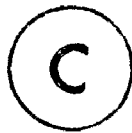


AN EXPERIMENTAL INVESTIGATION OF
DILUTE SLURRY SEDIMENTATION

by



T. E. POLLOCK, B. Eng., M. Eng.

A Thesis

Submitted to the Faculty of Graduate Studies

In Partial Fulfillment of the Requirements

for the Degree

Doctor of Philosophy

McMaster University

November, 1981

DOCTOR OF PHILOSOPHY
(Chemical Engineering)

McMASTER UNIVERSITY
Hamilton, Ontario

TITLE: An Experimental Investigation of Dilute Slurry
Sedimentation

AUTHOR: T. E. Pollock, B. Eng. (McMaster Univeristy)
M. Eng. (McMaster University)

SUPERVISOR: Dr. K. L. Murphy

NUMBER OF PAGES: xv, 270

ABSTRACT

The velocity and concentration of slurries of closely-sized, spherical particles in water were measured at several locations in the dilute blanket of a laboratory-scale, continuous, thickener-clarifier. Particle velocities were measured by the laser Doppler technique; particle concentrations were measured by local scattered light intensity and by optical transmittance.

Steady-state settling velocities as much as 70 percent higher than the average particle Stokes velocity occurred at slurry concentrations between 7.04×10^{-2} and 1.07×10^{-1} percent by volume. These findings contradicted all of the deterministic models commonly used to correlate slurry settling velocity with particle concentration. The failure of these models at dilute concentration was verified by flux measurements.

The formation of clusters, whereby several particles settle as a group rather than individually, was used to explain the high velocities. Based on a binomial spatial distribution of particles, large clusters at concentrations slightly higher than the bulk solution concentration were predicted to occur with high probability.

The few previous studies noting the formation of particle clusters were shown to have been dominated by wall effects at volumetric concentrations as low as 0.1 percent. The inverse variation of cluster size with slurry concentration accounted for the fact that the high velocities observed at low slurry concentrations have not been reported before.

The results of this investigation have significant implications for optimizing the design and control of those unit operations and unit processes which depend on relative motion between particles and fluid.

ACKNOWLEDGMENTS

Sincere thanks are extended to:

- (1) Dr. K. L. Murphy, for his support, encouragement and infinite patience throughout this investigation.
- (2) Mr. J. Newton and Mr. R. Dunn, for their many helpful contributions in designing and constructing the experimental apparatus.
- (3) Dr. C. Carter, for his help in designing and testing the electronic components.
- (4) Mr. D. Dolson, for his assistance in running the apparatus and collecting the data.
- (5) Dr. B. Latta, for his generous loan of the data logging instrumentation.
- (6) Mr. J. Hutchison and Mr. C. MacKay, for assembling many of the electronic components.
- (7) Dr. M. Baird, for the frequent use of his oscilloscope.
- (8) Dr. E. Ballik and Dr. B. Garside, for their helpful suggestions concerning the laser Doppler System.
- (9) Ms. P. Phillips for her prompt, accurate typing of the manuscript.

Financial assistance provided by the National Research Council of Canada and the Department of Chemical Engineering, McMaster University, is gratefully appreciated.

This thesis is dedicated to my parents.

TABLE OF CONTENTS

	Page
TITLE PAGE	i
SCOPE AND CONTENTS	ii
ABSTRACT	iii
ACKNOWLEDGMENTS	v
TABLE OF CONTENTS	vi
LIST OF FIGURES	xi
LIST OF TABLES	xiv
CHAPTER 1 INTRODUCTION	1
CHAPTER 2 MULTIPARTICLE SEDIMENTATION	7
2.1 Theoretical Models of Multiparticle Sedimentation	8
2.1.1 The Method of Reflections	9
2.1.2 The Method of Point Forces	11
2.1.3 The Cell Model Method	12
2.2 Semi-Theoretical Models of Multi- particle Sedimentation	14
2.3 Empirical Models of Multiparticle Sedimentation	24
2.4 Multiparticle Sedimentation at Very Dilute Concentration	32
CHAPTER 3 THE OPTICAL MEASUREMENT OF PARTICLE VELOCITY AND CONCENTRATION	38
3.1 The Optical Measurement of Particle Velocity	38
3.1.1 The Doppler Shift	38
3.1.2 The Heterodyne Detection of the Doppler Shift	42
3.1.3 The Laser Doppler Anemometer	44

Table of Contents (Cont'd.)

	Page
3.2 The Optical Measurement of Particle Concentration	49
3.2.1 The Estimation of Particle Concentration by Transmittance	52
3.2.2 The Estimation of Particle Concentration by Angular Scattering	56
3.2.3 Summary of the Optical Measurement of Particle Concentration	60
CHAPTER 4 THE LASER DOPPLER INSTRUMENT	63
4.1 Experimental Arrangement	63
4.2 The Laser	65
4.3 The Detector	65
4.4 The Incident Optics	68
4.5 The Detector Optics	72
4.6 The Electronic Signal Processing	74
4.7 The Data Logging Instrumentation	79
CHAPTER 5 MATERIALS AND METHODS	81
5.1 Sedimentation System	81
5.2 Slurry Particles	84
5.3 Settling Column	86
5.4 Traversing Mechanism	90
5.5 Base Plate	90
5.6 Feed Tank	91
5.7 Sedimentation System Start-Up	91
5.8 Sampling Locations	94
5.9 Procedure for Data Collection	96
CHAPTER 6 RESULTS AND INTERPRETATION	100
6.1 Particle Concentration	100
6.2 Particle Velocity	111
6.3 Velocity as a Function of Concentration	120
6.3.1 Comparison to Velocity Predicted by Literature Models	120
6.3.2 Comparison to Flux Predicted by Literature Models	128

Table of Contents (Cont'd.)

	Page
6.4 Dilute Slurry Sedimentation	130
6.4.1 The Probability of Cluster Formation at Very Dilute Concentrations	133
6.4.2 The Influence of Wall Effects on Cluster Settling Velocity . .	141
6.4.3 The Influence of Slurry Particle Velocity Distribution on Cluster Settling Velocity . . .	148
CHAPTER 7 CONCLUSIONS, RECOMMENDATIONS, AND ENGINEERING SIGNIFICANCE	152
7.1 Conclusions	152
7.2 Recommendations	153
7.3 Engineering Significance	154
REFERENCES	156
APPENDICES	
I CORRELATION BETWEEN PARTICLE CONCENTRATION AND AMPLITUDE OF THE DOPPLER SIGNAL	163
II CALIBRATION EXPERIMENTS FOR CONCENTRATION AND VELOCITY MEASUREMENTS	168
II.1 Calibration of Particle Concentration Measurements	168
II.1.1 Transmitted Intensity Calibration	169
II.1.2 Scattered Intensity Calibration	170
II.1.3 Combined Transmitted - Scattered Intensity Calibration	173
II.1.4 Transmittance Beam Reference Intensity	174
II.2 Calibration of Particle Velocity Measurement	177
II.2.1 Rotating Disc on Detector Side of Column	183
II.2.2 Rotating Disc on Laser Side of Column	185

Table of Contents (Cont'd.)

	Page
II.3	Verification of Doppler Signal 188
III	VARIANCES ASSOCIATED WITH CONCENTRATION, VELOCITY, AND FLUX ESTIMATES 196
III.1	Analysis of Variance for Concentration and Velocity Measurements . . . 196
III.2	Variance in Velocity Measurement for Estimating the Probability of Cluster Formation 197
III.3	Variance of Volumetric Flux Estimates 199
III.3.1	Variance of Measured Underflow Flux 199
III.3.2	Variance of Flux Predicted by Literature Models 203
III.3.3	Variance of Flux Calculated from Measured Velocity and Concentration 204
III.3.4	Comparison of Calculated and Predicted Fluxes to Measured Flux 205
IV	CHARACTERIZATION OF SLURRY PARTICLES 207
IV.1	Particle Size Distribution 207
IV.2	Particle Stokes Velocity Distribution 208
IV.3	Particle Density Determination 212
IV.4	Uncertainty in the Calculation of Stokes Velocity 216
V	CALIBRATION OF SIGNAL PROCESSING ELECTRONICS 218
V.1	Attenuator Calibration 221
V.2	Envelope Detector Output and Amplifier Gain Calibration 221
V.3	Bandpass Filter Calibration 225
V.4	Frequency Measurement Calibration 226
V.5	Voltmeter Calibration 229

Table of Contents (Cont'd.)

	Page
VI OPERATING CHARACTERISTICS OF THE LASER DOPPLER INSTRUMENT	231
VI.1 Photomultiplier Tube Calibration . . .	231
VI.1.1 Photomultiplier Tube Gain . .	231
VI.1.2 Photomultiplier Tube Dark Current	232
VI.2 Photomultiplier Tube Supply Voltage Calibration	237
VI.3 Laser Beam Power	239
VI.4 Effect of Optical Path Length Difference on Doppler Signal Amplitude	239
VI.5 Effects of Reference Beam Strength and False-Alarm Frequency on Doppler Signal Frequency and Amplitude	241
VII OPTICAL ALIGNMENT OF THE APPARATUS	250
VIII LINEAR LEAST-SQUARES REGRESSION PROCEDURE	256
IX MAJOR EQUIPMENT	258
X VELOCITY AND MASS CONCENTRATION AT EACH GRID POINT	259

LIST OF FIGURES

Figure		Page
1	CONVENTIONAL ACTIVATED SLUDGE SYSTEM	2
2	LIGHT SCATTERING BY A PARTICLE	39
3	TYPICAL LASER DOPPLER SYSTEM	45
4	TRANSMITTANCE VS. MASS CONCENTRATION	55
5	SCATTERING BEAM INTENSITY AND COMBINED SCAT- TERING BEAM-TRANSMITTANCE INTENSITIES VS. MASS CONCENTRATION	61
6	SCHEMATIC OF LASER DOPPLER SYSTEM	64
7	PHOTOMULTIPLIER TUBE HOUSING	67
8	PHOTOGRAPH OF INCIDENT OPTICS	69
9	SCHEMATIC OF DETECTOR OPTICS	73
10	SCHEMATIC OF SIGNAL PROCESSING ELECTRONICS	75
11	PHOTOGRAPH OF THE SIGNAL PROCESSING ELECTRONICS	76
12	SCHEMATIC OF THE EXPERIMENTAL APPARATUS	82
13	PHOTOGRAPH OF THE EXPERIMENTAL APPARATUS	83
14	CUMULATIVE PARTICLE SIZE DISTRIBUTION	85
15	CALCULATED PARTICLE STOKES VELOCITY DISTRIBUTION	87
16	SAMPLING LOCATIONS IN SETTLING COLUMN	95
17	EXPERIMENTAL DESIGN	101
18	PARTICLE CONCENTRATION VS. DEPTH	106

List of Figures (Cont'd.)

Figure	Page
19 CORRELATIONS AMONG THE THREE METHODS OF ESTIMATING PARTICLE CONCENTRATION	112
20 PARTICLE VELOCITY VS. DEPTH	119
21 COMPARISON BETWEEN LITERATURE MODELS AND MEASURED VELOCITY	122
22 COMPARISON BETWEEN FLUX PREDICTED BY LITERATURE MODELS AND MEASURED FLUX	129
23 VELOCITY VS. CONCENTRATION	132
24 BINOMIAL PROBABILITY VS. CLUSTER DIAMETER	137
25 BINOMIAL PROBABILITY VS. CLUSTER CONCENTRATION	138
26 CLUSTER DIAMETER VS. CLUSTER VELOCITY	140
27 THE INFLUENCE OF WALL EFFECTS ON CLUSTER VELOCITY	143
I-1 ENVELOPE DETECTOR OUTPUT VS. CONCENTRATION	165
II-1 CALIBRATION OF DOPPLER FREQUENCY	184
II-2 DOPPLER FREQUENCY VS. FALSE-ALARM FREQUENCY	187
II-3 AMPLITUDE OF DOPPLER SIGNAL VS. INPUT LIGHT INTENSITY	190
IV-1 PARTICLE SIZE DISTRIBUTION	209
IV-2 PARTICLE STOKES VELOCITY DISTRIBUTION	213
V-1 SCHEMATIC OF CALIBRATION OF SIGNAL PROCESSING ELECTRONICS	219
V-2 WIRING DIAGRAM FOR ELECTRONIC COMPONENTS	220
V-3 ATTENUATOR CALIBRATION	222
V-4 CALIBRATION OF ENVELOPE DETECTOR AND AMPLIFIER GAINS	224

List of Figures (Cont'd.)

Figure	Page
V-5 BANDPASS FILTER CHARACTERISTICS	227
V-6 CALIBRATION OF FREQUENCY MEASUREMENT	228
V-7 CALIBRATION OF AC VOLTMETER	230
VI-1 PHOTOMULTIPLIER TUBE GAIN	235
VI-2 PHOTOMULTIPLIER TUBE DARK CURRENT	236
VI-3 CALIBRATION OF PHOTOMULTIPLIER TUBE SUPPLY VOLTAGE	238
VI-4 CALIBRATION OF LASER POWER METER	240
VI-5 EFFECT OF PATH LENGTH DIFFERENCE ON DOPPLER SIGNAL FREQUENCY AND AMPLITUDE	242
VI-6 EFFECT OF REFERENCE BEAM INTENSITY ON FALSE- ALARM FREQUENCY	244
VI-7 EFFECT OF REFERENCE BEAM INTENSITY ON DOPPLER SIGNAL FREQUENCY AND AMPLITUDE	245
VI-8 EFFECT OF FALSE-ALARM FREQUENCY ON DOPPLER SIGNAL FREQUENCY	246

LIST OF TABLES

Table	Page
1 AVERAGE PARTICLE MASS FLOWRATES FOR FEED, OVERFLOW AND UNDERFLOW STREAMS	102
2 ANALYSIS OF VARIANCE FOR TRANSMITTANCE MEASUREMENTS	103
3 ANALYSIS OF VARIANCE FOR SCATTERING BEAM MEASUREMENTS	104
4 LEVEL AVERAGES OF MASS CONCENTRATION	107
5 RUN-AVERAGE ESTIMATES OF MASS CONCENTRATION	110
6 ANALYSIS OF VARIANCE FOR VELOCITY ESTIMATES	113
7 LEVEL AND RUN-AVERAGE VELOCITIES	115
8 THEORETICAL LITERATURE MODELS	123
9 SEMI-THEORETICAL LITERATURE MODELS	125
10 EMPIRICAL LITERATURE MODELS	126
11 POTENTIAL WALL EFFECTS ON CLUSTER VELOCITY	145
I-1 DOPPLER SIGNAL AMPLITUDE VS. MASS CONCENTRATION	166
II-1 CALIBRATION OF TRANSMITTED INTENSITY VS. MASS CONCENTRATION	171
II-2 CALIBRATION OF SCATTERED INTENSITY VS. MASS CONCENTRATION	172
II-3 LEAST-SQUARES MODELS FOR PHOTO-TUBE CALIBRATION	175
II-4 SEQUENCE OF MEASUREMENTS FOR ROTATING DISC EXPERIMENT	181
II-5 ROTATING DISC EXPERIMENT	186

List of Tables (Cont'd.)

Table	Page
II-6 LEVEL AVERAGE ESTIMATES OF PRE-AMPLIFIER INPUT AND LASER POWER	192
II-7 RUN-AVERAGE ESTIMATES OF PRE-AMPLIFIER INPUT AND LASER POWER	195
III-1 COMPONENT RANDOM VARIABLES FOR FLUX CALCULATIONS	201
III-2 VOLUMETRIC FLUX ESTIMATES	206
IV-1 DETERMINATION OF PARTICLE SIZE DISTRIBUTION . . .	210
IV-2 DETERMINATION OF PARTICLE DENSITY	214
VI-1 DETERMINATION OF PHOTOMULTIPLIER TUBE AMPLIFICATION	233
VI-2 INFLUENCE OF REFERENCE BEAM INTENSITY AND FALSE-ALARM FREQUENCY ON DOPPLER SIGNAL	247
VII-1 ALIGNMENT OF LASER DOPPLER INSTRUMENT	252

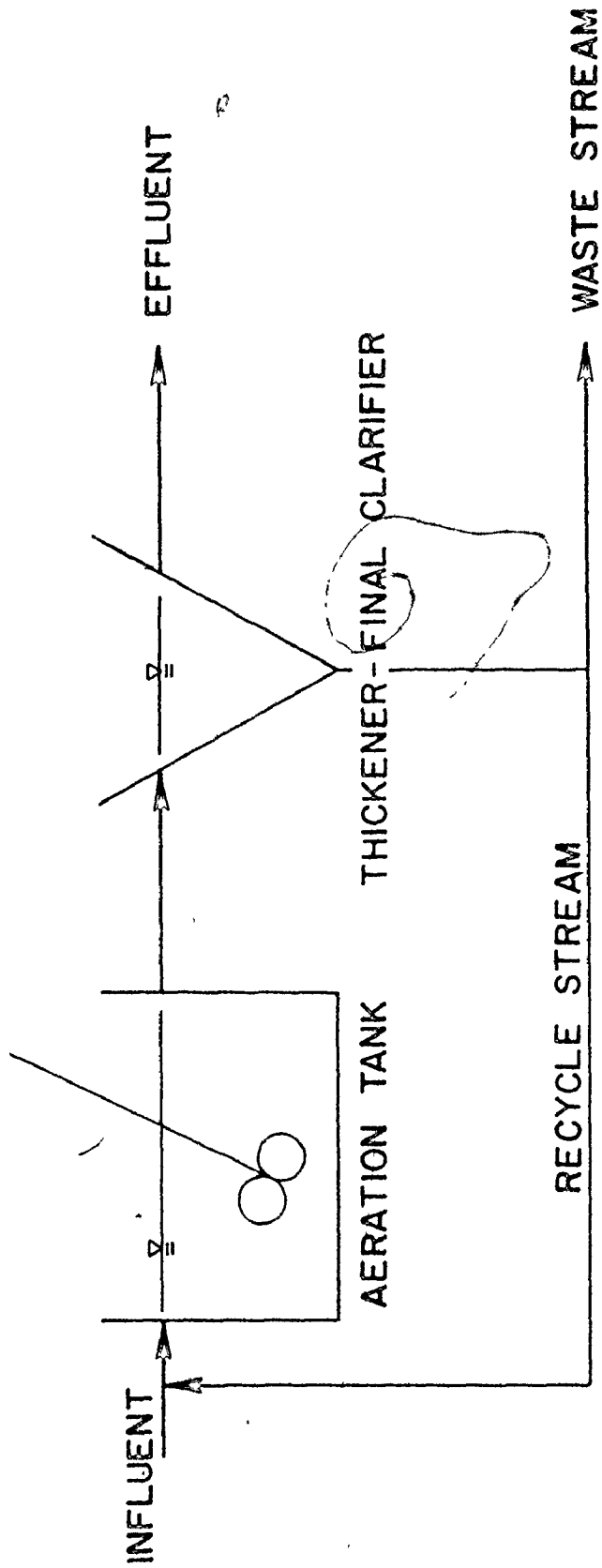
CHAPTER 1

INTRODUCTION

The conventional activated sludge system and its modifications are widely used for treating both industrial and domestic wastewaters. This system, shown in Figure 1, consists of a biological reactor, an aeration tank, followed by a final clarifier. In the aeration tank, the wastewater is contacted with microorganisms which convert the organic waste constituents to a wide variety of end products through a complex network of biochemical reactions. In the final clarifier, the microorganisms are removed from the carriage water by gravity sedimentation. Since the overall reaction rate is directly proportional to the biomass concentration, the concentrated biomass is collected at the underflow of the final clarifier and returned to the aeration tank. The clarified overflow from the final clarifier is discharged as system effluent. Since the utilization of substrate in the aeration tank results in the growth of microorganisms, biomass must be removed from the system on a regular basis. This is commonly practiced by diverting part of the recycle flow away from the system.

The final clarifier provides two major functions. It should be designed and operated such that suspended solids

FIGURE 1
CONVENTIONAL ACTIVATED SLUDGE SYSTEM



are not swept upward in the unit with the overflow thereby contaminating the system effluent. This is the clarification function. In addition, it should be designed and operated such that particulate material attains a high concentration in the underflow of the unit. This is the thickening function. In order to properly design and operate an activated sludge system, an adequate description must be available for the gravitational sedimentation of particles in the final clarifier. Since this component of the system performs the dual functions of clarification and thickening, it is evident that the sedimentation characteristics of the particles must be known over a broad range of slurry concentrations encompassing very low concentrations near the overflow, the clarification region, and very high concentrations near the underflow, the thickening region.

The problem of describing the relative velocity between a multiparticle cloud and a continuous fluid medium is common to many engineering fields and a tremendous amount of effort has been devoted to this topic. However, no comprehensive theoretical or empirical formulae have been developed to provide an adequate description of the phenomenon.

Several analyses have been published for fluid flow relative to assemblages of particles. Because of the non-linearity of the equations of motion due to the inclusion of inertial effects, theoretical analysis beyond the Stokes

region for multiparticle systems generally prove to be intractable. Consequently, theoretical studies have usually been restricted to systems defined by a single particle, or a few interacting particles, in creeping flow. Further, most analyses consider particles of well defined shape and many solutions are further restricted by a well ordered spatial arrangement of the particles. The difficulty of obtaining a convergent solution to this boundary value problem becomes enormous as these restrictions are relaxed, that is, as "real" systems are admitted.

Several investigations have treated multiparticle phenomena from a non-Newtonian point of view by assuming the slurry to be a homogeneous system which acts as a fluid with modified properties. These formulations define relationships between the settling velocity of the dispersed phase and the Stokes terminal velocity of a single particle which incorporate an empirical function of the dispersed phase volumetric concentration. This method of treatment generally adopts Burgers' (1942) approach of distinguishing between the effects of the motion and of the presence, even without motion, of neighbouring particles on a representative particle. The motion of other particles is represented by a simple function of the volumetric concentration of the dispersed phase. The presence of other particles is represented

through the use of an empirical viscosity function which is dependent on dispersed phase concentration.

Many strictly empirical models have been reported to describe multiparticle settling phenomena. These models have usually evolved from batch studies in which the settling behaviour of slurry particles in a quiescent fluid is determined. Experimental limitations have restricted the useful information which has been obtained from these investigations. The extreme difficulty of measuring particle motion in the interior of a multiparticle cloud without perturbing the flow has confined attention to the observation of particle motion close to the container walls or close to the solid-fluid interface where the settling characteristics may not be representative of the slurry as a whole.

Independent of the approach used to describe multiparticle sedimentation, the resulting models show the settling velocity of the dispersed phase to be a function of the local particle volumetric concentration only. This dependence has never been verified.

Most investigations have focused on the determination of multiparticle settling velocities at relatively high particle concentrations since this is an area of concern to many technologies. Relatively little attention has been given to the determination of the settling characteristics of multiparticle systems at dilute particle concentrations, and few

data are available in this region. The sedimentation characteristics in the dilute concentration region are usually estimated by extrapolation of the models developed for the more concentrated region. The accuracy of this approach for predicting dilute concentration sedimentation is not known.

It would be of benefit to determine the sedimentation characteristics of dilute concentration suspensions such as would occur in the clarification zone of a final clarifier. This could lead to improved design and operating criteria for the activated sludge system. A study was initiated to investigate this area. The specific objectives were:

- (1) to determine the dependence of dilute particle sedimentation on the local suspended solids concentration, and
- (2) to determine the accuracy of existing models for describing particle sedimentation in dilute slurries.

CHAPTER 2

MULTIPARTICLE SEDIMENTATION

Considerable attention has been given to describing particle sedimentation. For the case of a single spherical particle settling under the influence of gravity in an infinite fluid, a number of correlations are available to describe the settling velocity as a function of Reynolds number. For the conditions of very low Reynolds number, the creeping flow regime, particle sedimentation is adequately described by Stokes law:

$$V_{ST} = \frac{(\rho_p - \rho_f) D_p^2 g}{18\mu} \quad (2-1)$$

where: V_{ST} = Stokes velocity,
 ρ_p = particle density,
 ρ_f = fluid density,
 D_p = particle diameter,
 g = gravitational constant, and
 μ = fluid absolute viscosity.

If only a few identical particles are added to the fluid, the description of the motion of the particles becomes more complicated and the settling velocity of the individual particle is no longer described by Stokes law.

Investigators have used several approaches in an effort to describe multiparticle settling rate as a function of particle concentration. The various models reported in the literature can be conveniently, if somewhat arbitrarily, classified as theoretical, semi-theoretical and empirical.

2.1 THEORETICAL MODELS OF MULTIPARTICLE SEDIMENTATION

Several analyses have been presented for fluid flow relative to assemblages of particles. Analytical solutions of the equations of motion beyond the creeping flow regime for multiparticle systems have not been reported due to the non-linearity introduced by the inclusion of inertial effects. Further to the restriction of creeping flow, most investigators have used simplified systems consisting of identical spherical particles which do not collide or flocculate. Describing the motion of particles and fluid in multiparticle systems requires the specification of boundary conditions to account for the effect of neighbouring particles and vessel walls on the motion of a single particle. This difficult boundary value problem has been attempted using three major methods: the method of reflections, the method of point forces and the cell model method. Success has been claimed for all three methods for dilute suspensions; only the cell model method has been considered useful for more concentrated suspensions.

2.1.1 The Method of Reflections

This method was first used by Smoluchowski in 1911 and involves a piecewise matching of boundary conditions. For a suspension of particles, each moving at a constant velocity, the first reflection is the Stokes velocity field which would be established by each particle if it were moving at the same velocity but at infinite dilution. Assuming each particle in the suspension establishes such a velocity field, the net effect of the total field on an individual particle can be determined by reflecting from it the sum of the first reflections for all the other particles. In order for the particle to maintain a constant velocity, an equal and opposite field must be reflected from it. This reactive field influences the motion of all the other particles in the suspension. That is, the reactive field emanating from the subject particle is reflected off all other particles in the suspension. The disturbances produced by each particle in the suspension are reflected from the other suspension particles and the vessel walls to produce successively smaller effects with each successive reflection. As pointed out by Happel and Brenner (1965), an iterative solution scheme is established whereby particle-particle interactions can be taken into account. The accuracy of the solution is directly related to the number of reflections employed, subject to the constraint that a suitable coordinate system, that is, a

suitable spatial arrangement of particles, is employed. This method has proved successful for the condition of dilute concentration which allows each particle to be considered as a point.

The method of reflections has been used by McNown and Lin (1952), Burgers (1942) and Famularo and Happel (1965) for a cubic arrangement of particles and by Famularo and Happel (1965) for a rhombohedral and a random arrangement of particles. All of these solutions are of the form:

$$\frac{V_r}{V_{ST}} = \frac{1}{1 + K\phi^{1/3}} \quad (2-2)$$

where: V_r = particle velocity relative to the fluid,
 V_{ST} = Stokes velocity,
 ϕ = volumetric particle concentration, and
 K = constant.

The value of K ranges from 1.3 for the random spatial distribution to 1.92 for the cubic spatial distribution. Based on Famularo's (1962) work, Happel and Brenner (1965) suggest that the value of the parameter K in equation (2-2) should be independent of the spatial arrangement of particles provided that the distance between neighbouring particles is not greatly different from the mean interparticle spacing.

Burgers (1942) used the method of reflections for the assumption of random particle arrangement and obtained the solution:

$$\frac{V_r}{V_{ST}} = \frac{1}{1 + 6.88\phi} \quad (2-3)$$

The different functional dependence of sedimentation rate on concentration shown by equation (2-3) was ascribed by Happel and Brenner (1965) to possible errors in defining the spatial distribution of particles by Burgers (1942).

2.1.2 The Method of Point Forces

The method of point forces has been used by Hasimoto (1959), McNown and Lin (1952) and others [see, for example, Barnea and Mizrahi (1973)] to determine suspension settling rate as a function of concentration. In this method, the suspension particles, which are assumed to occupy a cubic array, are replaced by a point force which retards the fluid motion. The resulting cubic lattice of point forces is then used to modify the creeping flow equations. The form of solution obtained by this method is identical to equation (2-2). The values of the parameter, K , range from 1.6 according to McNown and Lin (1952) to 1.79 according to Hasimoto (1959).

It is interesting to note that the same form of dependence of settling velocity on concentration has been obtained by the method of reflections and the method of point forces. The variability in the parameter, K , reported in the literature is discussed by Happel and Brenner (1965) for the case of a cubic spatial arrangement of particles. They

ascribe this variability, in part, to the form of boundary condition used at the container wall. The no-slip assumption used by Hasimoto (1959) results in a value for K of 1.76; the perfect-slip assumption employed by Famularo (1962) results in a value for K of 1.91.

2.1.3 The Cell Model Method

The cell model method surrounds each particle in a symmetrical particle assemblage with a fluid envelope so that the suspension is assumed to consist of a number of identical cells. The dimensions of the fluid envelope are such that the ratio of the single particle volume to the cell volume is the same as the volumetric concentration of the suspension. For the case of one dimensional sedimentation, Happel (1958) derived the relationship:

$$\frac{v_r}{v_{ST}} = \left[\frac{3 - \left(\frac{9}{2}\right)\phi + \left(\frac{9}{2}\right)\phi^{5/3} - 3\phi^2}{3 + 2\phi^{5/3}} \right] \frac{\Delta P}{\Delta P_0} \quad (2-4)$$

where it was assumed that ΔP , the dynamic pressure drop, was equal to ΔP_0 , the dynamic pressure drop for Stokes flow.

This equation, which describes the settling velocity for a uniformly distributed particle assemblage, was obtained using a spherical fluid envelope for which the radial velocity component and the tangential shear stresses were identically zero at the surface, the so called free-surface assumptions. By means of the free-surface assumptions, the surface of the

fluid cell was made frictionless and the entire flow disturbance due to each particle was confined to the cell of fluid which surrounded it. The boundary value problem was thus reduced to a consideration of a single particle and its bounding envelope. Happel and Ast (1960) used the free surface approach for the case of a spherical particle bounded by an infinitely long frictionless cylinder. Good agreement was obtained between this model and the concentric sphere model for volumetric concentrations less than approximately 21 percent. This suggests that the free surface cell model is reasonably insensitive to the shape of the cells enveloping the particles.

Kuwabara (1959) used a treatment similar to Happel's free surface model. Instead of the assumption of zero tangential stress on the outer spherical envelope, Kuwabara used the boundary condition of zero vorticity. This zero vorticity model has been used by Gal-Or (1970) for the creeping flow regime and by LeClair and Hamielec (1968) for the intermediate Reynolds number range.

Solutions for the settling velocity of suspensions using the cell model method show the same functional dependence on particle concentration as equation (2-2).

All three theoretical methods of approach predict a decrease in settling velocity proportional to $\phi^{1/3}$. While this dependence has been widely accepted, Batchelor (1972) has shown that it results from the assumption of a regular arrangement of particles. A random particle distribution leads to a velocity decrease proportional to ϕ . The alleged experimental support

for the $\phi^{1/3}$ models has been based on the rate of fall of the interface which Tory and Pickard (1981) noted is often less than the mean velocity.

2.2 SEMI-THEORETICAL MODELS OF MULTIPARTICLE SEDIMENTATION

Several investigators have proposed relations of the form:

$$\frac{V}{\bar{V}_{ST}} = (1 - \phi)^2 \xi(\phi) \quad (2-5)$$

where: V = particle velocity relative to fixed reference frame, and

$\xi(\phi)$ = viscosity function,

to describe the settling velocity for multiparticle systems. Models of this form have evolved from the work of Burgers (1941, 1942) and modify Stokes law to account for the effects of the motion of and the presence of neighbouring particles in a suspension. These correcting factors are functions of particle volumetric concentration only.

According to Burgers (1941, 1942), the velocity field imparted to the fluid by a settling particle has the effect of inducing downward motion on neighbouring particles. Thus, each particle in a settling suspension experiences a downward drag, and its settling rate is therefore enhanced, due to the

sedimentation of all the other particles. As the particles move downward, each particle displaces a volume of fluid equal to the particle volume. This return fluid flow due to a single particle tends to decrease the settling rate of neighbouring particles. The net effect of the motion of the suspension particles on the settling rate of the multiparticle system is influenced by these two factors.

According to Burgers (1941, 1942), the presence of the suspension particles increases the stresses in the fluid. These stresses arise from the inability of the solid particles to deform in response to the velocity fields arising from the settling of neighbouring particles. As a result, the settling particles experience a resistance to settling. Burgers (1941, 1942) suggests that this effect can be accounted for by using a modified viscosity. A single particle, therefore, is considered to settle in a continuum consisting of a fluid with modified viscosity.

Another effect arising from the mere presence of particles in suspension was included in the analyses of Steinour (1949) and Hawksley (1951). They suggested that the effective buoyant force acting on a particle should depend on the density of the suspension as a whole, rather than on the density of the continuous phase only. This was later verified by Richardson and Meikle (1961).

The functional relationship expressed by equation (2-5) was originally proposed by Hawksley (1951) and Steinour (1949). In this equation, Stokes law is modified by the factor $(1-\phi)$ to account for the return flow effect; by a second factor $(1-\phi)$ to account for the modified buoyancy effect; and by the factor $\xi(\phi)$ to account for the modified viscosity effect. As noted by Zuber (1964), the validity of equation (2-5) was questioned since the development was not rigorous. Considerable support for the functional form of equation (2-5) was provided by Zuber (1964), who obtained the same dependence of multiparticle settling rate on particle concentration by an independent analysis. Zuber framed the one-dimensional steady-state settling problem in terms of four equations. The equation of motion for the mixture and the continuity equation for each phase were used to account for the effects of the motion of the two-phase continuum. The effects due to the presence of suspension particles were accounted for using a phenomenological equation which incorporated the apparent suspension viscosity to describe the motion of a single particle in the two-phase continuum.

The differences among the various semi-theoretical models of the form of equation (2-5) arise from the specification of the function $\xi(\phi)$. This function defines the viscosity of the multiparticle suspension, the apparent viscosity, as a function of particle volumetric concentration.

Einstein (1906) developed the theoretical expression:

$$\frac{\mu_a}{\mu_f} = (1 + K\phi) \quad (2-6)$$

where: μ_a = apparent viscosity,

μ_f = fluid viscosity, and

K = constant.

The parameter K was specified to be a function of the shape of the particles and was determined to be 2.5 for spheres. Einstein developed equation (2-6) for the assumptions of creeping flow conditions in a suspension sufficiently dilute that the particles did not interact hydrodynamically. This allowed a solution for the apparent viscosity of the solution as a whole by solving the equations of motion assuming no-slip conditions at the particle surfaces for the case of a single particle and then summing this solution to account for the other suspension particles. This solution was a limiting case of the method of reflections previously described and required only that the spacial distribution of the particles be specified. Cheng and Schachman (1955) have confirmed equation (2-6) in experiments using latex particles.

Guth and Simha (1936) extended the analysis of Einstein (1911) to include weak hydrodynamic interactions between the suspension particles at dilute concentration. They used the method of reflections, truncated after accounting for first reflection effects, to obtain:

$$\frac{\mu_a}{\mu_f} = 1. + 2.5\phi + 14.1\phi^2 \quad (2-7)$$

This equation was modified by Saito (1950) to account for the mutual volume of exclusion of the spheres to:

$$\frac{\mu_a}{\mu_f} = 1 + 2.5\phi + 12.6\phi^2 + \dots \quad (2-8)$$

Vand (1948) also used the method of reflections and included effects through second order reflections to obtain:

$$\frac{\mu_a}{\mu_f} = \exp \left[\frac{2.5\phi}{1 - (39/64)\phi} \right] \quad (2-9)$$

which assumed no attraction or repulsion between particles, and the relation

$$\frac{\mu_a}{\mu_f} = \exp \left[\frac{2 - 5\phi + 2.7\phi^2}{1 - (39/64)\phi} \right] \quad (2-10)$$

which took into account doublet collisions. Vand (1948) presented data which agreed very well with equation (2-10).

Several investigators have attempted to describe suspensions at high concentrations. At high concentration, the spatial distribution of particles and the interparticle hydrodynamic effects exert a more pronounced effect on multiparticle motion. In a semi-theoretical development, Mooney (1951) obtained:

$$\frac{\mu_a}{\mu_f} = \exp \left[\frac{2.5\phi}{1 - K\phi} \right] \quad (2-11)$$

which he claimed accounted for hydrodynamic interaction and particle crowding effects. The parameter, K , the crowding factor, apparently depended on the size distribution of the spherical particles. For a suspension containing a single size spherical particle, the estimated range for K given by Mooney (1951) is: $1.35 \cdot K \cdot 1.91$

It should be noted that the equations of Vand and Mooney show the same form of dependence of apparent viscosity on particle concentration. Empirical justification for this form of dependence was claimed by Barnea and Mizrahi (1973) who analyzed the data from sixteen sources and obtained:

$$\frac{\mu_a}{\mu_f} = \exp \left[\frac{1.66\phi}{1 - \phi} \right] \quad (2-12)$$

In determining the viscosity of concentrated suspensions, Brinkman (1952) extended Einstein's analysis by considering the effect of adding a single particle to a suspension. In this approach, the suspension was viewed as a fluid continuum of the same viscosity as the suspension. As noted by Frisch and Simha in Eirich (1956), this analysis is valid only for the case that the suspension is extremely dilute. The following model was obtained in this analysis:

$$\frac{\mu_a}{\mu_f} = (1 - K\phi)^{-2.5} \quad (2-13)$$

where: $K = 1$

This equation was derived independently by Roscoe (1952) who defined the parameter, K , to be a function of particle volumetric concentration. Maude and Whitmore (1952) were able to fit their experimental data for spherical particle suspensions with Roscoe's model.

Simha (1952) used the cell model approach previously described to derive an expression showing the dependence of the apparent suspension viscosity on particle concentration. He assumed each particle to be enveloped by a rigid spherical shell which was impermeable to the flow fields established by other particles of the suspension. By assuming no-slip at the boundary of the solid shell, he derived:

$$\frac{\mu_a}{\mu_f} = 1 + 2.5\phi \left[1 + \frac{25\phi}{4K^3} - \frac{21}{2K^3} \phi^{5/3} + \frac{625}{16K^6} \phi^2 + \dots \right] \quad (2-14)$$

and:

$$\frac{\mu_a}{\mu_f} = 1 + 2.5\phi \left[1 + \frac{25}{4K^3} + \frac{75}{4K^4} \phi^{4/3} + \frac{27}{K^5} \phi^{5/3} + \frac{785}{16K^6} \phi^2 + \dots \right] \quad (2-15)$$

for dilute and concentrated suspensions, respectively. The constant, K , was defined in terms of the maximum concentration and therefore is dependent on the spatial arrangement of the particles as well as being a function of particle concentration. Simha (1952) states that K ranges from close to unity for dilute suspensions to 1.81 for a concentrated hexagonal arrangement and to 1.61 for a concentrated cubic

arrangement. Cheng and Schachman (1955) provided empirical support for Simha's model for the case $K = 1.05$.

Hawksley (1951) used the apparent viscosity derived by Vand (1948) for his model. Using the data of Hanratty and Bandukwala (1957) and of Oliver (1961), Zuber (1964) claimed support for Hawksley's model as well as the Brinkman (1952)-Roscoe (1952) model for the region $0.05 \leq \phi \leq 0.65$. Further, since Zuber (1964) derived equation (2-5) by solving the two-phase continuity and momentum equations, he felt that the assumptions introduced by Hawksley (1951) with respect to the return flow effects and the buoyancy effects were correct.

Barnea and Mizrahi (1973) questioned the Hawksley model since it apparently predicts a weaker dependence of multiparticle settling velocity on concentration than had been observed empirically for very dilute suspensions. These investigators felt that an additional correction factor was needed to account for this deficiency. They derived an expression for the sedimentation velocity of a suspension by considering a force balance on a single particle in the suspension. In accordance with the approach of Burgers (1941, 1942), they incorporated a momentum transfer effect and a "wall hindrance" effect, both of which increased the drag force experience by the particle. The momentum transfer effect, which modified the interaction between the particles, was interpreted as being strongly related to, although not

equivalent to, the increase in the apparent viscosity of the suspension as seen by the particle. The fluid phase viscosity was replaced by the apparent viscosity in the drag relation using a correlation similar to that derived by Vand (1948):

$$\frac{u_a}{u_f} = \exp \left[\frac{K_1 \phi}{1 - K_2 \phi} \right] \quad (2-16)$$

The "wall hindrance" effect accounted for the increased drag experienced by the particle resulting from the return flow due to the motion of other particles. The particle settling velocity in the drag relation was replaced by a velocity specified by the form of correlation determined by the theoretical approach to multiparticle settling:

$$\frac{V_r}{V_{ST}} = \frac{1}{(1 + K_3 \phi^{1/3})} \quad (2-2)$$

Barnea and Mizrahi (1973) modified the buoyancy force experienced by the particle by replacing the specific gravity of the fluid phase with the specific gravity of the suspension, as suggested by Steinour (1949) and Hawksley (1951). The resulting model for the creeping flow range is:

$$\frac{V_r}{V_{ST}} = \frac{1 - \phi}{(1 + K_3 \phi^{1/3}) \exp\left(\frac{K_1 \phi}{1 - K_2 \phi}\right)} \quad (2-17)$$

To determine the values of the parameters, K_1 , K_2 and K_3 in equation (2-17), Barnea and Mizrahi correlated data for the

creeping flow range from eight literature sources by an iterative approximation scheme. They obtained: $K_1 = 5/3$, $K_2 = K_3 = 1.0$. The details of this nonlinear optimization are not presented, so it is not possible to estimate the correlation among the parameter values obtained. The investigators claimed that the model developed for the creeping flow range provides a good fit for data at much higher Reynolds numbers.

Brinkman (1947) considered the case of a spherical particle embedded in a porous medium. He obtained a solution in which the flow around the particle was described by the creeping flow equation of motion and the flow through the porous medium was described by a modification of Darcy's law:

$$\frac{V_r}{V_{ST}} = 1 + \frac{3}{4} \left[1 - \sqrt{\left(\frac{8}{3} - 3\right)} \right] \quad (2-18)$$

This approach has been criticized for lack of rigour due to the empirical nature of Darcy's law, [Happel and Brenner (1965)]. Barnea and Mizrahi (1973) compared the Brinkman model to the data from five published sources and noted the poor agreement obtained.

Loeffler and Ruth (1959) proposed a modified form of the Carman-Kozeny equation:

$$\frac{V_r}{V_{ST}} = \frac{1}{1 + \frac{2K_1}{(1 - \phi)^3}} \quad (2-19)$$

2.3 EMPIRICAL MODELS OF MULTIPARTICLE SEDIMENTATION

Steinour (1944) proposed a relationship of the form of equation (2-5) to describe multiparticle sedimentation to account for the presence and the motion of the suspension particles. Rather than using a theoretical development for the viscosity function $\epsilon(\phi)$ however, he used an empirical factor which he determined from his sedimentation experiments:

$$\frac{v_r}{v_{ST}} = (1 - \phi) \exp(-4.19\phi) \quad (2-20)$$

This correlation provided good agreement for his data in the concentration range studied, $0.076 \leq \phi \leq 0.498$, but, as noted by Barnea and Mizrahi (1973), the fit was not good outside this range.

Maude and Whitmore (1958) proposed the model:

$$\frac{v_s}{v_{ST}} = (1 - \phi)^n \quad (2-21)$$

where: v_s = superficial relative velocity, and

n = empirical constant,

to describe the dependence of multiparticle settling rate on particle concentration. The exponent, n , was specified to be a function of particle size distribution, particle shape, and Reynolds number. They reported exponent values of 5, 2 to 4, and 7 to 10, for uniform spheres in creeping flow, uniform

spheres in turbulent flow, and rough particles in creeping flow, respectively.

Richardson and Zaki (1954) developed an expression of the same form as equation (2-21) through the use of dimensional analysis and an experimental evaluation of the exponent. They assumed a spatial arrangement for the particles of the suspension in which identical horizontal layers of particles in hexagonal arrays were stacked vertically. As noted by Happel and Brenner (1965), they developed an approximate solution for the boundary value problem which broke down at infinite dilution. According to Richardson and Zaki (1954), the exponent, n , in equation (2-21) should be 4.65 for spheres in creeping flow. This model was intended to cover the range of dilute solution to $\phi = 0.5$.

Several investigators have proposed a correlation of the form of equation (2-21) to describe the dependence of multiparticle settling rate on particle concentration. For the case of spheres in creeping flow, the value of the exponent, n , ranges from 4.65 to 5.0.

Gasparyon and Zaminyon (1959) and Rutgers (1962) proposed a modified form of equation (2-21) to provide a better fit to experimental data in the dilute concentration range:

$$\frac{V}{V_{ST}} = K(1 - \phi)^n \quad (2-22)$$

The additional parameter, K , also a function of Reynolds number, apparently improved the model so that a good fit to

literature data was obtained by Barnea and Mizrahi (1973) for the condition $\phi \geq 0.1$.

A substantial body of work has evolved from the thickener design point of view. This approach is basically empirical in nature; no attempt is made to provide a fundamental hydrodynamic description of a single particle in the slurry, rather an overall point of view is adopted and the settling behaviour of the slurry as a whole is described.

Coe and Clevenger (1916) were the first investigators to attempt a comprehensive description of thickening. They introduced the concept that each horizontal plane in a continuous thickener had a capacity for transmitting solids that was determined by the solids concentration in the plane. That is, the particles in a continuous thickener settled at a rate determined by the local solids concentration. The area requirements for a continuous thickener would be determined by that combination of local solids concentration and local solids velocity which resulted in a minimum mass flux according to the relation:

$$G_i = \frac{V_i}{\frac{1}{\phi_i} - \frac{1}{\phi_u}} \quad (2-23)$$

where: G_i = particle flux,

V_i = settling velocity of particles at concentration ϕ_i , and

ϕ_u = underflow particle concentration.

Coe and Clevenger determined the particle settling velocity as a function of concentration from a series of batch tests in which the initial, linear, subsidence velocity of the solid-fluid interface was determined as a function of the initial uniform concentration. By employing initial concentrations covering those expected in the continuous thickener ranging between the feed concentration and the underflow concentration, the dependence of particle flux on concentration could be determined.

Kynch (1952) provided a mathematical framework for the observations of Coe and Clevenger. For the one dimensional batch sedimentation of an initially uniform suspension of identical spherical particles, Kynch postulated that infinitesimally thin bands of progressively increasing particle concentration propagated upward from the bottom of the container to intersect the solid-liquid interface at a velocity:

$$U = \frac{dG}{d\phi} \quad (2-24)$$

where: U = velocity of propagation through the suspension of a concentration discontinuity,

$d\phi$ = incremental change in concentration across the concentration discontinuity, and

dG = incremental change in flux across the concentration discontinuity.

By assuming that the subsidence velocity of the solid-fluid interface was a function of the particle concentration at the

interface, Kynch showed that the solid-fluid interface height versus time curve for a single batch test could be used to determine the dependence of velocity on concentration.

The slope of the tangent at a given point on the interface versus time curve is the instantaneous interface velocity corresponding to the instantaneous interface concentration:

$$\phi_1 = \frac{H_0 \phi_0}{H_I} \quad (2-25)$$

where: ϕ_i = interface particle concentration when the interface is at height H_i ,
 ϕ_0 = initial, uniform particle concentration,
 H_0 = initial height of slurry, and
 H_I = ordinate intercept of the tangent to the interface height-time curve at an interface height of H_i .

Kynch's analysis of batch sedimentation was adopted by Talmage and Fitch (1955) who derived a design procedure by which the required area for a thickener could be determined from a single batch settling test. This procedure depended on estimating the compression point on the interface height versus time curve. That is, it was necessary to determine the time at which the solid-fluid interface left the free settling region and entered the compression region where the interface solids received mechanical support from underlying particles. This issue was not resolved by Talmage and Fitch.

Two graphical approximation techniques have been used to estimate the point of compression. Roberts (1949) assumed that the time rate of change of concentration for solids in compression could be described by a rate equation, first order with respect to dilution:

$$\frac{dD}{dt} = K(D - D_{\infty}) \quad (2-26)$$

where: D = dilution at time t (weight of fluid divided by weight of particles),

t = time,

K = rate constant, and


D_{∞} = dilution at infinite time.

By plotting $(D - D_{\infty})$ versus time, the location of the compression point could be estimated as the point at which this relationship did not hold. It should be noted that this technique required an estimate of D_{∞} , the dilution at infinite time. Eckenfelder and Melbinger (1957) proposed a simpler technique for estimating the compression point. According to these workers, the compression point could be located as the intersection of the interface height versus time curve and the bisector of the angle contained between the tangents to the compression zone and the free settling zone, the two extremes of the interface height versus time curve.

Considerable controversy existed over whether multiple batch tests or a single batch test should form the basis

for thickener design. Behn and Liebman (1963) and Scott (1968) demonstrated that the batch settling curve could be constructed from multiple tangents drawn to a single interface height-time curve. Scott (1968) concluded from his studies using flocculated silica that the single batch test approach was at least as good as the multiple test procedure of Coe and Clevenger (1916). Shannon *et al.* (1964) determined that the velocity-concentration dependence as determined from the single test Kynch approach agreed well with that obtained from the multiple test approach for noncompressible slurries of glass beads in water. Subsequently, Tory and Shannon (1965) demonstrated a lack of correspondence between the two approaches for a compressible calcium carbonate slurry.* The discrepancy was ascribed to a nonrepresentative estimate of interface concentration in the single test approach due to the compression of already settled particles in the settling container. Tory and Shannon (1965) Shin and Dick (1974), and Shirato *et al.* (1970) have shown that significant compressive stresses are present in the compression zone of a batch settling test thereby suggesting that the Kynch (single test) approach would not apply to a compressible slurry.

The work of Coe and Clevenger (1916) and of Kynch (1952) on batch sedimentation forms the basis for most continuous thickener designs. The relationship between particle



flux (product of velocity and concentration) and particle concentration has been advocated for thickener design by Yoshioka *et al.* (1957) and Hassett (1958), and adopted for steady-state continuous operation by Keinath *et al.* (1976). The fundamental assumption for analyses of thickener design and operation is that local particle velocity is a function of local particle concentration. Considerable empirical evidence has been presented to support this assumption. Shannon and Tory and their coworkers [Shannon *et al.* (1963), Shannon and Tory (1966), and Tory and Shannon (1965)] demonstrated good correspondence between observed continuous thickener operation and that predicted by batch flux curves for incompressible slurries. Scott (1968, 1968a) worked with calcium carbonate slurries and silica suspensions and was able to predict underflow mass discharge rates and concentration profiles in continuous operation from batch flux data. Javaheri (1971) was able to predict continuous thickener performance from batch flux data for slurries of glass beads, calcium carbonate, and lime softening sludges. However, Comings (1940) measurements of concentration profiles in continuous thickeners and Scott and Alderton's (1966) measurement of limiting continuous flux are at variance with the Kynch assumptions. Mancini (1962) and Dick and Ewing (1967) have concluded that the Kynch assumptions are not valid for activated sludge suspensions. Dick, in particular, has done

considerable research attempting to relate the settling properties of activated sludge to the rheological properties of the suspension [Dick (1968)].

Much empirical evidence is available to demonstrate a strong correspondence between observed continuous steady-state thickener operation and measured batch flux analyses for incompressible slurries. Considerable uncertainty is apparent in the literature for the case of suspensions which are strongly non-ideal and for the case of non-steady-state operation. While a strong dependence of particle settling velocity on concentration is generally accepted, the nature of the dependence is ill-defined.

2.4 MULTIPARTICLE SEDIMENTATION AT VERY DILUTE CONCENTRATION

While most of the work on multiparticle sedimentation has been concerned with relatively concentrated slurries, some studies have considered particle sedimentation in very dilute suspensions. The case of two equal spheres settling together has been treated by Smoluchowski (1911) and Stimson and Jeffery (1926) and exact solutions for various two sphere arrangements have been given by Goldman *et al.* (1966). According to these studies, the two spheres always move in parallel with the same velocity. The vertical component of the settling velocity is enhanced, relative to the single particle Stokes velocity, by a factor of 1.4 when the two

spheres come in contact in the horizontal plane, and by a factor of 1.55 in the vertical plane. Particle interactions were shown to be important even when the particles were separated by several particle diameters. These theories are in good agreement with the data of Eveson *et al.* (1959) and Happel and Pfeffer (1960). Enhanced settling velocity due to hydrodynamic particle interaction has been described theoretically for very simple systems only; when several particles are present, the description of particle motion is much more complicated and analytical solutions are not available for these cases.

Kaye and Boardman (1962) were the first to experimentally measure an enhanced particle velocity for dilute slurries. In their batch sedimentation studies, the settling velocities of a few coloured spheres were observed in slurries of transparent spheres. By varying the number of transparent spheres, they were able to determine particle settling velocity as a function of particle concentration. They noted that particle settling velocity increased from the Stokes value at infinite dilution to a maximum value approximately one and one-half times the Stokes value at a volumetric concentration of about 1.2 percent. At greater volumetric concentrations the velocity decreased with increasing concentration. They speculated that the enhanced settling rates were caused by the formation of particle clusters, by

which a number of particles would become strongly enough associated to settle as a group rather than individually. That is, each cluster could be viewed as a single particle of modified density, whose size was determined by the number of particles in the group. According to Kaye and Boardman (1962), clusters were continually forming and disintegrating during the sedimentation process.

This work led others to investigate the behaviour of particles at dilute concentrations. Johne (1966) performed experiments with monodisperse suspensions of 200 μ m diameter glass spheres, a small number of which were radioactive. Mean velocities as a function of suspension concentration were determined by monitoring the time of fall of the radioactive particles with a scintillation counter. Johne (1966) confirmed Kaye and Boardman's (1962) observation that the maximum particle settling velocity occurred at a volumetric concentration of approximately 10^{-2} ; however, he measured a maximum velocity 2.1 times larger than the individual particle Stokes velocity. He ascribed the lower velocity enhancement reported by Kaye and Boardman (1962) to the fact that the tracer particles used in their experiments were of different size than the suspension particles. Data presented by Johne (1966) and Kaye and Boardman (1962) support this interpretation. Both groups showed that as the difference in size between the tracer spheres and the other suspension

spheres increased, the concentration at which the maximum settling velocity was observed increased but the extent of the velocity enhancement decreased.

Koglin (1972) extended Johne's work using the same experimental techniques and showed that, for a monodisperse suspension of spherical particles, a maximum settling velocity of three times the Stokes velocity occurred at a volumetric concentration of 1.3 percent. Through experiments with different diameter cylindrical containers, he demonstrated that the lower velocity values reported by Johne (1966) and by Kaye and Boardman (1962) could be explained by wall effects.

Koglin (1971) demonstrated that, for a given slurry concentration, the velocity distribution resulting from the dynamic formation and disintegration of particle clusters could be described by a logarithmic normal distribution at any given concentration.

In subsequent work, Koglin (1973) showed that the logarithmic normal distribution observed for spheres was also valid for plastic discs and irregularly shaped limestone particles. In these experiments using different particle shapes, it was shown that the extent of increase in the settling velocity relative to the Stokes velocity was inversely proportional to the square root of the particle sphericity and directly proportional to the square root of the number of

particles in the cluster. His data showed that the concentration at which the maximum velocity occurred, as well as the extent of velocity enhancement, decreased as the particle sphericity decreased. This was ascribed to the lower stability of the clusters formed by nonspherical particles. He claimed support for this interpretation using the data of Barford (1972) who performed settling experiments using irregularly shaped particles over the volumetric concentration range of 0.002 to 1.15 percent. He observed a maximum settling velocity approximately ten percent greater than the Stokes velocity at a concentration of 0.2 volume percent for three different mean particle sizes: 13 μ m, 22.5 μ m, and 30 μ m diameter. Barford (1972) assumed that the particles settled as if they were ordered in pairs with an assumed centre to centre separation and a random angle of inclination. By using a Poisson distribution of particles in the suspension and the calculations of Goldman *et al.* (1966), he was able to fit his data in the concentration range of 0.015 to 0.1 volumetric percent. Poor agreement with his data was evident outside this concentration range.

These studies suggest that the dynamic formation and disintegration of particle clusters accounts for the enhanced settling velocities observed for very dilute slurries. Conditions favouring cluster formation are apparently present in a slurry due to the random spatial distribution of the

particles. The extent of velocity enhancement depends on the size distribution, sphericity and concentration of the slurry particles.

CHAPTER 3
THE OPTICAL MEASUREMENT OF PARTICLE
VELOCITY AND CONCENTRATION

It is evident that the understanding of multiparticle sedimentation has been limited by the complexity of the governing equations and by the difficulty of empirically determining localized particle velocities and concentrations.

It would be beneficial to be able to measure localized velocities and concentrations in a settling slurry. These measurements would allow an evaluation of the universal assumption that localized particle velocity is a function of localized particle volumetric concentration and a determination of the influence of operating variables on the thickening and clarification functions of a final clarifier. The development of laser technology has made possible the measurement of particle motion with accuracy and precision.

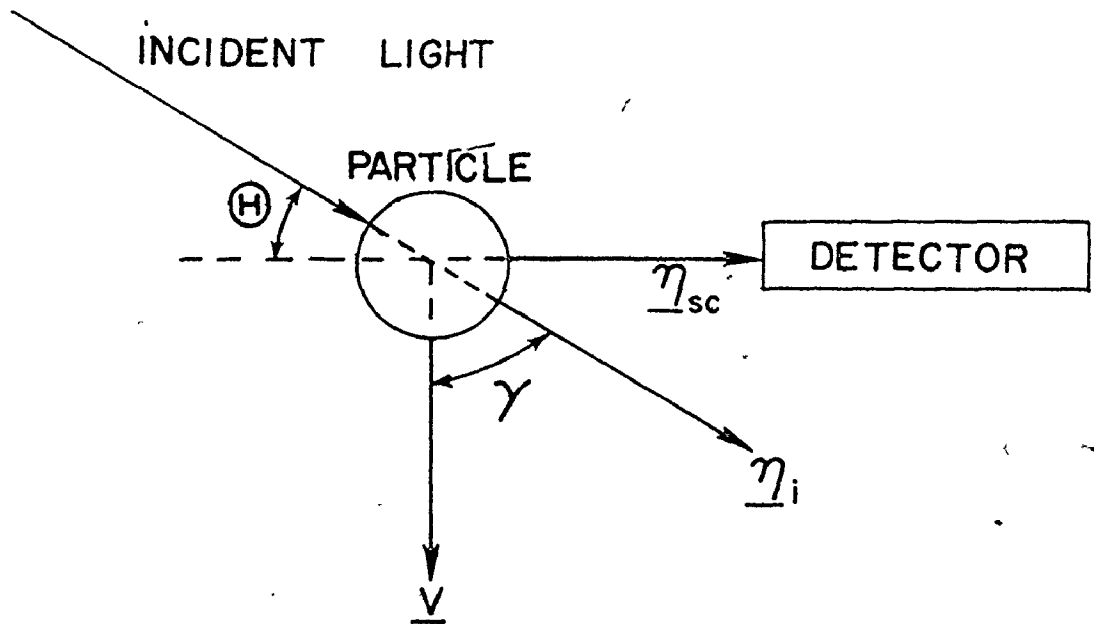
3.1 THE OPTICAL MEASUREMENT OF PARTICLE VELOCITY

3.1.1 The Doppler Shift

Consider monochromatic radiation of wavelength λ_i and speed c emanating from a stationary laser source and impinging a particle, (see Figure 2). The incident radiation moves in the direction defined by the unit vector \underline{n}_1 and

FIGURE 2

LIGHT SCATTERING BY A PARTICLE



illuminates a particle having a velocity \underline{v} where $|\underline{v}| \ll c$. For a stationary particle, the number of wavefronts striking it per unit time would be c/λ_i or ω_i , where ω_i is the frequency of the incident radiation. Since the difference between the velocity of the particle and the illumination is:

$$c - \underline{v} \cdot \underline{n}_i \quad (3-1)$$

the number of wavefronts incident upon the particle per unit time is:

$$\omega_p = (c - \underline{v} \cdot \underline{n}_i) / \lambda_i \quad (3-2)$$

where ω_p is the apparent frequency of the incident radiation to the particle and hence represents the number of wavefronts scattered by the moving particle per unit time.

For a fixed detector which collects radiation scattered in the direction \underline{n}_{sc} , the number of wavefronts collected is ω_p . After the scattering of one wavefront, the particle moves toward that wavefront with a speed $\underline{v} \cdot \underline{n}_{sc}$. Thus, when the next wavefront is scattered after a time interval $1/\omega_p$, the first wavefront is a distance $(c - \underline{v} \cdot \underline{n}_{sc})/\omega_p$ away from the particle. To the fixed detector, the apparent wavelength of the scattered radiation is:

$$\lambda_{sc} = (c - \underline{v} \cdot \underline{n}_{sc}) / \omega_p = \lambda_i [(c - \underline{v} \cdot \underline{n}_{sc}) / (c - \underline{v} \cdot \underline{n}_i)] \quad (3-3)$$

The frequency of the scattered radiation with respect to the fixed detector is:

$$\omega_{sc} = \frac{c}{\lambda_{sc}} = \frac{c}{\lambda_i} \left[\frac{c - \underline{v} \cdot \underline{n}_i}{c - \underline{v} \cdot \underline{n}_{sc}} \right] = \omega_i \left[\frac{1 - \frac{\underline{v} \cdot \underline{n}_i}{c}}{1 - \frac{\underline{v} \cdot \underline{n}_{sc}}{c}} \right] \quad (3-4)$$

and the difference in frequency between the scattered radiation and the incident radiation, the Doppler shift, is

$$\omega_D = \omega_{sc} - \omega_i \quad (3-5)$$

That is:

$$\omega_D = \omega_i \left[\frac{1 - \frac{\underline{v} \cdot \underline{n}_i}{c}}{1 - \frac{\underline{v} \cdot \underline{n}_{sc}}{c}} \right] - \omega_i = \frac{\omega_i}{c} \left[\frac{\underline{v} \cdot (\underline{n}_{sc} - \underline{n}_i)}{1 - \frac{\underline{v} \cdot \underline{n}_{sc}}{c}} \right] \quad (3-6)$$

Since $|\underline{v}| \ll c$, then

$$\omega_D \approx \frac{nv}{\lambda_0} \cdot (\underline{n}_{sc} - \underline{n}_i) \quad (3-7)$$

where: λ_0 = vacuum wavelength of incident radiation, and

n = index of refraction in the medium surrounding the particle.

The determination of particle velocity, therefore, involves the determination of the frequency shift, the Doppler shift, induced in the scattered radiation by virtue of the particle motion.

For fixed orientations of the incident and scattered light beams, the frequency shift, ω_D , gives the component of velocity in the direction $(\underline{n}_{sc} - \underline{n}_i)$. For the laser Doppler system used in this investigation, the vertical component of the particle settling velocity relative to a fixed observer was calculated using:

$$V = \frac{\omega_D}{127.289} \quad (3-8)$$

Refer to Appendix II.

3.1.2 The Heterodyne Detection of the Doppler Shift

Forrester *et al.* (1947) were the first to suggest that heterodyne detection could be achieved with signals of optical frequency and Forrester *et al.* (1955) subsequently demonstrated the effect. Conventional "monochromatic" light sources produce radiation with relatively large bandwidth and low intensity per unit bandwidth thereby limiting the optical heterodyne technique to the detection of frequency shifts greater than 10^9 Hz due to poor signal to noise ratios [Angus *et al.* (1969)]. With the development of gas lasers which produce essentially monochromatic radiation, heterodyning in the optical frequency range for frequency shifts less than 10^9 Hz became feasible [Forrester (1961), Stone (1963)]. The shift in frequency of laser light scattered from a moving object can be determined by optically mixing the scattered radiation with a reference beam of unshifted frequency from the same laser on the surface of a photosensitive square law detector.

For a square law detector, the emission of an electron from the photocathode is proportional to the intensity of incident light, that is, to the square of the total

electric field intensity. If two sine waves of different frequency are superimposed on a photocathode, the result is an output signal whose amplitude is modulated by the difference frequency, [Stone (1963)]. Consider two monochromatic light beams of slightly different frequency combined on the surface of a photocathode:

$$\begin{aligned} E_1 &= E_{10} \sin 2\pi\omega_0 t \\ E_2 &= E_{20} \sin 2\pi(\omega_0 + \omega_D)t \end{aligned} \quad (3-9)$$

where: $E_{1,2}$ = electric fields of signals 1 and 2,
 $E_{10,20}$ = amplitudes of signals 1 and 2,
 ω_0 = frequency,
 ω_D = frequency difference, and
 t = time.

The output current, i , is proportional to the square of the incident electric field:

$$i \propto (E_1 + E_2)^2 \quad (3-10)$$

Due to the frequency response characteristics of a photomultiplier tube, terms in the expansion of the output current having frequencies of the order of ω_0 will result in a DC current proportional to the time average of those terms.

For $\omega_D \ll \omega_0$:

$$i \propto \left[\frac{E_{10}^2 + E_{20}^2}{2} + E_{10} E_{20} \sin 2\pi(\omega_D t + \zeta) \right] \quad (3-11)$$

where the phase angle, ζ , is a constant if the two beams are coherent, [Goldstein and Kreid (1968)]. The first term in equation (3-11) is the DC current and the second term is the AC or Doppler current. Knowledge of the frequency of the Doppler current and the geometry of the light scattering system allows the particle velocity to be calculated according to equation (3-7).

3.1.3 The Laser Doppler Anemometer

A schematic of the components of a typical laser Doppler system is shown in Figure 3. The light from a laser source is split into two fractions, a reference beam and a scattering beam. These beams are made to intersect at the desired location in the fluid-solid system by various optical elements. Part of the light scattered from the intersection point is collected by the elements of the receiver optics and directed to the cathode of a photomultiplier tube. The geometrical arrangement of the incident and collection optical elements is such that that portion of the reference beam which reaches the detector has experienced no frequency shift while that portion of the scattering beam reaching the detector has been frequency shifted by the Doppler effect due to the motion of the scattering centres. The output current of the detector is then processed electronically to extract the desired frequency (and hence velocity) information. Many variations are possible with respect to the geometrical

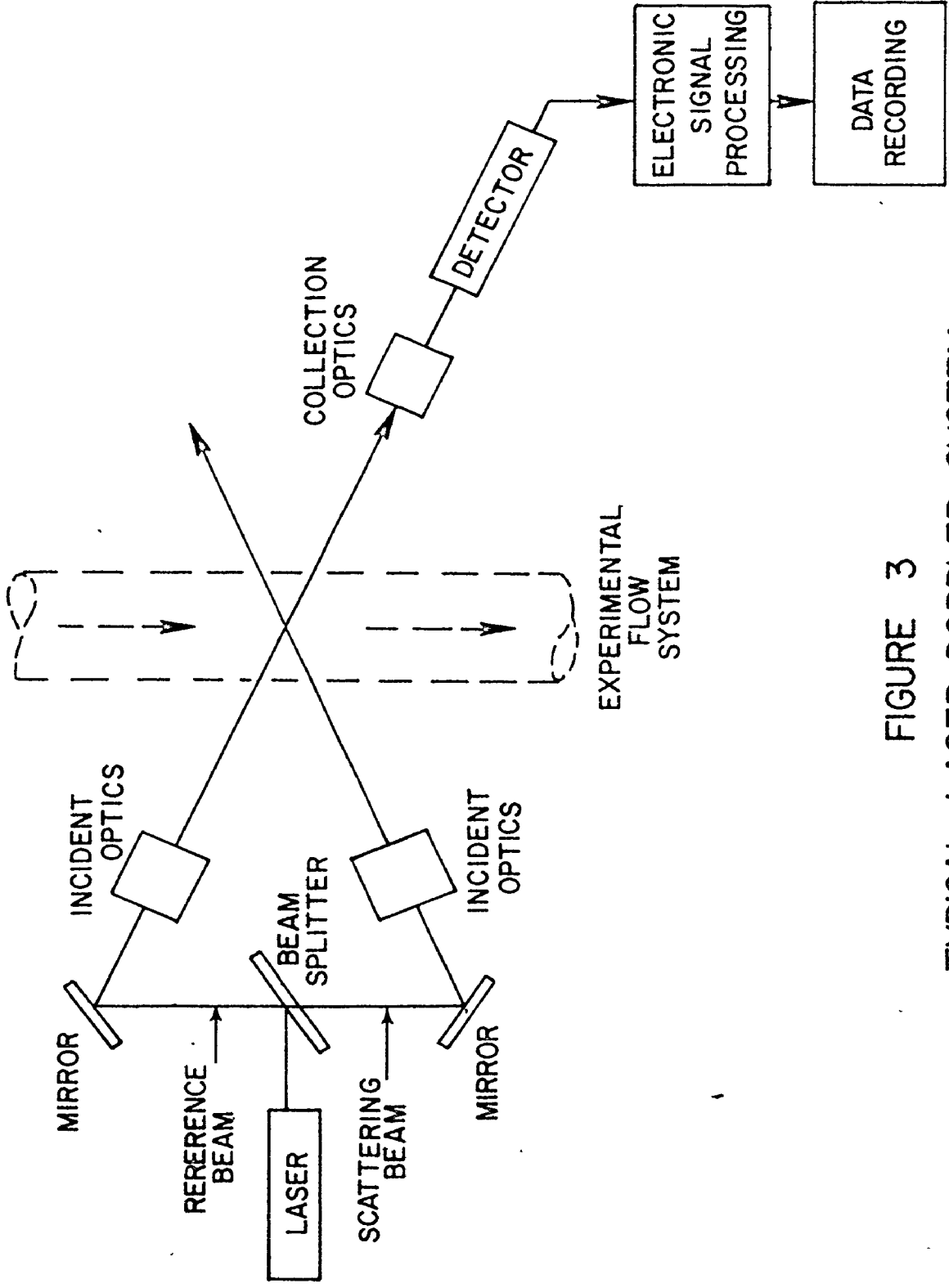


FIGURE 3
TYPICAL LASER DOPPLER SYSTEM

arrangement of the system components and the method of extracting the requisite velocity data from the detector output. The laser Doppler anemometer used in this study is described in Chapter 4.

The laser Doppler technique was developed in the middle 1960s. Yeh and Cummins (1964) measured the fully developed laminar flow profile for water flowing in a duct of circular cross-section. Laminar flow development was studied in a square duct by Goldstein and Kreid (1967) and in a round duct for water at low Reynolds number by Foreman *et al.* (1966) and Berman and Santos (1969). Studies were performed with water [Goldstein and Hagen (1967), and Pike *et al.* (1968)] and dilute water-polymer solutions [Goldstein *et al.* (1969)] for flows covering the range from the laminar region through transition to full turbulence. Studies of turbulent flow have been made in gases [Foreman *et al.* (1966) and Lewis *et al.* (1968)] and in rocket and jet exhausts [James *et al.* (1968)]. Since this pioneering work in the use of laser Doppler anemometry, the technique has been applied to a number of complex fluid flow problems [see, for example, the monograph by Durst *et al.* (1976)].

The accuracy of the velocity measurement varies inversely with the bandwidth of the Doppler signal. The total signal bandwidth is the sum of the broadening due to the bandwidths of: the laser source, the detector output

electronic processing instrumentation, the Brownian motion of the scattering particles, the velocity gradients in the scattering volume of the slurry, and the angular uncertainties inherent in the arrangement of the elements of the incident and collection optics [Angus *et al.* (1969); Goldstein and Kreid (1967)]. The broadening due to the laser source can be as small as 10 to 20 Hz for low power helium-neon lasers [Goldstein and Kreid (1967)], and as large as several hundred hertz for high power argon lasers [Bloom (1968)], while that due to the detector output instrumentation can be less than 10 Hz [Yeh and Cummins (1964); Goldstein and Kreid (1967)]. The broadening due to these effects and that due to Brownian motion [estimated to be about 10 Hz by Yeh and Cummins (1964) for spherical particles of diameter 0.5 micrometers and specific gravity 1.0] is constant and is significant only at very low levels of Doppler shift according to Goldstein and Kreid (1967). The broadening due to velocity gradients in the finite scattering volume observed by the detector has been reported to be directly proportional to the spatial resolution of the incident laser beam. Angus *et al.* (1969) found that a diffraction limited spot size of 10 micrometers was obtainable with a helium-neon laser, enabling them to sample across the laminar sublayer in turbulent pipe flow to within 10 micrometers of the wall. By proper design of the laser Doppler system, Angus *et al.* (1969) reported that

frequency changes of approximately 10 Hz out of absolute light frequencies on the order of 10^{14} Hz may be observed.

The high degree of resolution possible with the laser Doppler system has made possible the precise measurement of very low velocities. Angus *et al.* (1969) have claimed that the minimum detectable velocity with this technique is on the order of 10^{-5} m/sec with an average deviation of 0.24 percent from theoretical predictions for fully developed laminar flow in circular cylinders and square ducts. Yeh and Cummins (1964) reported that velocities as low as 7×10^{-5} m/sec could be measured and they and Foreman *et al.* (1965) demonstrated excellent agreement with the theory for the measurement of centre line velocities ranging from 10^{-3} to 1 m/sec for pipe flow. Goldstein and Kreid (1967) measured velocity profiles in a transparent tube with a low power helium-neon laser. Mean speeds of from 6.5×10^{-3} to 3.62×10^{-2} m/sec were measured with a reported accuracy of about 0.1 percent.

The laser Doppler technique appears to be well suited to a determination of localized particle velocity in a laboratory scale continuous sedimentation vessel. The technique offers a high degree of spatial resolution along with very good precision and accuracy. Measurements can be made with minimal perturbation of the slurry so that the velocity of the test system is not modified by the measuring

device. Further, the possibility of real time measurement of velocity is possible with this technique.

The advantages of laser Doppler anemometry appear to be significant when compared with the drawbacks associated with other means of obtaining velocity information. Techniques which require the collection of slurry samples or the insertion of probes have the obvious disadvantage of distorting the slurry sedimentation to an unknown degree. Techniques which depend on the monitoring of the motion of a small number of "tracer" particles in a slurry lack the spatial resolution of the laser Doppler technique.,

3.2 THE OPTICAL MEASUREMENT OF PARTICLE CONCENTRATION

Optical techniques offer the potential of continuously and remotely monitoring the localized concentration of particles in a slurry with minimum disturbance to the system. Suspended particles in a fluid scatter and absorb radiation to a degree depending on their size, shape, refractive index and the wavelength of the incident radiation. The scattering of light is the result of the interaction of electromagnetic waves and the electrons in the particle; the incident waves produce periodic oscillations in the system which then radiate secondary waves as the scattered radiation. This radiation includes the diffracted, refracted and reflected components.

There are two basic methods of approach to describing light scattering. In one approach, the charges resulting from the interaction of the incident radiation and the particles are represented as an array of linearly oscillating dipoles. This approach was developed by Rayleigh in the late 1800s and is applicable to particles much smaller than the wavelength of the incident radiation. In the other approach, electromagnetic field theory is used to describe the scattering phenomena. This approach was adopted by Mie (1908) who provided the theoretical framework which has been extended by others to provide a complete description of the theory of light scattering by spheres [see Van de Hulst (1957) and Kerker (1963)]. The Mie theory is not restricted by particle size and agrees with the Rayleigh theory for the limiting case in which the particles are much smaller than the wavelength of the incident radiation.

The Mie theory of light scattering allows for the absolute determination of particle concentration if the properties of the scattering system are known. However, the theory is valid only for cases in which single, independent scattering occurs. Van de Hulst (1957) notes that the assumption of independent scattering implies that there is no systematic relation between the phases of the radiation scattered by neighbouring particles. This condition is met by a random spatial distribution of scattering centres whose

centre to centre separation is not less than three times the particle radius, [Van de Hulst (1957)]. Churchill *et al.* (1960) verified this criterion for independent scattering by experiments with very dense hydrosols.

The assumption of single scattering is met by dilute suspensions. According to Green *et al.* (1964), the single scattering requirement is met when the light scattered by a suspension of N similar scattering particles is N times the intensity of that scattered by a single particle, and the energy removed from a beam of light traversing the suspension is N times that removed by a single particle. Van de Hulst (1957) points out that this simple proportionality to the number of particles holds only if the radiation to which each particle is exposed is essentially that of the original beam. In a suspension, however, each particle is also illuminated by light scattered by the other particles and light from the original beam is attenuated by the other particles. When these effects are strong, multiple scattering is said to occur and the simple proportionality does not exist. The problem of determining the scattered intensities inside and outside the suspension under the conditions of multiple scattering is a very difficult mathematical problem [Chandrasekhar (1950)], and solutions have been obtained for very simple cases only. Based on the work of Churchill *et al.* (1960), Green *et al.* (1964) suggest that multiple

scattering may be assumed to be insignificant for suspensions whose centre to centre particle spacing is greater than approximately three times the particle radius. This criterion neglects the optical thickness of the suspension which will have a strong influence on the degree of multiple scattering [Hodkinson (1966)]. Van de Hulst (1957) suggests that multiple scattering effects can be assumed to be insignificant if the intensity of a beam of light is attenuated less than 10 percent by the suspension.

For suspensions of spherical particles of uniform size and density, particle concentration can be determined by the Mie theory providing the criteria for single scattering and independent scattering are not violated. For the experimental apparatus employed in this study for measuring local particle velocity by laser Doppler anemometry, it was convenient to measure particle concentration by two methods: by the degree of extinction of a transmittance beam and by the intensity of light scattered by the slurry at a known angle.

3.2.1 The Estimation of Particle Concentration by Transmittance

According to the Bouguer Law, the transmitted and incident intensities are related by:

$$\frac{I}{I_0} = e^{-kx} \quad (3-12)$$

where: I = transmitted intensity,
 I_0 = incident intensity,
 k = extinction coefficient, and
 x = thickness of the suspension.

The extinction produced by one particle is described by the particle extinction coefficient, E , where:

$$E = \frac{\text{total flux scattered and absorbed by the particle}}{\text{total flux geometrically incident on the particle}}$$

If there are N particles of projected area A in a unit volume of suspension whose particles have identical extinction coefficients, the Bouguer Law may be expressed:

$$\frac{I}{I_0} = e^{-NAEx} \quad (3-13)$$

Since spherical particles of uniform diameter were employed in this study, and since the particle diameter was large relative to the wavelength of the incident radiation (particle size parameter $\alpha = 145$), the extinction coefficient was known to be identically two. Thus, knowing the suspension thickness, the projected area concentration, NA , could be determined from measured values of I and I_0 according to equation (3-13). Further, since the particle density and projected area were known, equation (3-13) could be expressed as:

$$\log_{10} \left(\frac{I}{I_0} \right) = -2.9655C \quad (3-14)$$

where: C = particle mass concentration.

The transmitted intensity was measured at each of several locations in the settling column for each run. The particle mass concentration was estimated from these measurements using the relationship:

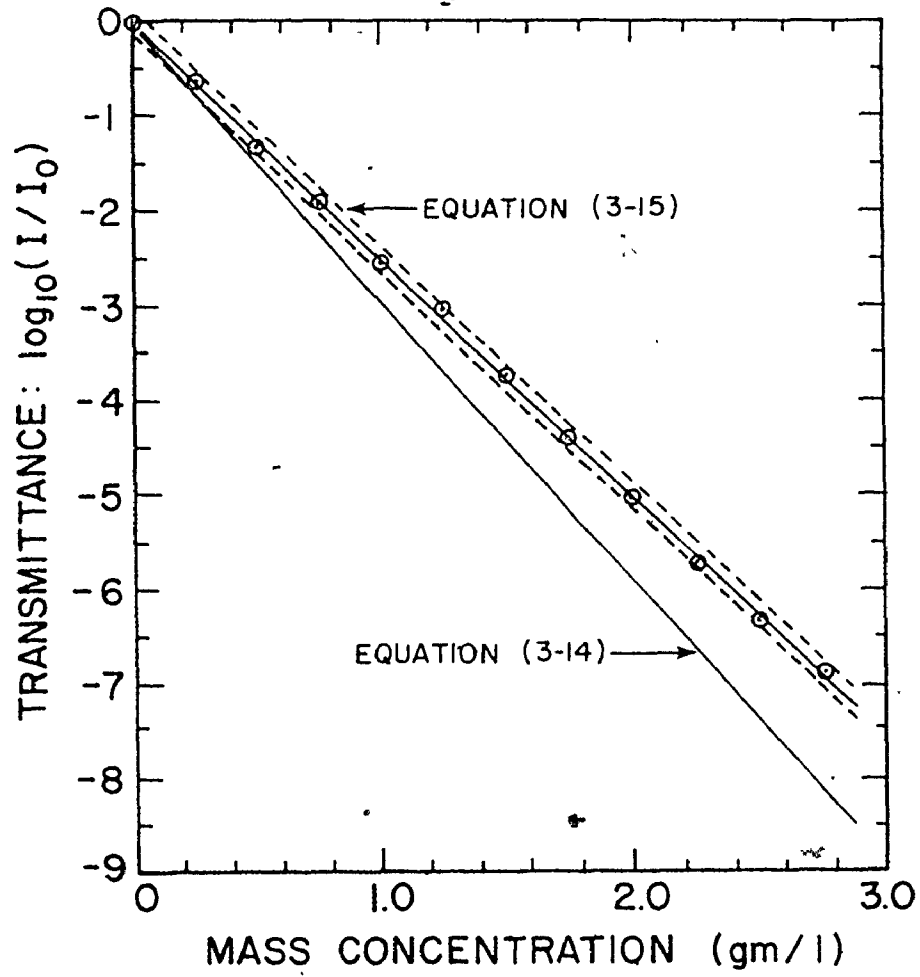
$$\log_{10} \left(\frac{I}{I_0} \right) = 2.0140 \times 10^{-3} - 2.5093 C \quad (3-15)$$

which was determined by least-squares techniques from the calibration experiments described in Appendix II. The transmittance with the settling column filled with water but devoid of particles, I_0 , was determined to be 571.348 volts, (see Section II.1.4). The measured correlation between transmitted intensity and particle mass concentration is shown in Figure 4. Also plotted is the relationship predicted by equation (3-14) which was determined from the measured values of particle diameter and density.

The divergence of these curves may result, in part, from uncertainty in the estimates of particle diameter and particle density, [which would influence the slope in equation (3-14)], and, in part, from the effects of multiple scattering, [which would influence the slope in equation (3-15)]. Hodkinson (1966) claims that a large amount of multiple scattering will not affect the Bouguer Law when the field of view of the detector is limited to:

$$\theta < \frac{3.84}{10 \alpha} \quad (3-16)$$

FIGURE 4
TRANSMITTANCE
VS
MASS CONCENTRATION



where: θ = detector field of view (radians), and
 α = particle size parameter:

$$\alpha = \frac{\pi D_p}{\lambda_{rel}}$$

where: D_p = particle diameter, and
 λ_{rel} = wavelength of radiation in the suspending medium.

The field of view of the detector employed in this study, $\theta = 5.88 \times 10^{-5}$ radians, was sufficiently small to meet Hodkinson's requirement, $\theta = 2.6461 \times 10^{-3}$ radians from equation (3-16), to ensure the absence of multiple scattering effects. Since this criterion takes no account of suspension thickness, however, the influence of multiple scattering could not be ignored. In fact, for the range of extinctions measured in this study, the work of Van de Hulst (1957) would suggest that multiple scattering was present. The suspension mass concentrations measured in this study were sufficiently low to meet the criterion for independent scattering according to the studies of Churchill *et al.* (1960) and Van de Hulst (1957).

3.2.2 The Estimation of Particle Concentration by Angular Scattering

According to Mie theory, the light scattered by an optically isotropic sphere of a given refractive index can be described as a spherical wave composed of two groups of partial waves:

$$I_{\theta} = \frac{\lambda_{\text{rel}}^2}{8\pi^2 R^2} (i_1 + i_2) \quad (3-17)$$

where: I_{θ} = intensity of light scattered in direction θ ,

λ_{rel} = wavelength of incident radiation in the suspending medium,

R = distance between the detector and the particle, and

i_1, i_2 = amplitude functions.

The values of i_1 and i_2 are defined in terms of the coefficients of the electric and magnetic waves. The result is expressed in a complicated series of terms involving Bessel, Hankel and Legendre functions as well as the particle size parameter, α , and the refractive index, m , of the particle relative to that of the medium in which it is suspended.

The angular distribution of intensity is a complicated function of the scattering angle, θ , and the degree of complexity increases with particle size. As particle size increases, the scattering pattern becomes more forward directed and develops an array of angular maxima and minima in addition to the principal forward maximum. Hodkinson (1966) notes that the number of minima in the pattern between $\theta = 0^\circ$ and $\theta = 180^\circ$ is approximately equal to α , the particle size parameter.

A further complication arises for the case of concentrated suspensions. In order to estimate particle concentration through the Mie theory, account must be taken of the

attenuation experienced by the incident radiation prior to reaching the local suspension volume from which the scattered intensity is to be measured and of the attenuation experienced by the scattered radiation as it traverses that portion of the slurry between the local scattering volume and the detector. Hodkinson (1966) suggests that this complication can be overcome by normalizing the scattered intensity, I_{θ} , by the transmittance, I . He presents a derivation to relate the normalized scattered intensity to the particle projected area concentration, C_a :

$$\frac{I_{\theta}}{I} = C_a (V) \gamma (i_1 + i_2) \quad (3-18)$$

where: $C_a = \frac{D_p^2}{4}$,

V = volume of suspension sampled, and

γ = solid angle subtended by the detector.

Equation (3-18) is claimed by Hodkinson to be valid for those situations in which the transmittance is within a few percent of 100 percent; that is, in the absence of significant multiple scattering.

As previously noted in the discussion of transmittance measurements, there is strong evidence to suggest that multiple scattering effects were appreciable throughout this study. In view of the documented breakdown of the Mie theory for small amounts of multiple scattering, it is evident that an absolute estimate of particle concentration could not be

obtained by the measurement of scattered light intensity at a given angle.

A series of experiments was performed (see Appendix II) to determine if a useful correlation could be obtained between scattered light intensity and particle mass concentration. It was determined that, within experimental error, the relation:

$$\log_{10} \left[\frac{I_{sca}}{I_o} \right] = -3.0802 - 0.7663 C \quad (3-19)$$

where: I_{sca} = scattered intensity at angle θ ,

I_o = incident transmittance intensity, (see Appendix VI), and

C = particle mass concentration,

described this dependence at the 95 percent confidence level for the range of particle mass concentrations used in this study. This correlation was observed to hold independent of the location of the scattering volume within the suspension.

Using Hodkinson's (1966) approach of normalizing the measured scattered intensity, the relation:

$$\log_{10} \left[\frac{I_{sca}}{I} \right] = -6.2759 + 1.7430 C \quad (3-20)$$

where: I = intensity of the transmittance beam,

was determined to describe the dependence of scattered intensity on particle mass concentration at the 95 percent confidence level for the case in which there were no concentration

gradients in the suspension. These correlations are shown in Figure 5.

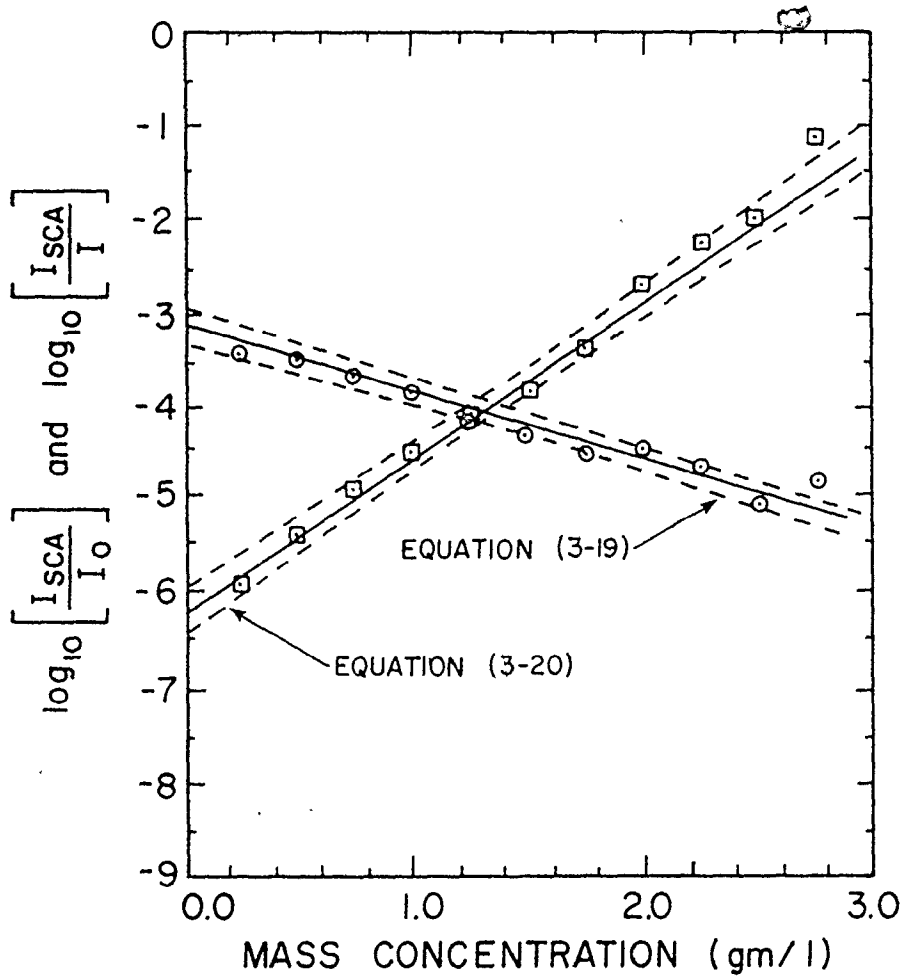
3.2.3 Summary of the Optical Measurement of Particle Concentration

The scattered light intensity and the transmittance were measured at each of the 40 sampling locations for each experimental run. The particle mass concentration was estimated from the measured transmittance using equation (3-15); from the scattered intensity using equation (3-19); and from both the measured transmittance and the measured scattered intensity using equation (3-20).

The transmittance measurement has the disadvantage of lacking spatial specificity along the axis of the incident radiation. The mass concentration determined by this method represents an estimate averaged along the longitudinal axis of the incident transmittance beam. With this measurement, it is not possible to discern variations in particle mass concentration in the direction parallel to the incident radiation.

The scattered intensity measurement has the advantage that an estimate of particle mass concentration can be obtained from a localized region within the slurry. Although the calibration experiments described in Appendix II demonstrate that the correlation of equation (3-19) is independent of location within the settling column for the case of

FIGURE 5
SCATTERING BEAM INTENSITY AND
COMBINED SCATTERING BEAM - TRANSMITTANCE
VS MASS CONCENTRATION



spatially uniform particle concentration, this correlation may not hold for the case of significant particle concentration gradients in the settling column. For a non-uniform particle distribution, account would have to be taken of the varying degrees of attenuation experienced by the incident and scattered radiation as a function of location within the column.

Hodkinson's (1966) approach of normalizing the scattered intensity with a measured transmittance value may alleviate some of the uncertainty inherent in the scattered intensity measurement due to particle concentration gradients. While this approach is convenient, it suffers from the fact that two measurements of light intensity must be made thereby increasing the variance of the estimate of particle mass concentration. In addition, since the correlation of equation (3-20) depends on a "correction" based on the measurement of transmittance, the advantage of a localized measurement of particle concentration is somewhat diminished.

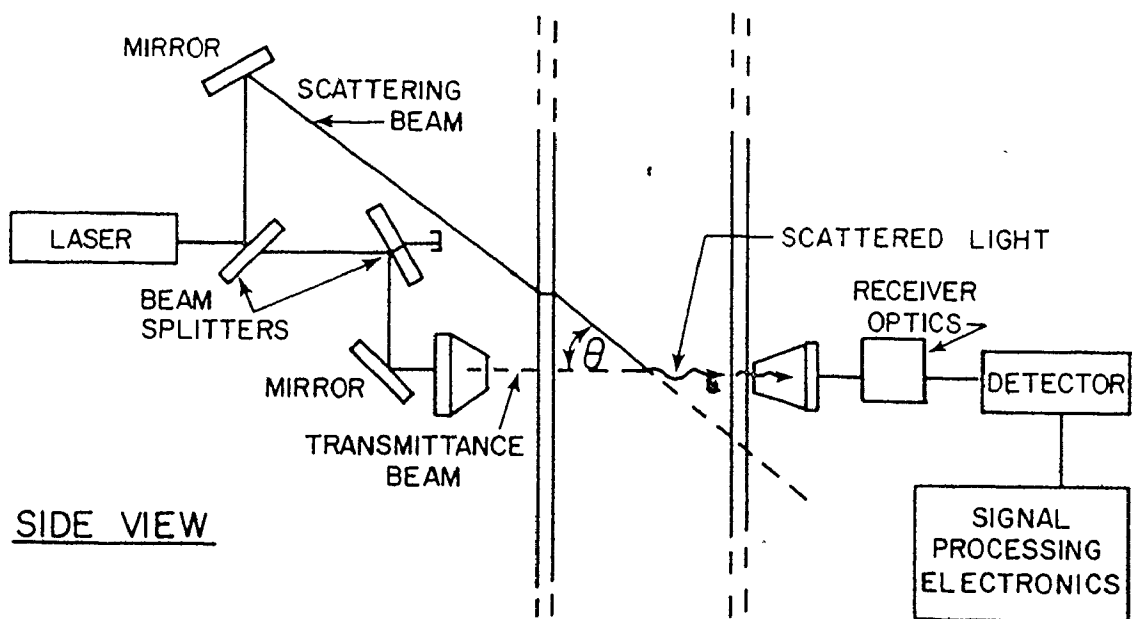
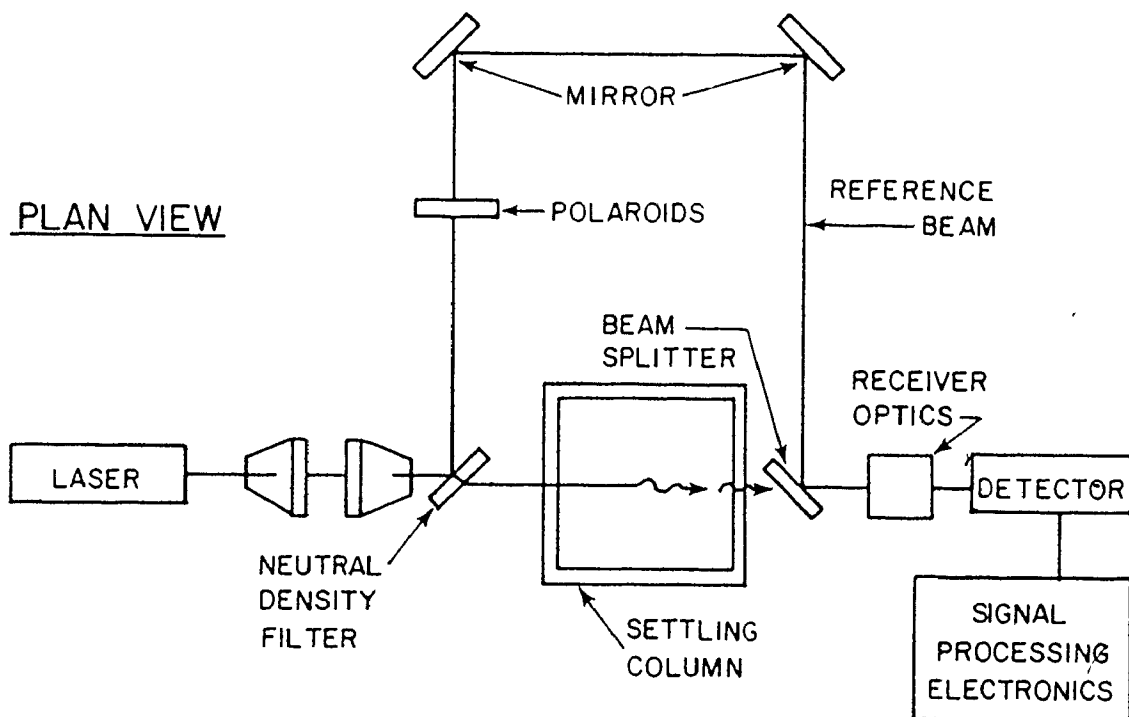
CHAPTER 4

THE LASER DOPPLER INSTRUMENT

4.1 EXPERIMENTAL ARRANGEMENT

A block diagram of the experimental apparatus is shown in Figure 6. The output from the laser source was split into three beams by the incident optics: the transmittance beam, the scattering beam, and the reference beam. The transmittance beam was used for aligning the settling column and the detector assembly. The scattering beam was directed into the settling slurry, in the same vertical plane as the transmittance beam, at an angle of 17 degrees to the horizontal. The reference beam was directed around the settling column to the receiving optics in the same horizontal plane as the transmittance beam. The receiver optics limited the field of view of the detector and directed the collected light to the photocathode of the photomultiplier tube. During the course of an experiment, measurements were made of the scattering beam, the reference beam, the transmittance beam and various combinations of these three beams. For those instances in which a particular beam was not needed for a measurement, a light trap was used to prevent unwanted laser light from entering the field of view of the detector. The detector output was processed electronically to determine

FIGURE 6
SCHEMATIC OF LASER DOPPLER SYSTEM



the Doppler frequency which was subsequently recorded on magnetic tape.

4.2 THE LASER

A Spectra Physics model 164 argon ion laser was used in this study. This laser was equipped with a prism assembly allowing single line operation at 4880 \AA and an inter-cavity aperture allowing single mode operation. A light stabilizer increased the stability of the output power (nominally $\pm 0.5\%$ over 10 hours) and decreased the output noise (nominally 0.2% rms, 10 Hz - 2 MHz). The use of this laser sacrificed the low noise operation of neutral atomic gas lasers such as helium-neon and helium-cadmium for the increased power attainable with an ion laser.

4.3 THE DETECTOR

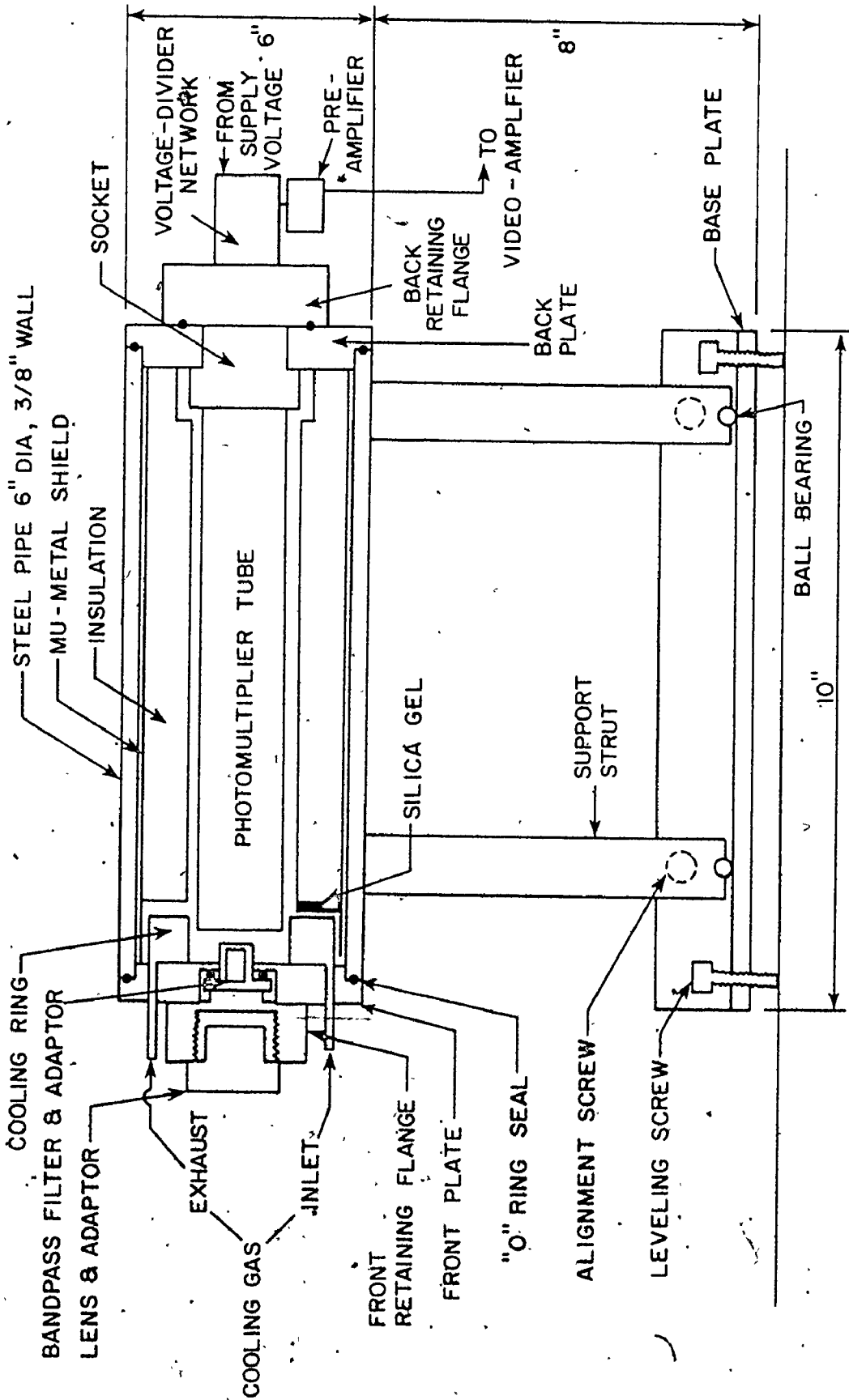
An RCA 7265 photomultiplier tube was used in this study. This detector, a 14-stage, head-on type with a multi-alkalai photocathode, provided a S-20 spectral response with high quantum efficiency and low dark current. The photomultiplier cathode was operated at a potential of minus 2200 volts DC relative to the anode by means of a regulated, Fluke Manufacturing Company model 415-B power supply and the voltage divider network recommended by the manufacturer.

To reduce photocathode thermionic emission noise, the photomultiplier was cooled to a temperature less than 5°C by

passing certified dry nitrogen gas, which had been cooled by a liquid nitrogen reservoir, through a hollow brass ring surrounding the head of the tube. Good thermal insulation was obtained from Urethane plastic foam. To reduce the possibility of frosting on the front window of the detector housing, (a $4880 \pm 20 \text{ \AA}$ bandpass filter), the entire housing was purged with certified dry nitrogen and then immediately sealed air-tight. A small quantity of silica gel was placed inside the housing to trap any residual moisture. The cross-sectional view of the housing is shown in Figure 7.

The photomultiplier tube was mounted horizontally in the housing and was wholly supported by the tube socket. Since the glass envelope of the tube was free from contact, noise due to charge distribution was minimized [Braddick (1960)]. This mounting configuration permitted operation of the photomultiplier in the grounded anode mode and damage to the semiconductor pre-amplifier from high voltage power switching transients was avoided. To reduce ohmic leakage noise [Lallemand (1962)], the photomultiplier tube and socket were carefully cleaned with acetone prior to installation. A mu-metal shield was installed to prevent noise from stray magnetic fields [Lallemond (1962)]. This shield was connected to the cathode terminal to limit leakage current [RCA (1968)].

FIGURE 7
PHOTOMULTIPLIER TUBE HOUSING



An enclosure made from a double layer of heavy black velvet cloth was placed around the detector housing and those components of the collection optics after the beam splitter to eliminate the leakage of stray laser light to the photocathode.

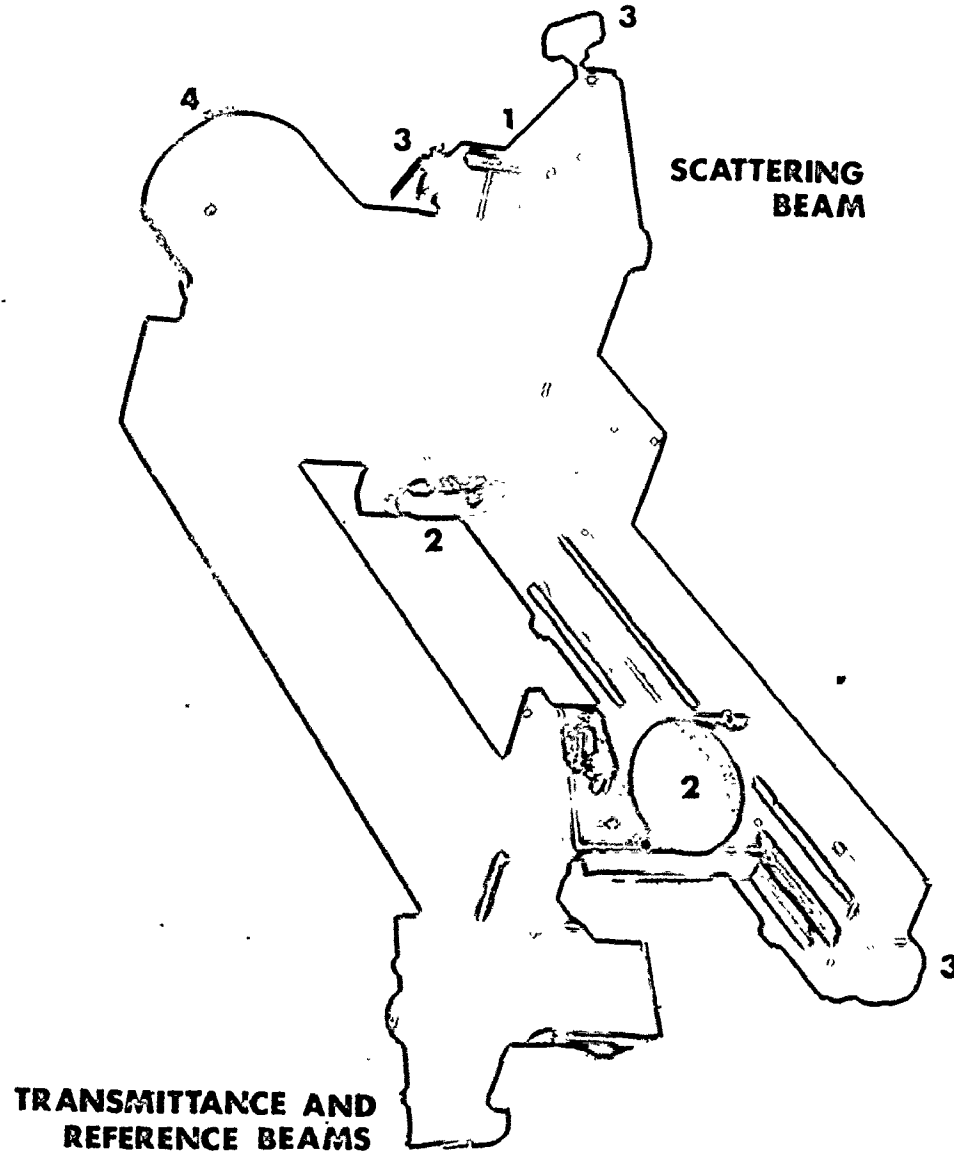
4.4 THE INCIDENT OPTICS

The incident optics are shown in Figure 8. Two components, each consisting of a beam splitter and a mirror, were attached to a precision slide in one leg of the support frame. A fine-pitch drive screw in each leg allowed approximately 6 inches of ganged horizontal translation parallel to the laser output for each beam splitter-mirror combination.

The beam splitter supports had a similar slide adjustment which allowed relative translation between the beam splitter and the mirror of each combination along the axis of the laser output. Each beam splitter could be rotated about that horizontal axis normal to the laser output. Each mirror could be rotated about the two axes normal to the laser output. The translational and rotational movement possible with this design was useful in aligning the optical system for a desired scattering angle.

The incident optical frame was mounted on the gimballed support of the laser output mirror. The entire assembly could be rotated about the axis of the laser output so that the incident optics could be aligned with the laser output

FIGURE 8
PHOTOGRAPH OF INCIDENT OPTICS



- 1 MIRROR**
- 2 BEAM-SPLITTER**
- 3 ADJUSTMENT SCREWS**
- 4 MOUNTING SLEEVE**

beam. An adjustable brace attached to the laser head cover maintained alignment of the laser cavity by alleviating the torque imposed on the laser output mirror gimbal due to the application of the optical assembly.

Approximately 72.1% of the vertically polarized laser output was reflected from the first beam splitter to the first mirror. This beam, the scattering beam, was directed into the experimental settling column in a vertical plane at an angle of 17 degrees from the horizontal as determined with the column filled with water.

Approximately 72.1% of that portion of the laser output transmitted by the first beam splitter was reflected to the second mirror by the second beam splitter. This beam was subsequently split by a neutral density filter which transmitted 41.5% and reflected 58.5%. The transmitted portion of this beam, the transmittance beam, was directed into the settling column in a horizontal plane, and was used to measure the optical density of the slurry and to align the detector.

The reflected portion of this beam, the reference beam, was directed around the experimental column in a horizontal plane by a series of mirrors as shown in Figure 6. These external mirrors could be rotated about two orthogonal axes in the plane normal to the axis of beam propagation, and translated along the axis of beam propagation. Two polaroid

elements were used to vary the intensity of the reference beam. The second polaroid was used to ensure that the direction of polarization of the reference beam was the same as that of the laser output.

To obtain a Doppler signal it was necessary to direct the reference beam around, rather than through, the settling column. In the latter case, the extent of line broadening experienced by the reference beam due to multiple scattering was apparently sufficient to introduce significant uncertainty in the determination of the Doppler frequency and thus in the estimate of particle velocity.

Transparent, one-inch diameter plastic tubes were suspended from the ceiling to provide a conduit which shielded the reference beam from air currents during its passage around the settling column. The line broadening of the reference beam due to air-borne particulates was a concern because of the long transmission path between the laser source and the detector optics required to maintain temporal coherence between the scattering beam and the reference beam. The path length of the reference beam was adjusted by trial and error to maximize the amplitude of the Doppler signal, Appendix VI.

4.5 THE DETECTOR OPTICS

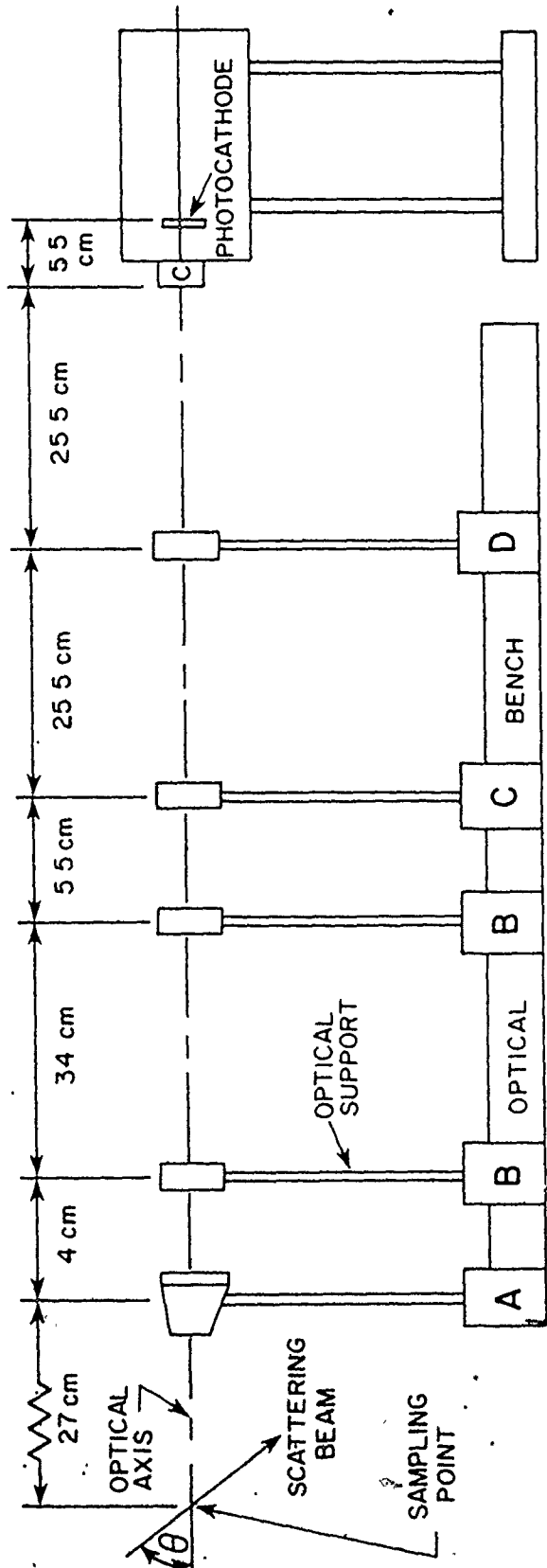
The light scattered from the sampling volume of the experimental slurry was collected and directed to the photocathode by the components shown in Figure 9.

The beam splitter was used to superimpose the light scattered from the slurry and the reference beam travelling around the settling column. The two pin hole apertures were positioned to limit the field of view of the detector to approximately 8.561×10^{-2} degrees. This field of view restriction was imposed to maintain spatial coherence for the light reaching the photocathode, [Goldstein and Kreid (1968)]. The size and spacing of the apertures ensured that the diameter of the first maximum in the Fraunhofer diffraction pattern of the first aperture, the Airy disc diameter, was larger than the diameter of the second aperture.

The volume of slurry observed by the detector was calculated using the dimensions of the laser beam and the angular field of view of the detector. For a 2 mm beam diameter oriented 17 degrees from the horizontal, the volume of the scattering volume was estimated to be $7.71 \times 10^{-3} \text{ cm}^3$. For the particle concentrations observed in this study, the approximate number of particles in the field of view of the detector ranged from 495 to 850.

The assembly of lenses shown in Figure 9 collected the light passing through the pin hole aperture and focused

FIGURE 9
DETECTOR OPTICS



NOTE: OPTICAL SUPPORTS HAVE ADJUSTMENT SCREWS
FOR TRANSLATION IN X, Y, Z
ROTATION ABOUT Y AND Z

- A = BEAM SPLITTER
- B = APERTURE, 0.010" DIA
- C = LENS, 5.5 cm FOCAL LENGTH
- D = LENS, 20 cm FOCAL LENGTH

it on the surface of the photocathode. The first lens in the assembly was positioned one focal length behind the second pin hole aperture. The second and third lenses were separated by the sum of their focal lengths. The third lens in the assembly was mounted on the detector housing by a fine pitch threaded support. This allowed relative translation between the third lens and the photocathode so that the collected light could be focused on the surface of the photocathode. This minimized the degradation of the Doppler signal due to the spatially distributed phase differences inherent in the photoemission process [RCA (1968)].

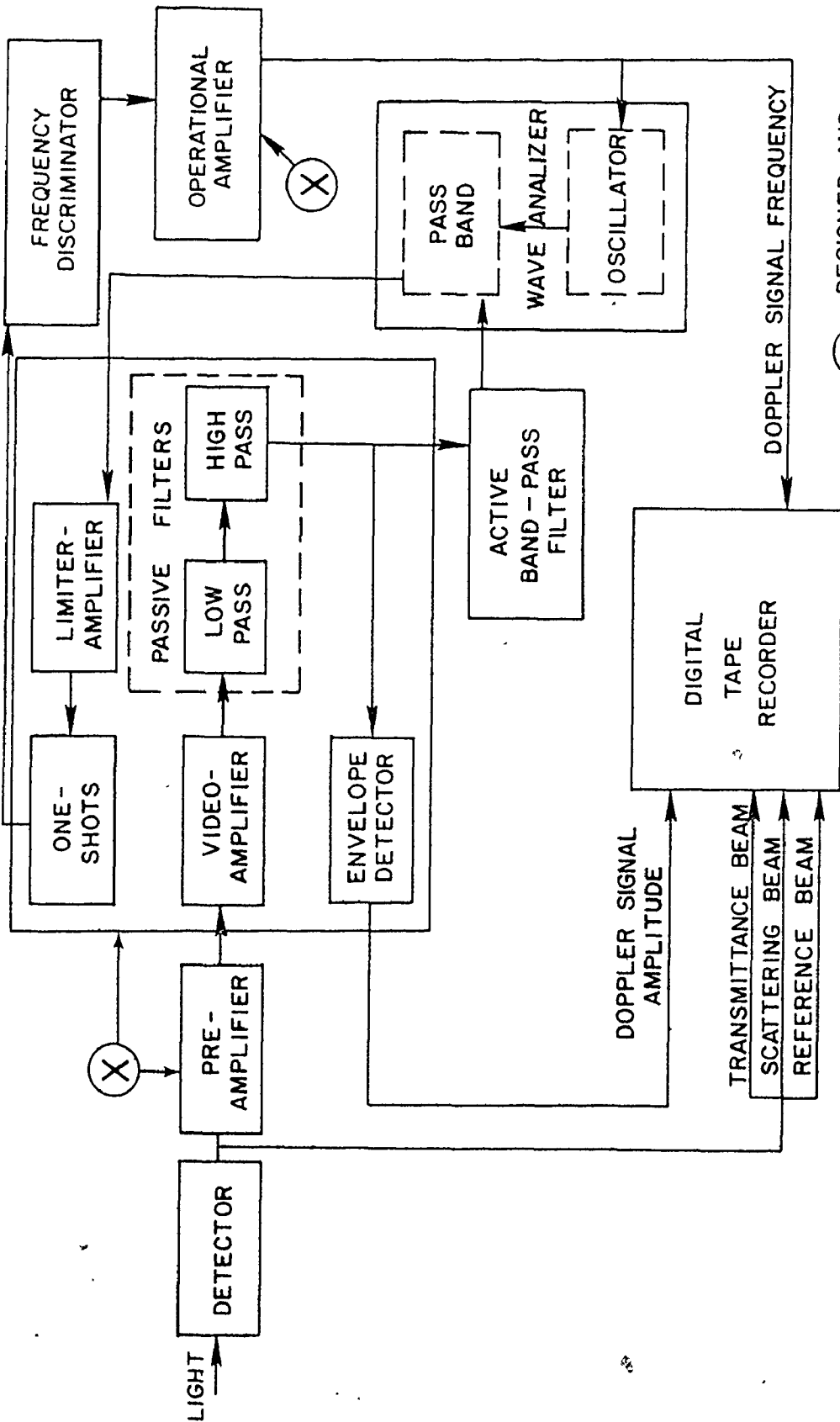
All of the optical elements were constructed of quartz of $\lambda/20$ surface quality. Each element was coated for use at 4880 \AA .

4.6 THE ELECTRONIC SIGNAL PROCESSING

The output from the photomultiplier tube was processed electronically to extract the velocity and concentration information. A block diagram of the electronics is shown in Figure 10. Figure 11 is a photograph of electronic components and the data logging system.

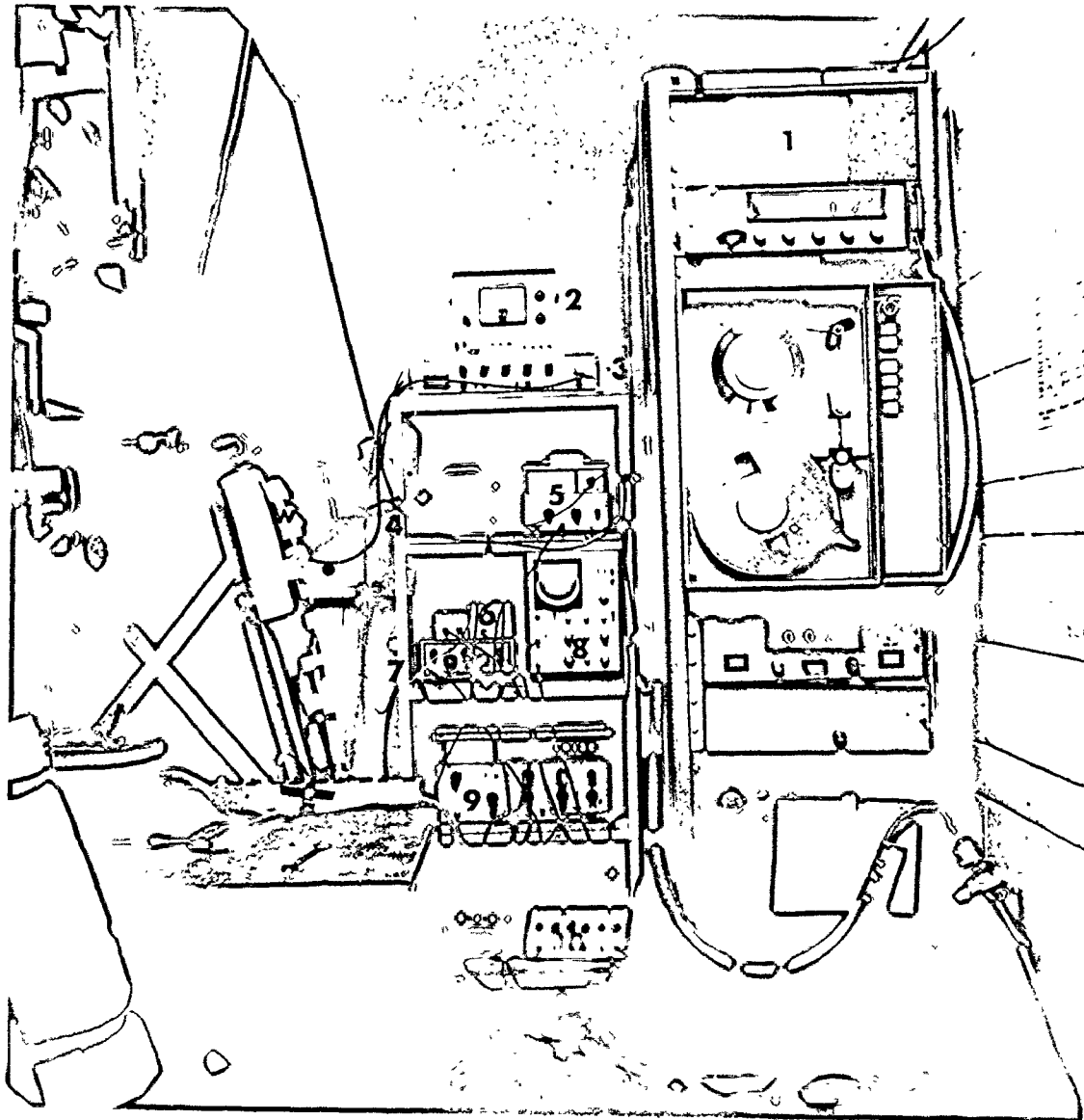
The low noise pre-amplifier was connected across the anode load resistor on the photomultiplier housing. The pre-amplifier boosted the signal level to decrease the significance of any subsequent electromagnetic noise which might otherwise decrease the signal to noise ratio. The

FIGURE 10
SIGNAL PROCESSING ELECTRONICS



(X) = DESIGNED AND CONSTRUCTED IN-HOUSE

FIGURE 11
PHOTOGRAPH OF THE SIGNAL PROCESSING ELECTRONICS



- 1 DATA LOGGER
- 2 THERMOMETER
- 3 DETECTOR POWER SUPPLY
- 4 COMPONENTS IN FIGURE V-2
- 5 FREQUENCY DISCRIMINATOR

- 6 OPERATIONAL AMPLIFIER
- 7 BANDPASS FILTER
- 8 OSCILLOSCOPE
- 9 WAVE ANALYZER
- 10 PILOT STRIP

pre-amplifier output was fed to the video-amplifier. The gain of the pre-amplifier was determined to be 193; that of the video-amplifier was determined to be 14.7. The gain of each amplifier was independent of signal frequency over the range of 50 Hz to 5000 Hz.

Low frequency and high frequency noise components were attenuated in the video-amplifier output by a passive bandpass filter with nominal corner frequencies of 233 Hz and 2250 Hz. The amplitude of this rough-filtered signal was measured at the output of the envelope detector and was used to estimate localized particle mass concentration, Appendix I.

Prior to the estimation of the frequency of the video-amplifier output, low and high frequency noise was further attenuated by active bandpass filters. The rough-filtered, amplified signal was fed to a Krohn-Hite model 3350 bandpass filter operated at a fixed bandpass (half-power frequencies of 200 Hz and 3000 Hz) and subsequently to a Hewlett-Packard model 3590A wave analyzer. The wave analyzer window was 1300 Hz wide at the half power points, and the centre frequency of the bandpass was made to track the measured Doppler signal frequency by a feedback loop. The shapes of the bandpass filters are shown in Appendix V.

The filtered output signal from the wave analyzer was fed to a limiter-amplifier. The gain of the wave analyzer

was manually adjusted so that the limiter-amplifier output was clipped and almost squared-off.

The clipped limiter output was fed to a "one-shot" which produced a square, one-volt pulse of uniform duration for every negative to positive zero crossing in the limiter-amplifier output waveform. The frequency of these pulses was converted to a DC voltage by a Hewlett-Packard model 5210A frequency discriminator. The output voltage of the frequency discriminator was fed to the wave analyzer oscillator to centre the fourth-order Butterworth bandpass filter at the Doppler frequency. An operational amplifier with an adjustable gain was used to match the frequency proportional output voltage of the frequency discriminator to the ramp voltage of the wave analyzer bandpass oscillator. The output voltage of this operational amplifier was proportional to the frequency of the Doppler signal frequency and was recorded on magnetic tape.

Care was taken to isolate the photomultiplier detector, the electronic processing, and the data logging instrumentation from electrical contact with the laboratory. Each of these components was chassis grounded and all power connections were made to a single pilot strip which was mains-grounded at a single electrical outlet. Coaxial cable and BNC connectors were used throughout with the exception of the leads between the pre-amplifier and the video-amplifier.

Here, special care was taken to minimize front end noise. Multi-strand, twisted pair copper leads encased in an aluminum foil shield with a copper drain line were used to reduce noise pickup, [Clevite (1970)]. Three, 1/4 inch diameter, multi-strand copper straps were connected to the chassis of the high voltage power supply of the photomultiplier tube to eliminate ground loops which resulted in spurious signals at harmonic 60 Hz frequencies.

With the exception of the active bandpass filters and the frequency discriminator, the entire signal processing instrumentation was designed and constructed in-house. A wiring diagram for these components is shown in Appendix V.

Details of calibration of the signal processing instrumentation are described in Appendix V.

4.7 THE DATA LOGGING INSTRUMENTATION

At each grid location in the column, the detector output was monitored for the various combinations of the three laser beams (reference, scattering and transmittance). Refer to Figure 6 for a schematic of these beams.

The analog DC voltages resulting after various stages of electronic processing of the detector output signal were fed to a Honeywell model 6305 digital multimeter (range: 10^{-6} to 7.5×10^2 volts) which converted the analog voltage to a five digit display. The output from the multimeter was fed to a Honeywell model 825E output control which encoded

the digital signals as seven-level BCD characters. The output from this device was coupled to a Honeywell model 6200 incremental digital recorder, which recorded the encoded digital signal on seven-track, 1/2 inch magnetic tape at a density of 200 bits per inch. While the multimeter had an adjustable sampling frequency ranging from 0.1 to 10^6 Hz, the output control and digital recorder limited the maximum data logging frequency to approximately 1.5 Hz, the signal sampling frequency used throughout this study. Subsequent data analysis was performed on a Control Data Corporation model 6400 digital computer.

CHAPTER 5
MATERIALS AND METHODS

5.1 SEDIMENTATION SYSTEM

A schematic of the experimental apparatus is shown in Figure 12 and a photograph of the system is shown in Figure 13. The slurry was pumped from the feed tank and entered the column through the inlet device which distributed the feed stream particles over the column cross-section. Those particles which were transmitted to the bottom of the settling column were discharged through the underflow and pumped to the feed tank. The column overflow discharged through a series of V-notch weirs to a launderer, and was returned by gravity to the feed tank. The volumetric discharge of the column overflow was established by the settings of the feed and underflow pumps.

For each combination of feed stream and underflow flowrates, the system was allowed to reach steady-state with respect to the particle mass concentrations and the slurry volumetric flowrates of the feed, underflow and overflow streams. Steady-state was assumed to have been reached when measurements of these parameters did not change significantly at the 95 percent confidence level over a six-hour period.

FIGURE 12
EXPERIMENTAL APPARATUS

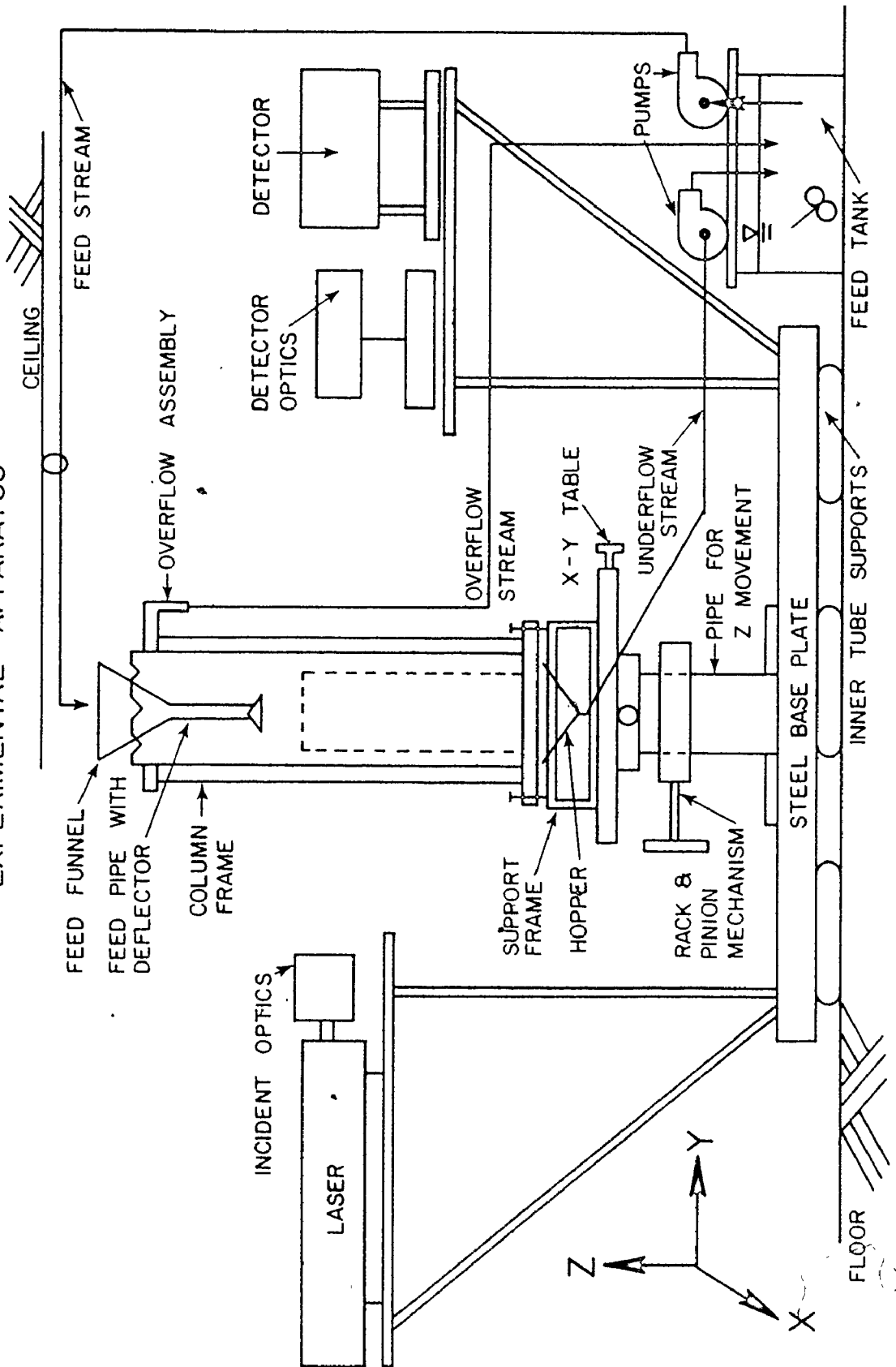
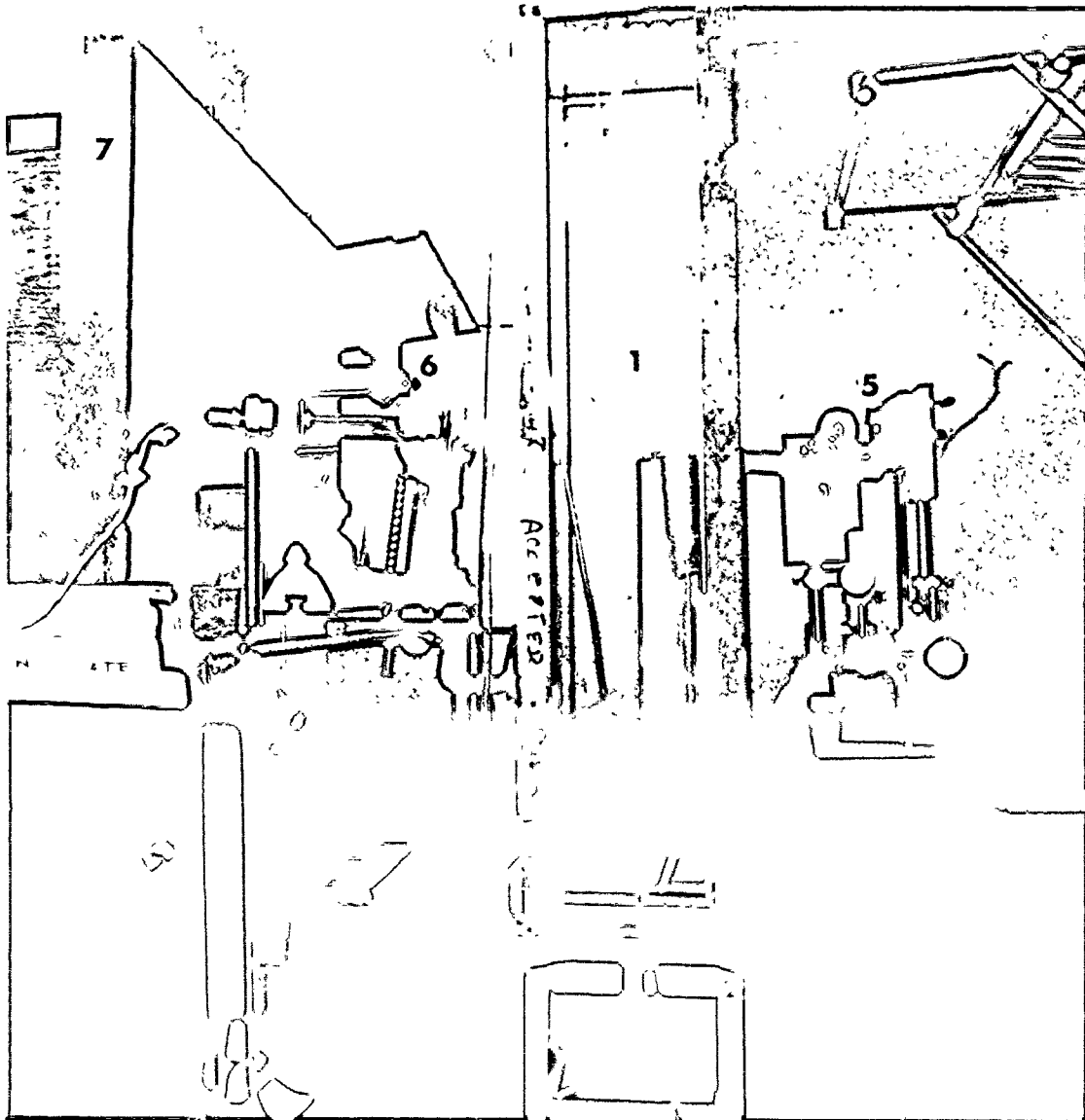


FIGURE 13
PHOTOGRAPH OF THE EXPERIMENTAL APPARATUS



- 1** SETTLING COLUMN
- 2** SUPPORT FRAME
- 3** HOPPER
- 4** PUMPS

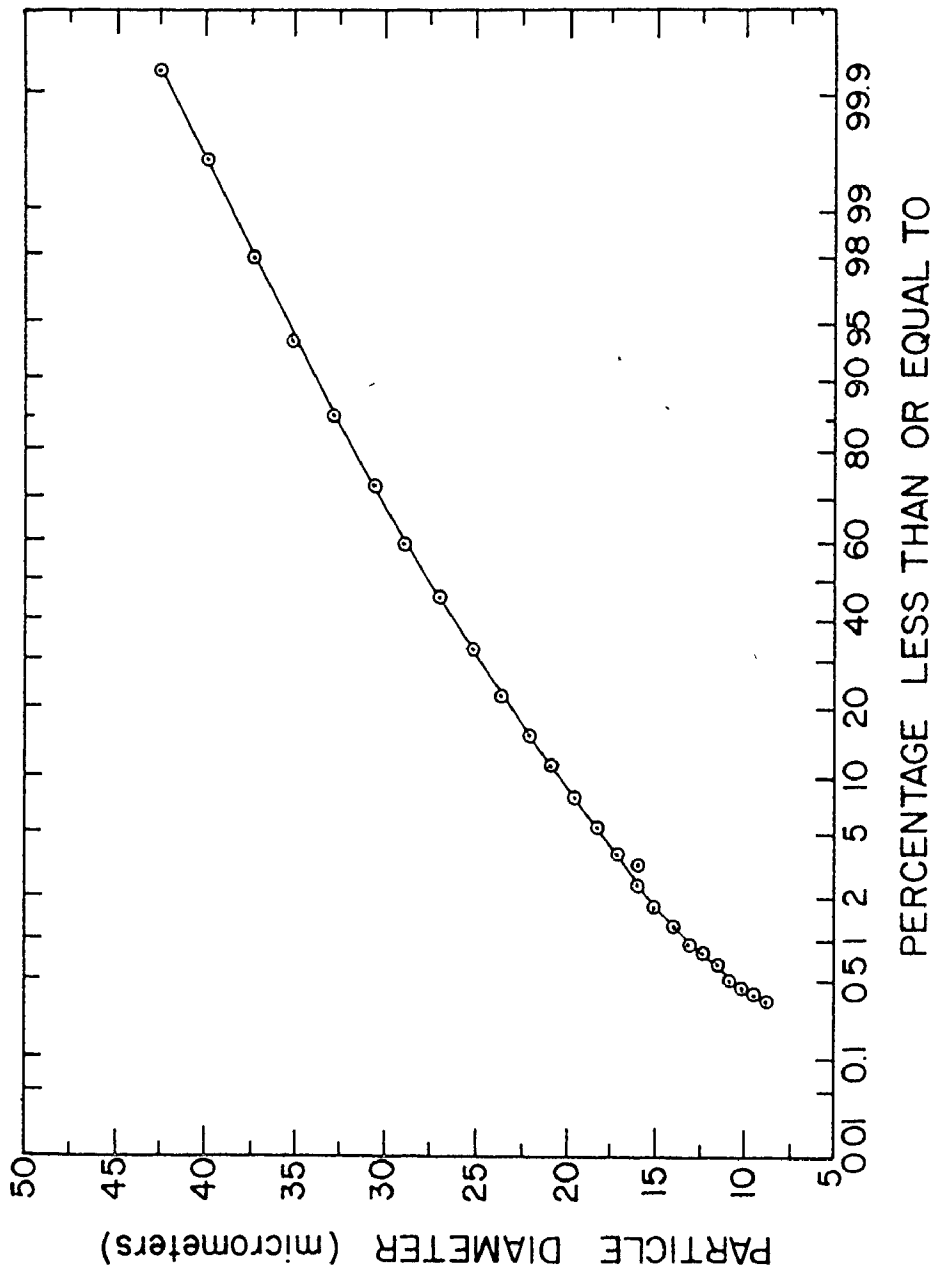
- 5** DETECTOR OPTICS
- 6** INCIDENT OPTICS
- 7** LASER HOUSING

Localized particle velocity and particle mass concentration were then measured at a number of locations in the dilute blanket by means of the laser Doppler system. At the completion of these measurements, timed volumetric samples were collected for the estimation of the particle mass concentrations and the slurry volumetric flowrates of the feed, underflow and overflow streams.

5.2 SLURRY PARTICLES

Glass particles (3M Company, catalogue number 380) were used in this study. These particles were supplied at a nominal mean particle diameter of 29 micrometers and were classified by the manufacturer so that less than one percent by weight of the particles had diameters less than 18 micrometers. These particles were further classified by rejecting that portion of them that were retained on a 37 micrometer, standard U.S. sieve, (No. 400). The resulting distribution of particle diameters was determined by means of a Zeiss Counter using photographs of the slurry particles taken at calibrated degrees of enlargement. The particle diameters were observed to be approximately normally distributed with a mean diameter of 27.5 micrometers and a standard deviation of 5.4 micrometers. The cumulative particle size distribution is shown in Figure 14.

FIGURE 14
CUMULATIVE PARTICLE SIZE DISTRIBUTION



The apparent density of the particles was determined by a standard density bottle analysis and was estimated to be 2.4348 ± 0.1199 gm/cc.

The average Stokes diameter of the slurry particles was estimated by batch sedimentation experiments. Insofar as was possible, single particles were introduced into a one litre graduated cylinder filled with water which had been allowed to equilibrate to room temperature. By measuring the time of fall of the individual particles over a distance of 10 cm, the mean terminal settling velocity was determined to be 3.031 cm/min with a standard deviation of 0.248 cm/min based on 100 observations.

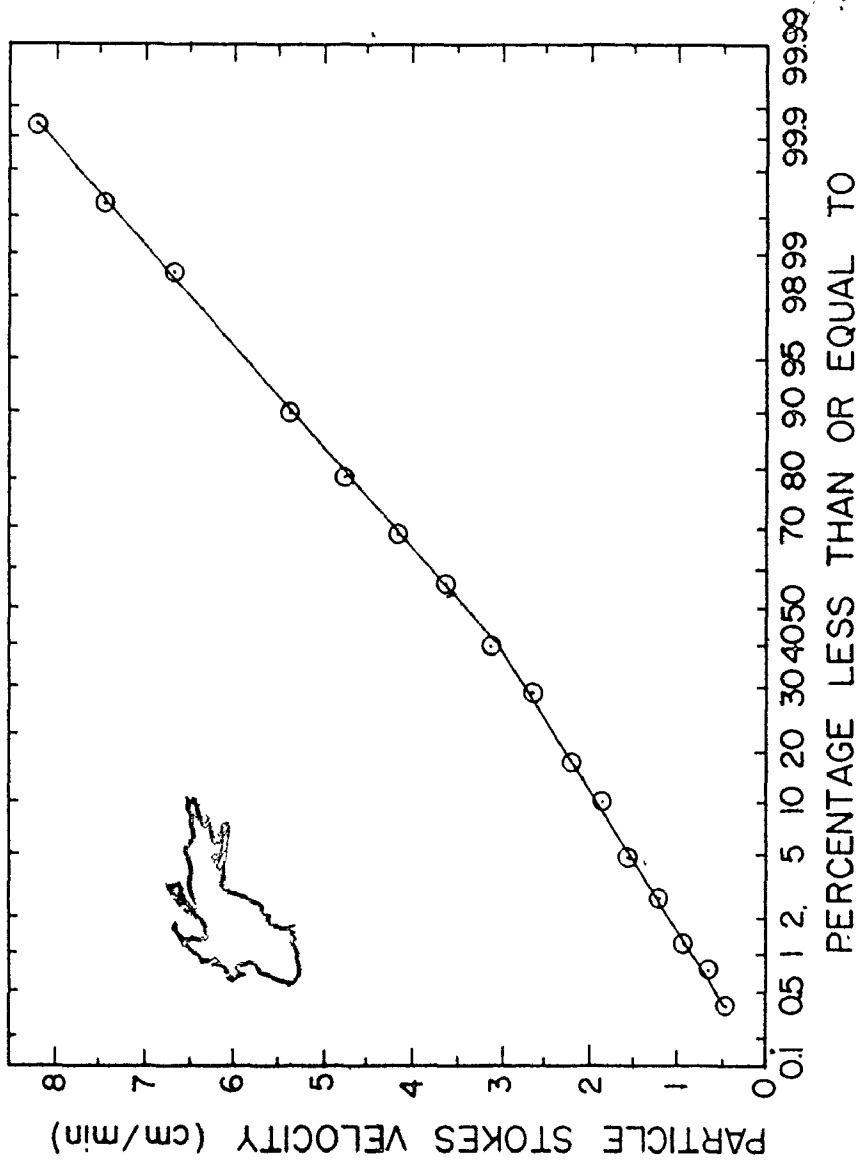
The measured terminal settling velocity agreed well with that predicted by Stokes Law using the empirical estimates of mean geometric particle size and mean particle density. This indicated that the particles could be assumed to be spherical without introducing significant error.

The cumulative Stokes velocity distribution, calculated using the measured size distribution and the measured density, is shown in Figure 15. Refer to Appendix IV for details of the characterization of the slurry particles.

5.3 SETTLING COLUMN

Since a settling column with a curved surface would act like a lens and greatly complicate the alignment of the optical system, a settling column with a square, (six inch by

FIGURE 15
CALCULATED PARTICLE STOKES VELOCITY DISTRIBUTION



six inch) cross-section was used. The size was selected to minimize the influence of container walls on the particle sedimentation rate.

The column was constructed of best commercial quality float glass held in a brass frame made from four pieces of 1 1/2-inch bar stock each of which was 37 3/4 inches long. The machined surfaces of the assembled frame were checked for parallelism of opposite faces and squareness of adjacent faces and were observed to vary not more than ± 0.003 inches over the entire length. The float glass was inserted into this frame and allowed to "ride" against the machined faces. The column was made water tight by the application of a thin bead of silicone rubber along the inside corners of the glass container.

A brass flange was bolted to the bottom of the frame and made water-tight by silicone rubber caulking. A hopper six inches square at the base and sloped at 60 degrees to the horizontal on four faces to an orifice of 3/4-inch diameter at the apex, was bolted to this flange. The sloping sides of the hopper directed settled solids to the underflow discharge where they were pumped back to the feed tank.

A plexiglass overflow assembly, six inches square and four inches in height, consisting of a series of V-notch weirs, launderer and downcomer was cemented to the top of the

glass settling column. The overflow discharge was returned by gravity to the feed tank through 1/2-inch tygon tubing.

The feed port consisted of an 18-inch-long, 1/2 inch ID plexiglass tube. An adapter containing a conical deflector element was attached to the bottom of the feed port. The adapter and feed pipe were threaded so that the clearance between the bottom of the feed pipe and the base of the deflector could be varied to provide a uniform distribution of the feed slurry over the column cross-section. It was necessary to separate the feed port from the feed line since pump vibrations were otherwise transmitted through the slurry and introduced intolerable noise to the scattered light. Therefore, the inlet tubing was suspended from a ceiling bracket and was positioned close to, but not touching, the bowl of a six-inch-diameter funnel attached to the top of the feed port. This arrangement enabled a complete traverse of the settling column cross-section without adjustment of the feed line.

Similarly, it was necessary to decouple the underflow pump and the settling column. A 100-cm³ separatory funnel inserted in the underflow-discharge line between the column and the feed tank effectively isolated the slurry from the pressure disturbances caused by the pump impeller. A four-inch-thick piece of foam rubber inserted between this separatory funnel and the table was helpful in reducing the effects

of vibration transmitted through the tubing walls. These measures reduced the amplitude of "pumping noise" in the detected signal to acceptable levels.

5.4 TRAVERSING MECHANISM

The assembled column rested on a support frame by means of four adjustment screws which were used to level the column. The support frame was bolted to a two-axis adjustable table which allowed a traverse of 12 inches in each of two orthogonal directions in the plane of the table surface. The fine thread manual drives on this table allowed very slow, smooth movement of the settling column through the laser beam. This table was mounted horizontally on the knee of a sleeve bearing which could be moved up and down a ten-inch-diameter, eight-foot section of machined pipe stock by means of a rack and pinion. The vertical movement possible with this arrangement allowed the probing of the entire depth of the column by the laser beam.

5.5 BASE PLATE

The three-axis traversing assembly was bolted to a 4-foot-wide by 6-foot-long by 2 1/4-inch-thick steel base-plate which rested on six, 18-inch-diameter, tire inner tubes. An A-frame was bolted to each end of the base plate. The laser and incident beam optics were mounted on one frame, the detector and collection optics were mounted on the other.

This arrangement helped to isolate the experimental system from building vibrations and significant noise from this source was not observed in the detection of the laser light.

5.6 FEED TANK

An 18-inch-diameter, 15 inch high cylindrical glass vessel was used as the feed tank. A fluid depth of 12 inches was maintained in the feed tank throughout this study. The feed slurry was agitated by two impeller mixers which maintained a uniformly mixed condition in the tank. A slurry temperature of $20^{\circ}\text{C} \pm 0.2^{\circ}\text{C}$ was maintained at all times.

5.7 SEDIMENTATION SYSTEM START-UP

Prior to the beginning of each run, the feed system was dismantled and thoroughly cleaned with a solution of soap and distilled water. A brush was used to remove particles adhering to the surfaces. The settling column was drained, rinsed thoroughly with distilled water, dried with lens paper and then cleaned with a commercial lens cleaning solution.

The plastic tubing used to transport the slurry from the feed tank to the settling column and to transport the overflow and underflow streams to the feed tank was replaced with fresh tubing which had been flushed with distilled water to remove particulate contaminants. Those sections of tubing passing through the pump heads were "worn-in" prior to run

initiation to prevent excessive drift in pump flowrates which otherwise occurred.

The feed tank and settling column were then filled with distilled water which had been filtered through a double layer of membrane filters, (0.45 micrometer pore size). To minimize the introduction of air-borne dust particles to the system, covers were placed over the feed tank and the column.

With the system filled with water, but not yet charged with particles, the apparatus was levelled by adjusting the air pressure in the support inner tubes. This ensured that the settling column was vertical. The settling column, detector and optical elements were aligned using the laser beam according to the procedure outlined in Appendix VII.

With the system so prepared, the feed tank mixers and temperature control system were turned on, and the detector output was monitored for any frequency components arising from these sources. Next, the feed and underflow pumps were started and the detector output was again monitored for any coupling of these components to the laser light system. These checks were made by clamping a piece of 1/4 inch plexiglass, whose surface had been scored with coarse sandpaper, to the outside surface of that column glass face nearest to the laser. The settling column was moved so that incident radiation scattered from this surface would be in the

detector field of view. The absence of a detectable output signal indicated that the settling column was sufficiently isolated from external vibrations.

The volumetric flowrates of the overflow, underflow and feed streams were measured by determining the time required to fill a volumetric flask. The size of flask used for each measurement was of sufficient capacity that at least three minutes would be required for the determination.

Particles, which had been acid washed, rinsed with distilled water and oven dried at 103°C, were then added to the feed tank. At the completion of each run, the particles were salvaged from the system and recleaned.

After the system had operated for a period of six hours, three replicate measurements of the volumetric flowrates of each of the three streams were made beginning with the overflow stream and finishing with the feed stream. After each measurement, the sampled slurry was immediately returned to the feed tank. Sampling in this sequence minimized the impact of sample collection on the operation of the settling column. The system was allowed to stabilize for a further three hours prior to data collection.

Periodically during a run, timed samples of the overflow discharge were collected to determine the overflow volumetric flowrate. In this way, a rough check on pumping rates

was maintained, since a changed throughput in either of the pumps would have immediately changed the overflow rate.

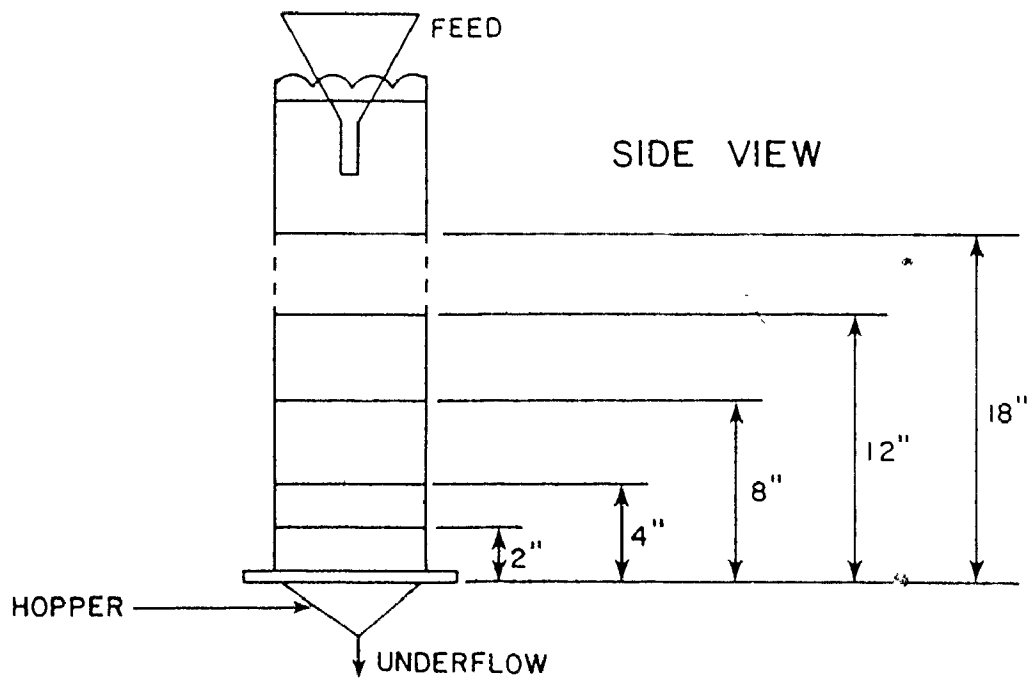
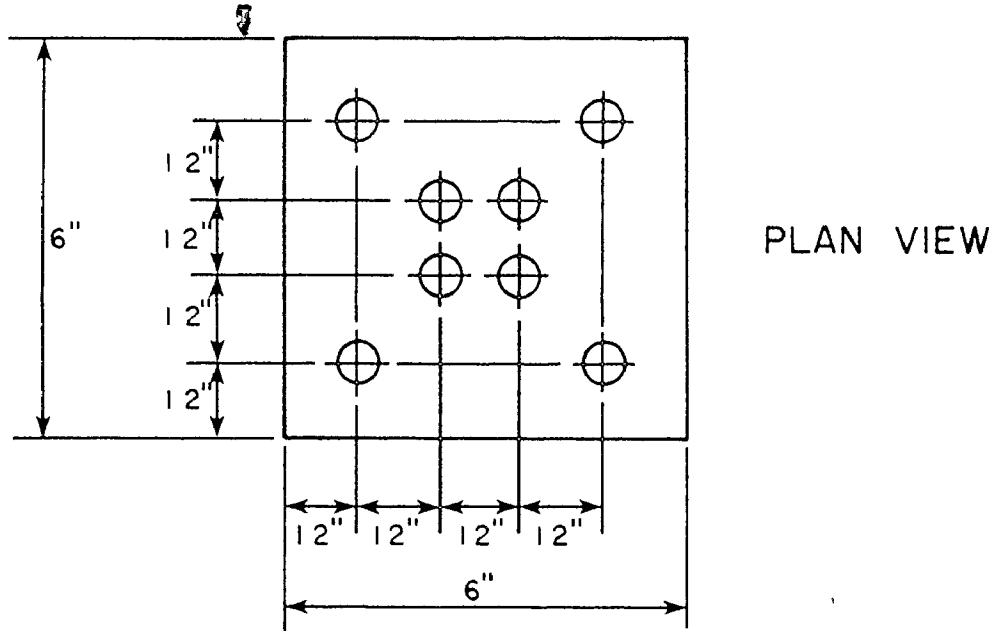
5.8 SAMPLING LOCATIONS

During the course of a run, the local particle velocity and concentration were measured at horizontal planes 2, 4, 8, 12 and 18 inches above the base of the underflow hopper. The bottom (2 inch) plane was the sampling location closest to the underflow that was possible with the apparatus; at greater column depths, the field of view of the detector was obscured by the settling column frame. The top (18 inch) plane was established by trial and error to be the approximate lower boundary of the mixing zone caused by the introduction of the slurry to the column.

At each of these five horizontal planes, eight locations were sampled for particle velocity and concentration. The sampling locations were defined by the diagonals of a 4 by 4 orthogonal, uniformly spaced grid. These sampling locations are shown in Figure 16.

At the start of each run, the settling column was positioned so that location 2-1 (two inch horizontal plane - grid point one, see Figure 16) was in the field of view of the detector. Data were collected for each grid location in turn proceeding from location 2-1 through location 2-8 in ascending numerical order. The column was then lowered so that location 4-8 was in the field of view of the detector.

FIGURE 16
 SAMPLING LOCATIONS IN SETTLING COLUMN



The four inch horizontal plane was monitored in descending grid location numerical order, finishing with location 4-1. This pattern of column movement was continued until all 40 grid locations had been monitored.

This sequence was used to minimize any disturbance to the solid-fluid flow caused by column movement. A stabilization period of 15 minutes was allowed after each change in grid location to reduce the effects of any residual bulk circulation in the column induced by such movement.

5.9 PROCEDURE FOR DATA COLLECTION

Prior to collecting data at each grid location, the alignment of the reference beam was checked by blocking the transmittance and scattering beams, and adjusting the orientation of the reference beam mirrors until the output of the detector pre-amplifier was 1.0 ± 0.05 mv. Since the reference beam supplied virtually all of the radiation incident on the photocathode surface, this adjustment ensured a uniform basis for the measurement of velocity and concentration as well as providing a uniform noise-in-signal for the detector.

With the reference beam aligned, the volume control setting of the limiter-amplifier input was adjusted so that the reference beam induced the baseline false alarm rate of 100 ± 10 Hz. This false alarm rate was found by trial and error to be a convenient trade-off between lower rates which

resulted in Doppler signal "drop-out" and higher rates which degraded the accuracy of the Doppler signal measurement.

The scattering beam light trap was then removed and the approximate frequency of the Doppler signal was estimated from the oscilloscope trace of the video-amplifier output. The bandpass of the wave analyzer was set at 3000 Hz to enable this instrument to observe and start tracking the Doppler signal. The wave analyzer bandpass filter was then reduced to 1000 Hz and visual comparison was made of the wave analyzer display frequency to that frequency estimated from the oscilloscope trace. Rough agreement between these frequencies indicated that the Doppler signal was being observed. The Doppler frequency was then recorded for approximately three minutes.

Following this measurement, the scattering beam light trap was inserted and the reference beam alignment was rechecked. If the output of the detector pre-amplifier had drifted from the set point of 1.0 ± 0.05 mv, the Doppler frequency data were discarded and a subsequent measurement of Doppler frequency was made. This procedure was repeated until changes in reference beam intensity during data recording were within the prescribed limits.

Immediately following this measurement of Doppler frequency, the false alarm frequency (amplified output voltage of frequency discriminator with transmittance beam and

scattering beam light traps inserted) was recorded for approximately 0.5 minutes. These data were accepted or rejected based on an immediate check of reference beam intensity drift as described above.

The scattering beam light trap was then removed and the output voltage of the envelope detector was recorded for approximately three minutes. These data were accepted if subsequent checks of reference beam intensity and false alarm frequency were within the limits prescribed above and were otherwise rejected. The scattering beam light trap was subsequently inserted and the envelope detector output was recorded for approximately 0.5 minutes to establish a background correction. Care was taken to ensure that the reference beam intensity did not drift during this measurement as described above.

Following these measurements, the detector pre-amplifier output voltage produced by each of the reference, scattering and transmittance beams were individually recorded for a period of approximately 0.5 minutes. After these measurements, light traps were inserted in the paths of all three beams and the detector pre-amplifier output was recorded for 0.5 minutes to provide an estimate of background noise.

While this sequence of measurements was being made, no adjustments were made to the laser, detector or electronic

signal processing components with one exception. It was determined part way through the experimental program that the detector pre-amplifier output voltage due to background noise (all three light traps inserted) was close to the threshold limit for the digital multimeter. For the last four runs, the background noise and the scattering beam intensity were measured at a detector supply voltage of minus 2700 volts. The gain calibration of the photomultiplier tube, Appendix VI, was used to scale these measurements to those levels which would have been observed had a detector supply voltage of minus 2200 volts been used. For all other measurements the detector power supply was maintained at minus 2200 volts. After each adjustment of the photomultiplier supply voltage, no data were collected for a period of five minutes to allow the detector to reach a steady-state.

Throughout the experimental period the laser system, the detector system and the electronic components used to process the detector output were kept on. The only exceptions to this occurred when the laboratory lights were switched on to clean the system between runs. On these occasions, the high voltage detector power supply was switched off to minimize the possibility of damaging the photocathode. In this way, spurious response of the laser system due to thermal transients was minimized.

CHAPTER 6

RESULTS AND INTERPRETATION

Six experimental runs were conducted at specific combinations of feed flowrate and underflow flowrate according to the experimental design shown in Figure 17. One set of conditions was replicated once to obtain an estimate of experimental error variance. The average flowrates and mass concentrations for each of the feed, underflow and overflow streams are listed in Table 1. The good closures obtained for the particle mass balances indicate that steady-state operation was reasonably approximated for each of the runs.

6.1 PARTICLE CONCENTRATION

The particle mass concentrations estimated from the transmitted intensity, equation (3-15), and the scattered intensity, equation (3-19), are listed in Appendix X. For both measurements, analysis of variance, Tables 2 and 3 and Appendix III, showed that the variations in particle mass concentration across each of the horizontal planes and over the depth of the column were significant at the 95 percent confidence level.

The variations in particle mass concentration for a given horizontal plane, although significant at the 95 percent confidence level due to the small error variances

FIGURE 17
EXPERIMENTAL DESIGN

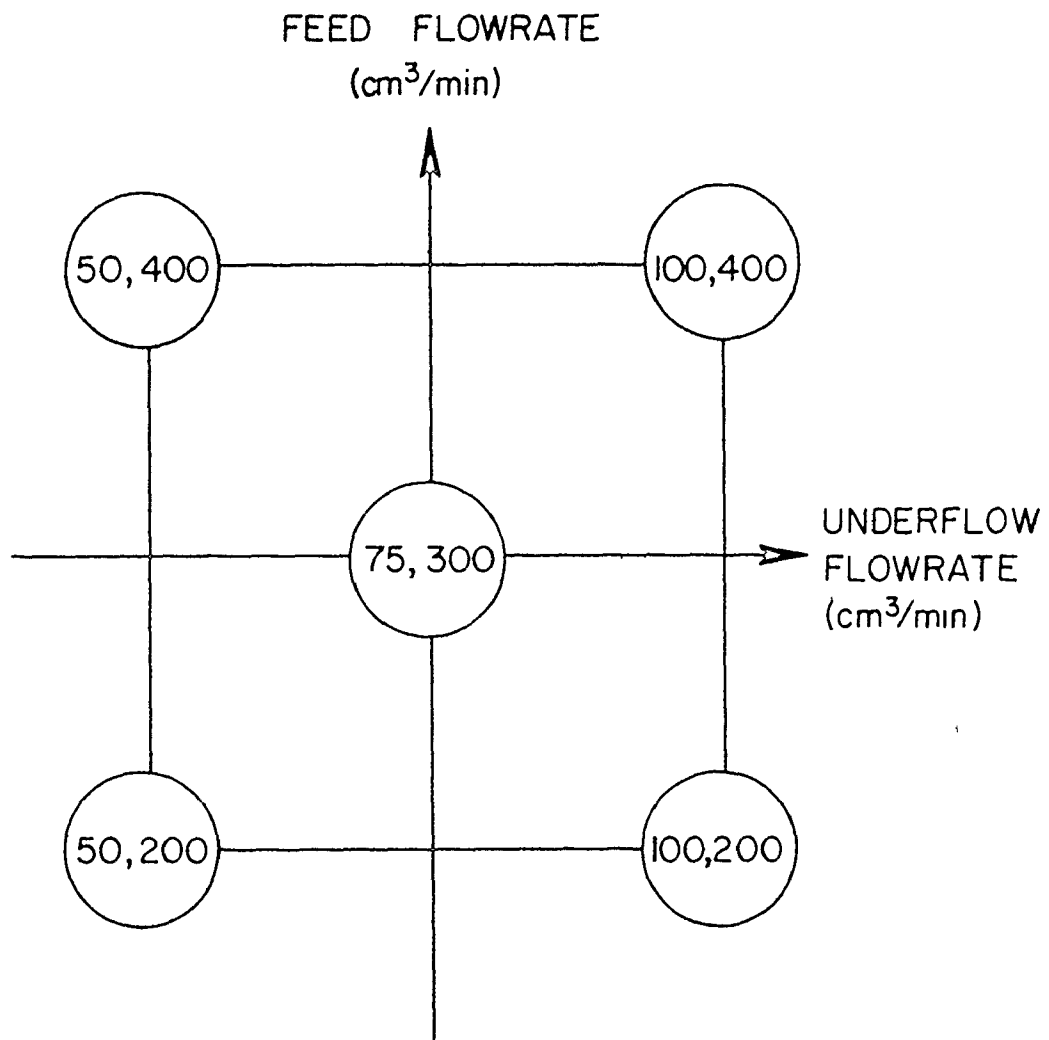


TABLE 1

AVERAGE PARTICLE MASS FLOWRATES FOR FEED, OVERFLOW AND UNDERFLOW STREAMS

Run	Volumetric Flowrate (cm^3/min)		Mass Concentration (gm/ℓ)		Mass Flowrate (gm/min)		Closure on Mass Flowrate $\Delta = Q_F C_F - (Q_O C_O + Q_U C_U)$				
	Feed Q_F	Overflow Q_O	Underflow Q_U	Feed C_F	Overflow C_O	Underflow C_U	Feed $Q_F C_F$	Overflow $Q_O C_O$	Underflow $Q_U C_U$	Δ (gm/min)	$\frac{\Delta}{Q_F C_F}$ (%)
1	300.11	233.49	72.51	15.562	8.307	42.217	4.670	1.940	3.061	-0.330	-7.07
2	199.23	85.01	114.05	18.593	6.210	23.699	3.704	0.528	2.703	0.473	12.77
3	198.43	149.50	48.87	10.723	0.014	42.538	2.128	0.002	2.079	0.047	2.21
4	400.20	301.01	97.06	7.605	0.374	29.617	3.044	0.113	2.875	0.056	1.84
5	396.38	299.18	96.30	7.432	0.164	26.427	2.946	0.049	2.545	0.352	11.95
6	395.77	346.13	49.22	9.363	0.105	58.895	3.706	0.036	2.899	0.771	20.80

TABLE 2

ANALYSIS OF VARIANCE FOR TRANSMITTANCE MEASUREMENTS
(Voltage Units)

Run	Population Variance Estimates, (volts) ²											
	Within Grid Points					Between Levels					Variance Ratio	
	Run Average	v	Run Average	v	Run Average	Within Run	Within Levels	Within Run	Within Grid Points	Within Run	Within Levels	
1	2.0904×10^{-8}	1284	1.0902×10^{-7}	35	3.3762×10^{-6}	4	5.22*	161*	31*			
2	3.7276×10^{-5}	1538	2.6382×10^{-4}	35	3.6764×10^{-3}	4	7.08*	99*	14*			
3	1.0594×10^{-4}	1446	1.4095×10^{-3}	35	7.8573×10^{-3}	4	13.3*	74*	5.57*			
4	4.9467×10^{-8}	1870	9.1527×10^{-7}	35	3.2729×10^{-5}	4	18.5*	662*	35.8*			
5	4.9681×10^{-7}	1561	1.1210×10^{-5}	35	7.4176×10^{-5}	4	22.6*	149*	6.62*			
6	2.5057×10^{-9}	1493	5.1142×10^{-8}	35	1.2790×10^{-6}	4	20.4*	510*	25.0*			

*Significant at 95% confidence level

TABLE 3
 ANALYSIS OF VARIANCE FOR SCATTERING BEAM MEASUREMENTS
 (Voltage Units)

Run	Population Variance Estimates (volts) ²									
	Within Grid Points		Between Grid Points		Between Levels		Within Levels		Variance Ratio	
	Run Average	v	Run Average	v	Run Average	v	Within Run	Within Grid Points	Within Run	Within Levels
1	2.1165×10^{-11}	1263	1.0564×10^{-10}	35	4.3041×10^{-10}	4	4.99*	20*	4.72*	
2	1.9821×10^{-11}	1491	4.9356×10^{-10}	35	9.5484×10^{-10}	4	24.9*	48*	1.93	
3	1.9822×10^{-10}	1446	4.4479×10^{-8}	35	3.6205×10^{-8}	4	22.5*	18.3*	0.814	
4	6.5020×10^{-11}	1779	8.3720×10^{-9}	35	3.9529×10^{-8}	4	12.9*	608*	4.72*	
5	5.5135×10^{-11}	1576	1.1849×10^{-8}	35	3.8054×10^{-8}	4	215*	69*	3.21*	
6	1.3719×10^{-3}	1417	3.3377×10^{-1}	35	9.9547×10^{-4}	4	243*	0.726	0.003	

*Significant at 95% confidence level

associated with measuring the transmitted and scattered intensities, were on the order of ten percent of the average particle concentration at each horizontal level and can probably be considered not significant from a practical viewpoint.

At the 95 percent confidence level, there was significant variation in particle mass concentration with column depth relative to that observed within the five horizontal planes for each run. Figure 18 shows the average concentration at each of the horizontal planes as a function of distance above the column hopper. For every run, the particle concentration decreased with increasing distance above the hopper; however, the maximum difference observed within a given run between the upper-most and lower-most horizontal planes was on the order of ten percent of the run-average concentration. For practical purposes, the particle mass concentration could be assumed to be uniform with depth.

The average concentration observed at each horizontal plane is shown in Table 4, the run-average concentrations are listed in Table 5. For comparative purposes, the mass concentrations estimated using the combined transmittance-scattered intensity correlation, equation (3-20), are listed in Tables 4 and 5 and Appendix X.

FIGURE 18

MASS CONCENTRATION VS. DEPTH

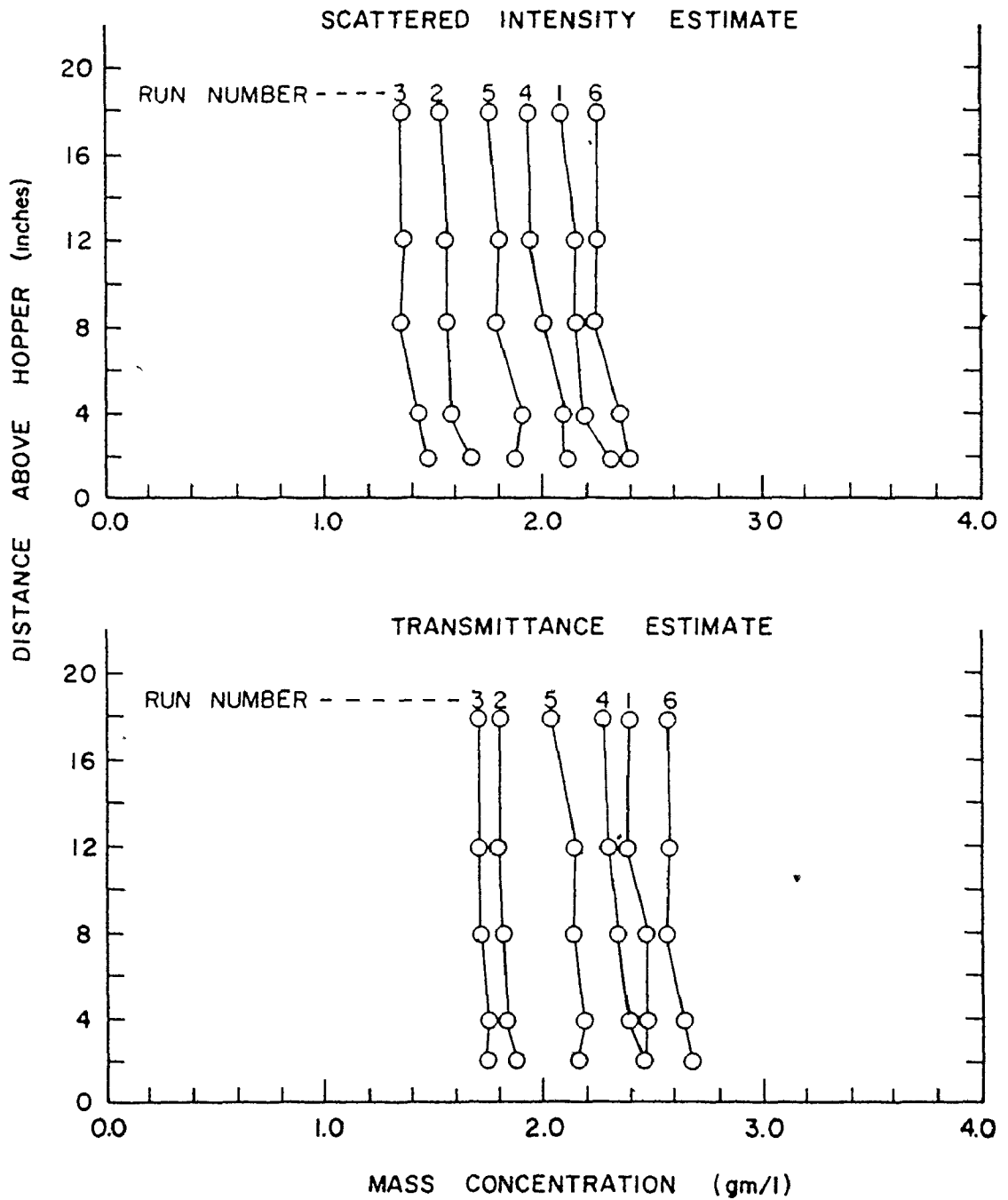


TABLE 4
LEVEL AVERAGES OF MASS CONCENTRATION

In Level	Distance Above Hopper (in)	Transmitted Intensity			Scattered Intensity			Combined Scattered-Transmitted Intensities		
		Mean (gm/l)	Variance (gm/l) ²	Degrees of Freedom for Variance	Mean (gm/l)	Variance (gm/l) ²	Degrees of Freedom for Variance	Mean (gm/l)	Variance (gm/l) ²	Degrees of Freedom for Variance
1	2	2.454	2.035x10 ⁻⁴	7	2.282	9.645x10 ⁻³	7	2.529	1.322x10 ⁻³	7
2	4	2.454	4.305x10 ⁻⁴	7	2.175	8.369x10 ⁻³	7	2.581	1.683x10 ⁻³	7
3	8	2.443	7.751x10 ⁻⁴	7	2.131	1.326x10 ⁻²	7	2.595	2.689x10 ⁻³	7
4	12	2.381	4.938x10 ⁻⁴	7	2.110	2.651x10 ⁻²	7	2.496	4.857x10 ⁻³	7
5	18	2.378	1.240x10 ⁻⁴	7	2.047	4.156x10 ⁻³	7	2.518	1.263x10 ⁻³	7
<hr/>										
1	2	1.863	2.644x10 ⁻⁴	7	1.642	6.739x10 ⁻³	7	1.953	1.232x10 ⁻³	7
2	4	1.829	1.334x10 ⁻³	7	1.568	3.083x10 ⁻³	7	1.939	2.765x10 ⁻³	7
3	8	1.800	4.589x10 ⁻⁴	7	1.550	5.244x10 ⁻⁴	7	1.903	1.080x10 ⁻³	7
4	12	1.785	5.124x10 ⁻⁴	7	1.537	2.687x10 ⁻³	7	1.899	2.589x10 ⁻³	7
5	18	1.771	8.564x10 ⁻⁴	7	1.506	3.414x10 ⁻³	7	1.893	5.541x10 ⁻⁴	7

Table 4 (Cont'd.)

Run Level	Distance Above Hopper (in)	Transmitted Intensity			Scattered Intensity			Combined Scattered-Transmitted Intensities		
		Mean (gm/l)	Variance (gm/l) ²	Degrees of Freedom for Variance	Mean (gm/l)	Variance (gm/l) ²	Degrees of Freedom for Variance	Mean (gm/l)	Variance (gm/l) ²	Degrees of Freedom for Variance
1	2	1.743	2.499x10 ⁻³	7	1.432	1.589x10 ⁻³	7	1.870	4.625x10 ⁻³	7
2	4	1.751	1.808x10 ⁻³	7	1.422	2.136x10 ⁻³	7	1.883	4.002x10 ⁻³	7
3	8	1.701	1.994x10 ⁻³	7	1.340	3.132x10 ⁻³	7	1.857	2.809x10 ⁻³	7
4	12	1.680	9.361x10 ⁻⁴	7	1.363	1.033x10 ⁻³	7	1.810	2.025x10 ⁻³	7
5	18	1.687	2.092x10 ⁻⁴	7	1.354	1.530x10 ⁻³	7	1.830	6.142x10 ⁻⁴	7
1	2	2.438	7.217x10 ⁻⁴	7	2.112	1.367x10 ⁻³	7	2.595	1.460x10 ⁻³	7
2	4	2.388	1.626x10 ⁻³	7	2.083	2.955x10 ⁻³	7	2.519	2.284x10 ⁻³	7
3	8	2.316	9.134x10 ⁻⁴	7	1.983	1.778x10 ⁻³	7	2.466	4.439x10 ⁻⁴	7
4	12	2.285	6.093x10 ⁻⁴	7	1.917	1.650x10 ⁻³	7	2.439	5.612x10 ⁻⁴	7
5	18	2.277	5.462x10 ⁻⁴	7	1.913	3.285x10 ⁻³	7	2.432	2.281x10 ⁻³	7

Table 4 (Cont'd.)

Run Level	Distance Above Hopper (in)	Transmitted Intensity			Scattered Intensity			Combined Scattered-Transmitted Intensities		
		Mean (gm/ℓ)	Variance (gm/ℓ) ²	Degrees of Freedom for Variance	Mean (gm/ℓ)	Variance (gm/ℓ) ²	Degrees of Freedom for Variance	Mean (gm/ℓ)	Variance (gm/ℓ) ²	Degrees of Freedom for Variance
1	2	2.166	1.662x10 ⁻³	7	1.863	4.368x10 ⁻³	7	2.295	2.947x10 ⁻³	7
2	4	2.178	4.995x10 ⁻⁴	7	1.890	3.151x10 ⁻³	7	2.302	5.864x10 ⁻⁴	7
5	8	2.139	1.795x10 ⁻³	7	1.795	2.326x10 ⁻³	7	2.275	1.039x10 ⁻³	7
4	12	2.138	1.523x10 ⁻³	7	1.803	6.366x10 ⁻⁴	7	2.299	1.444x10 ⁻³	7
5	18	2.094	1.131x10 ⁻³	7	1.737	2.574x10 ⁻³	7	2.237	9.539x10 ⁻⁴	7

1	2	2.671	4.508x10 ⁻⁴	7	2.389	2.257x10 ⁻³	7	2.805	5.558x10 ⁻⁴	7
2	4	2.625	9.516x10 ⁻⁴	7	2.320	2.450x10 ⁻³	7	2.751	7.711x10 ⁻⁴	7
6	8	2.549	2.110x10 ⁻³	7	2.223	2.116x10 ⁻³	7	2.668	1.128x10 ⁻³	7
4	12	2.573	7.443x10 ⁻⁴	7	2.249	2.341x10 ⁻³	7	2.698	1.127x10 ⁻³	7
5	18	2.531	7.329x10 ⁻⁴	7	2.232	2.663x10 ⁻³	7	2.669	2.252x10 ⁻³	7

TABLE 5

RUN-AVERAGE ESTIMATES OF MASS CONCENTRATION

Run	Transmitted Intensity			Scattered Intensity			Combined Scattered- Transmitted Intensities		
	Mean (gm/ℓ)	Variance (gm/ℓ) ²	Degrees of Freedom for Variance	Mean (gm/ℓ)	Variance (gm/ℓ) ²	Degrees of Freedom for Variance	Mean (gm/ℓ)	Variance (gm/ℓ) ²	Degrees of Freedom for Variance
1	2.422	1.527x10 ⁻³	4	2.149	7.643x10 ⁻³	4	2.544	1.794x10 ⁻³	4
2	1.810	1.354x10 ⁻³	4	1.561	2.582x10 ⁻³	4	1.917	7.188x10 ⁻⁴	4
3	1.721	9.775x10 ⁻⁴	4	1.382	1.743x10 ⁻³	4	1.850	8.845x10 ⁻⁴	4
4	2.357	4.785x10 ⁻³	4	2.002	8.500x10 ⁻³	4	2.490	4.602x10 ⁻³	4
5	2.143	1.049x10 ⁻³	4	1.818	3.628x10 ⁻³	4	2.282	7.328x10 ⁻⁴	4
6	2.590	3.309x10 ⁻³	4	2.283	4.958x10 ⁻³	4	2.718	3.490x10 ⁻³	4

In Figure 19, the run-average values of mass concentration determined from the scattered intensity correlation, and from the combined scattered intensity-transmittance correlation are plotted as a function of those values determined from the transmittance correlation. The combined scattered intensity-transmittance method predicts concentrations approximately 0.1 gm/ℓ higher, while the scattered intensity method predicts concentrations approximately 0.3 gm/ℓ lower than does the transmittance method. The vertical displacement between the three methods is probably a consequence of minor run to run variations in the alignment of the many elements in the optical path. For any of the three methods, a change in optical system alignment between the calibration experiment, Appendix II, and the experimental runs could result in such an occurrence. In this event, the transmittance method of estimating concentration would likely be the most accurate, since misalignment of the transmittance beam is less likely than misalignment of the scattering beam.

6.2 PARTICLE VELOCITY

The average values of the local particle velocity for each of the 40 grid points in each run are listed in Appendix X. Although significant differences were observed in the velocity estimates within a given horizontal plane for a given run, (see Table 6 and Appendix III), these differences appeared to be random with respect to position. No pattern

FIGURE 19
CORRELATION AMONG
CONCENTRATION ESTIMATES

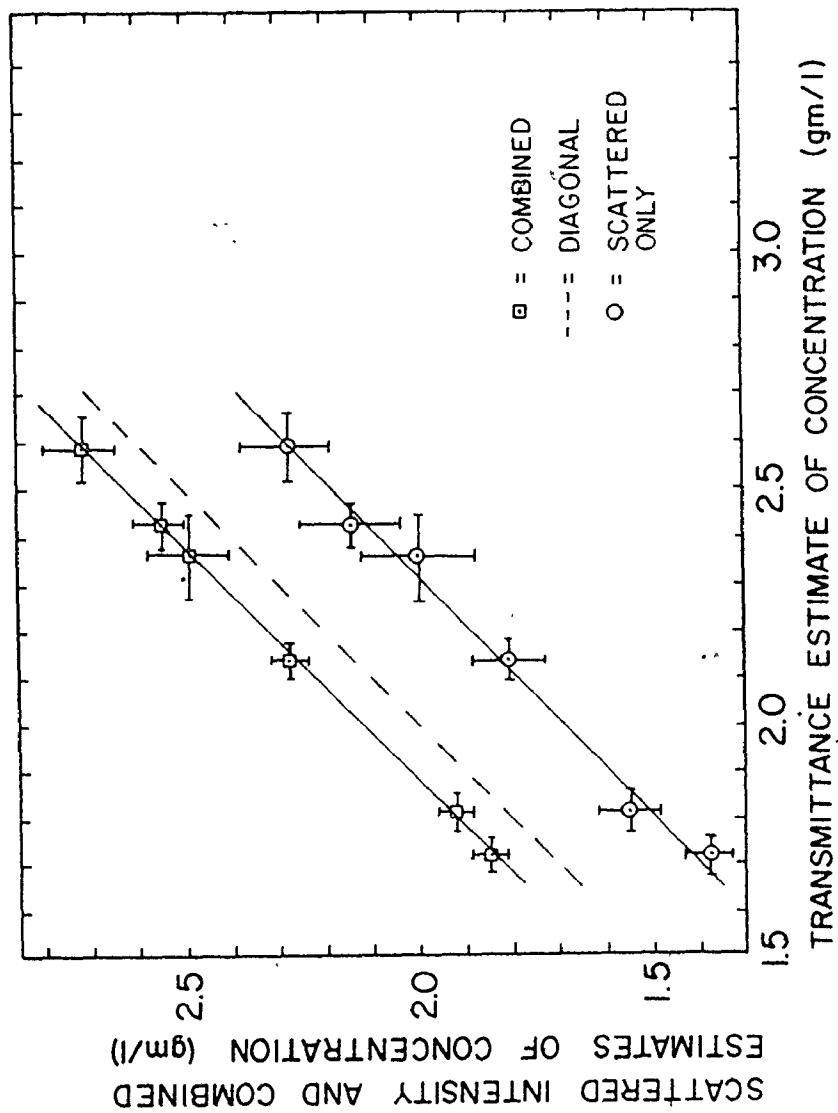


TABLE 6
ANALYSIS OF VARIANCE FOR VELOCITY ESTIMATES
(Voltage Units)

Run	Population Variance Estimates (volts) ²				Variance Ratio				
	Within Grid Points		Between Levels		Within Levels		Within Run		
	Run Average	ν	Run Average	ν	Run Average	ν	Run Average	ν	
1	1.5930x10 ⁻⁴	5902	2.6462x10 ⁻²	28	3.1250x10 ⁻²	3	166*	1962*	1.18
2	7.8996x10 ⁻⁴	6022	9.0126x10 ⁻²	28	1.5363x10 ⁻¹	3	114*	809*	1.70
3	6.7332x10 ⁻⁴	6878	5.7080x10 ⁻²	28	3.9684x10 ⁻¹	3	85*	590*	6.95*
4	9.5131x10 ⁻⁴	5593	2.6788x10 ⁻¹	28	4.0104x10 ⁻¹	3	282*	422*	1.50
5	9.0317x10 ⁻⁴	4882	4.2786x10 ⁻²	28	1.1171x10 ⁻¹	3	47*	124*	2.61
6	1.0363x10 ⁻³	4652	1.1346x10 ⁻¹	28	9.8910x10 ⁻¹	3	109*	955*	8.72*

*Significant at 95% confidence level

could be discerned to suggest that particles were settling faster in any particular region of the column. This indicated that stable, bulk circulation currents were not present in any of the runs. The variability of the velocity estimates within and between horizontal planes probably resulted from temporal changes over the sampling period. Six hours were required to sample a given horizontal plane; each run lasted 30 hours.

The eight estimates of velocity for each horizontal plane were averaged to provide a mean velocity estimate and a pooled variance. These data, summarized in Table 7, are shown in Figure 20 in which the average velocity is plotted as a function of column depth. The large variations in average velocity for those horizontal planes farthest from the column hopper are most probably due to mixing caused by the introduction of the slurry to the column. The influence of this mixing zone extended at least to the upper-most horizontal level at which measurements were made. At this level, the random motion of the particles caused the Doppler signal to change frequency faster than the tracking bandpass filter of the processing electronics could respond, resulting in frequent signal "drop-out." This problem was not encountered in any other region of the column. Although the particle velocity was unsteady in this region, the particle

TABLE 7
LEVEL AND RUN-AVERAGE VELOCITIES

Run	Level	Bulk Velocity (cm/min)	Mean Level Velocity (cm/min)		Variance of Velocity at Level (cm/min) ²		Distribution of Grid Point Means About Level Mean	v
			Relative to Fixed Observer	Relative to Slurry	Pooled from Individual Measurements	v		
	1		5.463	5.151	1.5192×10^{-1}	1436	2.1181×10^{-1}	7
	2		5.639	5.327	1.0685×10^{-1}	1479	1.6344×10^{-1}	7
1	3	0.3122	5.715	5.403	1.5401×10^{-1}	1489	1.0159×10^{-1}	7
	4		5.408	5.096	2.1643×10^{-1}	1498	9.0683×10^{-2}	7
	5		4.285	3.973	8.6536×10^{-1}	1505	1.3278×10^0	7
	1		5.808	5.317	4.9804×10^{-1}	1513	5.3697×10^{-1}	7
	2		6.488	5.997	1.0188×10^0	1506	2.3023×10^{-1}	7
2	3	0.4911	5.882	5.391	1.0054×10^0	1505	9.2895×10^{-1}	7
	4		5.878	5.387	6.0291×10^{-1}	1498	2.0007×10^{-1}	7
	5		5.627	5.136	1.2651×10^0	2743	1.0418×10^0	7

Table 7 (Cont'd.)

Run Level	Bulk Velocity (cm/min)	Mean Level Velocity (cm/min)		Variance of Velocity at Level (cm/min) ²		Distribution of Grid Point Means About Level Mean	v
		Relative to Fixed Observer	Relative to Slurry	Pooled from Individual Measurements			
1		6.126	5.915	6.6637×10^{-1}	1334	2.6684×10^{-1}	7
2		5.854	5.643	4.6540×10^{-1}	1520	4.0506×10^{-1}	7
3	0.2104	5.922	5.712	7.9963×10^{-1}	2147	2.2680×10^{-1}	7
4		6.894	6.684	6.7470×10^{-1}	1877	1.5143×10^{-1}	7
5		4.309	4.098	2.8612×10^0	1587	9.5623×10^{-1}	7
1		4.306	3.889	6.4705×10^{-1}	1329	6.1265×10^{-1}	7
2		3.486	3.068	6.6049×10^{-1}	1199	9.8946×10^{-1}	7
3	0.4176	3.426	3.008	9.2885×10^{-1}	1249	2.4336×10^0	7
4		4.438	4.020	1.3488×10^0	1816	2.0192×10^0	7
5		5.020	4.603	8.1507×10^{-1}	1908	2.1613×10^{-1}	7

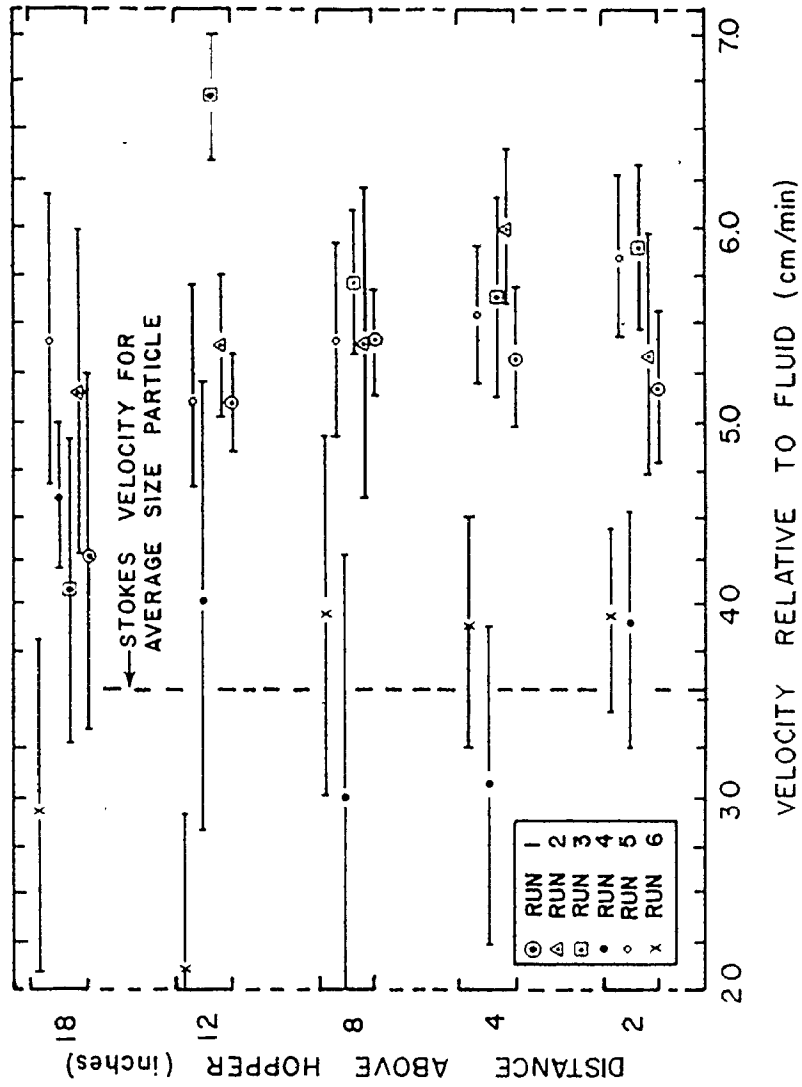
Table 7 (Cont'd.)

Run	Level	Bulk Velocity (cm/min)	Mean Level Velocity (cm/min)		Variance of Velocity at Level (cm/min) ²			
			Relative to Fixed Observer	Relative to Slurry	Pooled from Individual Measurements	\bar{v}	Distribution of Grid Point Means About Level Mean	
1			6.271	5.857	4.6302×10^{-1}	1166	2.5237×10^{-1}	7
2			5.969	5.554	6.5240×10^{-1}	1306	1.8262×10^{-1}	7
5	3	0.4146	5.808	5.393	8.2625×10^{-1}	1209	3.6530×10^{-1}	7
	4		5.554	5.139	1.6397×10^0	1201	3.0585×10^{-1}	7
	5		5.827	5.412	1.0761×10^0	1195	7.8206×10^{-1}	7
	1		4.165	3.953	1.0528×10^0	1178	3.3924×10^{-1}	7
	2		4.104	3.892	4.6406×10^{-1}	1151	5.2905×10^{-1}	7
6	3	0.2119	4.193	3.981	9.1286×10^{-1}	1146	1.2817×10^0	7
	4		2.325	2.113	1.6541×10^0	1177	9.2392×10^{-1}	7
	5		3.170	2.958	2.1189×10^0	1149	1.1122×10^0	7

TABLE 7
LEVEL AND RUN-AVERAGE VELOCITIES

Run	Run-Average Velocity (cm/min)	Variance of Run-Average Velocity, (cm/min) ²				ν	Distribution of Level Means About Run Mean	ν	V run / V Stokes
		Pooled from Individual Measurements	ν	ν	ν				
1	5.244	1.5753x10 ⁻¹	5902	2.0943x10 ⁻²	3	1.48	3	1.48	
2	5.523	7.8116x10 ⁻¹	6022	1.0091x10 ⁻¹	3	1.56	3	1.56	
3	5.988	6.6582x10 ⁻¹	6878	2.2815x10 ⁻¹	3	1.69	3	1.69	
4	3.496	9.4072x10 ⁻¹	5593	2.8327x10 ⁻¹	3	0.99	3	0.99	
5	5.486	8.9311x10 ⁻¹	4882	9.0247x10 ⁻²	3	1.55	3	1.55	
6	3.485	1.0248x10 ⁰	4652	8.3740x10 ⁻¹	3	0.98	3	0.98	

FIGURE 20
VELOCITY VS DEPTH



concentration was uniform and not significantly different from that observed at greater depths in the column.

With the exception of the upper-most regions of the column, the particle velocity appeared to be relatively uniform and independent of depth for each run, Table 6. The four lower-most horizontal planes were averaged to provide the run-average velocities listed in Table 7.

6.3 VELOCITY AS A FUNCTION OF CONCENTRATION

6.3.1 Comparison to Velocity Predicted by Literature Models

The velocities predicted by many of the models discussed in Chapter 2 were compared to the velocities measured in the experimental settling column. The particle mass concentration estimated by the transmittance measurement was converted to an estimated volumetric concentration using the measured particle parameters, and inserted in the various models to predict particle velocity. Although there was no basis for determining which of the three methods of estimating mass concentration was most accurate, it was felt that the transmittance method would be less susceptible to minor variations in system alignment which undoubtedly existed among the experimental runs and this method was used for the comparison.

The laser Doppler system measured particle velocity relative to a fixed observer. This velocity has two

components: the velocity of the particles relative to the fluid, and the bulk velocity superimposed on the slurry due to the underflow discharge:

$$V = V_r + V_f \quad (6-1)$$

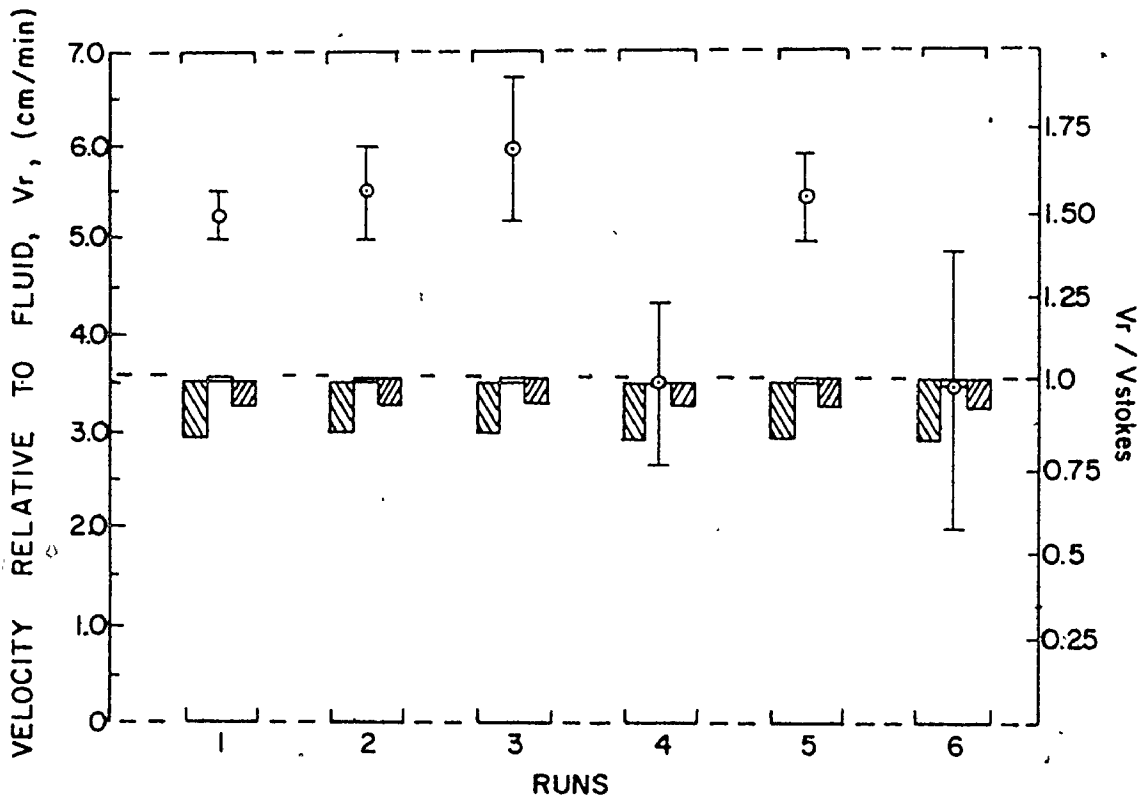
where: V = particle velocity relative to a fixed observer,
 V_r = relative velocity between the particle and the fluid, and
 V_f = fluid velocity relative to a fixed observed due to the underflow discharge.

Most of the models in the literature have been based on a relative velocity; however, different definitions of relative velocity have been used by different authors. In order to provide a uniform basis for comparison, the velocities in the literature models were modified to the same basis as those measured with the laser system according to equation (6-1). The fluid velocity component, V_f , was calculated from the measured underflow discharge, corrected for particle concentration, and was assumed to be uniform throughout the settling column.

Most of the literature models were developed for velocities normalized with respect to a measured or-calculated value of Stokes velocity. The Stokes velocity, V_{ST} , used in this comparison was that calculated from the measured particle properties, (see Appendix III).

Figure 21 shows the range of the predicted velocities for each run for the literature models listed in Tables 8, 9

FIGURE 21
VELOCITY COMPARISONS



▨ THEORETICAL MODELS, TABLE 8
 □ SEMI THEORETICAL MODELS, TABLE 9
 ▩ EMPIRICAL MODELS, TABLE 10
 ○ MEASURED BY LASER DOPPLER

TABLE 8
THEORETICAL LITERATURE MODELS

Source	Model (Figure 21)
Happel (1958)	$\frac{v_r}{v_{ST}} = \frac{1}{1 + 1.5\phi^{1/3}}$
McNown and Lin (1952)	$\frac{v_r}{v_{ST}} = \frac{1}{1 + 1.6\phi^{1/3}}$
Hasimoto (1959)	$\frac{v_r}{v_{ST}} = \frac{1}{1 + 1.76\phi^{1/3}}$
Famularo and Happel (1965)	$\frac{v_r}{v_{ST}} = \frac{1}{1 + 1.79\phi^{1/3}}$
Leclair and Hamielec (1968)	$\frac{v_r}{v_{ST}} = \frac{1}{1 + 1.8\phi^{1/3}}$
Smoluchowski (1911)	$\frac{v_r}{v_{ST}} = \frac{1}{1 + 1.92\phi^{1/3}}$
Uchida (1949)	$\frac{v_r}{v_{ST}} = \frac{1}{1 + 2.1\phi^{1/3}}$
Happel and Brenner (1965)	$\frac{v_r}{v_{ST}} = \frac{1 - \phi}{1 + 5.5\phi \left[\frac{4\phi^{7/3} - \frac{84}{11}\phi^{2/3} + 10}{10(1 - \phi^{10/3}) - 25\phi(1 - \phi^{4/3})} \right]}$

Table 8 (Cont'd.)

Source	Model (Figure 21)
Happel and Brenner (1965)	$\frac{v_r}{v_{ST}} = \frac{3 - (9/2)\phi^{1/3} + (9/2)\phi^{5/3} - 3\phi^2}{3 + 2\phi^{5/3}}$
Barnea and Mizrahi (1973)	$\frac{v_r}{v_{ST}} = \frac{1 - \phi}{(1 + \phi)^{1/3} \exp \frac{5\phi}{3(1 - \phi)}}$

Notes:

Working Models: Figure 22 $v = (1 - \phi) v_r + \frac{Q_u}{A}$

where: Q_u = measured underflow flowrate

A = cross-sectional area of column

TABLE 9
SEMI-THEORETICAL LITERATURE MODELS

Source	Model
Einstein (1906)	$\frac{\mu_a}{\mu_f} = 1 + 2.5\phi$
Guth and Simha (1936)	$\frac{\mu_a}{\mu_f} = \frac{1 + 0.5\phi - 0.5\phi^2}{1 - 2\phi - 0.6\phi^2}$
Vand (1948) and Hawksley (1951)	$\frac{\mu_a}{\mu_f} = \exp\left[\frac{2.5\phi}{1 - 0.609\phi}\right]$
Vand (1948)	$\frac{\mu_a}{\mu_f} = \exp\left[\frac{2.5\phi + 2.7\phi^2}{1 - 0.609\phi}\right]$
Mooney (1951)	$\frac{\mu_a}{\mu_f} = \exp\left[\frac{2.5\phi}{1 - 0.75\phi}\right]$
	$\frac{\mu_a}{\mu_f} = \exp\left[\frac{2.5\phi}{1 - 1.5\phi}\right]$
Brinkman (1952) and Roscoe (1952)	$\frac{\mu_a}{\mu_f} = \frac{1}{(1 - \phi)^{2.5}}$
Thomas (1965)	$\frac{\mu_a}{\mu_f} = [1 + 2.5\phi + 10.05\phi^2 + 0.00273 \exp(16.6\phi)]$

Notes:

Working Models: Figure 21: $V_r = (1 - \phi) \left(\frac{\mu_f}{\mu_a}\right) V_{ST}$

Figure 22: $V = (1 - \phi)V_r + \frac{Q_u}{A}$

where: Q_u = measured underflow flowrate

A = cross-sectional area of column

TABLE 10
EMPIRICAL LITERATURE MODELS

Source	Model (Figure 21)
Steinour (1944)	$\frac{v_r}{v_{ST}} = (1 - \phi) \exp(-4.19\phi)$
Richardson and Zaki (1954)	$\frac{v_{BS}}{v_{ST}} = (1 - \phi)^{4.65} \longrightarrow \frac{v_r}{v_{ST}} = (1 - \phi)^{3.65}$
Brinkman (1947)	$\frac{v_r}{v_{ST}} = 1 + \frac{3}{4}\phi \left[\frac{8}{\phi} - 3 \right]^{1/2}$
Loeffler and Ruth (1959)	$\frac{v_r}{v_{ST}} = \left[1 + \frac{5.70\phi}{(1 - \phi)^2} \right]^{-1}$
Oliver (1961)	$\frac{v_{BS}}{v_{ST}} = (1 - 0.75\phi^{1/3})(1 - 2.15\phi) \longrightarrow$ $\frac{v_r}{v_{ST}} = \frac{1}{(1 - \phi)}(1 - 0.75\phi^{1/3})(1 - 2.15\phi)$

Notes: v_{BS} = Velocity of interface in batch settling test

Working Models: Figure 22: $v = (1 - \phi) v_r + \frac{Q_u}{A}$

where: Q_u = measured underflow flowrate

A = cross-sectional area of column

and 10. Also shown in this figure are the run-average values of velocity measured in this study. The excellent agreement among the literature models and the poor agreement between the literature models and the measured velocities should be noted.

All of the literature models are structured in such a way that the maximum particle velocity, Stokes velocity, occurs at infinite dilution and that the particle velocity decreases as the particle concentration increases. The measurements obtained in this study suggest the same inverse variation of velocity with concentration; however, at the lowest volumetric concentration studied, 7×10^{-2} percent, the settling velocity was observed to approach twice the Stokes velocity of the average size particle. That is, in dilute slurries, the "hindered" settling velocity was observed to be larger than the single particle terminal velocity at infinite dilution.

The large velocities observed in the settling region cannot be accounted for by classification of the feed stream particles or by the particle velocity distribution of the feed stream particles. Figure 15 shows the cumulative Stokes velocity distribution calculated using the measured particle size distribution, Appendix IV, and the measured particle density. Also shown is the upflow steady-state velocity in the classification region for each run due to the overflow

discharge. This velocity was estimated by dividing the overflow flowrate by the cross-sectional area.

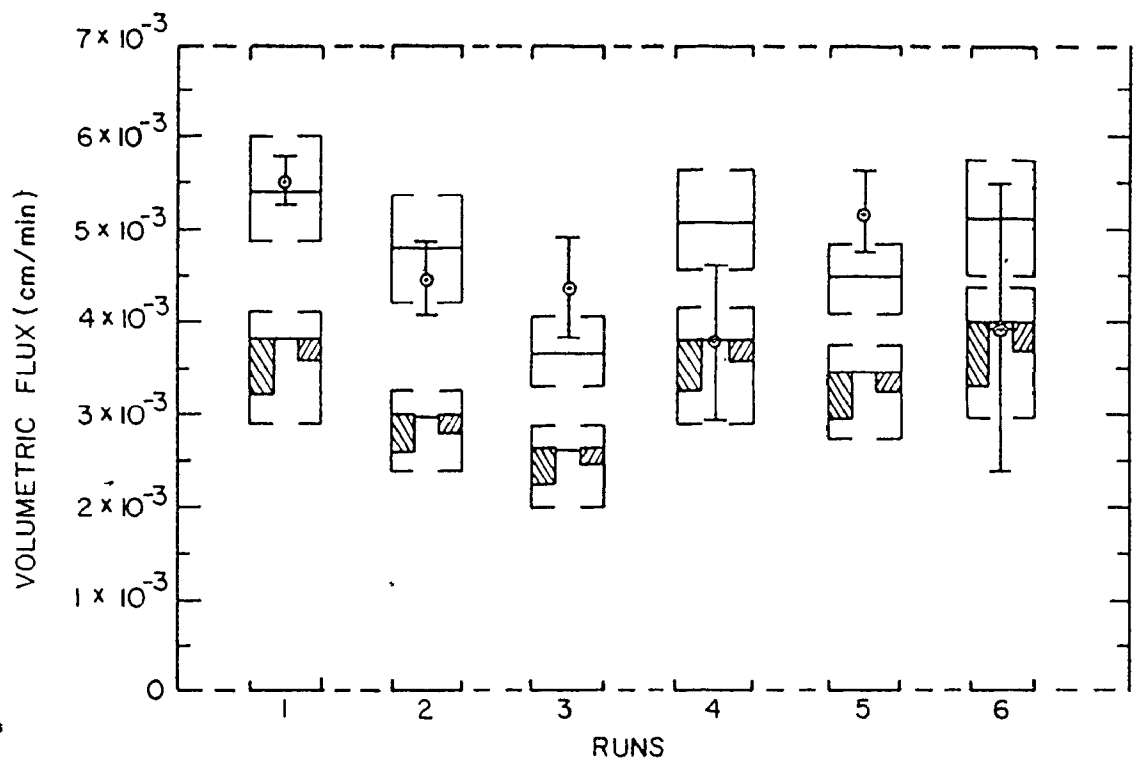
Even neglecting turbulent effects at the feed point, the extent of classification expected due to the distribution of particle velocities in the feed stream would be minor and the velocity distribution of the particles discharged in the underflow can reasonably be assumed to be the same as that of the particles in the feed stream. Except for runs 1 and 2 in which the settling column was overloaded due to an insufficient underflow flowrate, the small mass flowrate of particles in the overflow stream provides strong evidence for the absence of classification of the feed stream particles.

According to Figure 15: for run 3 only 4.5 percent of the feed stream particles, and for runs 1, 2, and 5 less than 10 percent of the feed stream particles had single particle, Stokes velocities as large as those measured for the slurry. This indicates that the large velocities observed in the settling column cannot be explained on the basis of the individual particle velocity distribution.

6.3.2 Comparison to Flux Predicted by Literature Models

Figure 22 shows the range of volumetric fluxes predicted by the literature models, the volumetric fluxes calculated from the optical measurements of velocity and concentration and the steady-state volumetric fluxes

FIGURE 22
FLUX COMPARISONS



MEAN AND 95% CONFIDENCE INTERVAL INDICATED

▨ PREDICTED BY THEORETICAL MODELS, TABLE 8

— PREDICTED BY SEMI-THEORETICAL MODELS, TABLE 9

▩ PREDICTED BY EMPIRICAL MODELS, TABLE 10

⊞ UNDERFLOW MEASUREMENT

⊙ OPTICAL MEASUREMENT

determined from the measurements of slurry flowrate and particle concentration at the column underflow for each set of experimental conditions.

Poor agreement was obtained between the measured steady-state fluxes and those predicted by the literature models. Assuming the concentration determined by the transmittance method is accurate, none of the literature models provides an accurate description of the dependence of velocity on concentration for the dilute slurries studied. The literature models underpredict particle velocity by as much as 100 percent.

Good agreement was obtained between the measured steady-state fluxes and those calculated from the optical measurements of velocity and concentration. As well as lending strong support to the accuracy of the laser Doppler system for measuring particle velocity, this demonstrates that "hindered" settling particle velocities significantly larger than single particle, Stokes velocity are attained in dilute slurries, (see Appendix III).

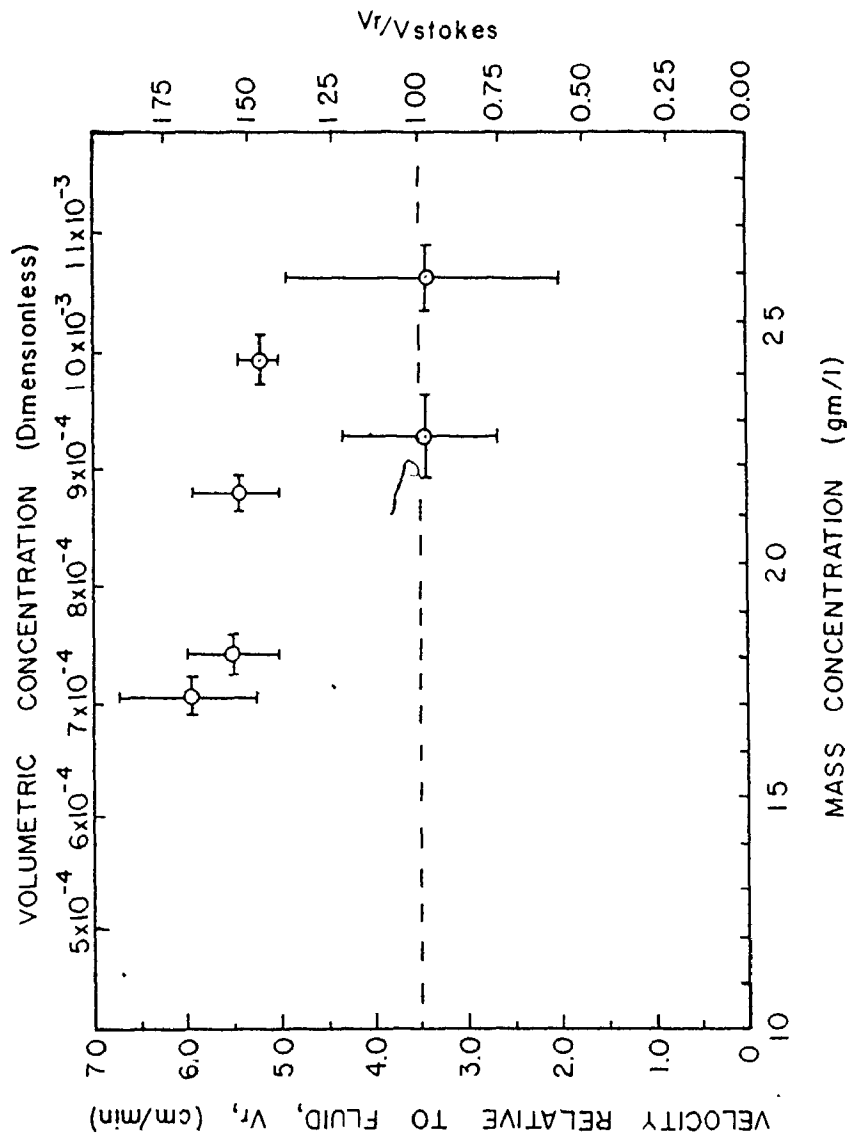
6.4 DILUTE SLURRY SEDIMENTATION

Previous studies using spherical particles at very dilute concentration have reported that enhanced velocities first become evident at volumetric concentrations between 10^{-3} and 10^{-2} ; the degree of enhancement increases to a

maximum at a concentration slightly greater than 10^{-2} ; and, thereafter, the velocity monotonically decreases with increasing concentration. It has generally been assumed that, at volumetric concentrations much less than 10^{-2} , the particles are so remote from each other that the probability of cluster formation becomes insignificant; this results in velocities not much different from the single particle Stokes value, [Kamel *et al.* (1979), Batchelor (1972), Tory and Pickard (1980)]. While the extent of enhancement has varied among studies, the concentration range over which the phenomenon has been observed has been remarkably consistent.

The results of this study do not agree with the experimental results available from the literature. In Figure 23, the run-average velocity, corrected for the velocity component due to the underflow discharge, is plotted as a function of run-average concentration. A maximum velocity 70 percent larger than the Stokes value for the average particle size was observed at the lowest volumetric concentration, 7.03×10^{-4} , a concentration more than one order of magnitude less than has been previously reported for the occurrence of maximum velocity. The extent of enhancement at this concentration is much larger than has previously been reported and there is no evidence to suggest that even higher velocities would not have been observed had lower concentrations been present in the settling column. To investigate this

FIGURE 23
VELOCITY VS CONCENTRATION



apparent anomaly, it would be instructive to estimate the probability of particle cluster formation in very dilute slurries.

6.4.1 The Probability of Cluster Formation at Very Dilute Concentrations

It has generally been agreed that cluster formation results as a consequence of the non-uniform spatial distribution of particles. Smith (1966) performed an interesting series of settling experiments at a single volumetric concentration of 0.025 which used a photographic technique to analyze suspensions of monodisperse spheres of different colours. He demonstrated that the settling particles were distributed in space according to a binomial distribution. Further, Johne (1966) and Barford (1972) claimed success in describing their particle sedimentation data by means of Poisson distributions, which, for the large particle numbers involved, can be considered good approximations to binomial distributions.

Following this work, a simple model of the slurry was formulated to accommodate the velocities observed in this study. In this model, local regions containing more than the bulk average number of particles were assumed to be present. That is, regions of volumetric concentrations slightly higher than the average concentration were assumed to occur. In these regions, the particles were assumed to be uniformly

distributed in a spherical drop whose density was greater than the average slurry density as a consequence of the higher particle concentration. The diameters of the slurry drops necessary to produce the run-average velocities observed in this study were calculated using Stokes law:

$$D_c = \sqrt{\frac{18 V_c \mu}{g (\rho_2 - \rho_1)}} \quad (6-2)$$

where: D_c = cluster diameter,
 V_c = observed velocity,
 g = gravitational constant,
 ρ_2 = cluster density, and
 ρ_1 = average slurry density.

For this calculation, the densities were estimated using:

$$\rho_2 = \phi_2 \rho_p + (1 - \phi_2) \rho_f \quad (6-4)$$

and

$$\rho_1 = \phi_1 \rho_p + (1 - \phi_1) \rho_f \quad (6-5)$$

where: ϕ_1 = slurry average volumetric concentration,
 ϕ_2 = cluster volumetric concentration,
 ρ_p = particle density, and
 ρ_f = fluid density.

For assumed values of cluster volumetric concentration, the number of particles of the mean diameter present in the cluster was determined. The binomial probability for the occurrence of clusters containing this number of particles

was estimated by integrating the individual probabilities over a range of particle numbers bracketing this value. The upper and lower bounds for this range of particle numbers was determined from the variance of the velocity measurement.

The variance associated with the mean velocity estimate at each location in the settling column should be related to the variations in cluster size and concentration occurring over the period for which the velocity was measured, Appendix III. The mean value of velocity determined at each location was used to estimate the mean cluster size and the mean cluster concentration. The 95 percent confidence limits of the mean velocity were used to establish a range of cluster sizes and densities which could be expected to occur with 95 percent confidence. Assuming a locally uniform distribution of particles within the cluster, the probability for the occurrence of this range of cluster sizes and concentrations was determined by means of the binomial distribution:

$$P_r = \sum_{n_1}^{n_2} \left[\binom{N}{n_i} z^{n_i} (1-z)^{N-n_i} \right] \quad (6-6)$$

where: P_r = binomial probability,
 N = maximum possible number of particles in the cluster,
 n_i = number of particles in the cluster,

n_1, n_2 = lower and upper limits for n_i , and

Z = probability of observing the bulk average number of particles in the cluster.

The summation limits, n_1 and n_2 , were established as the number of particles required to produce the lower and upper 95 percent confidence limits, respectively, for the mean velocity at a fixed cluster concentration. Smith (1966) demonstrated that the binomial probability function was relatively insensitive to the value selected for N , the maximum possible number of particles in the cluster. Following his recommendation, N was estimated by assuming a maximum possible particle volumetric concentration of 0.5. The value of Z , the probability of observing the bulk average number of particles in the cluster, was established as the ratio of the measured run-average volumetric concentration to the maximum possible volumetric concentration, 0.5.

The velocity at each grid point could be characterized by a mean value, plus or minus 2.5 percent at the 95 percent confidence level, (see Appendix III). For this range of velocity values, the probabilities for the occurrence of various cluster diameters are shown in Figure 24.

It is interesting to note that the observed velocities can be accounted for by localized regions at concentrations not much higher than the bulk average concentration. Figure 25 indicates that clusters with concentrations between

FIGURE 24.
BINOMIAL PROBABILITY VS CLUSTER DIAMETER

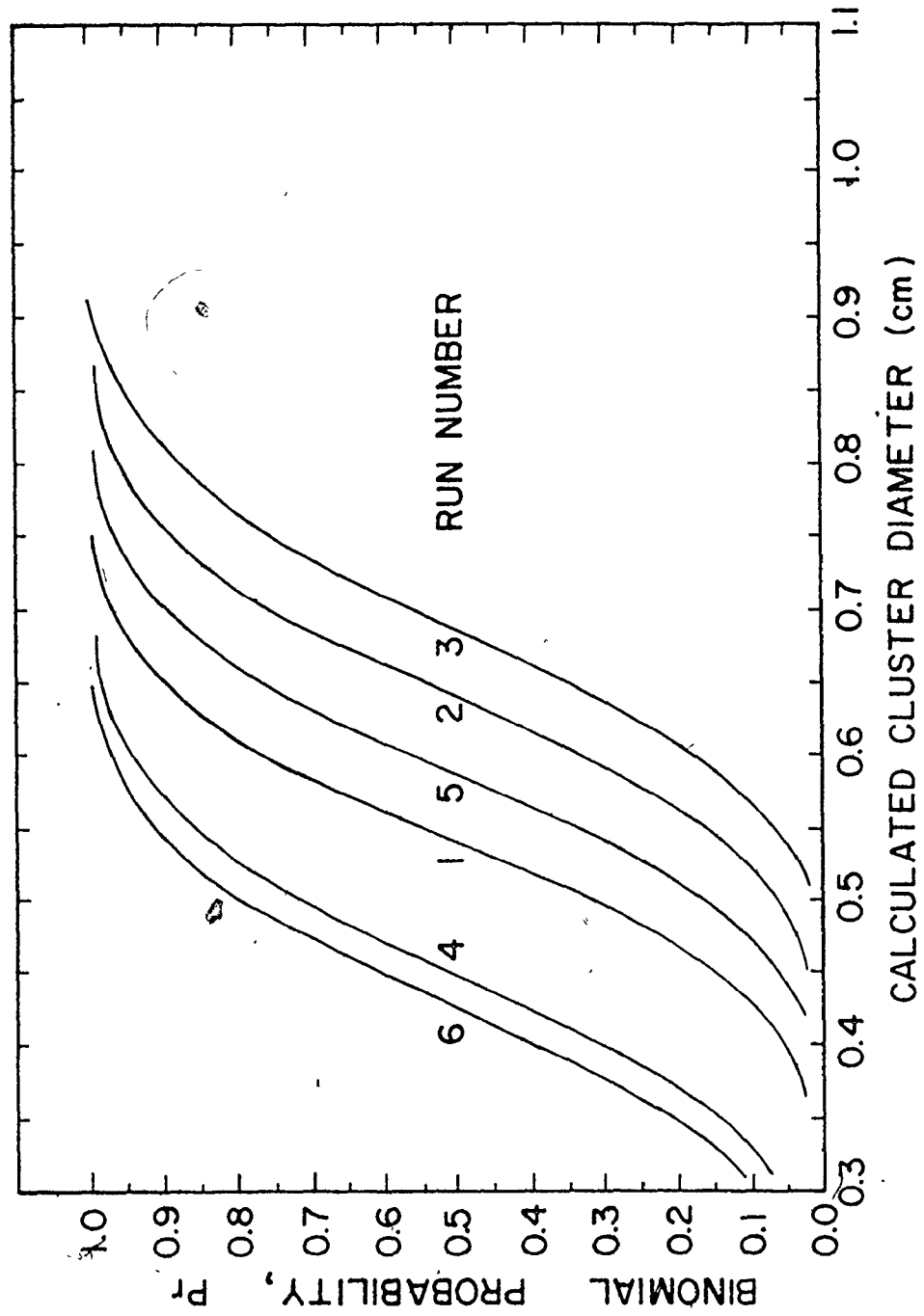
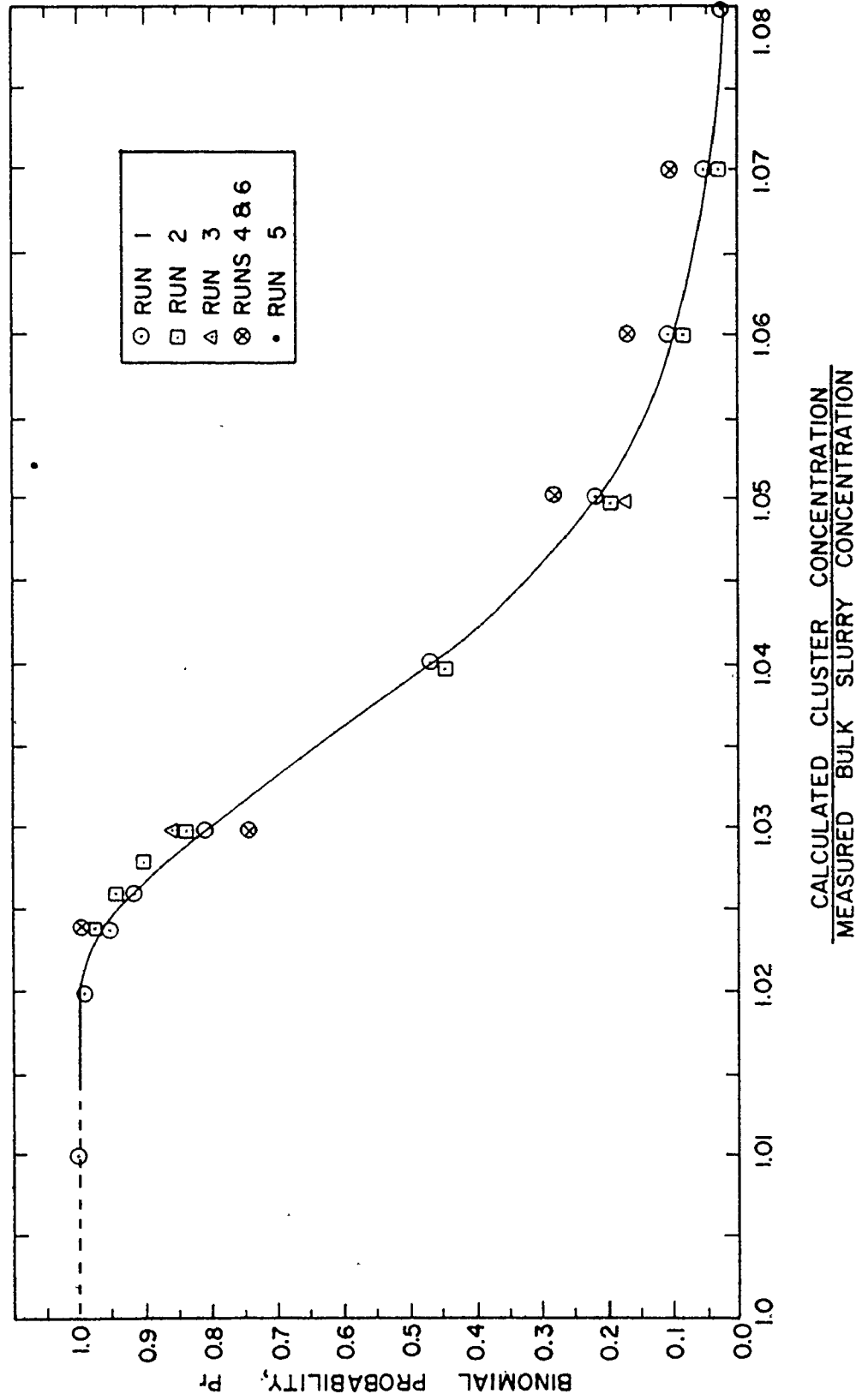


FIGURE 25
BINOMIAL PROBABILITY VS CLUSTER CONCENTRATION

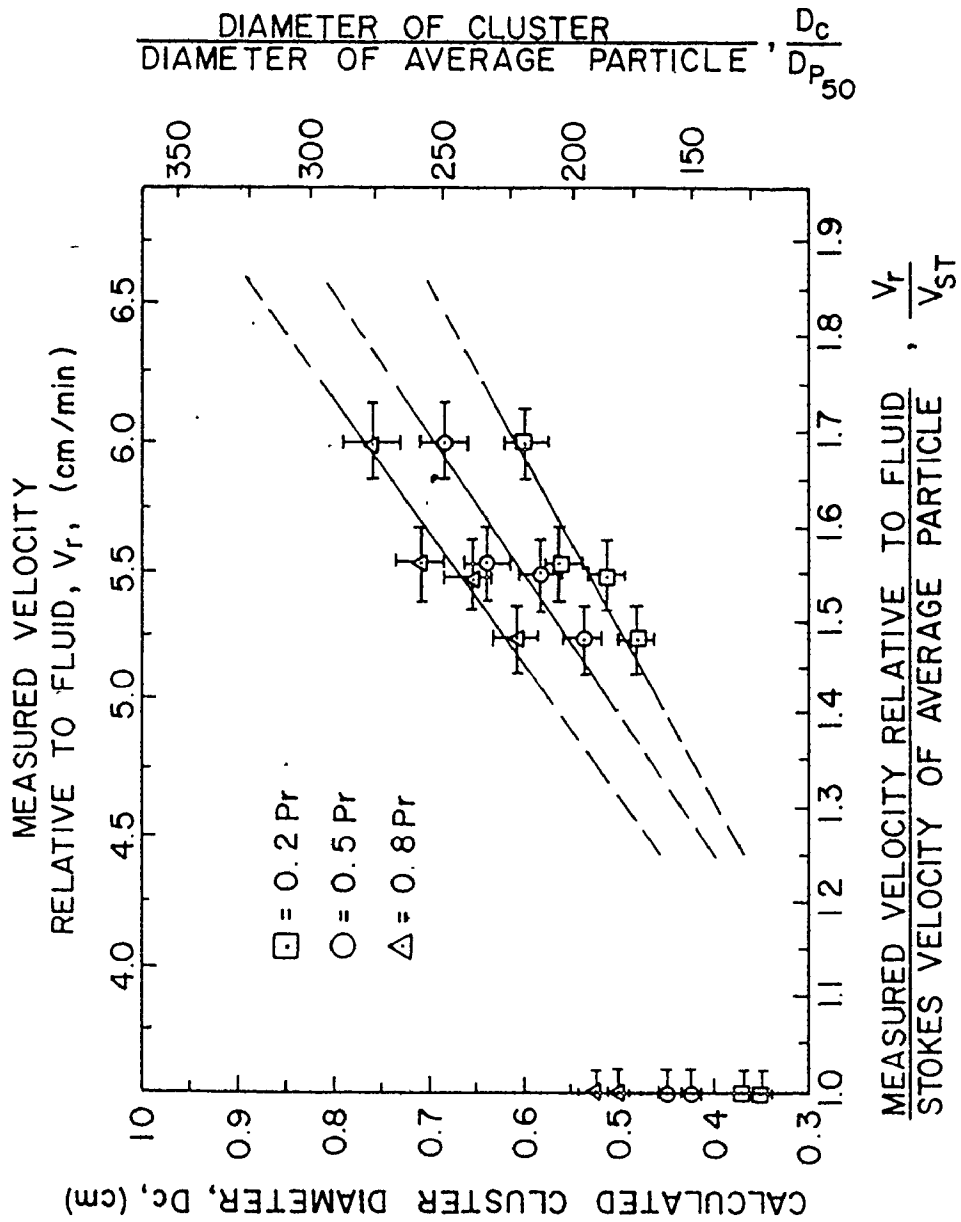


2.5 and 5 percent higher than the bulk average concentration could be expected to occur with high probability, while local regions with concentrations larger than the bulk average value by more than 5 percent would not be expected with high probability. According to the assumption of a binomial distribution of the slurry particles, therefore, very small local perturbations in the average particle number density can account for the enhanced settling velocities observed in this study.

The probabilities for the occurrence of clusters of various sizes is shown as a function of the run-average velocities in Figure 26. These data are a rearrangement of Figure 24. It is evident that relatively large clusters are predicted to occur with high probability. Assuming a 50 percent probability of occurrence, cluster sizes ranging from 5.5 to 6.9 mm are required to account for the enhanced velocities measured in this study.

With clusters this large, significant wall effects become a possible concern since, as noted by Koglin (1970), Tory and Pickard (1977) and Adachi *et al.* (1978), when particles became closely enough associated to form a cluster, the relevant particle size parameter for estimating wall effects is related to the dimensions of the cluster rather than to the dimensions of the individual particles.

FIGURE 26
 CLUSTER DIAMETER VS. CLUSTER VELOCITY



6.4.2 The Influence of Wall Effects on Cluster Settling Velocity

Koglin (1970) demonstrated the large influence of wall effects on the extent of velocity enhancement in dilute slurries. As the ratio of the average particle diameter to the diameter of his cylindrical settling vessel was decreased from 1.4×10^{-2} to 3.1×10^{-3} , the maximum velocity was observed to increase from approximately 1.5 to 3.0 times the Stokes value. His data showed that wall effects influenced the extent of velocity enhancement, but did not affect the particle volumetric concentration, 10^{-2} , at which the maximum velocity occurred. As the particle-to-container size ratio decreased, velocity enhancement became apparent at lower concentrations and persisted to higher concentrations. Although appreciable velocity enhancement was not apparent at concentrations as low as 10^{-3} due to the wall effects, the possibility of observing enhanced velocities at concentrations this low was demonstrated. Hestroni *et al.* (1970) and Koglin (1973) suggest that wall effects should be estimated assuming a spherical drop with the same dimensions as the cluster, an approach which accommodates the simple cluster model used in this analysis.

According to Happel and Brenner (1965), who summarized Faxen's work, the velocity of a sphere (that is, a cluster) moving parallel to two stationary walls can be approximated by:

$$\frac{V_C}{V_{CStokes}} = 1 - 0.6526 \left(\frac{R_C}{x}\right) + 0.1475 \left(\frac{R_C}{x}\right)^3 - 0.13 \left(\frac{R_C}{x}\right)^4 - 0.064 \left(\frac{R_C}{x}\right)^5 \quad (6-7)$$

for the case in which the particle is one-quarter way between the two walls, and:

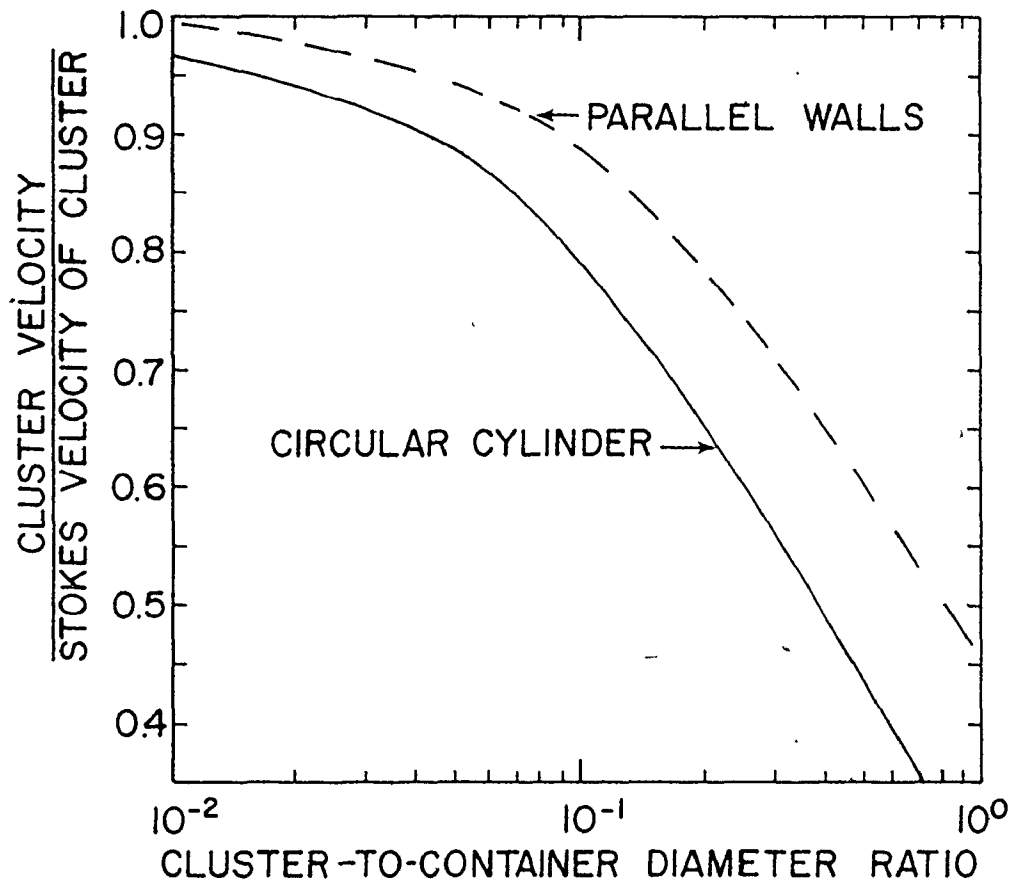
$$\frac{V_C}{V_{CStokes}} = 1 - 1.004 \left(\frac{R_C}{x}\right) + 0.418 \left(\frac{R_C}{x}\right)^3 + 0.21 \left(\frac{R_C}{x}\right)^4 - 0.169 \left(\frac{R_C}{x}\right)^5 \quad (6-8)$$

for the case in which the particle is mid-way between the two walls.

where: V_C = cluster velocity,
 $V_{CStokes}$ = Stokes velocity for the cluster,
 R_C = radius of the cluster, and
 x = separation between the stationary walls.

The relative velocities predicted by these two equations were averaged to provide an estimate of the wall effects on the settling velocity of the clusters in the experimental column. The relative cluster velocity is plotted as a function of the ratio of cluster diameter to the container wall separation in Figure 27. It is evident that, for the cluster sizes predicted in this analysis, the experimental column used in this study could be expected to decrease the cluster settling velocity by only approximately 5 percent. That is, wall effects were apparently of minor importance in this study.

FIGURE 27
VESSEL WALL EFFECTS



The same conclusion, however, may not be warranted for previous studies which have reported cluster formation with spherical particles. Also plotted in Figure 27 is the relative cluster velocity as a function of the ratio of cluster diameter to container diameter for a cylindrical container. This curve was estimated from the model of Happel and Brenner (1965):

$$\frac{V_c}{V_{c\text{Stokes}}} = \frac{1}{1 + f(\beta) \left(\frac{D_c}{D}\right)} \quad (6-9)$$

where: $f(\beta)$ = a function of the distance of the particle from the cylinder axis,

D = cylindrical container diameter, and

D_c = cluster diameter.

An unweighted average of Happel and Brenner's (1965) data, $f(\beta) = 2.621395$, was used for the location parameter in equation (6-9). Table 11 lists the container sizes and particle sizes used by previous investigators, and the cluster-to-container diameter ratio assuming cluster sizes similar to those determined for this study. It is evident from Figure 27 that wall effects would be significant in these studies for cluster sizes on the order of several millimeters. It is interesting to note that, had comparable cluster-to-container size ratios been employed in this study, no velocity enhancement would have occurred.

TABLE 11
POTENTIAL WALL EFFECTS ON CLUSTER VELOCITY

Source	Particle Size (μm)			Stokes Velocity Range				Cylindrical Container Diameter D (mm)	Cluster Diameter and Velocity*					
	$D_{P0.05}$	Mean $D_{P0.50}$	$D_{P0.95}$	$V_{D_{P0.05}}$	$V_{D_{P0.95}}$	$V_{D_{P0.50}}$	$V_{D_{P0.05}}$		$V_{D_{P0.95}}$	$V_{D_{P0.50}}$	$\frac{D_C}{D}$	$\frac{D_C}{D}$ (mm)	$\frac{V_C}{V_{C\text{Stokes}}}$	$\frac{V_C}{V_{D_{P0.50}}}$
Kaye and Boardman (1962)	80 350 700	100 400 820	120 450 940	2.25 1.65 1.80	1.44 1.26 1.31	0.64 0.77 0.73	0.64 0.77 0.73	70 70 70	23.0 91.9 188.3	3.28×10^{-1} 1.31 2.69	0.54 -- --	0.86 -- --		
Johne (1966)	180	200	220	1.57	1.1	0.7	0.7	35	45.9	1.31	--	--		
Koglin (1972)	180 180 180	200 200 200	220 220 220	1.57 1.57 1.57	1.1 1.1 1.1	0.7 0.7 0.7	0.7 0.7 0.7	35 20 65	45.9 45.9 45.9	1.31 2.30 7.06×10^{-1}	-- -- 0.35	-- -- 0.56		
Barford (1972)	7.9 12.2 19.8	13 22.2 29	24.3 25.0 40.0	9.46 4.20 4.08	3.50 1.23 1.90	0.37 0.30 0.47	0.37 0.30 0.47	57 57 57	3.0 5.1 6.7	5.24×10^{-2} 8.94×10^{-2} 1.17×10^{-1}	0.88 0.81 0.77	1.40 1.30 1.23		
Present Study	11.32	27.0	42.68	14.20	2.50	0.176	0.176	152.4**	6.2***	4.07×10^{-2}	0.96	1.54***		

*Assuming: $V_{C\text{Stokes}} = 1.6 V_{D_{P0.50}}$ at $\phi = 10^{-3}$
 **Square Cross-Section
 ***Average value for present study

The influence of container size on the settling velocity of clusters can be estimated as a function of the average slurry particle size using a rearrangement of equation (6-2):

$$D_c = \left[\frac{V_c 18\mu}{\gamma \phi_{AV} (\rho_p - \rho_f) g} \right]^{1/2} \quad (6-10)$$

where: D_c = cluster diameter,
 V_c = cluster velocity,
 ρ_p, ρ_f = particle and fluid densities,
 ϕ_{AV} = bulk average slurry volumetric concentration,
 and
 γ = fractional increase in ϕ_{AV} for the cluster,

that is:

$$\gamma = \frac{\phi_c - \phi_{AV}}{\phi_{AV}} \quad (6-11)$$

where: ϕ_c = cluster volumetric concentration.

Consider two slurries of monodisperse particles of the same density at the same (dilute) volumetric concentration in identical containers. Assume one slurry is comprised of particles with diameter D_{p1} , and the other of particles with diameter D_{p2} . For the same extent of velocity enhancement in each slurry:

$$\frac{V_{c1}}{V_{PStokes1}} = \frac{V_{c2}}{V_{PStokes2}} \quad (6-12)$$

and the same cluster volumetric concentration, (that is, $\gamma_1 = \gamma_2$), the cluster diameters are related by:

$$\frac{D_{c1}}{D_{c2}} = \left[\frac{V_{c1}}{V_{c2}} \right]^{1/2} = \frac{D_{p1}}{D_{p2}} \quad (6-13)$$

It is evident that, for a given probability of cluster formation (that is, a given γ), and for a given extent of velocity enhancement (that is a given $V_c/V_{p_{Stokes}}$), the cluster size increases as the slurry particle size increases. The wall effects on the settling velocity of the clusters formed in the slurry comprised of the larger particles would be greater than those for the other slurry.

Table 11 lists the cluster size and the cluster-to-container diameter ratio which would obtain in previous investigations assuming the same extent of velocity enhancement as was observed in this study at a volumetric concentration of 10^{-3} . It is obvious from Figure 27 that wall effects were dominant in the other studies and can account for the lack of velocity enhancement reported at concentrations as low as 10^{-3} .

For the dilute concentration range, the correlations of velocity with concentration reported by all previous workers may be artifacts of the particle-to-container size ratios employed. In these studies, the wall effects were apparently dominant until the cluster diameter decreased as a

consequence of increased slurry concentrations for ϕ_{AV} levels close to 10^{-2} , [see equation (6-10)].

6.4.3 The Influence of Slurry Particle Velocity Distribution on Cluster Settling Velocity

It has generally been assumed that the increase in velocity observed as the concentration increases from infinite dilution results from the random spatial distribution of the particles. As the concentration increases, the probability that several particles are in close proximity increases and hence the probability of cluster formation increases. The data available in the literature for the settling of spherical particles at dilute concentration predict maximum velocity enhancement at a volumetric concentration of about one percent. The monotonic decrease in observed velocity as the volumetric concentration is increased beyond this level has been ascribed to the return flow arising from the fluid displaced by the settling particles.

The trend of the data obtained in this study suggests a decrease in particle velocity as the concentration increases from 7×10^{-4} to 2.4×10^{-3} . These data suggest that at concentrations much above 10^{-3} , the particle velocity approaches the Stokes velocity for the average size particle. This apparent anomaly is probably a consequence of the low cluster stability prevalent in this study.

Cluster stability has been reported to be a function of the number of particles in the cluster. Jayaweera *et al.* (1964) observed that when six or less particles were introduced into a quiescent fluid, the particles positioned themselves in a regular polygon in a horizontal plane. These investigators did not observe stable clusters when more than six particles were present, a finding substantiated by the semi-theoretical analysis of Hocking (1964). This horizontal arrangement among the particles is at variance with the experimental results of Smith (1966) who noted a small vertical association among the particles of a suspension but no significant horizontal association. This discrepancy may be due to the fact that Jayaweera *et al.* (1964) observed the motion of very few particles introduced into a fluid devoid of other particles, while Smith (1966) worked with an initially well mixed slurry.

Koglin (1972) was able to measure the settling velocities of clusters containing up to ten particles. He noted, however, that cluster stability varied inversely with the number of particles in the cluster. Clusters containing many particles tended to shed particles much more frequently than did those containing fewer particles.

Cluster stability has been shown to be a function of volumetric concentration. As noted by Tory and Pickard (1977), Koglin's data demonstrated high cluster stability

when dense clusters fell through clear fluid or through suspensions of concentration less than 5.0×10^{-3} . Koglin (1973) found that the correlation length, a measure of the mean distance over which a particle is associated with a settling cluster, decreased with increasing concentration. Tory and Pickard (1977) and Koglin (1973) have suggested that clusters become less stable as concentration increases due to the increased probability of particles in the bulk suspension interfering with the passage of the cluster.

Cluster stability has also been shown, implicitly, to be a function of the size distribution of the slurry particles. Kaye and Boardman (1962) and Johne (1966) performed experiments in which the settling velocity of uniformly sized tracer particles were measured in monodisperse slurries whose particles were of different size than the tracer particles. These data showed that the extent of velocity enhancement, and therefore probably cluster stability, decreased in direct proportion to the size difference between the tracer particles and the slurry particles.

Most investigators have worked with suspensions of very narrow particle size distributions, and, due to the relatively large particle sizes employed, with suspensions of very narrow particle velocity distributions. Although the particles used in this investigation were closely sized, they exhibited a rather large velocity distribution as a

consequence of the relatively small average particle size, Table 11.

This large velocity distribution would result in a wide range of single particle settling velocities in the experimental column. The probability of clusters formed by the smaller slurry particles being disrupted by the larger slurry particles would be much greater in the present study than in previous studies using spherical particles. Further, this probability should increase with increasing particle number concentration. This lower cluster stability probably accounts for the decrease in particle velocity observed in this study for volumetric concentrations much above 10^{-3} .

It is interesting to note that Barford (1972), the only other worker to use particles of size similar to those used in this study, observed a similar rapid decrease in velocity enhancement at volumetric concentrations greater than 10^{-3} . Although Koglin (1972) ascribed Barford's observations to the fact that irregularly shaped particles were used in his study, his data probably reflect the small cluster stability resulting from the large particle velocity distribution.

CHAPTER 7
CONCLUSIONS, RECOMMENDATIONS, AND
ENGINEERING SIGNIFICANCE

7.1 CONCLUSIONS

For the materials and methods of this investigation, it is concluded that:

- (1) Stable particle concentration and velocity gradients were not present in the dilute blanket of the continuous thickener-clarifier.
- (2) Average slurry velocities up to 70 percent higher than the mean particle Stokes velocity occurred at dilute blanket concentrations between 7.04×10^{-2} and 1.07×10^{-1} percent by volume under steady-state thickener-clarifier operation.
- (3) None of the deterministic literature models commonly used to describe particle settling velocity as a function of particle concentration accurately predicted the relative slurry velocities at dilute concentrations.
- (4) Assuming the particles in the dilute blanket were spatially distributed according to a binomial distribution, local regions with

concentrations slightly higher than the bulk solution concentration were predicted to occur with high probability. These particle clusters could account for the high slurry velocities which were observed.

- (5) Previous studies reporting particle cluster formation have been influenced by container wall effects at volumetric concentrations as low as 10^{-3} .
- (6) Cluster stability was probably inversely related to the slurry concentration and to the variance of the velocity distribution of the constituent slurry particles. Cluster stability appeared to decrease at volumetric concentrations approaching 10^{-3} .

7.2 RECOMMENDATIONS

Based on the results of this investigation, it is recommended that:

- (1) The laser Doppler technique should be used with more concentrated suspensions and/or larger settling columns to establish the upper limits of multiple scattering for which the technique can be employed.
- (2) The influence of the variance of the velocity distribution of the constituent slurry particles

on the stability of particle clusters should be investigated.

- (3) The influence of the settling column walls on the formation and settling velocity of particle clusters should be investigated as a function of settling column size, slurry particle size, and slurry particle concentration.
- (4) Similar experiments should be performed over a broader range of particle concentrations to determine the dependence of slurry settling velocity on concentration.
- (5) Similar experiments should be performed to investigate the importance of cluster formation in slurries of flocculent particles.

7.3 ENGINEERING SIGNIFICANCE

This investigation has demonstrated that enhanced slurry settling velocities occur at very dilute concentration due to the formation of particle clusters. The extent of velocity enhancement has been shown, implicitly, to be influenced by the container-to-particle size ratio and by the velocity distribution of the slurry particles. These findings have important practical implications.

For those applications in which the object is to remove a solid from a fluid, (such as countercurrent and cocurrent separation processes), fluxes may be significantly

increased by operating at relatively more dilute rather than relatively more concentrated suspension concentrations. The separator cross-section should be designed taking particle size into account to minimize the influence of wall effects on the solid-fluid relative velocity.

For those applications in which the object is hydrodynamic particle classification, (such as particle size distribution measurements), the classification accuracy may be significantly improved by proper design of the classification vessel. The vessel cross-section should be selected to retard cluster formation by taking into account particle size and particle concentration.

For those applications which depend on contact time as well as relative particle-fluid motion, (such as fluidized bed reactors and processes involving simultaneous momentum transfer and heat or mass transfer), improved efficiency may result by designing and operating the process to promote cluster formation. That is, consideration should be given to the particle concentration and the particle-to-container size ratio.

REFERENCES

- (1) ADACHI, K., S. KIRIYAMA, and N. YOSHIOKA, Chem. Engin. Sci., 33, 115, (1978).
- (2) ANGUS, John C., David L. MORROW, John W. DUNNING, Jr., and Michael J. FRENCH, Ind. and Engin. Chem., 61 (2), 8, (1969).
- (3) BARFORD, N., Powder Tech., 6, 39, (1972).
- (4) BARNEA, E., and J. MIZRAHI, The Chem. Engin. J., 5 171, (1973).
- (5) BATCHELOR, G. K., J. Fluid Mech., 52, 245, (1972).
- (6) BERMAN, N. S., and V. A. SANTOS, AIChE J., 15(3), 323, (1969).
- (7) BEHN, V. C., and J. C. LIEBMAN, J. San. Engin. Div., ASCE, 89, SA3, Proc. Paper 3535, (1963).
- (8) BLOOM, Arnold L., "Gas Lasers", John Wiley and Sons, Inc., New York, N.Y., (1968).
- (9) BRADDICK, H. F. F., "Reports on Progress in Physics", ed. A. C. Strickland, XXIII, 154. The Physical Society, London, (1960).
- (10) BRINKMAN, H. C., Appl. Sci. Res., A1, 27, (1947).
- (11) BRINKMAN, H. C., J. Chem. Phys., 20, 571, (1952).
- (12) BURGERS, J. M., Proc. Koninkl. Akad. Wetenschap, (Amsterdam), 44, 1045, (1941).
- (13) BURGERS, J. M., Proc. Koninkl. Akad. Wetenschap, (Amsterdam), 45, 9, (1942).
- (14) CHANDRASEKHAR, S., "Radiative Transfer", Clarendon Press, Oxford, (1950).
- (15) CHENG, P. Y. and H. K. SCHACHMAN, J. Polymer Sci., 16, 19, (1955).
- (16) CHURCHILL, S. W., G. C. CLARK, and C. M. SLIENCEVICH, Disc. Faraday Soc., 30, 192, (1960).

- (17) CLEVITE CORP., "Elimination of Noise in Low-Level Circuits", Form No. LLS, Clevite Corp., Cleveland, Ohio, (1970).
- (18) COE, H. S., and G. H. CLEVINGER, Trans. A.I.M.E., 55, 356, (1916).
- (19) COMINGS, E. W., Ind. Engin. Chem., 32, 663, (1940).
- (20) DAVIES, Owen L., and Peter L. GOLDSMITH, "Statistical Methods in Research and Production", Oliver and Boyd, Edinburgh, (1972).
- (21) DICK, R. I., Proc., Fourth International Conf. on Water Poll. Res., Prague, 625, (1968).
- (22) DICK, R. I., and B. B. EWING, J. Water Poll. Control Fed., 39(4), 543, (1967).
- (23) DURST, F., A. MELLING, and J. H. WHITELOW, "Principles and Practice of Laser Doppler Anemometry", Academic Press Inc., London, (1976).
- (24) ECKENFELDER, W. W., Jr., and J. L. MANCINI, Paper presented at the National Symposium on Sanitary Engineering Research, Development, and Design. The Pennsylvania State Univ., University, Penn., (1965).
- (25) EINSTEIN, A., Ann. Phys., 19, 371, (1906).
- (26) EVESON, G. F., E. W. HALL, and S. G. WARD, Brit. J. Appl. Phys., 10, 43, (1959).
- (27) FAMULARO, J., Eng. Sc. D. Thesis, New York University, New York, N.Y., (1962)
- (28) FAMULARO, J., and J. HAPPEL, AIChE J., 11, 981, (1965).
- (29) FOREMAN, J. W., E. W. GEORGE, and R. D. LEWIS, Appl. Phys. Letters, 7, 77, (1965).
- (30) FOREMAN, J. W., R. D. LEWIS, J. R. THORTON, and H. J. WATSON, Proc. IEEE, 54, 425, (1966).
- (31) FORRESTER, A. T., J. Opt. Soc. Amer., 31, 253, (1961).
- (32) FORRESTER, A. T., R. A. GUDMUNDSEN, and P. O. JOHNSON, Phys. Rev., 99, 1691, (1955).

- (33) FORRESTER, A. T., W. E. PARKINS, and E. GERJUOY, *Phys. Rev.*, 72, 728, (1947).
- (34) FRISCH, H. L., and R. SIMHA, in "Rheology-Theory and Applications", Vol. I, ed. by F. R. Eirich, Academic Press, N.Y., (1956).
- (35) GAL-OR, B., *Can. J. Chem. Engin.*, 48, 526, (1970).
- (36) GASPARYAN, A. M., and A. A. ZAMINYAN, *Izvest. Akad. Navk Arminian SSR, Ser. Tekh Navk*, 12, 31, (1959).
- (37) GOLDMAN, A. J., R. G. COX, and H. BRENNER, *Chem. Engin. Sci.*, 21, 1151, (1966).
- (38) GOLDSTEIN, R. J., and W. F. HAGEN, *Phys. of Fluids*, 10, 1349, (1967).
- (39) GOLDSTEIN, R. J., and D. K. KREID, *J. Appl. Mech.*, 34-E, 813, (1967).
- (40) GOLDSTEIN, R. J. and D. K. KREID, HTL TR No. 85, University of Minnesota, Minneapolis, Minn., (1968).
- (41) GOLDSTEIN, R. J., R. J. ADRIAN, and D. K. KREID, *Ind. Engin. Chem. Fundamentals*, 8, 498, (1969).
- (42) GREEN, H. L., and W. R. LANE, "Particulate Clouds: Dusts, Smokes and Mists", E and F. N. Spon, Ltd., London, (1964).
- (43) GUTH, E., and R. SIMHA, *Kolloid Z.*, 74, 266, (1936).
- (44) HANRATTY, T. J., and A. BANDUKWALA, *Amer. Inst. Chem. Engrs. J.*, 3, 293, (1957).
- (45) HAPPEL, J., *AIChE J.*, 4, 197, (1958).
- (46) HAPPEL, J., and P. A. AST, *Chem. Engin. Sci.*, 11, 286, (1960).
- (47) HAPPEL, John, and Howard BRENNER, "Low Reynolds Number Hydrodynamics", Prentice-Hall Inc., Englewood Cliffs, N.J., (1965).
- (48) HAPPEL, J., and R. PFEFFER, *AIChE J.*, 6, 129, (1960).
- (49) HASIMOTO, H., *J. Fluid Mech.*, 5, 317, (1959).

- (50) HASSETT, N. J., *Ind. Chemist*, 34, 116; 34, 169; 34, 489, (1958).
- (51) HAWKSLEY, P. G. W., in "Some Aspects of Fluid Flow", Paper No. 7, Inst. Phys. and E. Arnold, London, (1951).
- (52) HESTRONI, G., S. HABER, and E. WACHOLDER, *J. Fluid Mech.*, 41, 689, (1970).
- (53) HOCKING, L. M., *J. Fluid Mech.*, 20, 129, (1964).
- (54) HODKINSON, J. R., in "Aerosol Science", ed. by C. N. Davies, Academic Press, London, (1966).
- (55) JOHNE, R., *Chemie Ing. Tech.*, 38, 428, (1966).
- (56) JAMES, R. N., W. R. BABCOCK, and H. S. SIEFERT, *A.I.A.A. J.*, 6, 160 (1968).
- (57) JAVAHERI, A. B., Ph.D. Dissertation, University of Illinois, Urbana, Ill., (1971).
- (58) JAYAWEERA, K. O. L. F., B. J. MASON, and G. W. SLACK, *J. Fluid Mech.*, 20, 121, (1964).
- (59) KAYE, B. H., and R. P. BOARDMAN, *Proc. Symp. Interaction between Fluid and Particles*, Inst. Chem. Engrs., 17, (1962).
- (60) KAMEL, M. T., E. M. TORY, and W. S. JODREY, *Powder Tech.*, 24, 19, (1979).
- (61) KEINATH, Thomas M., Mark D. RYCKMAN, Caleb H. DANA, and David A. HOFER, *J. Envir. Engin. Div., ASCE*, 103, 829, (1977).
- (62) KELLY, Louis G., "Handbook of Numerical Methods and Applications", Addison-Wesley Inc., Reading, Mass., (1967).
- (63) KENNEDY, John B., and Adam M. NEVILLE, "Basic Statistical Methods for Engineers and Scientists", IEP, New York, N.Y., (1976).
- (64) KERKER, M., Ed. "Interdisciplinary Conference on Electromagnetic Scattering", Pergamon Press Inc., New York, N.Y., (1963).

- (65) KOGLIN, Bernd, in "Particle Size Analysis", Univ. of Bradford, ed. by M. J. Groves and J. L. Wyatt-Sargent, The Soc. for Analytical Chem., London, (1970).
- (66) KOGLIN, B., *Chemie Ing. Tech.*, 43, 761, (1971).
- (67) KOGLIN, B., *Chemie Ing. Tech.*, 44, 515, (1972).
- (68) KOGLIN, B., *Proc. Conf. Particle Technology*, Chicago, Ill., 265, (1973).
- (69) KUWABARA, S., *J. Phys. Soc., Japan*, 14, 527, (1959).
- (70) KYNCH, G. J., *Trans. Faraday Soc.*, 28, 166, (1952).
- (71) LALLEMAND, A., in "Astronomical Techniques", ed. by W. A. Hiltner, *University of Chicago Press*, Chicago, Ill., (1962). 6
- (72) LECLAIR, B. P., and A. E. HAMIELEC, *Ind. Engin. Chem. Fundamentals*, 7, 542, (1968).
- (73) LEWIS, R. D., J. W. FOREMAN, and H. J. WATSON, *Phys. of Fluids*, 11, 433, (1968).
- (74) LOEFFLER, A. L., Jr., and B. F. RUTH, *AIChE J.*, 5, 310, (1959).
- (75) MANCINI, J. L., *Proc. 17th Industrial Waste Conf.*, Purdue University, 267, (1962).
- (76) MAUDE, A. D., and R. L. WHITMORE, *Brit. J. Appl. Phys.*, 9, 477, (1958).
- (77) McNOWN, J. S., and P. N. LIN, *Proc. Second Midwestern Conf. Fluid Mechanics*, Iowa State University, (1952).
- (78) MIE, G., *Ann. Phys. Lpz.*, 25, 377, (1908).
- (79) MOONEY, M., *J. Colloid Sci.*, 6, 162, (1951).
- (80) OLIVER, D. R., *Chem. Engin. Sci.*, 15, 230, (1961).
- (81) PIKE, E. B., D. A. JACKSON, P. J. BOURKE, and D. I. PAGE, *J. Sci. Inst.*, 1, 727, (1968).
- (82) RCA, "Phototubes and Photocells", *Technical Manual PT-60*, RCA, Harrison, N.J., (1968).

- (83) RICHARDSON, J. F., and R. A. MEIKLE, Trans. Instn. Chem. Engrs., 39, 348, (1961).
- (84) RICHARDSON, J. F., and W. H. ZAKI, Chem. Engin. Sci., 3, 65, (1954).
- (85) ROBERTS, E. J., Mining Engineering, 1, 61, (1949).
- (86) ROLFE, E., J. K. SILK, S. BOOTH, K. MEISTER, and R. M. YOUNG, Report No. CR-1199, NASA, (1968).
- (87) ROSCOE, R., Brit. J. Appl. Phys., 3, 267, (1952).
- (88) RUTGERS, I. R., Rheol. Acta, 2, 202, (1962).
- (89) SAITO, N. J., Phys. Soc., Japan, 5, 4, (1950).
- (90) SCOTT, K. J., Ind. Engin. Chem. Fundamentals, 7, 484, (1968).
- (91) SCOTT, K. J., Ind. Engin. Chem. Fundamentals, 7, 582, (1968a).
- (92) SCOTT, K. J., and J. L. ALDERTON, Trans. Inst. Mining Met., 75, C201, (1966).
- (93) SHANNON, P. T., R. D. DEHASS, E. P. STROUPE, and E. M. TORY, Ind. Engin. Chem. Fundamentals, 3, 250, (1964).
- (94) SHANNON, P. T., E. P. STROUPE, and E. M. TORY, Ind. Engin. Chem. Fundamentals, 2, 203, (1963).
- (95) SHANNON, P. T., and E. M. TORY, Trans. Soc. Mining Engin., 235, 375, (1966).
- (96) SHIN, B. S., and R. I. DICK, Proc., Seventh International Conf. on Water Poll. Res., Paris, (1974).
- (97) SHIRATO, M., H. KATO, K. KOBAYASHI, and H. SAKAZAKI, J. Chem. Engin., Japan, 3, 98, (1970).
- (98) SIMHA, R., J. Appl. Phys., 23, 1020, (1952).
- (99) SMITH, T. N., J. Fluid Mech., 32, 203, (1968).

- (100) SMOLUCHOWSKI, M., Bull. Acad. Sci., Cracow, 1A, 28, (1911).
- (101) STEINOUR, H. H., Ind. Engin. Chem., 36, 618; 36, 840; 36, 901, (1944).
- (102) STEINOUR, H. H., Ind. Engin. Chem., 52, 277, (1949).
- (103) STIMSON, M., and G. B. JEFFERY, Proc. Royal Soc., London, A111, 110, (1926).
- (104) STONE, J. M., "Radiation and Optics", McGraw-Hill Book Co. Inc., New York, N.Y., (1963).
- (105) TALMAGE, W. P., and E. B. FITCH, Ind. Engin. Chem., 47, 38, (1955).
- (106) THOMAS, D. G., J. Colloid Sci., 20, 267, (1965).
- (107) TORY, E. M., and D. K. PICKARD, Can. J. Chem. Engin., 55, 659, (1977).
- (108) TORY, E. M., and D. K. PICKARD, Fourth Can. Symp. Fluid Dynamics, Calgary, (1980).
- (109) TORY, E.M., and P.T. SHANNON, Ind. Engin. Chem., 57 (2), 18, (1965).
- (110) UCHIDA, S., Rept. Inst. Sci. Tech., Univ. Tokyo, 3, 97, (1949).
- (111) VAN DE HULST, H. C., "Light Scattering by Small Particles", John Wiley and Sons, Inc., New York, N.Y., (1957).
- (112) VAND, V. J., J. Phys. Colloid. Chem., 52, 277, (1948).
- (113) VOLK, William, "Applied Statistics for Engineers", McGraw-Hill Book Co. Inc., New York, N.Y., (1958).
- (114) YEH, Y., and H. Z. CUMMINS, Appl. Phys. Letters, 4(10), 176, (1964).
- (115) YOSHIOKA, N., Y. HOTTA, S. TANAKA, S. NAITO, and S. TSUGAMI, Kagaku Kogaku, 21, 66, (1957).
- (116) ZUBER, N., Chem. Engin. Sci., 19, 897, (1964).

APPENDIX I

CORRELATION BETWEEN PARTICLE CONCENTRATION AND AMPLITUDE OF THE DOPPLER SIGNAL

It was desired to determine if the time average of the amplitude of the Doppler signal could be used as an estimate of particle mass concentration. The envelope detector output voltage at each of the 40 grid points for a given run was compared to the corresponding mass concentration estimate. In Chapter 3 it was stated that theory predicts that the amplitude of the Doppler signal and the scattered intensity should be correlated. Therefore, the transmittance estimate of concentration was used in this comparison since this measurement was independent of the Doppler signal.

In order to make this comparison, it was necessary to account for the amplitude-frequency characteristics of the signal processing electronics. The Doppler frequency was estimated from the Doppler voltage measurement as previously described. The measured Doppler amplitude was then converted to that amplitude which would have been observed had the Doppler frequency been 1000 Hz using equation (V-4). This correction accounted for the non-linear attenuation of signal amplitude with frequency due to the bandpass filtering employed in the electronic processing.

The modified values of Doppler signal amplitude are plotted against estimated transmittance mass concentration in Figure I-1. These data, listed in Table I-1, are level-average values from each run. It is evident that a strong negative correlation exists between the amplitude of the Doppler signal and the particle mass concentration. A linear relationship was assumed between these variables and the least-squares model:

$$A = 5.0843 \times 10^{-2} - 1.6597 \times 10^{-2} C \quad (I-1)$$

where: A = envelope detector output, volts, and

C = mass concentration, gm/l,

was determined. It appears that, for a given Doppler anemometry instrument, it would be possible to obtain an estimate of the particle mass concentration by monitoring the amplitude of the Doppler signal.

FIGURE I-1
 ENVELOPE DETECTOR OUTPUT
 VS. CONCENTRATION

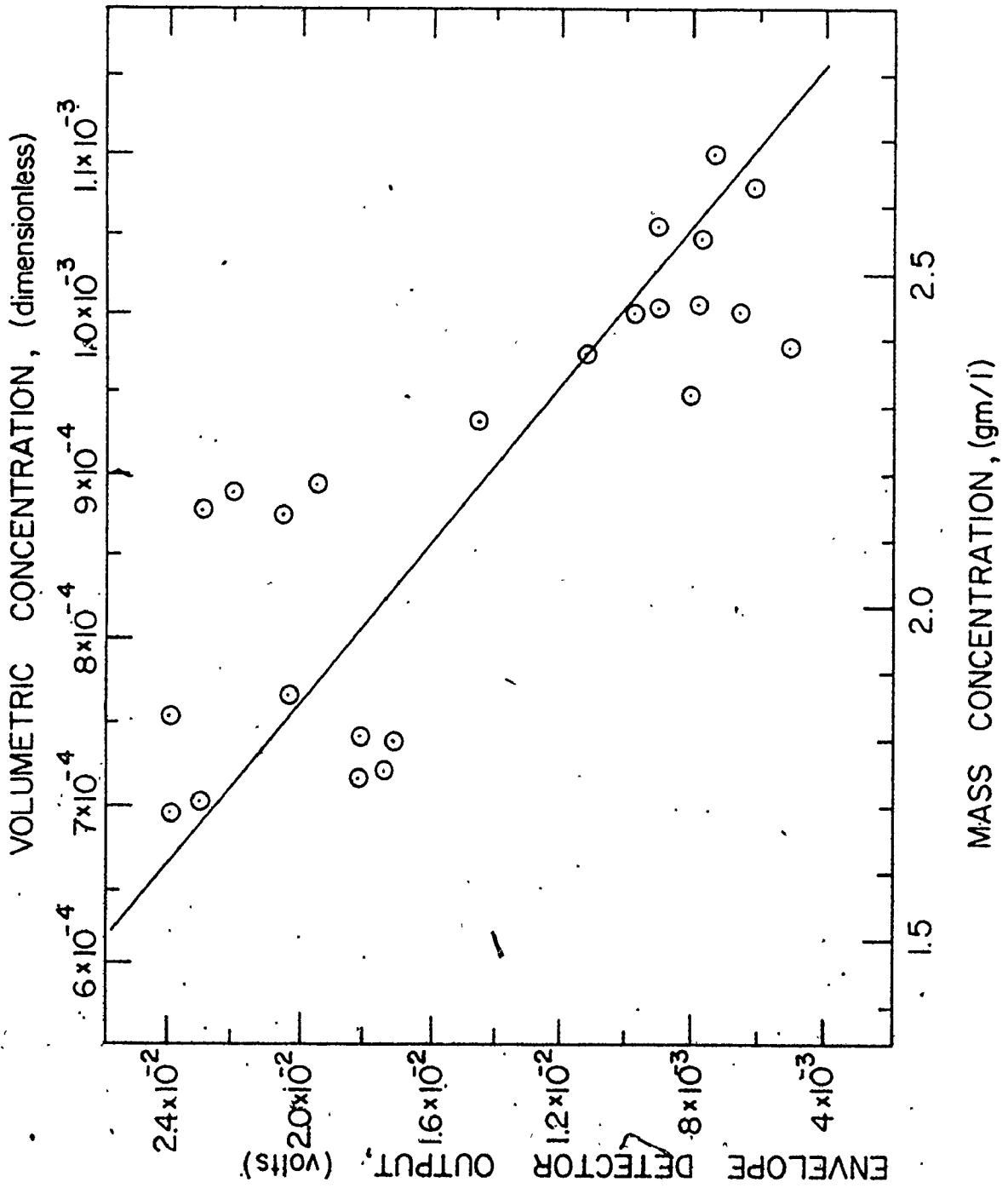


TABLE I-1
DOPPLER SIGNAL AMPLITUDE VS. MASS CONCENTRATION

Run	Level	Corrected Envelope Detector Output (volts)		Concentration (gm/l)	
		Mean	Variance*	Mean	Variance*
1	1	7.8852×10^{-3}	4.4953×10^{-6}	2.4541	2.0347×10^{-4}
	2	9.2285×10^{-3}	6.6111×10^{-6}	2.4540	4.3054×10^{-4}
	3	9.9199×10^{-3}	5.7402×10^{-6}	2.4433	7.7510×10^{-4}
	4	1.1264×10^{-2}	9.9450×10^{-6}	2.3809	4.9380×10^{-4}
2	1	2.0302×10^{-2}	1.5242×10^{-5}	1.8633	2.6435×10^{-4}
	2	2.4044×10^{-2}	2.5481×10^{-5}	1.8293	1.3343×10^{-3}
	3	1.8150×10^{-2}	3.6143×10^{-5}	1.8002	4.5889×10^{-4}
	4	1.7241×10^{-2}	2.0661×10^{-5}	1.7851	5.1237×10^{-4}
3	1	1.8162×10^{-2}	1.1097×10^{-5}	1.7428	2.4997×10^{-3}
	2	1.7456×10^{-2}	3.8907×10^{-5}	1.7505	1.8084×10^{-3}
	3	2.3058×10^{-2}	2.6509×10^{-5}	1.7005	1.9943×10^{-3}
	4	2.4021×10^{-2}	2.6315×10^{-5}	1.6800	9.3608×10^{-4}
4	1	6.7278×10^{-3}	3.0378×10^{-6}	2.4384	7.2169×10^{-4}
	2	5.1127×10^{-3}	6.2160×10^{-6}	2.3882	1.6257×10^{-3}
	3	8.1047×10^{-3}	2.4064×10^{-5}	2.3157	9.1341×10^{-4}
	4	1.4632×10^{-2}	2.2234×10^{-5}	2.2846	6.0925×10^{-4}

Table I-1 (Cont'd.)

Run	Level	Corrected Envelope Detector Output (volts)		Concentration (gm/l)	
		Mean	Variance*	Mean	Variance*
5	1	2.2088×10^{-2}	2.9430×10^{-5}	2.1658	1.6621×10^{-3}
	2	1.9539×10^{-2}	2.4957×10^{-5}	2.1782	4.9951×10^{-4}
	3	2.0622×10^{-2}	1.4032×10^{-5}	2.1389	1.7950×10^{-3}
	4	2.3013×10^{-2}	2.2457×10^{-5}	2.1375	1.5225×10^{-3}
6	1	7.5364×10^{-3}	2.9423×10^{-6}	2.6707	4.5078×10^{-4}
	2	6.2460×10^{-3}	9.7371×10^{-6}	2.6250	9.5163×10^{-4}
	3	7.8226×10^{-3}	4.1240×10^{-6}	2.5485	2.1094×10^{-3}
	4	9.2224×10^{-3}	1.3082×10^{-5}	2.5728	7.4433×10^{-4}

*Degrees of freedom = 7

APPENDIX II
CALIBRATION EXPERIMENTS FOR CONCENTRATION
AND VELOCITY MEASUREMENTS

II.1 CALIBRATION OF PARTICLE
CONCENTRATION MEASUREMENTS

Calibration experiments were performed for the transmitted intensity, the scattered intensity, and the combined transmittance-scattered intensity methods of estimating particle concentration. For these experiments, the experimental arrangement was identical to that used during the runs with two exceptions: a different laser source was used, and the experimental column was replaced with an aquarium.

The Spectra Physics 164 laser was not available for this phase of the study and was replaced by a Coherent Radiation model 54-A argon ion laser. The replacement laser produced an output with the same nominal specifications as did the Spectra Physics laser. However, apparent aging of the laser cavity decreased the output power to a level, (approximately 35 milliwatts at 4880 Å), significantly less than that used during the experimental runs, (approximately 1 watt at 4880 Å). Boiling of the cooling water as it circulated around the laser cavity caused the laser cavity to vibrate, and resulted in a noisy output beam.

An aquarium with the same cross-sectional area as the settling column was filled with three litres of distilled water which had been filtered through a double layer of 0.45 μm pore size membrane filters. Weighed quantities of the same particles used during the experimental runs were sequentially added.

After each addition of particles, the photomultiplier tube supply voltage was adjusted as described below and the detector ~~output~~ output voltage produced by each of the transmittance and scattering beams was recorded. After these measurements, light traps were inserted in the paths of both beams and the detector output was recorded to provide an estimate of background noise. Following each change in detector supply voltage, no data were collected for a period of ten minutes to allow the detector to reach a steady-state.

Care was taken during the alignment of the system to ensure that the aquarium face was normal to the transmittance beam and that incident laser beams were out of the zone of influence of the vortex caused by the magnetic mixer used to maintain completely mixed conditions in the aquarium.

II.1.1 Transmitted Intensity Calibration

To ensure stable operation of the photomultiplier tube, it was necessary to limit the photomultiplier anode current to a maximum of 10^{-6} amperes. Therefore, for each particle concentration measured by the transmittance method,

the absolute value of the photocathode supply voltage was increased in 100 volt steps until the detector output voltage was between 10 and 200 mv. The transmittance beam intensity was then measured at this supply voltage. The photomultiplier tube gain calibration, equation (VI-1), was used to determine the detector output voltage that would be observed at that photocathode supply voltage, (minus 2200 VDC), used throughout the experimental runs. Table II-1 lists these data. At the 95 percent confidence level, the model:

$$\log_{10} \left(\frac{I}{I_0} \right) = 2.0140 \times 10^{-3} - 2.5093 C \quad (\text{II-1})$$

where: I = transmittance beam voltage at mass concentration C , supply voltage = -2200 VDC, and

I_0 = transmittance beam voltage at mass concentration $C = 0$, supply voltage = -2200 VDC,

fit the data, Figure 4.

II.1.2 Scattered Intensity Calibration

Since the output power of the laser used in these calibration experiments was relatively low, the photocathode was operated at a higher absolute supply voltage (minus 2900 VDC) than during the experimental runs (minus 2200 VDC). This was necessary in order to obtain a measurable output voltage due to the low levels of scattered light reaching the photocathode. The photomultiplier gain calibration was used to account for this operating difference, Table II-2. The linear least-squares model:

TABLE II-1
 CALIBRATION OF TRANSMITTED INTENSITY VERSUS MASS CONCENTRATION

Mass Concentration (gm/l)	Operating Photomultiplier Supply Voltage, VDC (DC volts)	Transmitted Intensity (Volts)			Corrected for Background and Normalized
		Total	Background	Corrected for Background	
0	-1400	2.1859×10^{-1}	1.0105×10^{-4}	2.1849×10^{-1}	1.0000
0.25	-1400	5.4851×10^{-2}	9.9210×10^{-5}	5.4752×10^{-2}	2.5059×10^{-1}
0.50	-1400	1.0693×10^{-2}	9.7368×10^{-5}	1.0596×10^{-2}	4.8495×10^{-2}
0.75	-1800	3.9158×10^{-2}	9.6944×10^{-5}	3.9061×10^{-2}	1.4079×10^{-2}
1.00	-1800	8.4460×10^{-3}	9.7105×10^{-5}	8.3488×10^{-3}	3.0093×10^{-2}
1.25	-2400	4.6541×10^{-2}	9.9459×10^{-5}	4.6442×10^{-2}	9.1264×10^{-3}
1.50	-2400	9.7378×10^{-3}	9.9459×10^{-5}	9.6383×10^{-3}	1.8940×10^{-4}
1.75	-3000	2.0699×10^{-2}	1.0194×10^{-4}	2.0597×10^{-2}	4.2383×10^{-4}
2.00	-3000	4.6030×10^{-3}	1.0054×10^{-4}	4.5025×10^{-3}	9.2647×10^{-6}
2.25	-3000	1.0164×10^{-3}	1.0081×10^{-4}	9.1558×10^{-4}	1.8840×10^{-6}
2.50	-3000	3.4167×10^{-4}	1.0162×10^{-4}	2.4004×10^{-4}	4.9394×10^{-7}
2.75	-3000	1.7000×10^{-4}	1.0108×10^{-4}	6.8919×10^{-5}	1.4181×10^{-7}
3.00	-3000	1.1086×10^{-4}	1.0514×10^{-4}	5.7220×10^{-6}	1.1774×10^{-8}
3.25	-3000	1.1051×10^{-4}	1.0385×10^{-4}	6.6670×10^{-6}	1.3719×10^{-8}
3.50	-3000	1.0372×10^{-4}	1.0278×10^{-4}	9.4300×10^{-7}	1.9404×10^{-9}

TABLE II-2
 CALIBRATION OF SCATTERED INTENSITY VERSUS MASS CONCENTRATION

Mass Concentration (gm/ℓ)	Photomultiplier Supply = -2900 volts		Photomultiplier Supply = -2200 volts	
	Total (volts)	Background (volts)	Corrected for Background (volts)	Corrected for Background (volts)
0	1.0237×10^{-4}	1.0105×10^{-4}	1.3150×10^{-5}	8.0476×10^{-8}
0.25	1.9389×10^{-4}	9.9210×10^{-5}	9.4679×10^{-5}	5.7942×10^{-6}
0.50	1.7556×10^{-4}	9.7368×10^{-5}	7.8188×10^{-5}	4.7850×10^{-6}
0.75	1.4892×10^{-4}	9.6944×10^{-5}	5.1975×10^{-5}	3.1808×10^{-6}
1.00	1.2972×10^{-4}	9.7105×10^{-5}	3.2617×10^{-5}	1.9961×10^{-6}
1.25	1.1944×10^{-4}	9.9459×10^{-5}	1.9985×10^{-5}	1.2230×10^{-6}
1.50	1.0973×10^{-4}	9.9459×10^{-5}	1.0270×10^{-5}	6.2854×10^{-7}
1.75	1.0917×10^{-4}	1.0194×10^{-4}	7.2230×10^{-6}	4.4204×10^{-7}
2.00	1.0811×10^{-4}	1.0054×10^{-4}	7.5670×10^{-6}	4.6309×10^{-7}
2.25	1.0553×10^{-4}	1.0081×10^{-4}	4.7150×10^{-6}	2.8855×10^{-7}
2.50	1.0361×10^{-4}	1.0162×10^{-4}	1.9890×10^{-6}	1.2172×10^{-7}
2.75	1.0444×10^{-4}	1.0108×10^{-4}	3.3630×10^{-6}	2.0581×10^{-7}
3.00	1.0583×10^{-4}	1.0514×10^{-4}	6.9800×10^{-7}	4.2717×10^{-8}
3.25	1.0417×10^{-4}	1.0385×10^{-4}	3.2100×10^{-7}	1.9645×10^{-8}
3.50	1.0316×10^{-4}	1.0278×10^{-4}	3.8000×10^{-7}	2.3256×10^{-8}

$$\log_{10} \left[\frac{I_{sca}}{I_o} \right] = -3.0802 - 0.7663 C \quad (II-2)$$

where: I_{sca} = scattering beam voltage at mass concentration C , supply voltage = -2200 VDC, and

I_o = transmittance beam voltage at mass concentration $C = 0$, supply voltage = -2200 VDC,

was found to describe the dependence of adjusted voltage on mass concentration at the 95 percent confidence level, Figure 5.

The adjusted scattering beam voltages were normalized by the adjusted transmittance beam reference voltage to account for the difference in laser power between the experimental runs and the calibration experiment, (see section VI.3).

II.1.3 Combined Transmitted - Scattered Intensity Calibration

The least-squares model:

$$\log_{10} \left[\frac{I_{sca}}{I} \right] = -6.2759 + 1.7430 C \quad (II-3)$$

described the dependence of scattered intensity, normalized by the transmittance, on particle mass concentration at the 95 percent confidence level, Figure 5. The detector output voltages were corrected for background noise and adjusted to the supply voltage reference value of minus 2200 VDC as previously described.

II.1.4 Transmittance Beam Reference Intensity

The intensity of the transmittance beam with the settling column filled with water but devoid of particles was used as the reference intensity, I_0 , for estimating particle concentration by the transmittance method, equation (3-15), and by the scattered intensity method, equations (3-19) and (II-2). In the strict sense, the reference intensity of the scattering beam should be used in equation (3-19) and equation (II-2); however, it was impossible to accurately measure this intensity with the experimental arrangement employed. The transmittance beam reference intensity could be accurately measured. Since the polarization and wavelength of the laser source used in the calibration experiments were the same as those of the laser source used in the experimental runs, the ratio of transmittance beam reference intensity to scattering beam reference intensity could be assumed to be the same for both laser sources. Therefore, the transmittance reference intensity could be used to scale the scattered intensity calibration obtained with one laser source, equation (II-2), for use with the different laser source used during the experimental runs.

The reference intensity of the transmittance beam was measured immediately prior to the experimental runs. The photomultiplier output voltage was measured at four levels of detector supply voltage, (-800 to -1100 volts in -100 volt

increments), for each of seven nominal laser output powers (0.4 to 1.0 watts in 0.1 watt increments). For each laser output power, a least-squares model of the form:

$$\log_{10}(V_{\text{out}}) = \theta_0 + \theta_1 \log_{10}(V_{\text{supply}}) \quad (\text{II-4})$$

was observed to fit the data at the 95 percent confidence level. These models are listed in Table II-3; the data are plotted in Figure VI-1.

The variations in the intercepts among these models were probably caused by minor changes in the location of the laser output on the front mirror of the laser cavity as the output power was changed. The differences in the slopes among these models were significant at the 95 percent confidence level. This suggests that the amplification characteristic of the photomultiplier tube was a function of the input light intensity. This may have been due to increases in detector noise as the incident intensity increased, (so called "noise-in-signal"). Each of the slopes of the models listed in Table II-3 was significantly different from that determined at the termination of the experimental runs, 10.1126, [[see equation (VI-1)], and that provided by the photomultiplier tube manufacturer, 11.25. However, each of these slopes was determined for a different incident light intensity.

Since the experimental runs were conducted at a nominal laser output power of 1 watt, the model:

TABLE II-3
 LEAST-SQUARES MODELS FOR PHOTOMULTIPLIER
 TUBE CALIBRATION

Nominal Laser Output Power (watts)	Parameters in the Model $\log_{10}(V_{out}) = \theta_0 + \theta_1 \log_{10}(V_{supply})$	
	θ_0	θ_1
1.0	-36.7896 ^a	11.8317
0.9	-36.7140	11.7824
0.8	-36.6035	11.7185
0.7	-36.3925	11.6291
0.6	-36.4448	11.6218
0.5	-36.3430	11.5679
0.4	-36.1370	11.4777

$$\log_{10}(V_{\text{out}}) = -36.7896 + 11.8317 \log_{10}(V_{\text{supply}}) \quad (\text{II-5})$$

was used to estimate that transmitted reference intensity ($I_0 = 571.348$ volts) that would have been observed at a detector supply voltage of -2200, the supply voltage used in the experimental runs. The same model was used to estimate the transmitted reference intensity at a supply voltage of -2200, ($I_0 = 21.109$ volts), for the calibration experiments.

II.2 CALIBRATION OF PARTICLE VELOCITY MEASUREMENT

The frequency of the Doppler signal was calculated from the amplified output voltage of the frequency discriminator using equation (V-5). The particle velocity was calculated from the Doppler signal frequency using equation (3-7). Using the symbols in Figure 2 and performing the dot product in equation (3-7) gives:

$$W_D = \frac{nv}{(60)(\lambda_0)} \cos(\theta + \alpha) - \cos(\alpha) \quad (\text{II-6})$$

where: W_D = Doppler shift, Hz,

n = refractive index of water, 1.333,

λ_0 = vacuum wavelength of the incident light,
4.88 x 10⁻⁵ cm,

θ = angle between the scattering beam and the horizontal, 17°,

α = angle between scattering beam and the velocity vector, 73°; and

v = velocity relative to fixed reference frame,
cm/min.

That is:

$$v = \frac{W_D}{133.105} \quad (\text{II-7})$$

Equation (II-7) gives that component of the particle velocity relative to a fixed observer, in the direction $(\underline{n}_{sc} - \underline{n}_i)$.

The vertical component of this velocity is:

$$v = \frac{-W_D}{(133.105) \cos(\theta)} = \frac{-W_D}{127.289} \quad (\text{II-8})$$

This equation was used to calculate the particle settling velocities in this investigation.

Although the particle velocity could be calculated directly from equation (II-8) using the measured Doppler shift, a series of experiments was performed to calibrate the laser Doppler instrument. For this determination, the frequency shift in the light scattered from a transparent disc rotating at known angular speed was measured.

A six-inch-diameter, 1/8-inch-thick plexiglass disc was mounted on the shaft of a clock motor so that it rotated in a vertical plane normal to the transmittance beam at 1/5 rpm. The scattering beam and the transmittance beam intersected on the front surface of the disc in the same horizontal plane as the motor shaft. This ensured that the scattering point was aligned with the optical axis of the detector and that the velocity vector was vertical. To increase the amount of light scattered by the disc, one half of the front

surface was scored with a series of radial grooves at 0.5 degree increments.

The experimental apparatus was set up in the same manner as during the experimental runs. The angular velocity of the disc was measured with the laser Doppler instrument for two experimental arrangements. In one arrangement, the disc was positioned on the laser side of the settling column so that the light scattered by the disc passed through the settling column prior to reaching the detector. In the other arrangement, the disc was positioned on the detector side of the settling column so that the incident scattering beam passed through the settling column prior to reaching the disc. With the feed tank and the column filled with water, and the feed and underflow pumps operating, but with no particles added to the system, the Doppler shift was measured to calibrate the velocity measurement.

To determine the possibility of degrading the Doppler signal by multiple scattering of the incident scattering beam prior to reaching the sample volume and by multiple scattering of the scattered light as it traversed that portion of the slurry between the sample volume and the detector, weighed packets of slurry particles were sequentially added to the feed tank for both of the experimental arrangements. After each addition of particles, the settling column was

operated for approximately 8 hours so that a steady-state slurry concentration could be approached.

After each addition of particles, the absolute value of the photomultiplier supply voltage was increased in 100 volt steps until the measured intensity of the scattering beam was larger than the tube background (all light traps inserted) by a factor between 1.5 and 2.0. The intensity of the reference beam was then adjusted until the detector pre-amplifier output voltage was 1.0 ± 0.1 mv. This procedure ensured that the electronic processing instrumentation would "observe" the same Doppler signal amplitude relative to background and the same noise-in-signal as during the experimental runs.

For each particle concentration established in the settling column, the sequence of measurements shown in Table II-4 was followed. Measurements of the frequency and amplitude of the Doppler signal were discarded if the reference beam intensity changed by more than ten percent during these measurements. It will be noted from Table II-4 that the photocathode was operated at supply voltages other than the standard value used during the runs for the measurement of scattered light intensity and transmittance. This operational difference was accounted for using the amplification characteristics of the detector as previously described.

TABLE II-4
SEQUENCE OF MEASUREMENTS FOR ROTATING DISC EXPERIMENT

Step	Quantity Measured	Disc Motion	Laser Beams Applied		Photomultiplier Supply Voltage (DC volts)
			Reference Scattering	Transmittance	
1	Reference beam intensity	--	yes	no	Operating*
2	Doppler signal frequency	Rotating	yes	no	Operating
3	False alarms	Stationary	yes	no	Operating
4	False alarms	Rotating	yes	no	Operating
5	Reference beam intensity	--	yes	no	Operating
6	Doppler signal amplitude	Rotating	yes	no	Operating
7	Background for step 6	Rotating	yes	no	Operating
8	Background for step 6	Stationary	yes	no	Operating
9	Reference beam intensity	--	yes	no	Operating
10	Transmittance	Rotating	no	yes	-1500

Table II-4 (Cont'd.)

Step	Quantity Measured	Disc Motion	Laser Beams Applied		Photomultiplier Supply Voltage (DC volts)
			Reference Scattering	Transmittance	
11	Scattering beam intensity	Rotating	no	yes	-3000
12	Scattering beam intensity	Rotating	no	yes	Operating
13	Background for steps 10 and 12	Rotating	no	no	Operating

*Operating voltage is that level set by the criteria described/in text

It should be noted that the quality of the data collected in this calibration experiment was low due to the cavity generated frequency noise present in the laser output.

II.2.1 Rotating Disc on Detector Side of Column

The velocity determined from equation (II-8) is shown as a function of the transmittance estimate of slurry concentration in Figure II-1. The velocity estimate appeared to be independent of the slurry concentration for the range studied. This indicated that the velocity measurement was not sensitive to multiple scattering of the incident radiation prior to reaching the "sampling point."

For this experimental arrangement, the disc was positioned so that the angular velocity of a point 3.6 cm distant from the centre of the disc was measured. The angular velocity at this radial distance was determined from the equation:

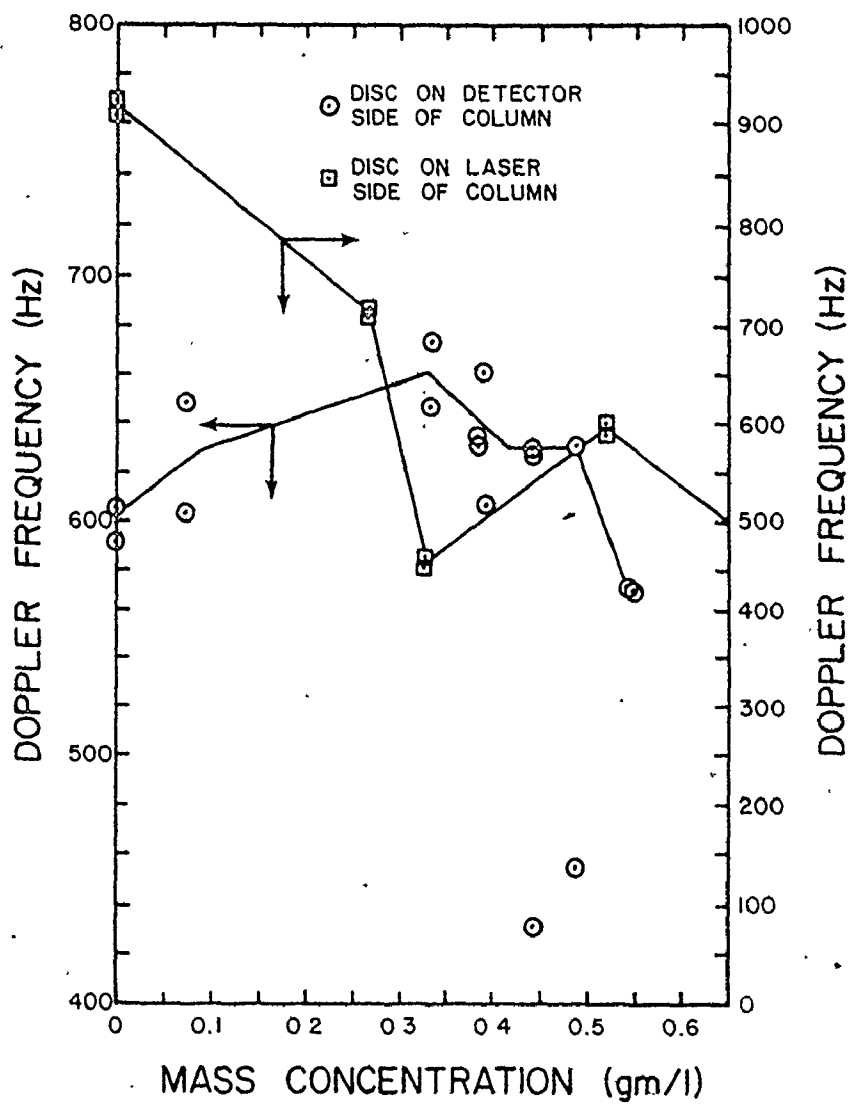
$$V = Wr \quad (\text{II-9})$$

where: V = angular velocity at radial distance r , and

W = rotational frequency of disc,

to be 4.52 cm/min, a value not too different from the particle velocities observed in the experimental runs. The mean value of the disc velocity, (see Table II-5), was not significantly different from the calculated velocity at the 95 percent confidence level, thereby demonstrating the accuracy of the laser Doppler instrument.

FIGURE II-1
DISC EXPERIMENT:
DOPPLER FREQUENCY VS. CONCENTRATION



II.2.2 Rotating Disc on Laser Side of Column

The disc velocity measured for this experimental arrangement is plotted as a function of the transmittance estimate of slurry concentration in Figure II-1. The measured velocity decreased as the slurry concentration increased. While these data might suggest that the multiple scattering experienced by the light scattered from the sampling volume affected the accuracy of the Doppler frequency determination, it is evident from Table II-5 that the frequency measurements for these data were inadvertently collected at an improper setting of the signal false-alarm level. As noted in Chapter 5, a false-alarm frequency of 100 ± 5 Hz was used throughout the experimental runs. This frequency was found to be a convenient trade-off between lower rates, which resulted in Doppler signal drop-out, and higher rates which degraded Doppler signal accuracy. The dependence of the measured frequency shift on the false-alarm rate for both experimental arrangements is shown in Figure II-2.

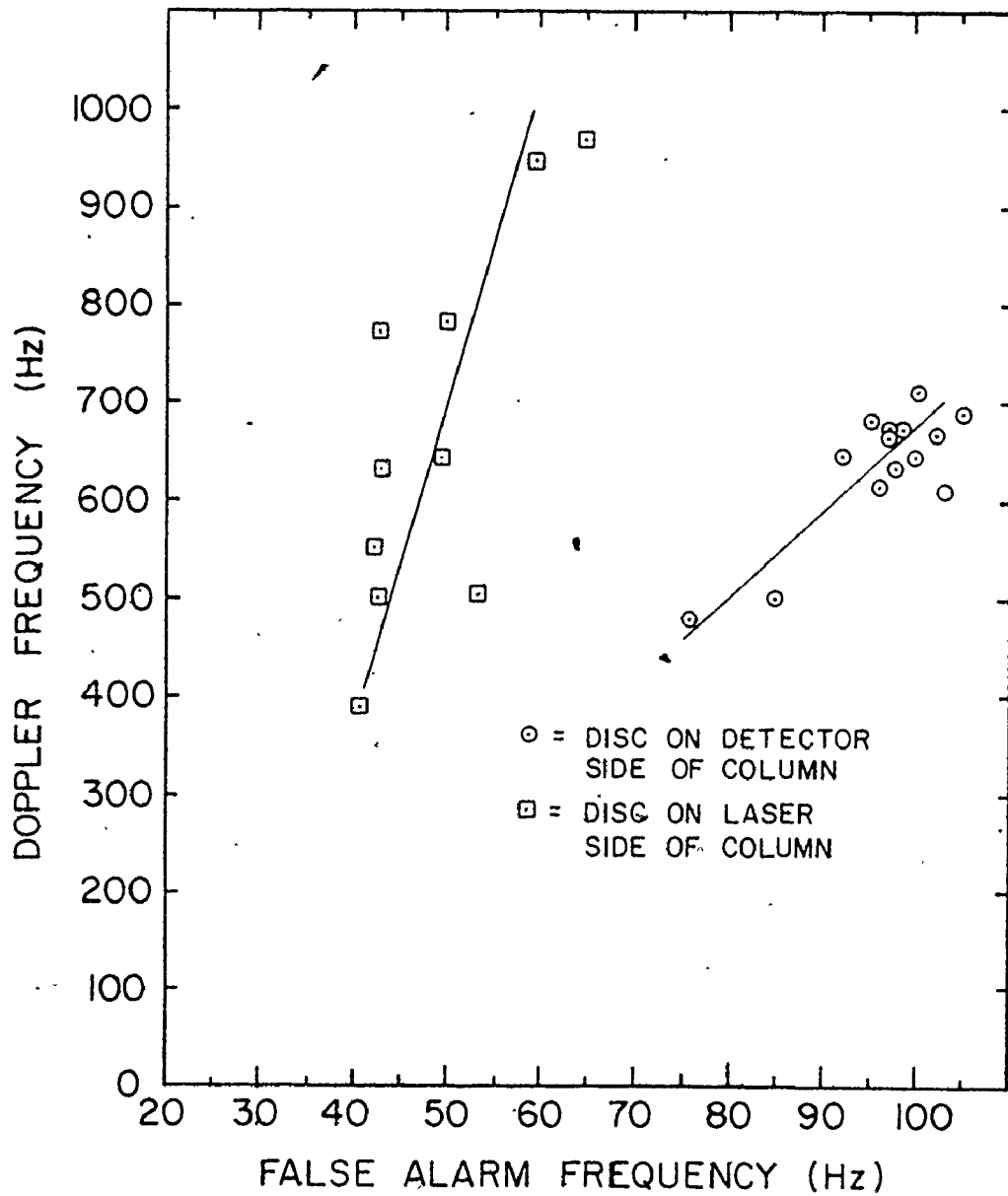
For the experiments in which the rotating disc was positioned on the laser side of the settling column, the velocity of a point 6 cm from the disc centre was measured. According to equation (II-9), a velocity of 7.53 cm/min should have been observed.

TABLE II-5

ROTATING DISC EXPERIMENT

Disc on Laser Side of Column				Disc on Detector Side of Column			
Slurry Concentration (gm/l)	Doppler Frequency (Hz)	Velocity (cm/min)	False-Alarm Frequency (Hz)	Slurry Concentration (gm/l)	Doppler Frequency (Hz)	Velocity (cm/min)	False-Alarm Frequency (Hz)
0.0	599	4.5	99	0.0	917	6.89	62
7.22×10^{-2}	625	4.7	98	2.66×10^{-1}	740	5.56	46
3.39×10^{-1}	659	4.96	97	2.74×10^{-1}	458	3.44	43
3.85×10^{-1}	637	4.79	97	5.20×10^{-1}	594	4.45	47
3.91×10^{-1}	635	4.77	92	7.65×10^{-1}	423	3.18	41
4.43×10^{-1}	628	4.72	102				
4.85×10^{-1}	634	4.76	97				

FIGURE II-2
DISC EXPERIMENT:
DOPPLER FREQUENCY
VS.
FALSE ALARM FREQUENCY



The low velocity values measured, and the apparent dependence of measured disc velocity on slurry concentration are probably artifacts of the low levels of false-alarm frequency employed in this portion of the calibration experiment.

II.3 VERIFICATION OF DOPPLER SIGNAL

It will be recalled from Chapter 3 that the amplitude of the Doppler signal is proportional to the square root of the power of the scattered radiation. That is:

$$i \propto \left[(P_{\text{sca}} + P_{\text{ref}}) + 2\sqrt{P_{\text{sca}}P_{\text{ref}}} \text{SIN } 2\pi(W_D t + \xi) \right] \quad (\text{II-10})$$

where: P_{sca} = power of scattered beam,

P_{ref} = power of reference beam,

W_D = Doppler frequency, and

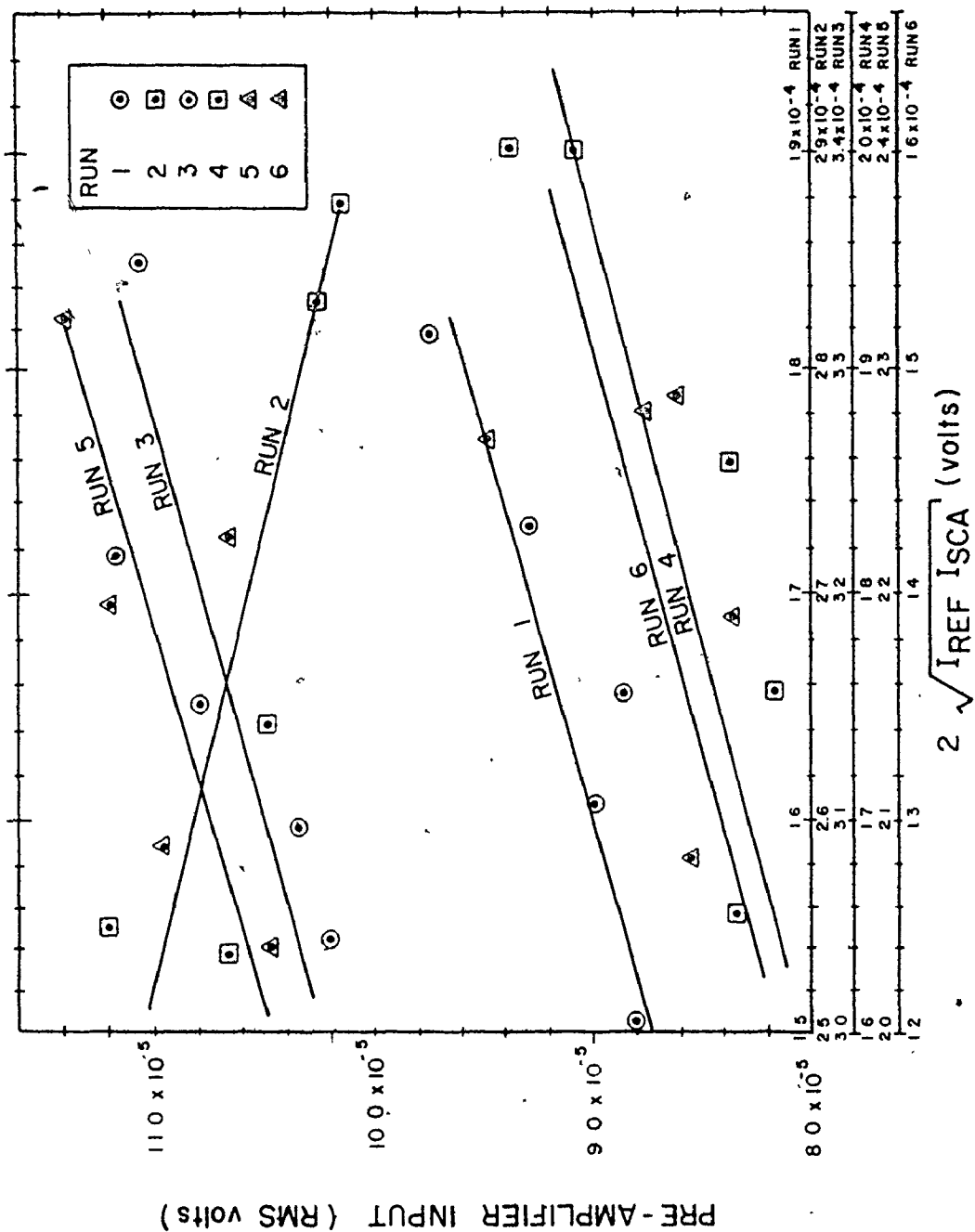
ξ = constant phase angle.

The first term in this equation is the DC current and the second term is the AC or Doppler current. Rolfe *et al.* (1968) note that, due to effects such as imperfect alignment between the scattered and reference beams at the photocathode and loss of coherence between the two beams, the Doppler amplitude is less than $2\sqrt{P_{\text{sca}}P_{\text{ref}}}$. This suggests that, for a given alignment of the laser Doppler instrument (that is, a given experimental run), the amplitude of the Doppler signal should be a linear function of $\sqrt{P_{\text{sca}}P_{\text{ref}}}$.

The correlation between the measured amplitude of the Doppler signal and the measured powers of the scattered and reference beams was determined for each of the experimental runs. In order to make this determination, it was necessary to account for the amplitude-frequency characteristics of the signal processing electronics. The Doppler frequency was estimated from the Doppler voltage measurement using equation (II-6). The envelope detector output voltage was then converted to that value which would have been observed had the Doppler frequency been 1000 Hz using equation (V-4). This correction accounted for the non-linear attenuation of signal amplitude with frequency due to the bandpass filtering employed in the signal processing. This equivalent envelope detector output was then corrected for the gain of the electronic system using equation (V-3) to provide an estimate of the voltage which would have been measured across the load at the photomultiplier anode. The output voltages of the photomultiplier tube when each of the scattered beam and the reference beam were individually applied were used as estimates of the power of these beams.

The modified values of the envelope detector output voltage are plotted as a function of the estimates of beam power in Figure II-3. These data are the average values for each of the five horizontal planes of each run. With the exception of run 2, a strong positive correlation exists

FIGURE II-3
PRE-AMPLIFIER INPUT
VS
LASER POWER



between the envelope detector output and the square root of the product of the estimates of beam power. It should be noted that the slopes of the linear least-squares correlations for each run are similar. The vertical displacement among the curves is probably due to differences in heterodyning efficiencies caused by run-to-run variations in optical alignment. Table II-6 lists these data. The run-average data are listed in Table II-7.

These correlations provide strong evidence that the AC signal measured during the experimental runs was caused by frequency differences between the scattered beam and the reference beam. The fact that the frequency of these signals could be used to predict the flux of particles through the column (see Chapter 6) provides strong evidence that a Doppler signal was measured.

TABLE II-6

LEVEL AVERAGE ESTIMATES OF PRE-AMPLIFIER INPUT AND LASER POWER

Run	Pre-Amplifier Input		Reference and Scattered Beam Powers		
	Level Distance Above Hopper (in)	Mean (volts)	Variance (volts) ²	Mean (volts)	Variance (volts) ²
1	2	8.600×10^{-5}	2.003×10^{-12}	1.504×10^{-4}	1.899×10^{-10}
2	4	8.860×10^{-5}	2.944×10^{-12}	1.655×10^{-4}	2.734×10^{-10}
3	8	9.001×10^{-5}	1.230×10^{-11}	1.606×10^{-4}	9.774×10^{-10}
4	12	9.289×10^{-5}	5.442×10^{-12}	1.729×10^{-4}	4.490×10^{-10}
5	18	9.737×10^{-5}	2.296×10^{-11}	1.816×10^{-4}	1.241×10^{-10}
1	2	1.066×10^{-4}	4.913×10^{-11}	2.537×10^{-4}	3.278×10^{-10}
2	4	1.122×10^{-4}	2.350×10^{-11}	2.550×10^{-4}	2.320×10^{-10}
3	8	1.048×10^{-4}	3.543×10^{-11}	2.641×10^{-4}	3.577×10^{-10}
4	12	1.024×10^{-4}	2.732×10^{-11}	2.835×10^{-4}	3.932×10^{-10}
5	18	1.014×10^{-4}	1.659×10^{-11}	2.876×10^{-4}	1.580×10^{-10}

Table II-6 (Cont'd.)

Run	Level		Pre-Amplifier Input			Reference and Scattered Beam Powers		
	No.	Distance Above Hopper (in)	Mean (volts)	Variance (volts) ²	v	Mean (volts)	Variance (volts) ²	v
1	2		1.020x10 ⁻⁴	1.765x10 ⁻¹¹	5	3.045x10 ⁻⁴	4.356x10 ⁻¹¹	5
2	4		1.032x10 ⁻⁴	5.688x10 ⁻¹¹	5	3.096x10 ⁻⁴	1.294x10 ⁻¹⁰	5
3	8		1.107x10 ⁻⁴	3.174x10 ⁻¹¹	5	3.349x10 ⁻⁴	3.631x10 ⁻¹⁰	5
4	12		1.119x10 ⁻⁴	1.528x10 ⁻¹¹	5	3.216x10 ⁻⁴	5.572x10 ⁻¹¹	5
5	18		1.079x10 ⁻⁴	2.218x10 ⁻¹¹	5	3.150x10 ⁻⁴	3.379x10 ⁻¹⁰	5
1	2		8.351x10 ⁻⁵	9.054x10 ⁻¹²	5	1.659x10 ⁻⁴	1.402x10 ⁻¹⁰	5
2	4		8.147x10 ⁻⁵	6.934x10 ⁻¹¹	5	1.756x10 ⁻⁴	6.561x10 ⁻¹¹	5
3	8		8.372x10 ⁻⁵	6.819x10 ⁻¹²	5	1.857x10 ⁻⁴	7.649x10 ⁻¹¹	5
4	12		9.381x10 ⁻⁵	1.238x10 ⁻¹¹	5	2.000x10 ⁻⁴	3.090x10 ⁻¹¹	5
5	18		9.094x10 ⁻⁵	5.824x10 ⁻¹²	5	2.001x10 ⁻⁴	9.750x10 ⁻¹¹	5

Table II-6 (Cont'd.)

Run	Level No.	Distance Above Hopper (in)	Pre-Amplifier Input		Reference and Scattered Beam Powers		
			Mean (volts)	Variance (volts) ²	Mean (volts)	Variance (volts) ²	$2\sqrt{V_{ref} V_{sca}}$
1	2		1.097×10^{-4}	3.088×10^{-11}	2.087×10^{-4}	1.773×10^{-10}	5
2	4		1.045×10^{-4}	6.511×10^{-11}	2.040×10^{-4}	8.940×10^{-11}	5
3	8		1.065×10^{-4}	2.612×10^{-11}	2.224×10^{-4}	8.448×10^{-11}	5
4	12		1.119×10^{-4}	1.825×10^{-11}	2.193×10^{-4}	3.107×10^{-11}	5
5	18		1.139×10^{-4}	3.258×10^{-11}	2.325×10^{-4}	2.951×10^{-10}	5
1	2		8.553×10^{-5}	5.861×10^{-12}	1.282×10^{-4}	4.119×10^{-10}	5
2	4		8.349×10^{-5}	2.699×10^{-11}	1.390×10^{-4}	5.758×10^{-11}	5
3	8		8.609×10^{-5}	1.433×10^{-11}	1.487×10^{-4}	8.937×10^{-11}	5
4	12		9.489×10^{-5}	1.286×10^{-10}	1.466×10^{-4}	4.189×10^{-11}	5
5	18		8.748×10^{-5}	9.173×10^{-12}	1.480×10^{-4}	3.535×10^{-11}	5

TABLE II-7
 RUN-AVERAGE ESTIMATES OF PRE-AMPLIFIER INPUT AND LASER POWER

Run	Pre-Amplifier Input		Reference and Scattered Beam Powers	
	Mean (volts)	Variance (volts) ²	Mean (volts)	Variance (volts) ²
1	8.865×10^{-5}	8.250×10^{-12}	1.624×10^{-4}	8.903×10^{-11}
2	1.065×10^{-4}	2.423×10^{-11}	2.641×10^{-4}	1.891×10^{-10}
3	1.070×10^{-4}	2.571×10^{-11}	3.177×10^{-4}	1.836×10^{-10}
4	8.563×10^{-5}	3.079×10^{-11}	1.818×10^{-4}	2.126×10^{-10}
5	1.081×10^{-4}	1.084×10^{-11}	2.135×10^{-4}	7.537×10^{-11}
6	8.750×10^{-5}	2.552×10^{-11}	1.406×10^{-4}	8.598×10^{-11}

APPENDIX III

VARIANCES ASSOCIATED WITH CONCENTRATION, VELOCITY, AND FLUX ESTIMATES

III.1 ANALYSIS OF VARIANCE FOR CONCENTRATION AND VELOCITY MEASUREMENTS

Analyses of variance were performed to estimate whether or not the observed variations in particle velocity and concentration within and between horizontal planes were significant relative to analytical error. A standard analysis for hierarchic classification with three sources of variation, (variation due to measurement at a single grid point; variation between the grid points within a single horizontal plane; and, variation between the horizontal planes within a given run), was used. For the concentration measurements, Tables 2 and 3, all five horizontal planes of a given run were used in the analysis. For the velocity measurements, Table 6, the top horizontal plane was not used in the analysis due to the influence of the slurry feed port at this level.

These analyses were performed for measurements in voltage units. The photomultiplier output voltages, corrected for background, due to the scattering beam and due to the transmittance beam were used as the two "concentration"

measurements. The amplified output voltage of the frequency discriminator was used as the "velocity" measurement.

In estimating the sums of squares for calculating the mean squares associated with variation between grid points within a single horizontal plane and those associated with variation between horizontal planes within a given run, a run-average value was used for the number of replicate measurements at single grid points, [Kennedy and Neville (1976)]. This value was within 10 percent of the number of replicate measurements made at any given grid point. The details of the analysis procedure are available in Davies and Goldsmith (1972).

III.2 VARIANCE IN VELOCITY MEASUREMENT FOR ESTIMATING THE PROBABILITY OF CLUSTER FORMATION

The variances of the velocity estimates were determined from the variances associated with measuring the frequency proportional output voltage of the frequency discriminator. Combining equations (V-5) and (II-6), the velocity was calculated from:

$$V = \frac{V_{\text{out}} - 4.906 \times 10^{-3}}{(127.289)(2.500 \times 10^{-4})} \quad (\text{III-1})$$

where: V = particle velocity relative to a fixed observer, cm/min, and

V_{out} = DC operational-amplifier output, volts.

The variance of the calculated velocity was estimated using a Taylor series expansion, [Volk (1958)]:

$$\text{Var}(v) = \left[\frac{\partial v}{\partial v_{\text{out}}} \right]^2 \text{Var}(v_{\text{out}}) = 988.864 \text{Var}(v_{\text{out}}) \quad (\text{III-2})$$

The variances of the least-squares parameter estimates in equation (V-5) were orders of magnitude less than those of the voltage measurements and were ignored for this determination.

Table 7 lists the average variance of the mean velocity for a grid point, (calculated from the distribution of replicate measurements about grid point means); the average variance of the mean velocity for a horizontal plane (calculated from the distribution of grid point means about horizontal plane means); and the variance of the mean velocity for each run, (calculated from the distribution of horizontal plane means about the global mean for each run). These average variances were calculated from an unweighted pooling over each run.

It is evident that those variances which include variations between grid points were significantly larger than those that did not. The former included contributions from relatively long term temporal variations in system operation while the latter did not. That is, the former were likely to include variations in velocity resulting from a relatively broad range of cluster sizes and concentrations; the latter were not. For the measured cluster velocities and the

predicted cluster sizes, the three minute sampling period at a single grid point resulted in the observation of a small number, (in the range of 2 to 4), of clusters. Therefore, that variance which included only variations within grid points provided the more accurate estimates of the true range of cluster sizes, (that is, the true range of the number of particles in a cluster), for calculating the probability of cluster formation. The individual run values of the variance of the mean velocity for a grid point were pooled for estimating n_1 and n_2 in equation (6-6).

For the magnitudes of velocity measured in this study, this resulted in 95 percent confidence limits which bracketed the mean velocities by plus and minus approximately 2.5 percent of the mean value.

III.3 VARIANCE OF VOLUMETRIC FLUX ESTIMATES

The measured underflow fluxes were compared to the fluxes predicted from the literature models listed in Tables 8, 9 and 10 and to the fluxes calculated from the run-average values of velocity and concentration. The 95 percent confidence intervals for each of these flux estimates, shown in Figure 22, were determined from the calculated flux variances.

III.3.1 Variance of Measured Underflow Flux

For each run, three replicate measurements were made for the underflow slurry volumetric flowrate, (Q_u , cm^3/min),

200

and for the underflow particle mass concentration, (C_u , gm/l). The volumetric flux, (ψ , cm/min), was determined from the relation:

$$\psi = \frac{C_u Q_u}{1000 \rho_p A} \quad (\text{III-3})$$

where: ρ_p = measured particle density, (gm/cm³), and
 A = column cross-sectional area, (cm²).

The variance of this flux was determined from the approximation:

$$\begin{aligned} \text{Var}(\psi) &= \left[\frac{\partial \psi}{\partial C_u} \right]^2 \text{Var}(C_u) + \left[\frac{\partial \psi}{\partial Q_u} \right]^2 \text{Var}(Q_u) + \left[\frac{\partial \psi}{\partial \rho_p} \right]^2 \text{Var}(\rho_p) \\ &= \left[\frac{Q_u}{1000 \rho_p A} \right]^2 \text{Var}(C_u) + \left[\frac{C_u}{1000 \rho_p A} \right]^2 \text{Var}(Q_u) \\ &\quad + \left[\frac{-C_u Q_u}{\rho_p^2 1000 A} \right]^2 \text{Var}(\rho_p) \end{aligned} \quad (\text{III-4})$$

using the data in Table III-1. The variance of the particle density, ρ_p , is determined in Appendix IV. The 95 percent confidence limits were determined using the t statistic:

$$\psi \pm t_{0.05, \nu} \sqrt{\text{Var}(\psi)} \quad (\text{III-5})$$

Two degrees of freedom, ν , were used for this determination since this was the minimum number of degrees of freedom associated with any of the random variables in equation (III-3). This resulted in a conservative estimate of the 95 percent confidence interval for ψ .

TABLE III-1
 COMPONENT RANDOM VARIABLES FOR FLUX CALCULATIONS

Run	Underflow Flowrate		Underflow Concentration	
	Mean (cm^3/min)	Variance* (cm^3/min) ²	Mean (gm/ℓ)	Variance* (gm/ℓ) ²
1	72.51	3.1611×10^0	42.2774	2.3210×10^{-2}
2	114.05	3.2242×10^1	23.7027	2.3052×10^{-2}
3	48.87	5.1131×10^{-2}	42.6889	2.5517×10^{-1}
4	97.06	9.5010×10^{-1}	29.6226	3.3744×10^{-1}
5	96.30	3.6839×10^{-1}	26.4310	2.1937×10^{-1}
6	49.22	6.9972×10^{-1}	58.9156	1.7089×10^0

*Note: All variances are variance of mean values

TABLE III-1
COMPONENT RANDOM VARIABLES FOR FLUX CALCULATIONS

Run	Run-Average Doppler Velocity		Run-Average Volumetric Concentration		Maximum Literature Model Velocities $V = V_{\text{model}} + \frac{Q_u}{A}$ (cm/min)
	Mean (cm/min)	Variance* (cm/min) ²	Mean (Dimensionless)	Variance* (Dimensionless)	
1	5.556	5.2358×10^{-3}	9.9475×10^{-4}	5.1517×10^{-11}	4 3.85
2	6.014	2.5229×10^{-2}	7.4339×10^{-4}	4.5680×10^{-11}	4 4.03
3	6.198	5.7038×10^{-2}	7.0684×10^{-4}	3.2978×10^{-11}	4 3.75
4	3.914	7.0818×10^{-2}	9.6806×10^{-4}	1.6143×10^{-10}	4 3.95
5	5.901	2.2562×10^{-2}	8.8016×10^{-4}	3.5390×10^{-11}	4 3.95
6	3.697	2.0935×10^{-1}	1.6638×10^{-3}	1.1164×10^{-10}	4 3.75

*Note: All variances are variance of mean values

III.3.2 Variance of Flux Predicted by Literature Models

For this comparison, the flux predicted by the literature models was determined from the relation:

$$\psi = (V_{\text{model}} + \frac{Q_u}{A}) \phi \quad (\text{III-6})$$

where: V_{model} = relative velocity predicted by the literature model, cm/min, and

ϕ = run-average volumetric concentration.

The literature models are of the form:

$$V_{\text{model}} = V_{\text{ST}}(\zeta) \quad (\text{III-7})$$

where: V_{ST} = Stokes velocity estimate, cm/min, and

ζ = function modifying Stokes velocity, dimensionless.

The variance of the flux was determined from the approximation:

$$\begin{aligned} \text{Var}(\psi) &= \left[\frac{\partial \psi}{\partial \phi} \right]^2 \text{Var}(\phi) + \left[\frac{\partial \psi}{\partial Q_u} \right]^2 \text{Var}(Q_u) \\ &+ \left[\frac{\partial \psi}{\partial V_{\text{ST}}} \right]^2 \text{Var}(V_{\text{ST}}) = \left[V_{\text{model}} + \frac{Q_u}{A} \right]^2 \text{Var}(\phi) \\ &+ \left[\frac{\phi}{A} \right]^2 \text{Var}(Q_u) + [\phi(\zeta)]^2 \text{Var}(V_{\text{ST}}) \quad (\text{III-8}) \end{aligned}$$

The variance of the Stokes velocity estimate is determined in Appendix IV.

The 95 percent confidence interval was determined using equation (III-5). A conservative estimate of this interval was obtained by using the minimum number of degrees

of freedom, $\nu = 2$, associated with any of the random variables in equation (III-6).

The Stokes velocity calculated from the measured parameters for the mean size particle, $V_{ST} = 3.54667 \pm 2.96301 \times 10^{-1}$ cm/min, was used in the literature models rather than the measured terminal settling velocity of 100 individual slurry particles, $V_{ST} = 3.03136 \pm 0.546618$ cm/min. The calculated value resulted in predicted fluxes 15 percent higher than those predicted using the measured value. That is, the literature models were placed in the best possible light for the comparison to the measured underflow fluxes.

It should be noted that there was no significant difference between the two estimates of the individual particle Stokes velocity at the 95 percent confidence level.

III.3.3 Variance of Flux Calculated from Measured Velocity and Concentration

The flux determined from the run-average estimates of velocity and concentration were determined from:

$$\psi = V\phi \quad (\text{III-9})$$

where: V = measured velocity relative to fixed observer, cm/min, and

ϕ = volumetric concentration.

The variance of the calculated flux was determined using the approximation:

$$\begin{aligned}\text{Var}(\psi) &= \left[\frac{\partial \psi}{\partial \phi} \right]^2 \text{Var}(\phi) + \left[\frac{\partial \psi}{\partial V} \right]^2 \text{Var}(V) \\ &= v^2 \text{Var}(\phi) + \phi^2 \text{Var}(V)\end{aligned}\quad (\text{III-10})$$

Three degrees of freedom were used in equation (III-9) for the determination of the 95 percent confidence interval.

III.3.4 Comparison of Calculated and Predicted Fluxes to Measured Flux

The t statistic was used to compare the volumetric fluxes calculated from the run-average velocity and concentrations and the volumetric fluxes predicted by the literature models to those measured at the column underflow, Table III-2.

With the exception of run 4, there was no significant difference at the 95 percent confidence level between the calculated fluxes and the measured fluxes. This lends strong support to accuracy of the laser Doppler measurement of particle velocity in this study.

At the 95 percent confidence level, none of the literature models predicted fluxes which agreed with the measured underflow fluxes. This indicates that none of the literature models accurately described the dependence of velocity on concentration for the range studied.

TABLE III-2

VOLUMETRIC FLUX ESTIMATES

Run	Measured at Underflow		Calculated from Doppler Velocity and Measured Concentration		Maximum Predicted from Literature Models		t Statistics	
	Mean (cm/min)	Variance (v=2) (cm/min) ²	Mean (cm/min)	Variance (v=3) (cm/min) ²	Mean (cm/min)	Variance (v=2) (cm/min) ²	Calculated: Measured	Literature: Measured
1	5.41308x10 ⁻³	5.94316x10 ⁻⁸	5.5270x10 ⁻³	6.7714x10 ⁻⁹	3.8224x10 ⁻³	4.7780x10 ⁻⁹	1.12	6.28*
2	4.77986x10 ⁻³	6.05730x10 ⁻⁸	4.4708x10 ⁻³	1.5594x10 ⁻⁸	2.9922x10 ⁻³	3.6811x10 ⁻⁹	0.44	7.05*
3	3.67583x10 ⁻³	3.97810x10 ⁻⁹	4.3812x10 ⁻³	2.9764x10 ⁻⁸	2.6473x10 ⁻³	2.8105x10 ⁻⁹	3.84	12.5*
4	5.08343x10 ⁻³	1.59314x10 ⁻⁸	3.7886x10 ⁻³	6.8838x10 ⁻⁸	3.8248x10 ⁻³	6.9431x10 ⁻⁹	4.45*	8.32*
5	4.50008x10 ⁻³	9.81738x10 ⁻⁹	5.1935x10 ⁻³	1.8710x10 ⁻⁸	3.4759x10 ⁻³	4.2074x10 ⁻⁹	4.11	8.65*
6	5.12596x10 ⁻³	2.39834x10 ⁻⁸	3.9326x10 ⁻³	2.3842x10 ⁻⁷	3.9825x10 ⁻³	6.9241x10 ⁻⁹	2.329	6.50*

*Significant at 95 percent confidence level

APPENDIX IV
CHARACTERIZATION OF SLURRY PARTICLES

IV.1 PARTICLE SIZE DISTRIBUTION

The particle size distribution was measured with a Zeiss model TGZ 3 counter using photographs of the particles taken at a calibrated degree of enlargement. This instrument produced a histogram of particle numbers as a function of the diameter of a circular spot of light, which diameter was adjusted to match the diameter of a large number of particles, one at a time.

The iris diameter of the counter was continuously adjustable between 1.0 and 9.0 mm; this range was divided into 48 segments for recording the distribution histogram. In order to approximate a uniform counting variance over all 48 intervals, the iris diameter was exponentially related to the interval number. Use of the instrument in the exponential mode necessitated applying a separate correction factor to the observed number of particles in each interval. These factors were provided by the instrument manufacturer.

In order to obtain an accurate representation of the particle distribution, over six thousand particles were counted from photographs taken at an enlargement of 184.8. The degree of enlargement was determined from the measurements

of the distance between random pairs of adjacent markings of a scale with 500 micrometer divisions. This calibration scale was included in each photograph of the slurry particles.

The instrument was calibrated from measurements of interval number as a function of iris diameter. The latter was measured with a precision scale for 20 settings of iris diameter over the approximate range of 1.5 to 8.5 mm. These data, corrected for magnification, were used to determine the relationship between particle diameter and interval number. The model:

$$\log_{10}(D_p) = 2.1190 \times 10^{-1} + 3.1029 \times 10^{-2} I \quad (\text{IV-1})$$

where: D_p = particle diameter, micrometers, and
 I = interval number.

fit these data at the 95 percent confidence level.

The particle size distribution is shown in Figure IV-1; Figure 14 is a plot of the cumulative particle size distribution calculated from the data in Table IV-1. From Figure 14, it can be seen that the particle diameters were approximately normally distributed with a mean of 27.5 micrometers and a standard deviation of 5.4 micrometers.

IV.2 PARTICLE STOKES VELOCITY DISTRIBUTION

The particle Stokes velocity distribution was calculated from the measured particle size distribution using equation (2-2):

FIGURE IV-1

PARTICLE SIZE DISTRIBUTION

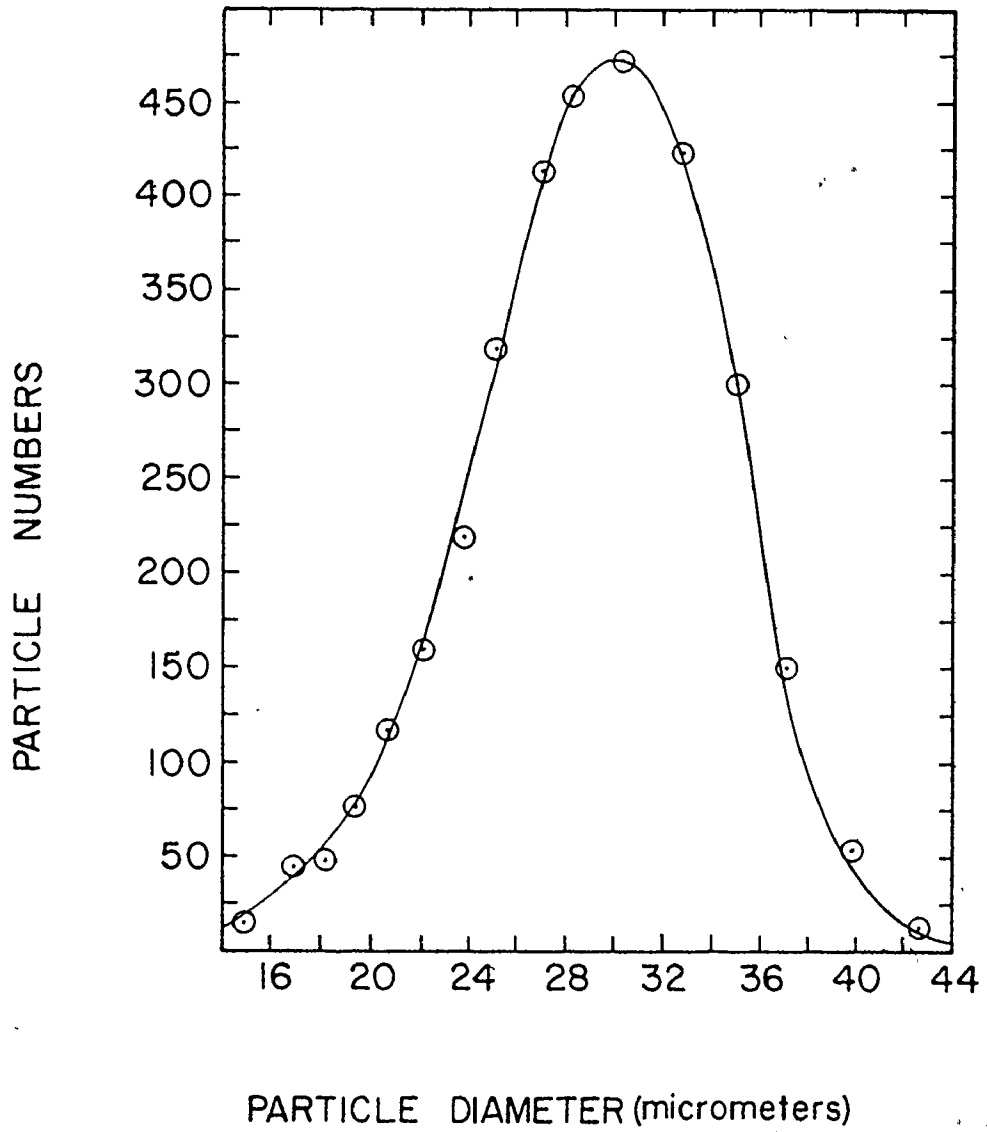


TABLE IV-1

DETERMINATION OF PARTICLE SIZE DISTRIBUTION

Interval Number	Number of Particles		Particle Diameter (micrometers)	Particle Velocity (cm/min)	Corrected Cumulative Distribution (Percentage Σ)	
	Observed	Corrected			Number	Velocity
21	2	3.66	8.33	0.325	0.110	0.356
22	4	6.84	8.87	0.369	0.315	0.980
23	1	1.62	9.47	0.421	0.364	1.12
24	1	1.51	10.12	0.480	0.409	1.24
25	2	2.84	10.80	0.547	0.495	1.44
26	4	5.28	11.53	0.624	0.653	1.74
27	4	4.96	12.34	0.714	0.802	2.01
28	3	3.48	13.10	0.805	0.907	2.17
29	8	8.72	14.02	0.922	1.17	2.53
30	16	16.32	14.99	1.054	1.66	3.41
31	25	24.00	15.96	1.195	2.38	4.63
32	52	46.80	17.05	1.363	3.78	6.85
33	58	48.72	18.18	1.550	5.25	9.02
34	97	76.63	19.42	1.769	7.55	12.22
35	157	116.18	20.73	2.105	11.04	16.76

Table IV-1 (Cont'd.)

Interval Number	Number of Particles		$\frac{\text{Corrected}}{2K D_p}$	Particle Diameter (micrometers)	Particle Velocity (cm/min)	Corrected Cumulative Distribution (Percentage Σ)	
	Observed	Corrected				Number	Velocity
36	233	160.77	774.52	22.13	2.297	15.86	22.64
37	336	218.40	984.53	23.65	2.623	22.42	30.12
38	524	319.64	1351.21	25.22	2.983	32.02	40.38
39	726	413.82	1640.70	26.89	3.391	44.45	52.84
40	855	453.15	1677.48	28.80	3.890	58.05	65.58
41	940	470.00	1633.24	30.68	4.414	72.16	77.98
42	901	423.47	1378.96	32.74	5.027	84.88	88.45
43	652	286.88	870.87	35.12	5.785	93.49	95.07
44	349	143.09	409.21	37.28	6.518	97.79	98.18
45	157	59.66	159.69	39.83	7.440	99.58	99.39
46	34	12.24	30.72	42.48	8.463	99.95	99.62
47	5	1.70	4.00	45.35	9.645	100	99.66
48	0	--	--	--	--	--	--

$$V_{ST} = K D_p^2 \quad (IV-2)$$

where: V_{ST} = particle Stokes velocity, cm/min,
 D_p = particle diameter, micrometers, and
 $K = \frac{(\rho_p - \rho_f)g}{18\mu}$.

The value of K was calculated to be 4.68988×10^{-3} cm/(micrometer²·min) using the measured particle density.

The particle Stokes velocity distribution is shown in Figure IV-2. This was obtained from the particle size distribution, Figure IV-1, by dividing the ordinate values by the factor $(2K D_p)$ and by multiplying the abscissa values by the factor, $(K D_p)$. The cumulative particle Stokes velocity distribution, Figure 15, was obtained from the cumulative particle size distribution, Figure 14, by multiplying the abscissa values by the factor $(K D_p)$.

The Stokes velocities of the slurry particles were observed to be approximately normally distributed, Figure 15, with a mean of 3.4 cm/min and a standard deviation of 1.45 cm/min.

IV.3 PARTICLE DENSITY DETERMINATION

The apparent density of the particles was estimated using a standard density bottle analysis, Table IV-2. This determination was performed using three 25 cm³ density bottles. The volume of each bottle was determined by the difference in weights between the empty bottle and the bottle filled with

FIGURE IV-2
STOKES VELOCITY DISTRIBUTION

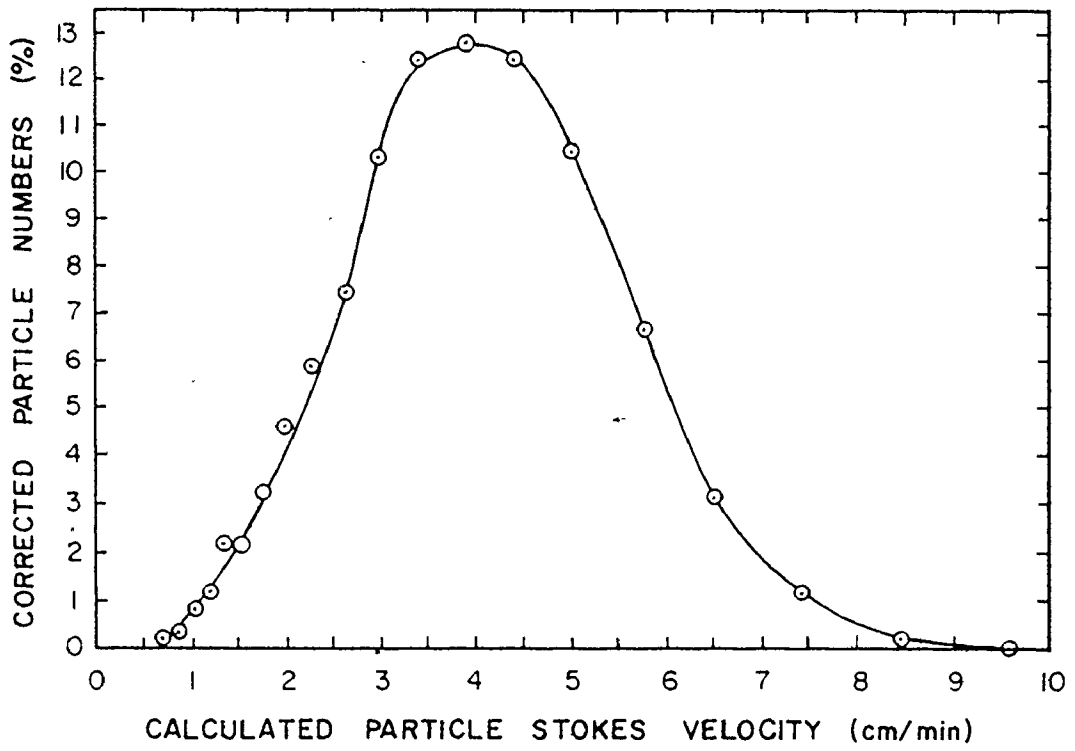


TABLE IV-2

DETERMINATION OF PARTICLE DENSITY

Bottle Number	Bottle Volume Determination			Density of Water (gm/cm ³)	Volume of Bottle (cm ³)
	Empty Bottle	Weight (gms) Bottle Plus Water	Water		
1	16.2872	41.1645	24.8773	0.99711	24.9494
2	15.4053	40.3652	24.9599	0.99711	25.0322
3	15.8312	40.7510	24.9198	0.99711	24.9920

✓

Table IV-2 (Cont'd.)

Bottle Number	Particle Density Determination						Particle Density (gm/cm ³)
	Weight (gms)			Volume (cm ³)			
	Bottle Plus Particles	Bottle Plus Particles Plus Water	Water	Water	Water	Particles	
1	21.9145	44.4561	22.5416	22.60693	2.34247	2.40229	
2	19.7616	42.9205	23.1589	23.22602	1.80622	2.41183	
3	17.7345	41.8922	24.1577	24.22772	0.76431	2.49022	

water. The determination was performed under conditions of thermal equilibrium; the ambient air temperature and the fluid temperature differed by less than 0.10°C . All temperatures were measured with a digital thermometer; all weighings were made on a Mettler balance to $\pm 1.0 \times 10^{-4}$ gms. The mean apparent particle density was determined to be $2.4348 \pm 1.1987 \times 10^{-1}$ gm/cm³ at the 95 percent confidence level.

IV.4 UNCERTAINTY IN THE CALCULATION OF STOKES VELOCITY

Stokes velocity was calculated from the measured particle diameter and density using equation (2-2):

$$V_{ST} = \frac{(\rho_p - \rho_f) D_p^2 g}{18\mu}$$

The variance of the Stokes velocity calculations were estimated using a Taylor series approximation, [Volk (1958)]:

$$\begin{aligned} \text{Var}(V_{ST}) &= \left[\frac{\partial V_{ST}}{\partial \rho_p} \right]^2 \text{Var}(\rho_p) + \left[\frac{\partial V_{ST}}{\partial D_p} \right]^2 \text{Var}(D_p) \\ &= \left[\frac{D_p^2 g}{18\mu} \right]^2 \text{Var}(\rho_p) + \left[\frac{2(\rho_p - \rho_f) D_p g}{18\mu} \right]^2 \text{Var}(D_p) \end{aligned} \quad (\text{IV-3})$$

Using the mean values for particle density and particle diameter, the variance of the Stokes velocity was calculated to be 5.4287×10^{-4} (cm/min)². The contribution to this variance due to the uncertainty in the estimation of particle density, the first term in equation (IV-3), was more than two orders of magnitude less than that due to uncertainty in the estimation

of particle diameter, the second term in equation (IV-3).

Therefore, since the particle diameters were normally distributed to a close approximation, an infinite number of degrees of freedom, ($t_{0.05} = 1.96$), was assumed in estimating the 95

percent confidence limits of the Stokes velocity for the mean particle size: $V_{ST} = 3.5467 \pm 4.5667 \times 10^{-2}$ cm/min.

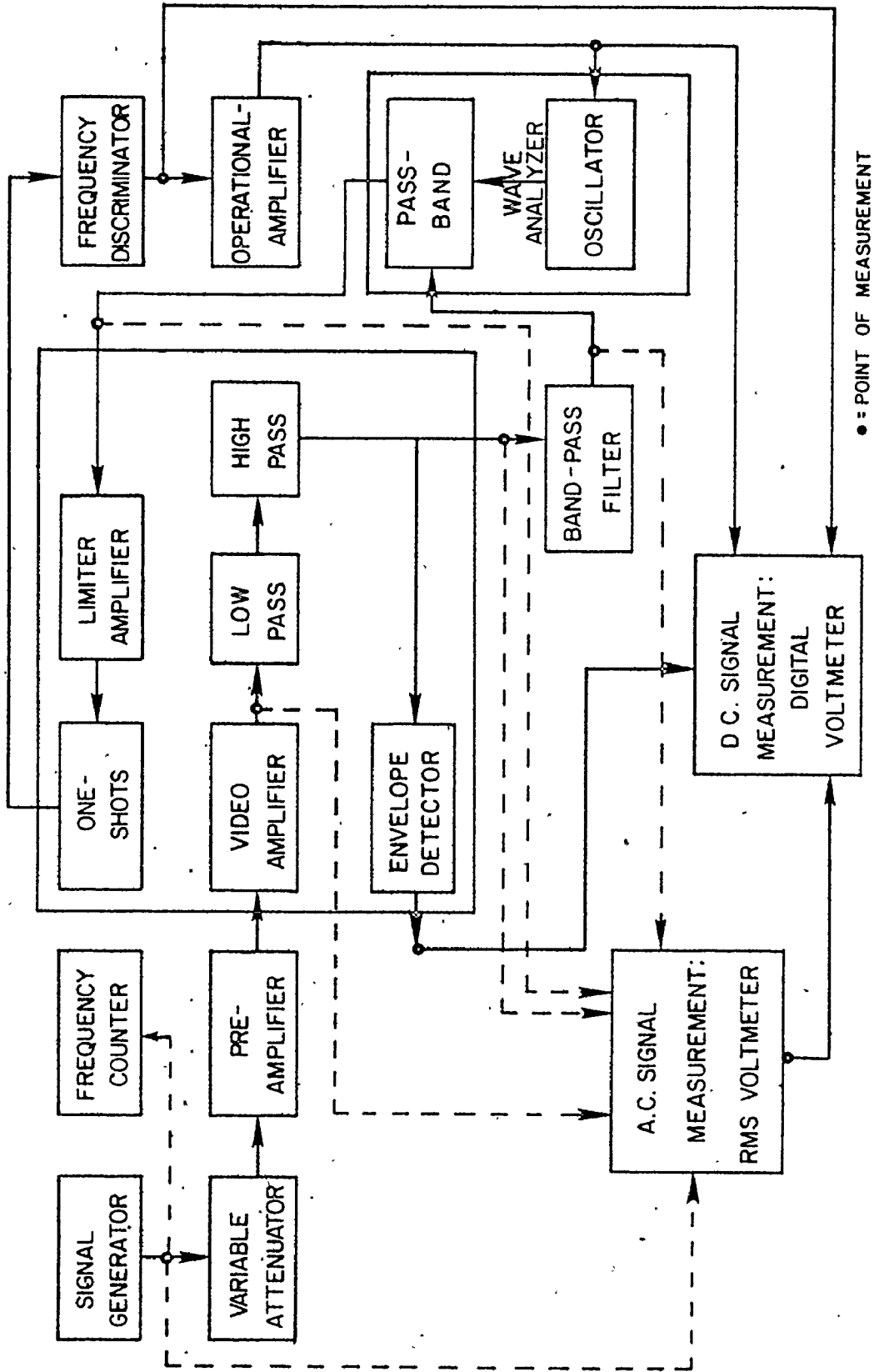
APPENDIX V
CALIBRATION OF SIGNAL PROCESSING
ELECTRONICS

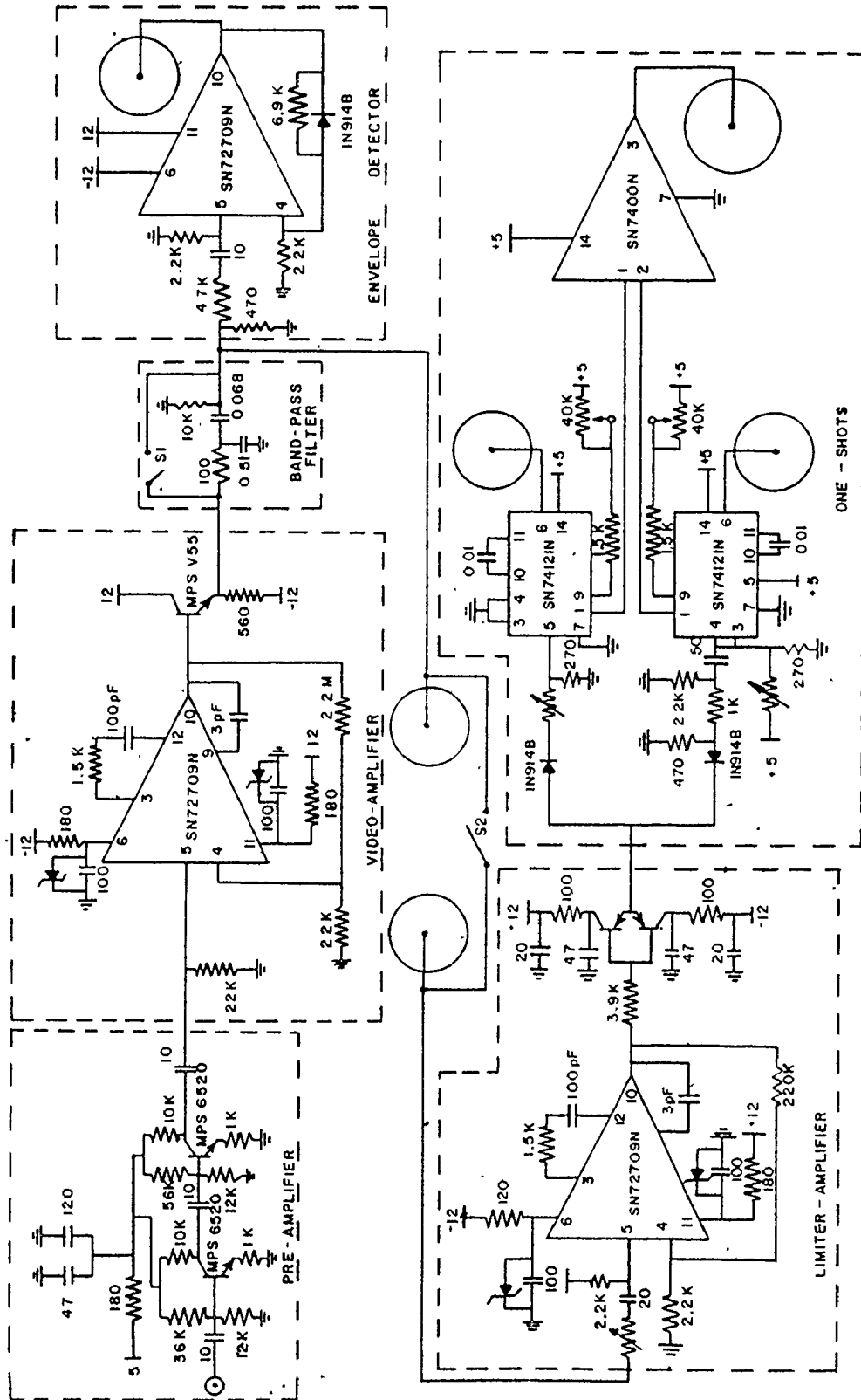
A series of experiments was performed to calibrate the electronic instrumentation used for the measurement of particle velocity and concentration. A signal generator (General Radio Corp., model 1210-C oscillator with model 1203-B power supply) was used to provide a sine wave to the pre-amplifier input. A variable attenuator (Kay Electronics Corp., model 461B) was used to decrease the amplitude of the applied signal to levels similar to those of the Doppler signals measured during the experimental runs.

In these experiments, signal frequencies were measured with a General Radio Corp. model 1192 digital counter; signal amplitudes were measured with a Hewlett-Packard model 3400 RMS voltmeter which produced a DC voltage proportional to the RMS amplitude of the AC signal. All DC voltages were measured with a Fluke Manufacturing Co. model 8300 A digital voltmeter.

A block diagram of the experimental set-up is shown in Figure V-1. Wiring diagrams for those electronic components designed and constructed in-house are shown in Figure V-2.

FIGURE V-1
 SCHEMATIC FOR CALIBRATION OF
 SIGNAL PROCESSING ELECTRONICS





NOTE: UNLESS OTHERWISE INDICATED
 (1) ALL RESISTANCES IN OHMS
 (2) ALL CAPACITANCE IN MICROFARADS

FIGURE V-2
 WIRING DIAGRAM

○ = BNC CONNECTOR

V.1 ATTENUATOR CALIBRATION

An input signal of constant amplitude, (1.1256×10^{-2} volts RMS), and constant frequency, (999 Hz), was applied to the attenuator and the signal amplitude at the output was measured for various degrees of attenuation. For attenuations between 20 and 46 decibels, the linear least-squares model:

$$\log_{10} \left[\frac{V_{\text{out}}}{V_{\text{in}}} \right] = -1.7058 - 0.0477 (\text{DB}) \quad (\text{V-1})$$

where: V_{out} = RMS amplitude of attenuator, output, volts,
 V_{in} = RMS amplitude of attenuator input, volts, and
 DB = nominal attenuation, decibels.

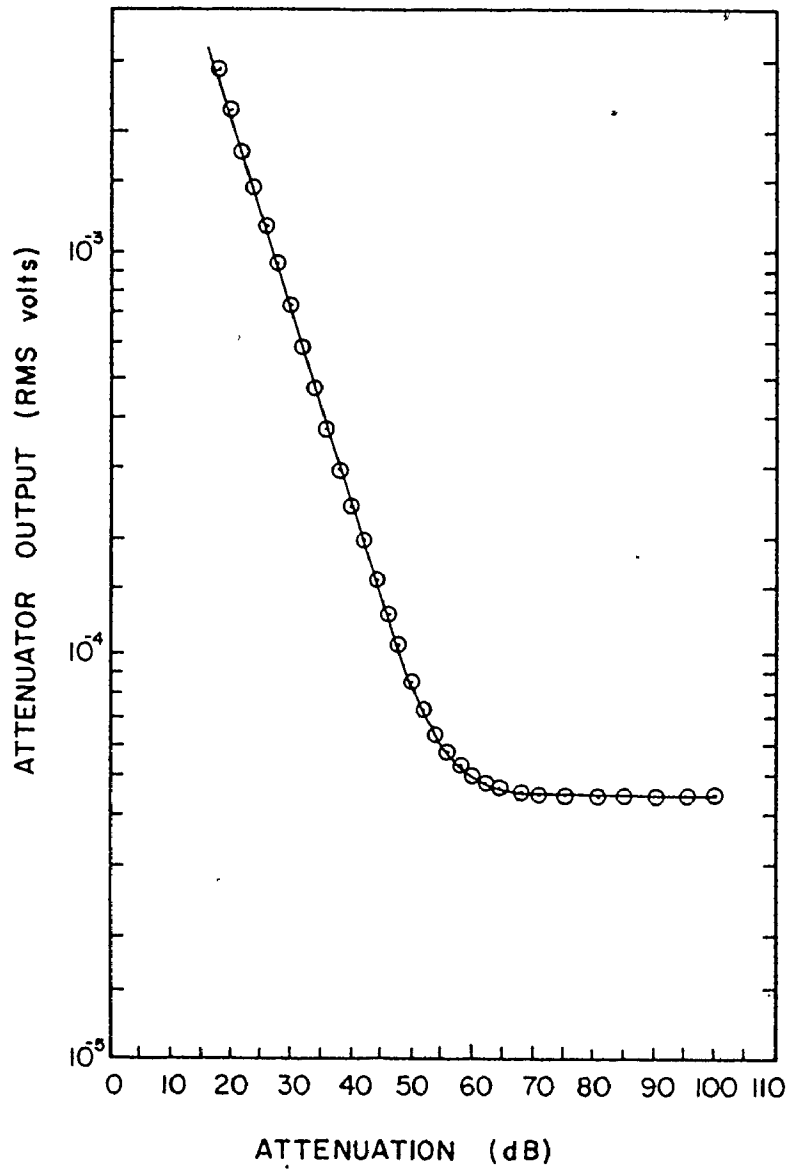
fit these data at the 95 percent confidence level. The curvature evident in Figure V-3 for attenuations greater than 50 decibels was caused by the non-linearity of the RMS voltmeter as the threshold detection level was approached.

For subsequent calibration experiments, equation (V-1) was used to estimate the RMS amplitude of the input signal to the pre-amplifier using the measured RMS amplitude of the signal generator output.

V.2 ENVELOPE DETECTOR OUTPUT AND AMPLIFIER GAIN CALIBRATION

As part of the verification that the Doppler signal was measured during the experimental runs, the extent of correlation between the amplitude of the Doppler signal and

FIGURE V-3
ATTENUATOR CALIBRATION



the independent measurements of reference beam and scattered beam voltages was determined, Appendix II. This required conversion of the DC output of the envelope detector to an equivalent AC signal amplitude at the input to the pre-amplifier.

A signal of constant frequency, (1000 Hz), and constant amplitude, (1.3881×10^{-2} volts RMS), was applied to the pre-amplifier input and the DC output voltage of the envelope detector was measured for various degrees of attenuation.

The linear least-squares model:

(V-2)

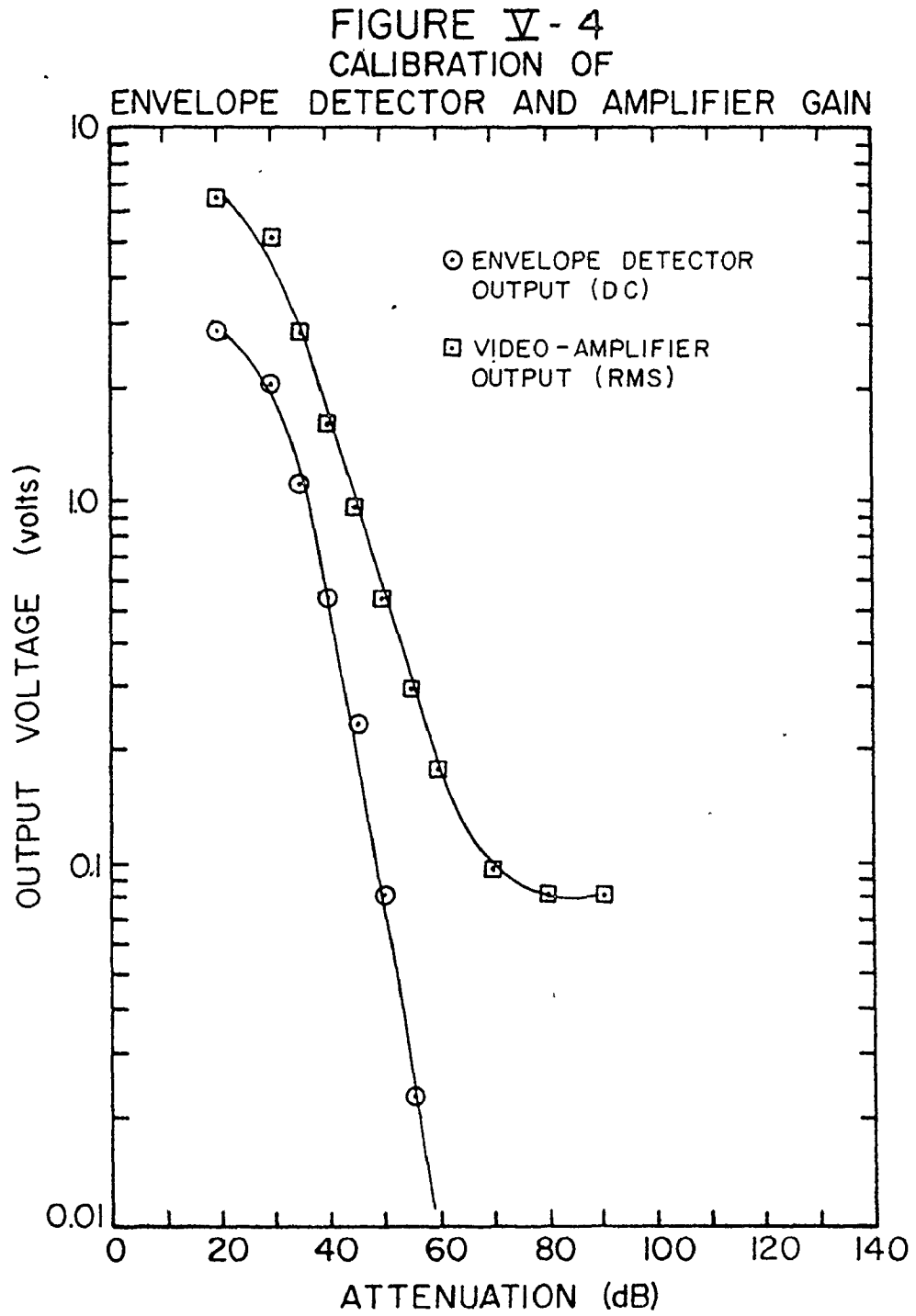
where: V_{out} = RMS amplitude of envelope detector output, volts, and

V_{in} = RMS amplitude of pre-amplifier input, volts,

fits these data at the 95 percent confidence level, Figure V-4.

During this experiment, the RMS amplitude of the output of the passive bandpass filters was measured to determine the combined gain of the pre-amplifier, the video-amplifier and the passive filters. These data, shown in Figure V-4, were fitted by the linear least-squares model:

$$V_{out} = -3.5515 \times 10^{-2} + 3.2212 \times 10^3 V_{in} \quad (V-3)$$



where: V_{out} = RMS amplitude of passive filter output, volts,
and

V_{in} = RMS amplitude of pre-amplifier input, volts.

At high levels of signal input, saturation of the video-amplifier was approached and at low levels of signal input, the electronic noise limit was approached. These factors caused the curvature evident in the data of Figure V-4.

V.3 BANDPASS FILTER CALIBRATION

In order to determine the extent of correlation between the DC voltage output of the envelope detector and the local particle concentration measured during the experimental runs, Appendix I, it was necessary to account for the frequency dependent attenuation of Doppler signal amplitude due to the passive bandpass filters.

The output of the passive bandpass filters was measured as a function of the frequency of a signal of constant amplitude, (9.993×10^{-5} volts RMS), applied to the input of the pre-amplifier. These data were fitted by linear least-squares. The model:

$$V_{out} = 1.205263 \times 10^{-2} + 9.173724 \times 10^{-3} F - 7.878426 \times 10^{-6} F^2 + 2.253354 \times 10^{-9} F^4 \quad (V-4)$$

described the dependence of RMS output voltage, V_{out} , on input signal frequency, F , over the range $100 \text{ Hz} \leq F \leq 1200 \text{ Hz}$.

During this experiment, the RMS amplitudes of the active filter output signals were also measured as a function of input signal frequency, Figure V-5. For this determination, the wave analyzer filter was centred at 1000 Hz and the bandpass was set at 1000 Hz. The upper and lower limits of the Krohn-Hite filter were set at 3000 Hz and 200 Hz respectively, the values used during the experimental runs.

V.4 FREQUENCY MEASUREMENT CALIBRATION

The measurement of Doppler signal frequency was calibrated by monitoring the DC output of the operational-amplifier (used to match the frequency discriminator output to the ramp voltage of the wave analyzer oscillator) as a function of input signal frequency. A signal of constant amplitude (9.9925×10^{-5} volts RMS) was used for this determination. These data are plotted in Figure V-6. For input frequencies in the range 500 Hz to 1600 Hz, the linear least-squares model:

$$V_{\text{out}} = 4.90591 \times 10^{-3} + 2.5001 \times 10^{-4} F \quad (\text{V-5})$$

where: V_{out} = DC operational-amplifier output, volts, and

F = input signal frequency, Hz,

fit the data at the 95 percent confidence level.

This experiment calibrated the joint operation of the wave analyzer, the limiter-amplifier, the one-shots, the frequency discriminator and the matching operational-amplifier, Figure V-1.

FIGURE V-5
BANDPASS FILTER CHARACTERISTICS

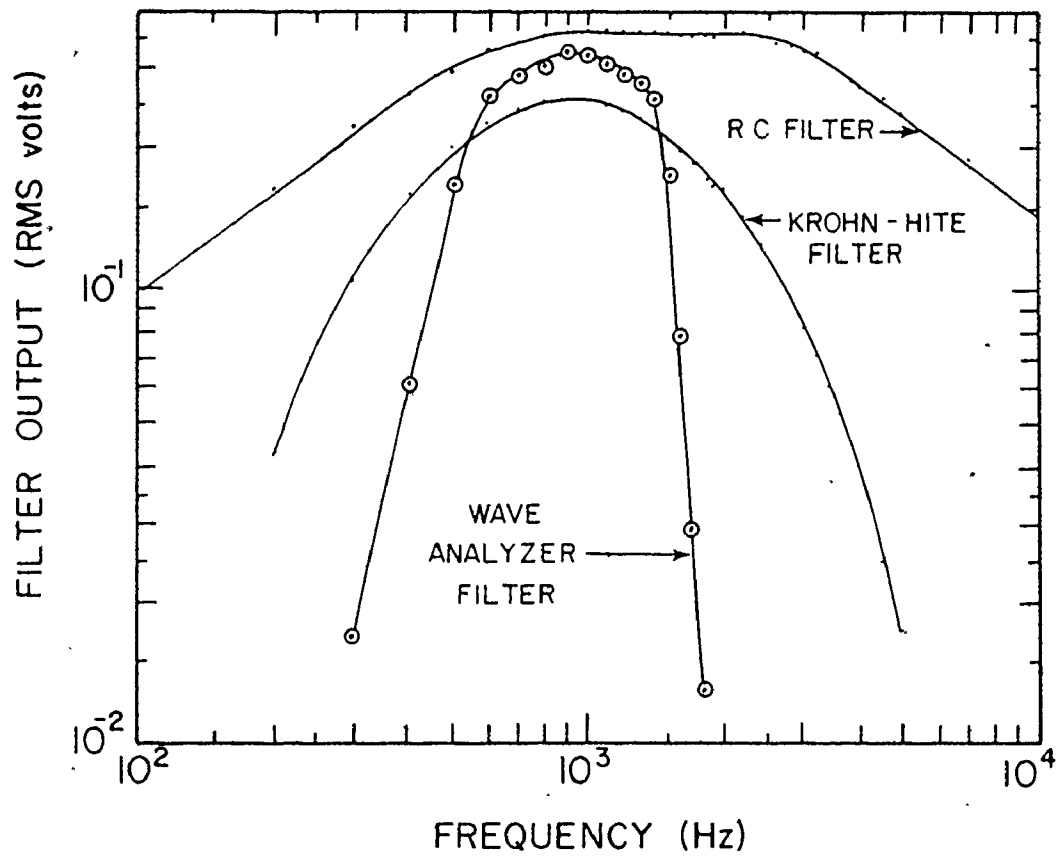
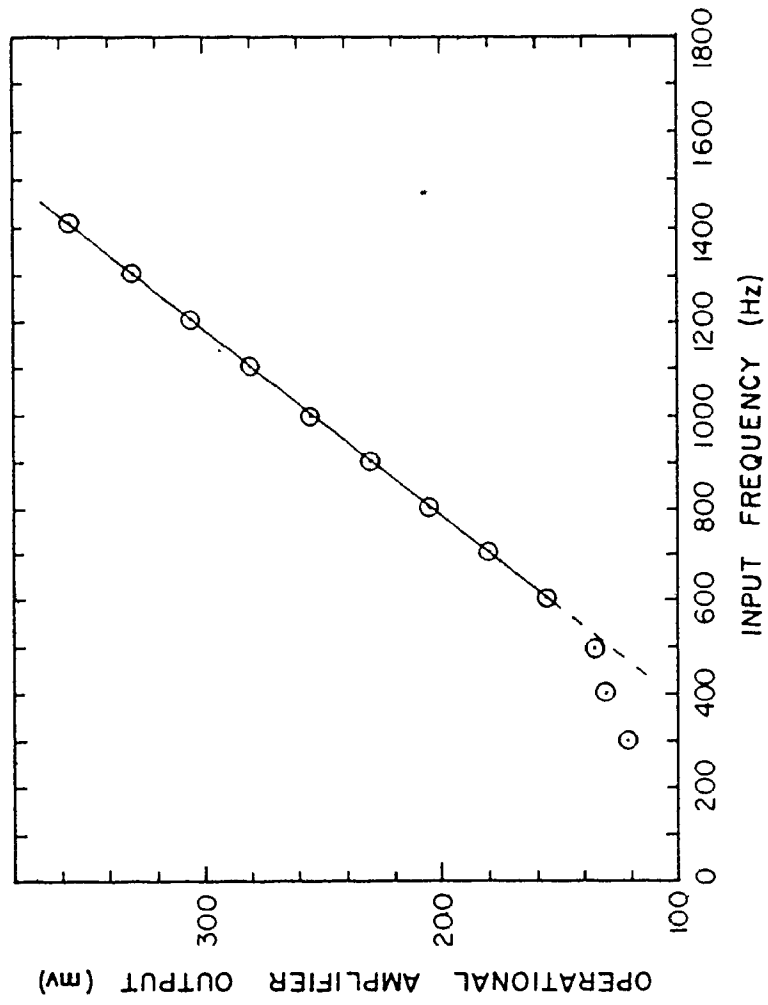


FIGURE V-6
FREQUENCY MEASUREMENT CALIBRATION



V.5 VOLTMETER CALIBRATION

The accuracy of the Hewlett-Packard RMS voltmeter used to measure RMS amplitudes in the calibration experiments was checked with an oscilloscope. The amplitude of a signal of constant frequency, (1000 Hz), was varied at the input to the RMS meter. The amplitude proportional DC voltage generated by the meter was measured and correlated with the peak-to-peak voltage observed on the oscilloscope. These data are plotted in Figure V-7. For all ranges of RMS meter operation, the meter response and the oscilloscope measurements were linearly related with slopes not significantly different from $2\sqrt{2}$ thereby demonstrating the meter accuracy.


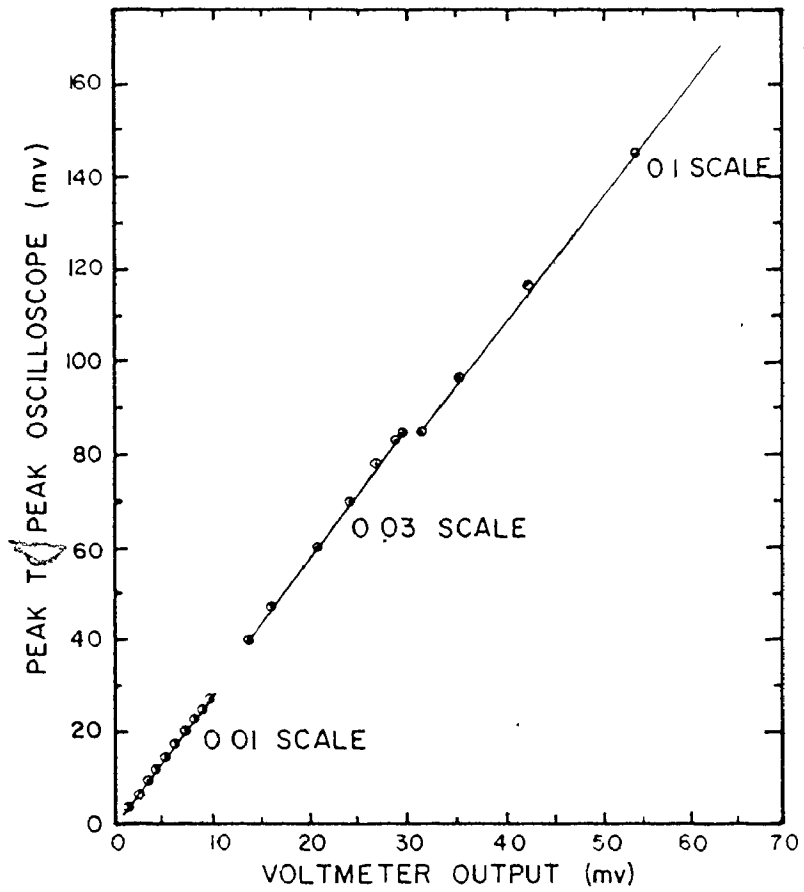


FIGURE V-7
CALIBRATION OF A.C. VOLTMETER



APPENDIX VI
OPERATING CHARACTERISTICS OF THE
LASER DOPPLER INSTRUMENT

VI.1 PHOTOMULTIPLIER TUBE CALIBRATION

VI.1.1 Photomultiplier Tube Gain

At the completion of the experimental runs, the DC output voltage across the photomultiplier anode load was measured as a function of photomultiplier supply voltage to determine the detector amplification characteristics. For this determination, the intensity of the reference beam was measured at supply voltages between -1700 and -3000 in -100 volt increments. After each change in supply voltage, the detector was allowed to stabilize for 10 minutes before readings were taken. After each measurement, the detector output was measured at the reference supply voltage of -2200 to ensure that the experiment was conducted at a constant light intensity.

The model:

$$\log_{10}(V_{\text{out}}) = 36.7876 + 10.1126 \log_{10}(V_{\text{supply}}) \quad (\text{VI-1})$$

where: V_{out} = DC photomultiplier output, volts, and

V_{supply} = absolute value of photomultiplier supply voltage, volts.

described the amplification characteristics at the 95 percent confidence level. The data are listed in Table VI-1 and plotted in Figure VI-1.

Equation (VI-1) was used to scale those scattered beam voltages measured at detector supply voltages of -2700 in runs 3 through 6 to those levels that would have been observed had supply voltages of -2200 been used. This provided a uniform basis across all experimental runs for the measurement of particle concentration using the scattered intensity correlation and the combined transmittance-scattered intensity correlation.

As noted in Appendix II, equation (VI-1) was used to scale the data to a reference detector supply voltage of -2200 during the calibration experiments for estimating particle concentration.

VI.1.2 Photomultiplier Tube Dark Current

The dark current (photomultiplier tube output with no light input) was measured as a function of photomultiplier supply voltage for detector operation at ambient temperature, (approximately 20°C), and for detector operation at a temperature less than 5°C. For this determination, the DC voltage at the envelope detector output was measured. Following each change in supply voltage, no data were collected for a period of 10 minutes to allow the detector to reach a steady-state.

It is evident from Figure VI-2 that dark current was appreciable at supply voltages less than -2400 for ambient

TABLE VI-1
 DETERMINATION OF PHOTOMULTIPLIER
 TUBE AMPLIFICATION

Photomultiplier Supply Voltage (DC volts)	Photomultiplier Output Voltage		
	Mean (DC volts)	Variance (DC volts) ²	Degrees of Freedom
-2200	1.04154×10^{-3}	1.44939×10^{-10}	38
-1700	1.34000×10^{-4}	2.47059×10^{-11}	34
-2200	1.04471×10^{-3}	1.34759×10^{-10}	33
-1800	1.82286×10^{-4}	3.57983×10^{-11}	34
-2200	1.03167×10^{-3}	2.08571×10^{-10}	35
-1900	2.69118×10^{-4}	8.28877×10^{-12}	33
-2200	1.01491×10^{-3}	2.14343×10^{-10}	54
-2000	4.03000×10^{-4}	5.74359×10^{-11}	39
-2200	1.02311×10^{-3}	3.62828×10^{-10}	44
-2100	6.47059×10^{-4}	8.80570×10^{-11}	33
-2200	9.99756×10^{-4}	3.57439×10^{-10}	40
-2300	1.59588×10^{-3}	6.06774×10^{-10}	33
-2200	1.01625×10^{-3}	3.31731×10^{-10}	39
-2400	2.47529×10^{-3}	1.74688×10^{-9}	33
-2200	9.97059×10^{-4}	5.42602×10^{-10}	33
-2500	3.74412×10^{-3}	5.89162×10^{-9}	33
-2200	1.00156×10^{-3}	1.87802×10^{-10}	31
-2600	5.63000×10^{-3}	1.47514×10^{-8}	37

Table VI-1 (Cont'd.)

Photomultiplier Supply Voltage (DC volts)	Photomultiplier Output Voltage		
	Mean (DC volts)	Variance (DC volts) ²	Degrees of Freedom
-2200	9.88857×10^{-4}	3.45714×10^{-10}	34
-2700	8.27000×10^{-3}	2.05080×10^{-8}	50
-2200	9.83830×10^{-4}	2.28492×10^{-10}	46
-2800	1.14970×10^{-2}	6.94343×10^{-8}	32
-2200	9.44286×10^{-4}	3.01681×10^{-10}	34
-2900	1.67465×10^{-2}	6.92660×10^{-8}	33
-2200	9.72143×10^{-4}	2.12369×10^{-10}	41
-3000	2.42842×10^{-2}	1.87749×10^{-7}	37

FIGURE VI-1
PHOTOMULTIPLIER TUBE GAIN

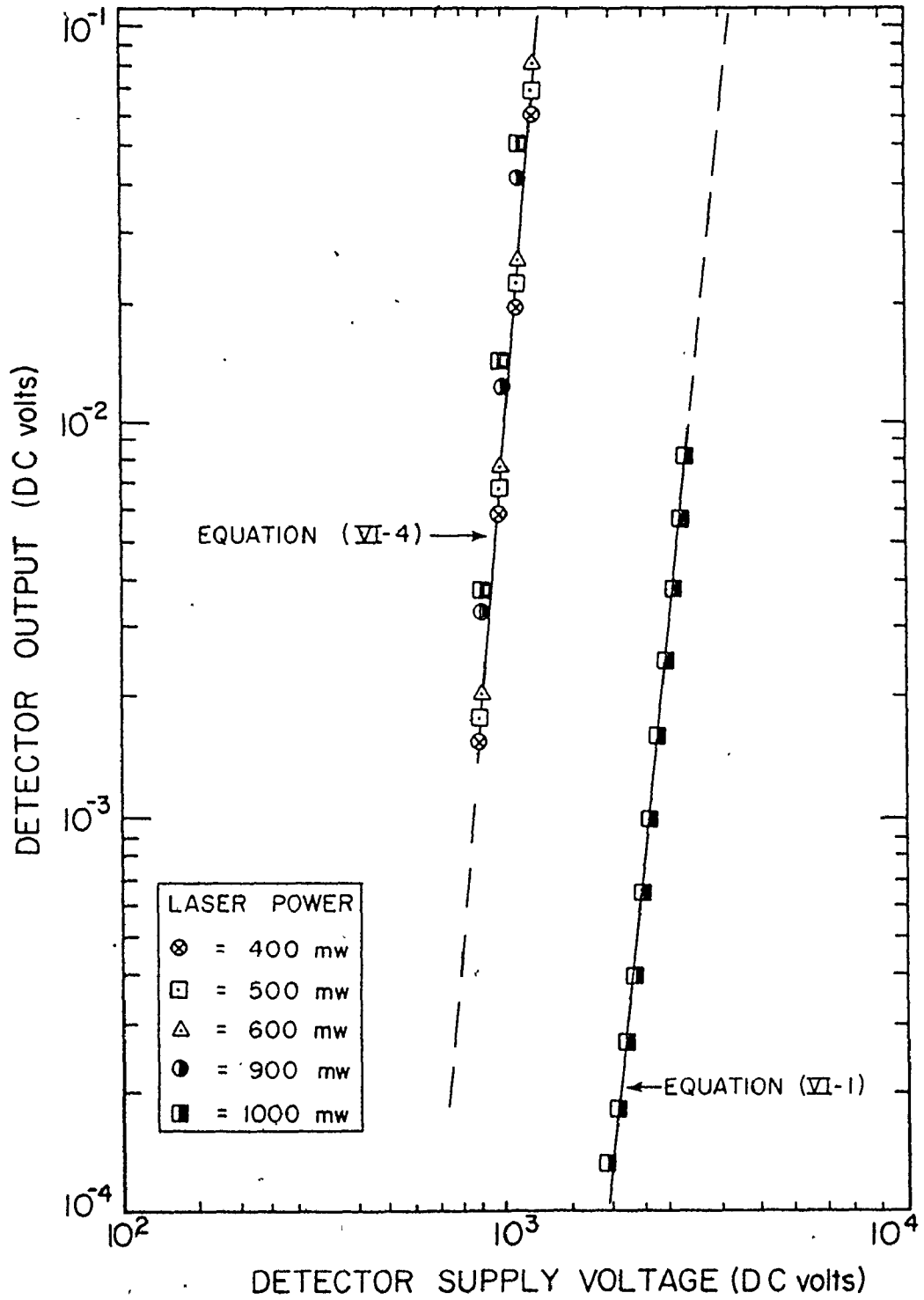
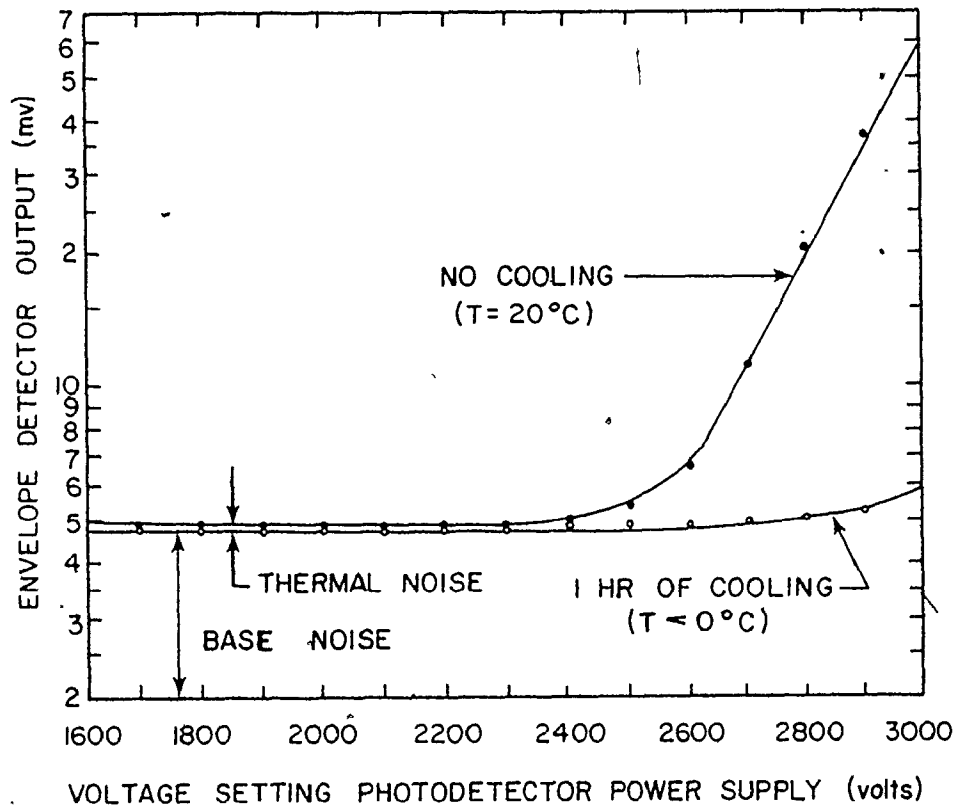


FIGURE VI-2
PHOTOMULTIPLIER DARK CURRENT



temperature operation. Under cooled operation, dark current was almost independent of supply voltage and was not much different from the broadband electronic noise. At supply voltages greater than -2300, detector cooling provided only minor benefits in reducing system noise.

It should be noted that, throughout the experimental runs, the detector was operated at a temperature less than 5°C.

VI.2 PHOTOMULTIPLIER TUBE SUPPLY VOLTAGE CALIBRATION

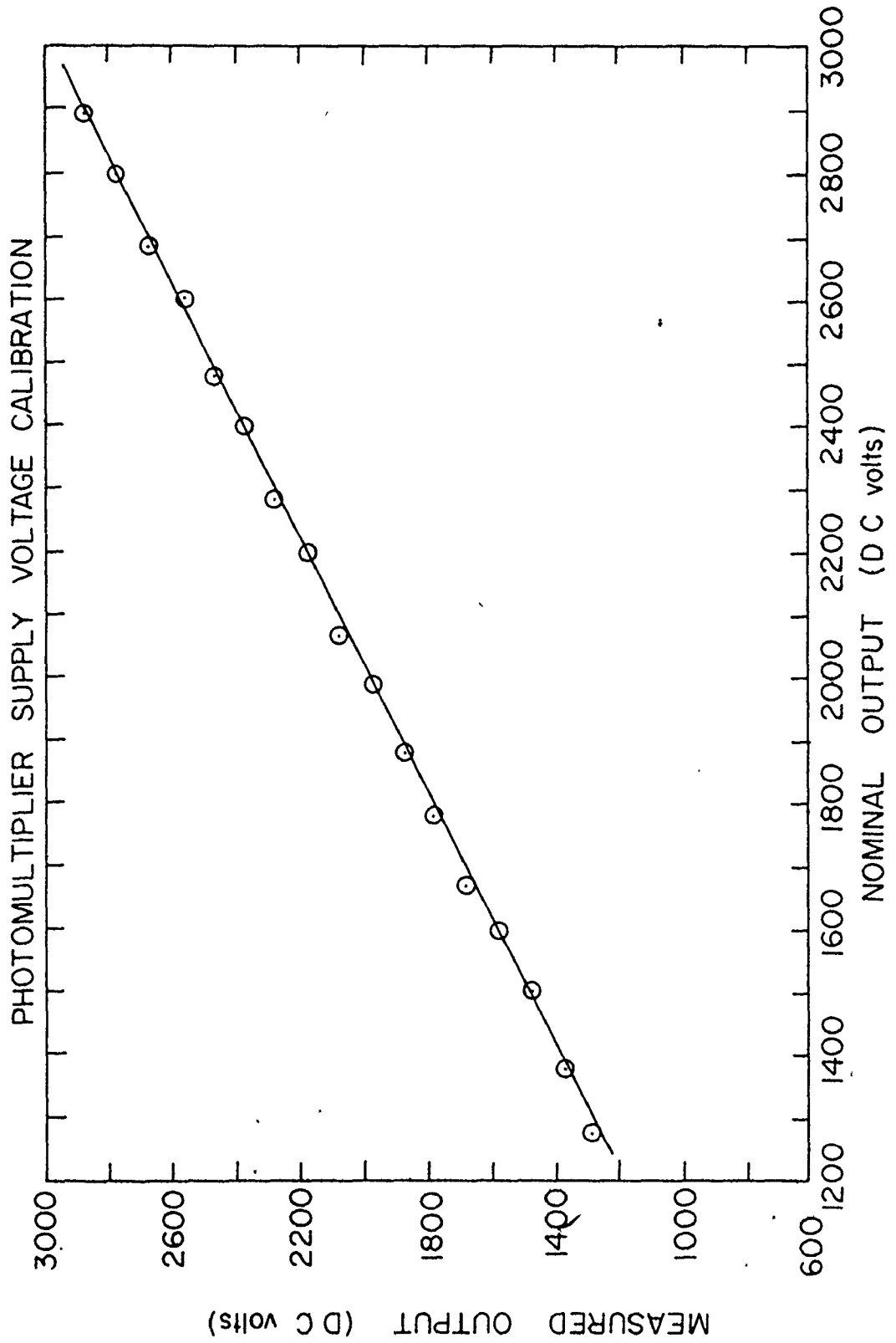
The detector high voltage DC power supply was checked for accuracy. The output voltage was measured using an analog DC voltmeter with a full scale deflection of 600 volts. For this determination, the voltmeter was connected in parallel with a 1.5 megaohm precision resistor to provide a combined resistance of 1.5 megaohms. This combination was connected in series with six, precision (± 0.1 percent) one-megaohm resistors. The output voltage of the power supply was measured over the range of -1000 volts to -3000 volts, Figure VI-3. The power supply output voltage was determined to be accurate within the precision of the analog voltmeter (± 0.5 percent) according to the least-squares model:

$$V_{\text{out}} = 7.5829 + 9.9201 \times 10^{-1} V \quad (\text{VI-2})$$

where: V_{out} = output voltage of power supply, volts, and

V = front panel voltage setting of power supply.

FIGURE VI-3



VI.3 LASER BEAM POWER

Throughout the experimental runs, the laser was operated at a total output power of approximately 950 mw. The powers of the scattering beam, reference beam, and transmittance beam were measured using a Spectra Physics model 401C power meter. This meter, designed for use with helium-neon lasers, was fitted with an adapter to accommodate light at 4880 Å. The DC output voltage of the meter was calibrated against the front panel meter of the laser power supply, Figure VI-4. Using least-squares regression models which described the linear dependence of output voltage on light power, the powers of the scattering, transmittance and reference beams were determined to be 619.458 mw, 99.697 mw, and 140.539 mw respectively.

VI.4 EFFECT OF OPTICAL PATH LENGTH DIFFERENCE ON DOPPLER SIGNAL AMPLITUDE

For maximum heterodyning efficiency, and therefore maximum Doppler signal amplitude, the optical path length of the scattering beam between the laser output mirror and the detector photocathode must differ from the optical path length of the reference beam between the laser output mirror and the detector photocathode according to the relation:

$$\Delta P = n2L \quad (\text{VI-3})$$

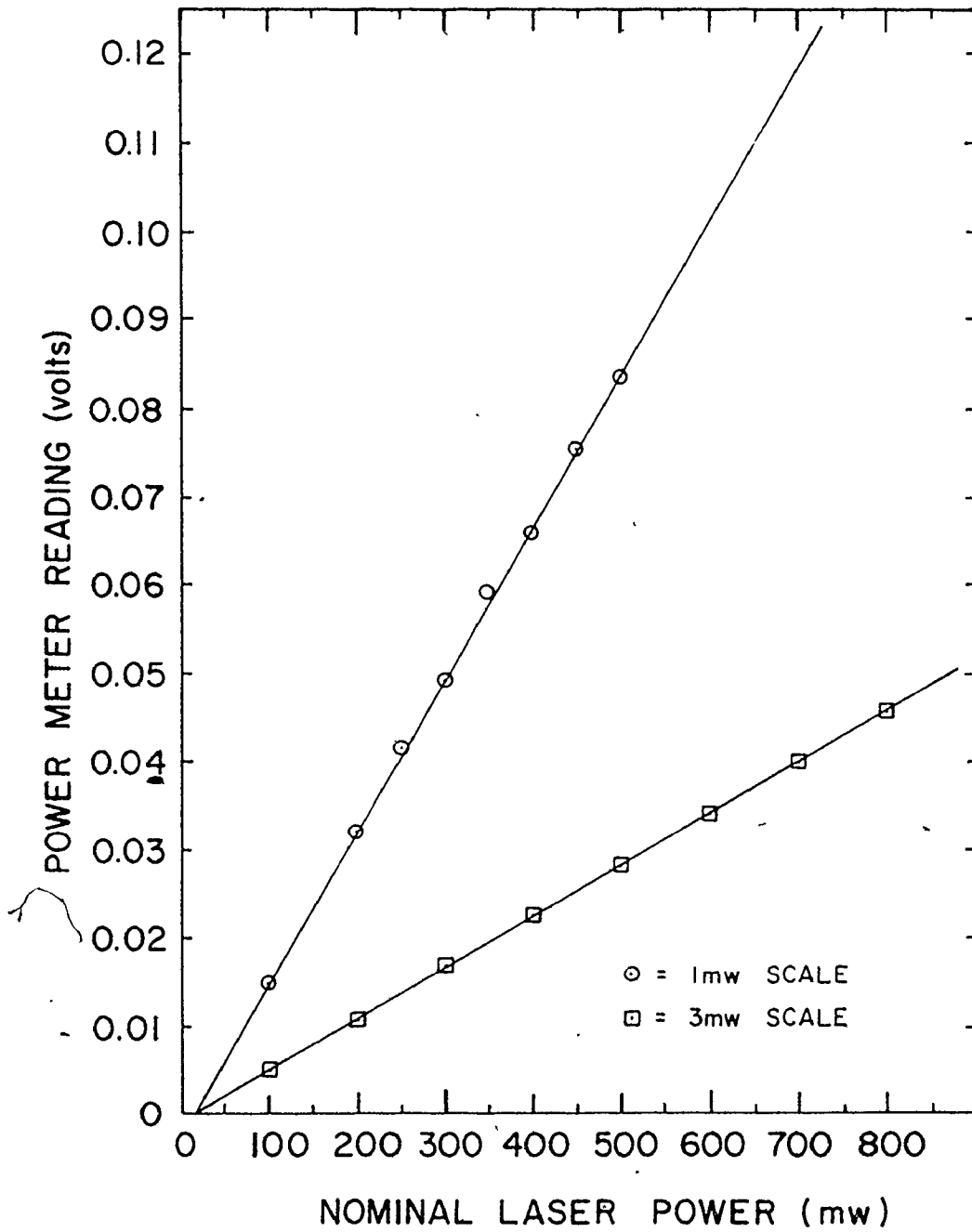
where: ΔP = path length difference between the reference and scattering beams,

L = length of laser cavity, and

n = an integer.

FIGURE VI-4

CALIBRATION OF POWER METER

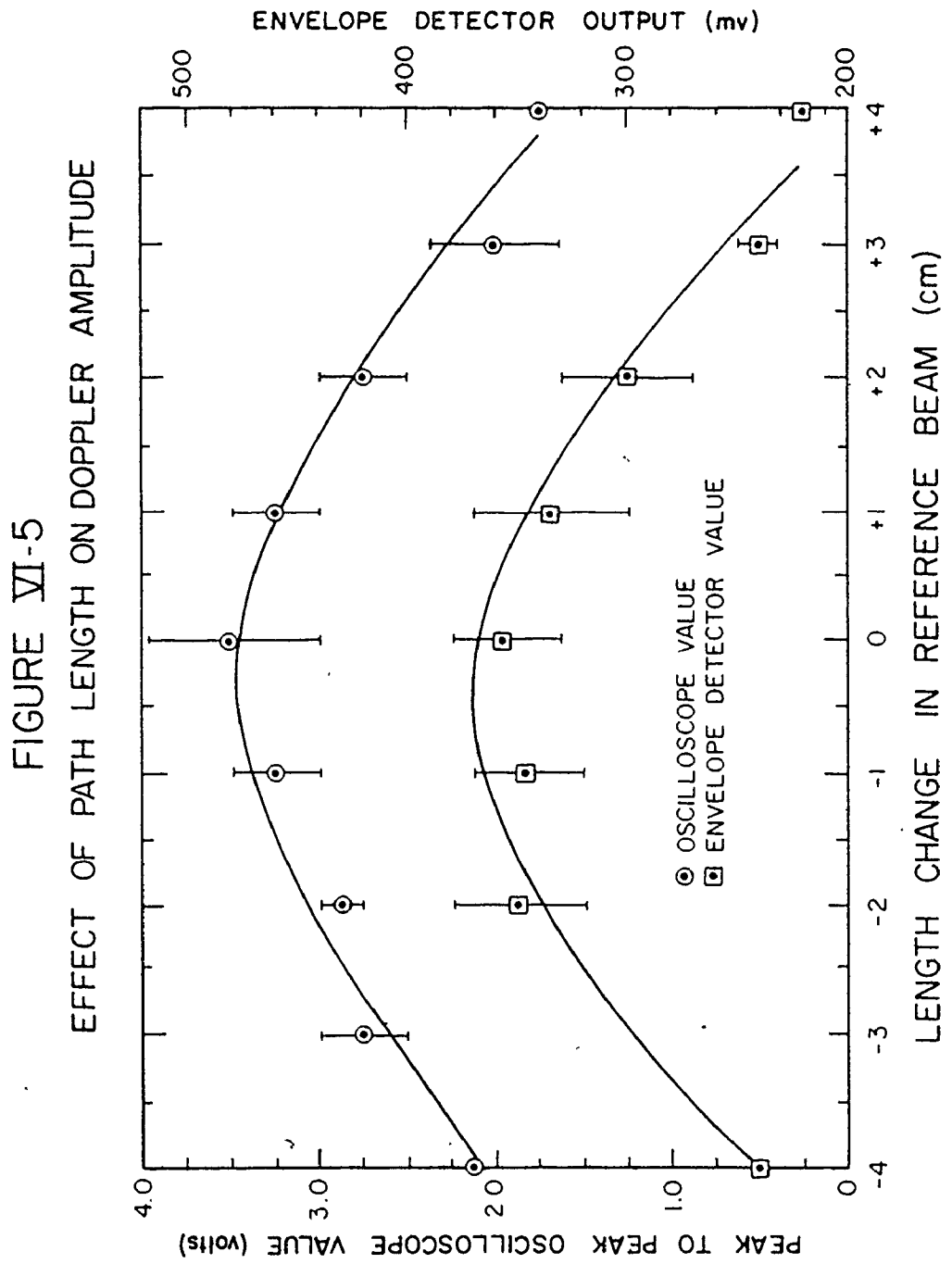


The effect of path length difference on the amplitude of the Doppler signal is shown in Figure VI-5. These data were collected using the same arrangement of apparatus as during the experimental runs, except that the settling column was replaced with a transparent disc mounted on the shaft of a clock motor which rotated at constant speed. As the optical path length of the reference beam was varied, the peak-to-peak amplitude of the Doppler signal was observed on an oscilloscope and the envelope detector output was monitored with a digital voltmeter. It is evident that the Doppler signal amplitude decreased by almost 40 percent for a path length difference of three centimeters.

For each of the experimental runs, the optical path length of the reference beam was adjusted to maximize the amplitude of the Doppler signal.

VI.5 EFFECTS OF REFERENCE BEAM STRENGTH AND FALSE-ALARM FREQUENCY ON DOPPLER SIGNAL FREQUENCY AND AMPLITUDE

An experiment was performed to determine the sensitivities of the measurements of Doppler signal frequency and amplitude to variations in reference beam strength and false-alarm levels. Using the same apparatus as during the experimental runs, the reference beam strength, measured across the detector load, was varied from 1.0 mv, the value used throughout the experimental runs, to 2.5 mv. For each level of reference beam strength, the Doppler frequency and the



envelope detector output were measured at a single location in the settling column for two operational conditions. Under one condition, the volume control of the wave analyzer was adjusted to provide a false-alarm frequency of 100 Hz for each value of reference beam strength. Under the other condition, the volume control of the wave analyzer was held constant at that setting required to provide a false-alarm frequency of 100 Hz at a reference beam strength of 1.0 mv. Under the latter condition, the false-alarm frequency increased as a function of reference beam strength, Figure VI-6.

It is evident from Figures VI-7 and VI-8 and Table VI-2 that the velocity measurement was independent of reference beam strength but strongly correlated with false-alarm frequency over the range studied.

Also shown in Figures VI-7 and VI-8 and Table VI-2 are the envelope detector output voltages, corrected for background (that is, output with scattering beam blocked). This measurement was made upstream from the wave analyzer and therefore was independent of false-alarm frequency. The envelope detector output was strongly correlated with reference beam strength.

A reference beam strength of 1.0 ± 0.05 mv was employed throughout the experimental runs. As well as maintaining a constant noise-in-signal for the photomultiplier

FIGURE VI-6
FALSE ALARM FREQUENCY
VS
REFERENCE BEAM INTENSITY

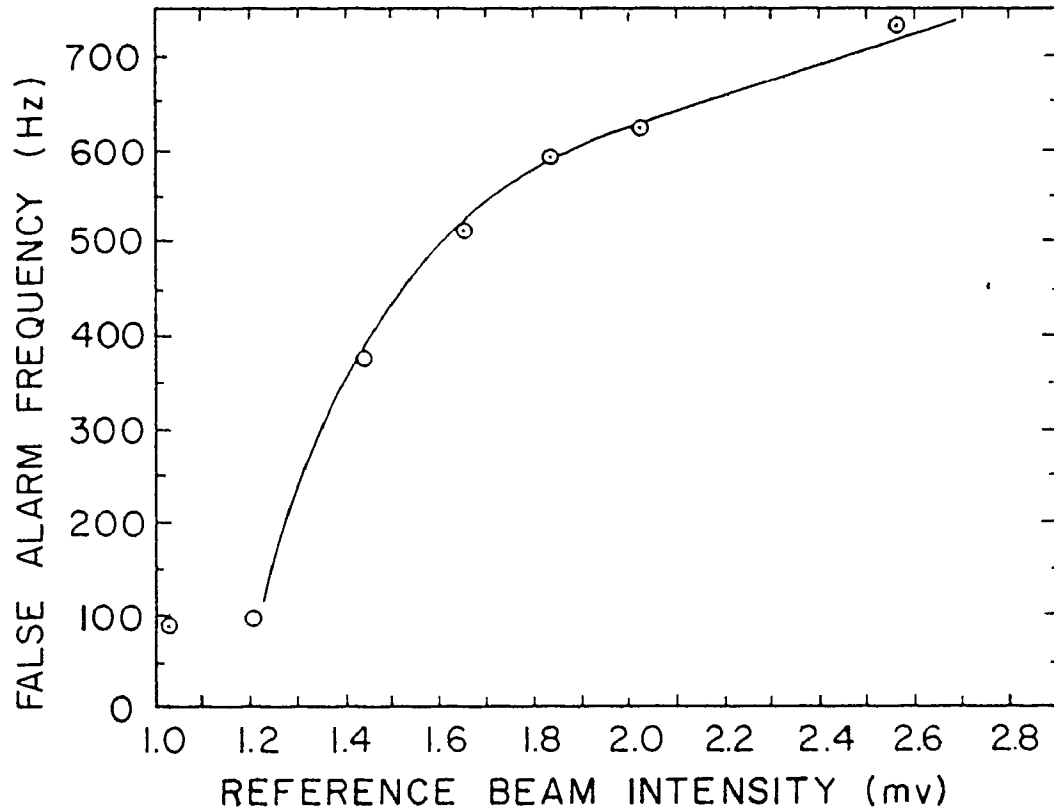


FIGURE VI-7
 DOPPLER SIGNAL AMPLITUDE AND FREQUENCY
 VS
 REFERENCE BEAM INTENSITY

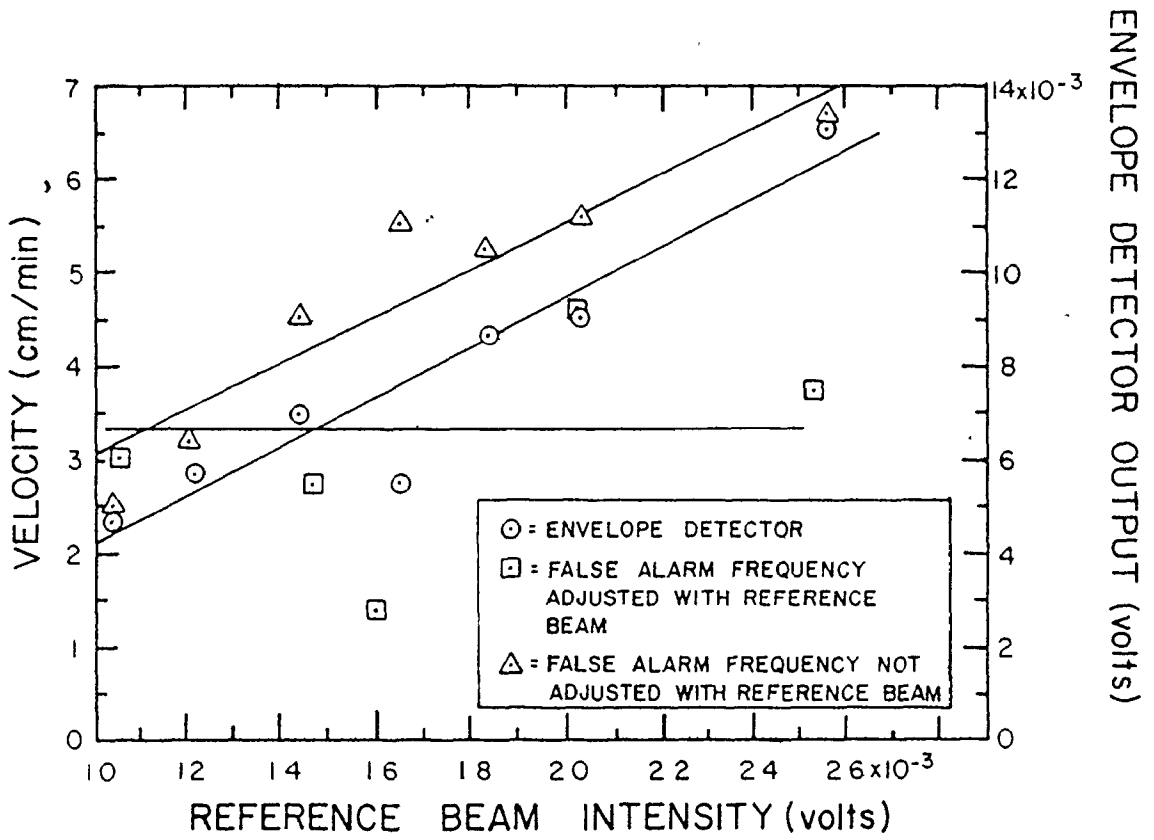


FIGURE VI-8
 DOPPLER SIGNAL AMPLITUDE AND FREQUENCY
 VS. FALSE ALARM FREQUENCY

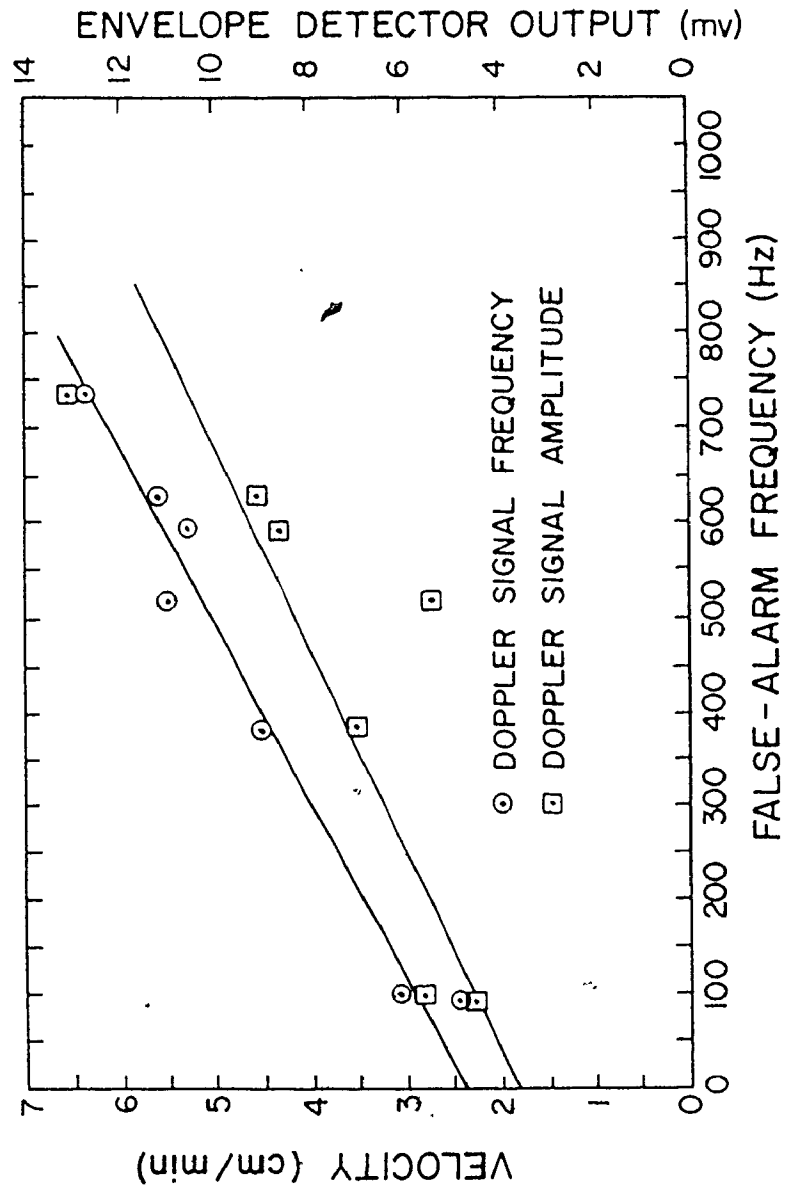


TABLE VI-2

INFLUENCE OF REFERENCE BEAM INTENSITY AND FALSE-ALARM FREQUENCY ON DOPPLER SIGNAL

Reference Beam Intensity (volts)	Changing False-Alarm Frequency									
	Doppler Signal Amplitude (volts)		False-Alarm Frequency		Doppler Signal Frequency		Doppler Signal Frequency		Velocity (cm/min)	
	Signal Plus Background	Background	Signal	Volts	Hz	Volts	Hz	Volts	Hz	Velocity
1.02556×10^{-3}	2.24234×10^{-2}	1.77261×10^{-2}	4.697×10^{-3}	2.74571×10^{-2}	90	8.69137×10^{-2}	328			2.47
1.20887×10^{-3}	2.51788×10^{-2}	1.95092×10^{-2}	5.670×10^{-3}	2.9507×10^{-2}	98	1.11754×10^{-1}	427			3.21
1.43900×10^{-3}	3.13720×10^{-2}	2.43863×10^{-2}	6.986×10^{-3}	9.93676×10^{-2}	378	1.55587×10^{-1}	602			4.53
1.65107×10^{-3}	3.58866×10^{-2}	3.03789×10^{-2}	5.508×10^{-3}	1.3363×10^{-1}	514	1.88420×10^{-1}	734			5.52
1.82528×10^{-3}	4.28286×10^{-2}	3.41159×10^{-2}	8.713×10^{-3}	1.52611×10^{-1}	590	1.79716×10^{-1}	699			5.26
2.01974×10^{-3}	4.72272×10^{-2}	3.80918×10^{-2}	9.135×10^{-3}	1.60977×10^{-1}	624	1.91060×10^{-1}	744			5.60
2.55865×10^{-3}	6.24235×10^{-2}	4.93140×10^{-2}	1.311×10^{-2}	1.88698×10^{-1}	735	2.17887×10^{-1}	851			6.41
							Mean			4.72
							Variance			1.978

Table VI-2 (Cont'd.)

Reference Beam Intensity (volts)	Doppler Signal Amplitude (volts)		Constant False-Alarm Frequency		Doppler Signal Frequency		Velocity (cm/min)
	Signal Plus Background	Background	Signal	False-Alarm Frequency	Volts	Hz	
1.04910×10^{-3}	---	--	--	2.6220×10^{-2}	1.05535×10^{-1}	402	3.03
1.22222×10^{-3}	---	--	--	2.89167×10^{-2}	1.15221×10^{-1}	441	3.32
1.46469×10^{-3}	---	--	--	2.77000×10^{-2}	9.56901×10^{-2}	363	2.73
1.59271×10^{-3}	---	--	--	2.79189×10^{-2}	5.17988×10^{-2}	187	1.41
1.78875×10^{-3}	---	--	--	2.67317×10^{-2}	1.48253×10^{-1}	573	4.31
2.02324×10^{-3}	---	--	--	2.83864×10^{-2}	1.59437×10^{-1}	618	4.65
2.53380×10^{-3}	---	--	--	2.53750×10^{-2}	1.29556×10^{-1}	498	3.75
1.04547×10^{-3}	---	--	--	2.72368×10^{-2}	1.14732×10^{-1}	436	2.29
						Mean	3.31
						Variance	1.002

tube, this provided a uniform basis for estimating particle concentration from the envelope detector output, Appendix I. Throughout the experimental runs, a false-alarm frequency of 100 ± 5 Hz was employed. This level was selected as a trade-off between lower frequencies which resulted in Doppler signal "drop-out" and higher frequencies which resulted in the measurement of broadband noise rather than the Doppler signal.

APPENDIX VII
OPTICAL ALIGNMENT OF THE APPARATUS

Prior to system alignment, the laser was operated at a nominal output of 1 watt for a period of three days in the temperature controlled (± 1 C) laboratory to ensure thermal equilibrium of the laser cavity. The apparatus was then aligned by following the steps in Table VII-1.

For the levelling of the base plate and the settling column (steps 1 through 6) and for the alignment of the detector optics (steps 10 through 15), the settling column, filled with water, was positioned so that the optical "sampling point," (intersection of scattering beam and transmittance beam), was located in the centre of the column. For the alignment of the incident beam optics (steps 7 through 9), the column was moved out of the optical axis.

A deflection gage which measured hundredths of an inch was mounted on each corner of the base plate following the levelling of the base plate and the settling column (steps 1 and 2).

All 40 grid points could be sampled without causing noticeable deflection of the gages. Periodically during each run, the deflection gages were checked and the inflation pressures in the inner tubes were adjusted as required, to

maintain the base plate in a horizontal plane. This ensured that the axis of the settling column remained vertical throughout the experimental period.

A quadrant detector was used to align the scattering beam, steps 7 and 8. This device was a photocell whose entrance window was divided into four equal area quadrants by two fine cross-hairs oriented 45° to the horizontal. The east-west and north-south pairs of quadrant were electrically connected to an X and a Y output jack, respectively. The quadrants were electronically matched so that a zero output voltage resulted at each jack when the laser beam was centred on the cross-hairs and a DC voltage, positive for north and east, negative for south and west, otherwise occurred. This device allowed positioning of the laser beam within ± 0.01 inches.

"Spacing rods" were used to position the quadrant detector, (step 7), and to provide the proper spacing between the various elements of the detector optics, (steps 12 and 15). These rods were made of $1/8$ inch diameter steel and were machined to the appropriate length, ± 0.005 inches.

TABLE VII-1
ALIGNMENT OF LASER DOPPLER INSTRUMENT

Step	Component Aligned	Purpose of Step	Alignment	
			Adjustment	Measurement
1	Base plate	Ensure base plate and X-Y table are horizontal	Individual adjustment of air pressure in the six inner-tube supports	Precision spirit level and deflection gauges
2	Settling Column	Ensure column axis is vertical to plane of X-Y table	Adjust threaded column supports	Precision spirit level
3	Laser	Ensure laser output is normal to settling column wall	Adjust threaded laser supports	Coincidence on laser output mirror of laser output and back reflection of laser output from settling column wall
4	Beam splitters of incident optics	Ensure incident optics support frame is aligned with laser cavity	Manual rotation about axis of laser output and rotation about axes normal to laser output by adjustment screws of incident optics support frame	Coincidence on laser output mirror of laser output and back reflections from beam splitters
5	Transmittance beam mirror, incident optics	Ensure transmittance beam is normal to settling column wall	Rotate mirror about those horizontal and vertical axes normal to laser output with precision adjustment screws	Coincidence on transmittance mirror of laser output and back reflection from settling column wall

Table VII-1 (Cont'd.)

Step	Component Aligned	Purpose of Step	Adjustment	Alignment	Measurement
6	Scattering beam mirror, incident optics	Ensure that scattering beam is in same vertical plane as transmittance beam	Rotate mirror about those horizontal and vertical axes normal to laser output with precision adjusting screws	Coincidence on scattering beam mirror of laser output and back reflection from setting column wall	
7	Quadrant detector for location of "sampling" point	Ensure quadrant detector is aligned with transmittance beam at desired intersection point	Quadrant detector photocell: (a) placed proper distance from incident optics (b) normal to axis of transmittance beam (c) centred on transmittance beam	(a) spacing rod (b) back reflection on transmittance mirror as in step 5 (c) null voltage of X and Y outputs of quadrant detector	
8	Scattering beam mirror, incident optics	Orient mirror so that scattering beam is centred in detector field of view and makes proper angle to horizontal (17° in water; 22.9° in air)	Rotate mirror about that horizontal axis normal to laser output with precision adjusting screw	Null voltage at X and Y outputs of quadrant detector	
9	Nil	Check of step 8	Measure angle between transmittance and scattering beams	Measure distance between beams in a vertical plane a known distance (4 ft) from intersection point	

Table VII-1 (Cont'd.)

Step	Component Aligned	Purpose of Step	Adjustment	Alignment	Measurement
10	Detector	Ensure axis of detector coincides with axis of transmittance beam	Detector rotated about those horizontal and vertical axes normal to axis of transmittance beam by precision adjustment screws	D.C. output voltage of detector maximized (laser power and detector supply voltage reduced to protect detector)	
11	First aperture, detector optics	Centre aperture with respect to transmittance beam	Translation and rotation of precision, gimballed, X-Y, optical support	Same as step 10	
12	Second aperture, detector optics	(a) place aperture cm behind first aperture to limit detector field of view (b) same as step 11	Same as step 11	(a) spacing rod (b) same as step 10	
13	Beam splitter, detector optics	Ensure surface of beam splitter is in a vertical plane oriented 45° to axis of transmittance beam	Same as step 11	Same as step 10	

Table VII-1 (Cont'd.)

Step	Component Aligned	Purpose of Step	Adjustment	Alignment	Measurement
14	Reference beam mirrors	(a) direct reference beam around settling column in same horizontal plane as transmittance beam (b) adjust path length of reference beam to maximize Doppler signal	Same as step 11	(a) same as step 10 (b) see section VI.5	
15	Lenses, detector optics	Ensure lenses are (a) correctly spaced (b) centred on detector axis in vertical plane normal to transmittance beam	Same as step 11	(a) spacing rod (b) rough adjustment by centring back reflection of laser output from detector entrance window on second aperture. Fine adjustment same as step 10	

APPENDIX VIII

LINEAR LEAST-SQUARES REGRESSION
PROCEDURE

Linear least-squares polynomial models of the form:

$$y = \sum_{i=0}^n \theta_i x^i + \epsilon \quad (\text{VIII-1})$$

where: y = predicted response of dependent variable,

x = independent variable,

θ_i = regression parameters, and

ϵ = experimental error, (assumed to be a normally distributed random variable with zero mean),

were used to describe the dependence of one variable on another. It was necessary to determine the number of terms to be included in the model and the values of the regression parameters, $\theta_0, \theta_1, \dots, \theta_n$.

Starting with the zero-order polynomial, ($n=0$), terms of increasing powers in x were added one at a time and the residual sum of squares of the data about the model was determined after each addition. The number of terms to be retained in a model was estimated from the mean square associated with the reduction in the residual sum of squares attributable to each parameter. This quantity was approximated for the k^{th} parameter by the difference in the residual sums of squares between the polynomial in $(k-1)$ terms and the polynomial in k

terms. When this reduction in residual sums of squares was significantly different from the residual mean square for the polynomial in k terms, the k^{th} parameter was retained in the model and the $(k+1)^{\text{th}}$ term was subsequently checked for significance. This procedure was continued until the addition of the $(n+2)^{\text{th}}$ term to the model did not result in a significant reduction in the residual sum of squares. The n^{th} order polynomial in $(n+1)$ terms was used to describe the data. Decisions concerning the acceptance or rejection of a parameter in the model were inferred from the F statistic at the 95 percent confidence level.

The parameters in the model were estimated using a least-squares analysis based on Forsythe orthogonal polynomials. This procedure avoided ill-conditioned normal equations; improved accuracy was further obtained by normalizing the independent variable over the range -2 to 2 . Details of the procedure are available in Kelly (1967).

For those instances in which the variance of the dependent variable was not homogeneous over the range of the independent variable, [determined using Bartlett's multiple F test, see Volk (1958)], the inverse of the variances of the observed responses were used as a weighting vector in the least-squares analysis.

APPENDIX IX

MAJOR EQUIPMENT

- (1) Lasers: (a) Spectra-Physics Inc., model 164; (b) Coherent Radiation Inc., model 54-A
- (2) Photomultiplier tube: RCA, model 7265
- (3) Photomultiplier supply voltage: John Fluke Manufacturing Co., model 415 B
- (4) Wave analyzer: Hewlett-Packard Inc., model 3590-A wave analyzer with model 3594 A oscillator
- (5) Active bandpass filter: Krohn-Hite Corp., model 3550
- (6) Data logging instrumentation: Honeywell Instruments Inc., model 6305 digital multimeter, model 825 E encoder, model 6200 incremental digital recorder
- (7) Frequency discriminator: Hewlett-Packard Inc., model 5210-A
- (8) Optical elements: (a) Spectra-Physics Inc., model 515-81 polarizing beamsplitter, model 540-0129 bandpass filter, model 576-21 front surface mirror, model 511-0021 beamsplitter; (b) Broomer Research Corp., fused silica schlieren grade focusing lenses
- (9) Quadrant detector: Metrologic Inc., model 60-228
- (10) Mu-metal shield: Magnetic Metals Co.
- (11) Particle sizing: Carl Zeiss Co., model TGZ3
- (12) Particles: 3M Company, catalogue number 380
- (13) Pumps: Cole Parmer Co., Masterflex model C-7554-10

APPENDIX X

VELOCITY AND MASS CONCENTRATION AT EACH GRID POINT

Run Number 1					
Level Number	Grid Point Number	Mass Concentration (gm/l)			Velocity (cm/min)
		Transmitted Intensity	Combined Transmitted-Scattered Intensities	Scattered Intensity	
1	1	2.4399	2.5533	2.1819	5.1524
	2	2.4570	2.4883	2.3858	5.4137
	3	2.4529	2.5290	2.2797	5.7896
	4	2.4400	2.4892	2.3281	5.2062
	5	2.4485	2.5808	2.1476	5.5063
	6	2.4837	2.5349	2.3941	5.4892
	7	2.4484	2.4080	2.5403	4.8574
	8	2.4627	2.4794	2.4248	4.3813
2	1	2.4224	2.5839	2.0549	5.5535
	2	2.4454	2.5351	2.2413	5.5770
	3	2.4684	2.6287	2.1040	5.7514
	4	2.4569	2.5988	2.1339	5.7262
	5	2.4573	2.5290	2.2942	5.5181
	6	2.4929	2.6125	2.2209	5.4290
	7	2.4416	2.3806	2.5803	4.7296
	8	2.4471	2.3475	2.6735	4.8544
3	1	2.4915	2.6506	2.1296	5.1602
	2	2.4245	2.6083	2.0062	5.5036
	3	2.4298	2.5939	2.0563	5.8209
	4	2.4567	2.6222	2.0803	5.8798
	5	2.4686	2.5939	2.1836	5.7024
	6	2.4467	2.4978	2.3306	5.3325
	7	2.4184	2.5186	2.1905	5.1924
	8	2.4099	2.4689	2.2757	5.1349

Appendix X (Cont'd.)

Run Number 1 (Cont'd.)					
Level Number	Grid Point Number	Mass Concentration (gm/l)			Velocity (cm/min)
		Transmitted Intensity	Combined Transmitted- Scattered Intensities	Scattered Intensity	
4	1	2.3857	2.5430	2.0277	4.8905
	2	2.3862	2.5229	2.0752	5.3689
	3	2.3291	2.4661	2.0174	5.4799
	4	2.3842	2.5787	1.9415	5.5905
	5	2.4027	2.4858	2.2135	4.9852
	6	2.3823	2.3802	2.3873	4.8390
	7	2.3806	2.4014	2.3335	4.9701
	8	2.3962	2.4001	2.3874	5.2495
5	1	2.3871	2.5372	2.0457	5.1530
	2	2.3793	2.5424	2.0084	4.9181
	3	2.3775	2.5582	1.9664	4.3483
	4	2.3605	2.5133	2.0129	5.2038
	5	2.3616	2.4043	2.1280	4.5200
	6	2.3754	2.4885	2.1183	2.4007
	7	2.3908	2.5256	2.0842	3.5943
	8	2.3846	2.3457	2.4731	3.6433

Appendix X (Cont'd.)

Run Number 2					
Level Number	Grid Point Number	Mass Concentration (gm/l)			Velocity (cm/min)
		Transmitted Intensity	Combined Transmitted-Scattered Intensities	Scattered Intensity	
1	1	1.8789	1.9752	1.6601	5.4167
	2	1.8343	1.9222	1.6342	6.2527
	3	1.8559	1.9955	1.5383	6.2359
	4	1.8517	1.9772	1.5664	6.1995
	5	1.8632	1.9396	1.6897	5.8877
	6	1.8622	1.9059	1.7627	5.1554
	7	1.8832	1.8628	1.9295	4.4036
	8	1.8767	1.8752	1.8802	4.8793
2	1	1.8437	1.9733	1.5487	5.7144
	2	1.8008	1.9122	1.5472	6.3297
	3	1.8885	2.0138	1.6035	7.0154
	4	1.7774	1.9101	1.4756	5.9836
	5	1.7919	1.8672	1.6206	6.2924
	6	1.8511	1.9557	1.6132	6.6590
	7	1.8395	1.8402	1.5545	5.8552
	8	1.8413	1.7998	1.9358	5.7857
3	1	1.7838	1.8841	1.5559	5.7568
	2	1.8368	1.9641	1.5471	6.2437
	3	1.7811	1.8899	1.5336	7.1248
	4	1.7951	1.9175	1.5166	5.7791
	5	1.7964	1.8903	1.5828	4.3964
	6	1.7792	1.8751	1.5610	6.0031
	7	1.8013	1.8181	1.7631	4.3928
	8	1.8277	1.8788	1.7115	5.3048

Appendix X (Cont'd.)

Run Number 2 (Cont'd.)					
Level Number	Grid Point Number	Mass Concentration (gm/l)			Velocity (cm/min)
		Transmitted Intensity	Combined Transmitted-Scattered Intensities	Scattered Intensity	
4	1	1.8230	1.9478	1.5390	6.1908
	2	1.7812	1.8659	1.5886	5.9301
	3	1.8166	1.9767	1.4525	6.1398
	4	1.7644	1.8808	1.4998	5.4056
	5	1.7776	1.8675	1.5732	4.9966
	6	1.7665	1.8540	1.5686	5.6101
	7	1.7675	1.6973	1.9272	5.4071
	8	1.7836	1.7958	1.7559	5.2901
5	1	1.7979	1.8972	1.5722	5.3319
	2	1.7898	1.9119	1.5122	6.1833
	3	1.7759	1.9068	1.4781	5.7012
	4	1.7254	1.8600	1.4193	5.1710
	5	1.7514	1.8682	1.4859	5.7331
	6	1.8091	1.9148	1.5689	5.9249
	7	1.7402	1.7370	1.7474	3.1036
	8	1.7765	1.8048	1.7121	5.9003

Appendix X (Cont'd.)

Run Number 3					
Level Number	Grid Point Number	Mass Concentration (gm/l)			Velocity (cm/min)
		Transmitted Intensity	Combined Transmitted-Scattered Intensities	Scattered Intensity	
1	1	1.8466	2.0056	1.4850	6.0960
	2	1.7154	1.8359	1.4414	6.6313
	3	1.6955	1.8353	1.3775	5.7893
	4	1.7174	1.8597	1.3936	5.8365
	5	1.7354	1.8590	1.4541	5.5893
	6	1.7081	1.8250	1.4423	6.1075
	7	1.7854	1.8432	1.6537	4.9034
	8	1.7387	1.8095	1.5779	5.9087
2	1	1.7342	1.8866	1.3876	5.7195
	2	1.7193	1.8502	1.4215	5.7339
	3	1.8146	1.9825	1.4325	6.1430
	4	1.7518	1.9208	1.3673	4.3314
	5	1.6852	1.8023	1.4190	6.2741
	6	1.7456	1.8527	1.5019	5.8143
	7	1.7479	1.7967	1.6369	5.2062
	8	1.8054	1.8723	1.6534	5.5629
3	1	1.7488	1.8970	1.4118	6.0088
	2	1.6295	1.7700	1.3098	5.1515
	3	1.6697	1.8393	1.2841	6.0434
	4	1.7063	1.8898	1.2887	6.1360
	5	1.7390	1.9117	1.3462	5.4254
	6	1.7033	1.8358	1.4018	5.2528
	7	1.6583	1.6696	1.6326	5.1560
	8	1.7488	1.8167	1.5942	6.1324

Appendix X (Cont'd.)

Run Number 3 (Cont'd.)					
Level Number	Grid Point Number	Mass Concentration (gm/l)			Velocity (cm/min)
		Transmitted Intensity	Combined Transmitted- Scattered Intensities	Scattered Intensity	
4	1	1.6897	1.8357	1.3576	6.4100
	2	1.6217	1.7370	1.3595	6.5252
	3	1.6518	1.7911	1.3349	7.2734
	4	1.7065	1.8700	1.3345	6.6942
	5	1.6841	1.8223	1.4198	6.9206
	6	1.6884	1.8056	1.4219	6.5446
	7	1.6796	1.7094	1.6120	6.1364
	8	1.7184	1.7792	1.5800	6.2299
5	1	1.6715	1.8097	1.3572	3.8797
	2	1.6659	1.7928	1.3771	4.1344
	3	1.6823	1.8443	1.3140	4.4610
	4	1.6882	1.8590	1.2998	4.2926
	5	1.6912	1.8273	1.3815	4.8381
	6	1.7088	1.8460	1.3967	5.5803
	7	1.7028	1.7700	1.5500	2.5418
	8	1.6833	1.7581	1.5130	3.2377

Appendix X (Cont'd.)

Run Number 4					
Level Number	Grid Point Number	Mass Concentration (gm/l)			Velocity (cm/min)
		Transmitted Intensity	Combined Transmitted-Scattered Intensities	Scattered Intensity	
1	1	2.4221	2.5460	2.1404	4.9211
	2	2.4279	2.5826	2.0762	4.5994
	3	2.4546	2.6107	2.0995	4.3648
	4	2.4826	2.6601	2.0786	2.7700
	5	2.4387	2.5858	2.1040	4.2683
	6	2.4557	2.5810	2.1704	2.5011
	7	2.4333	2.4645	2.3624	3.9552
	8	2.3922	2.4327	2.3002	4.5651
2	1	2.3412	2.4546	2.0835	3.5562
	2	2.3282	2.4727	1.9994	4.7497
	3	2.4240	2.5694	2.0932	3.7979
	4	2.3750	2.5129	2.0614	3.2112
	5	2.4027	2.5376	2.0957	1.4042
	6	2.4439	2.5657	2.1670	3.7615
	7	2.3765	2.4115	2.2971	3.2130
	8	2.4140	2.4454	2.3427	2.9755
3	1	2.3323	2.4646	2.0313	4.5861
	2	2.3202	2.47636	1.9712	3.1511
	3	2.3055	2.4652	1.9424	4.2328
	4	2.2881	2.4462	1.9284	4.4722
	5	2.3547	2.5011	2.0217	3.9474
	6	2.3076	2.4427	2.0002	9.1459
	7	2.2665	2.3102	2.1672	1.0173
	8	2.3507	2.4139	2.2071	3.8860

Appendix X (Cont'd.)

Run Number 4 (Cont'd.)					
Level Number	Grid Point Number	Mass Concentration (gm/l)			Velocity (cm/min)
		Transmitted Intensity	Combined Transmitted- Scattered Intensities	Scattered Intensity	
4	1	2.3018	2.4633	1.9345	5.3151
	2	2.2643	2.4165	1.9182	4.9265
	3	2.2380	2.4049	1.8582	4.3278
	4	2.2714	2.4401	1.8877	4.8342
	5	2.2976	2.4590	1.9304	4.8035
	6	2.3056	2.4506	1.9758	4.7870
	7	2.2896	2.3327	2.1910	1.0442
	8	2.3086	2.3546	2.2039	3.9116
5	1	2.2777	2.4149	1.9654	4.5272
	2	2.2512	2.4041	1.9036	4.9341
	3	2.2792	2.4667	1.8527	5.6218
	4	2.3140	2.5128	1.8617	4.6095
	5	2.2770	2.4000	1.9975	4.8426
	6	2.2419	2.3926	1.8991	5.1912
	7	2.2780	2.3043	2.2181	4.3720
	8	2.3005	2.3747	2.1317	4.3085

Appendix X (Cont'd.)

Run Number 5					
Level Number	Grid Point Number	Mass Concentration (gm/l)			Velocity (cm/min)
		Transmitted Intensity	Combined Transmitted- Scattered Intensities	Scattered Intensity	
1	1	2.0992	2.2210	1.8222	6.3165
	2	2.1710	2.2634	1.9607	6.4641
	3	2.22234	2.3643	1.9028	6.3105
	4	2.1134	2.2638	1.7714	5.2516
	5	2.1877	2.3392	1.8430	5.7120
	6	2.1840	2.3183	1.8786	6.4873
	7	2.1830	2.2293	2.0779	5.4315
	8	2.1644	2.1945	2.0958	6.0028
2	1	2.1681	2.2836	1.9054	5.1629
	2	2.1688	2.3244	1.8149	5.5761
	3	2.1326	2.2687	1.8229	5.2035
	4	2.2081	2.3330	1.9239	5.8552
	5	2.1902	2.3069	1.9248	5.9180
	6	2.1881	2.2950	1.9449	6.3718
	7	2.1828	2.2198	2.0984	5.5860
	8	2.1866	2.2416	2.0614	5.9887
3	1	2.0903	2.2249	1.7833	6.2798
	2	2.1240	2.2952	1.7343	5.9986
	3	2.1094	2.2467	1.7971	6.1165
	4	2.1233	2.2852	1.7551	5.4868
	5	2.1642	2.3092	1.8345	4.5031
	6	2.1609	2.2916	1.8634	5.4669
	7	2.1153	2.1353	2.0698	5.4333
	8	2.2237	2.2840	2.0867	5.1458

Appendix X (Cont'd.)

Run Number 5 (Cont'd.)					
Level Number	Grid Point Number	Mass Concentration (gm/l)			Velocity (cm/min)
		Transmitted Intensity	Combined Transmitted-Scattered Intensities	Scattered Intensity	
4	1	2.1941	2.3467	1.8468	5.2982
	2	2.1052	2.2530	1.7692	4.7545
	3	2.1663	2.3303	1.7933	6.0527
	4	2.1428	2.2909	1.8059	4.6574
	5	2.1192	2.2601	1.7985	5.7084
	6	2.1593	2.3148	1.8055	4.7828
	7	2.0690	2.0955	2.0085	5.7689
	8	2.1441	2.1899	2.0399	5.4663
5	1	2.0865	2.2351	1.7485	5.5836
	2	2.0519	2.1882	1.7417	6.2230
	3	2.0450	2.2179	1.6517	6.1466
	4	2.0993	2.2666	1.7188	6.1105
	5	2.1287	2.2702	1.8067	4.9611
	6	2.0918	2.2409	1.7528	6.3508
	7	2.1092	2.1441	2.0297	5.3427
	8	2.1411	2.1788	2.0555	3.8602

Appendix X (Cont'd.)

Run Number 6					
Level Number	Grid Point Number	Mass Concentration (gm/l)			Velocity (cm/min)
		Transmitted Intensity	Combined Transmitted-Scattered Intensities	Scattered Intensity	
1	1	2.6702	2.8238	2.3210	4.5768
	2	2.6701	2.8061	2.3609	2.8606
	3	2.7092	2.8387	2.4145	3.6277
	4	2.6679	2.8019	2.3630	4.4553
	5	2.6858	2.7788	2.4415	4.1943
	6	2.6744	2.7813	2.4313	4.3642
	7	2.6677	4.4361	0.0000	3.8503
	8	2.6305	2.6673	2.5469	3.9339
2	1	2.6177	2.7471	2.3233	4.6027
	2	2.6128	2.7460	2.3097	3.9672
	3	2.5846	2.7285	2.2573	4.5515
	4	2.5880	2.7208	2.2858	4.6180
	5	2.6755	2.7960	2.4015	4.0151
	6	2.6388	2.7702	2.3398	3.8033
	7	2.6508	2.7107	2.5146	2.8606
	8	2.6322	2.6701	2.5458	2.9779
3	1	2.5246	2.6560	2.2259	4.1681
	2	2.4913	2.6077	2.2267	2.6298
	3	2.5362	2.7080	2.1456	4.9308
	4	2.5349	2.6811	2.2024	4.7482
	5	2.5506	2.6747	2.2685	4.7924
	6	2.5227	4.2480	0.0000	4.6075
	7	2.5878	2.6766	2.3860	4.1663
	8	2.6400	2.6903	2.5254	2.0380

Appendix X (Cont'd.)

Run Number 6 (Cont'd.)					
Level Number	Grid Point Number	Mass Concentration (gm/l)			Velocity (cm/min)
		Transmitted Intensity	Combined Transmitted-Scattered Intensities	Scattered Intensity	
4	1	2.5578	2.6993	2.2359	2.0503
	2	2.5584	2.7086	2.2166	1.6630
	3	2.5707	2.7157	2.2410	3.3859
	4	2.5418	2.6908	2.2031	1.7855
	5	2.5454	2.6359	2.3396	3.9119
	6	2.5895	2.7344	2.2598	2.0181
	7	2.6035	2.6734	2.4466	1.3273
	8	2.6157	2.6703	2.4916	1.6480
5	1	2.5472	2.7016	2.1961	2.8955
	2	2.4867	2.6099	2.2066	3.5071
	3	2.5266	2.6702	2.2001	3.7444
	4	2.5753	2.7431	2.1936	4.7356
	5	2.5355	2.6416	2.2941	2.4146
	6	2.5421	2.6474	2.3028	3.3267
	7	2.5281	2.5841	2.4007	1.9317
	8	2.5032	2.5149	2.4764	1.6953